Investigating the GBA1-dependent regulation of GBA2 activity in *Gaucher* disease

Dissertation

zur

Erlangung des Doktorgrades (Dr. rer. nat.)

der

Mathematisch-Naturwissenschaftlichen Fakultät

der

Rheinischen Friedrich-Wilhelms-Universität Bonn

vorgelegt von

Sophie Schonauer

aus

Bonn

Bonn 2016

Angefertigt mit Genehmigung der Mathematisch-Naturwissenschaftlichen Fakultät
der Rheinischen Friedrich-Wilhelms-Universität Bonn

1. Gutachter:	PD Dr. D. Wachten
2. Gutachter:	Prof. Dr. C. Thiele
Tag der Promotion:	21. Dezember 2016
Erscheinungsjahr:	2017

Declaration

Parts of this thesis have already been published or submitted for publication:

Publications:

Körschen, H. G., Yildiz, Y., Raju, D. N., **Schonauer, S.**, Bönigk, W., Jansen, V., Kremmer, E., Kaupp, U. B., and Wachten, D. (2013). The Non-lysosomal beta-Glucosidase GBA2 Is a Non-integral Membrane-associated Protein at the Endoplasmic Reticulum (ER) and Golgi. J Biol Chem. 288(5):3381-93.

Schonauer, S., Körschen, H. G., Penno, A., Rennhack, A., Breiden, B., Sandhoff, K., vom Dorp, K., Dörmann, P., Raju, D., Haberkant, P., Gerl, M., Brügger, B., Zigdon, H., Futerman, A. H., Thiele, C., and Wachten, D. (2016). GBA1-dependent regulation of GBA2 activity in Gaucher disease. *Submitted for publication in Journal of Biological Chemistry.*

Posters:

Schonauer, S., Körschen, H. G., Raju, D.N., Breiden, B., Sandhoff, K., and Wachten, D. Investigating the cross-talk between GBA1 and GBA2 in Gaucher disease. Annual meeting of the “Bonner Forum Biomedizin”, 06.-07.02.2014, Sportschule Hennef, Hennef, Germany.

Schonauer, S., Raju, D.N., Körschen, H. G., Breiden, B., Sandhoff, K., and Wachten, D. Investigating the cross-talk between GBA1 and GBA2 in Gaucher disease. Keystone Symposium on “Lipid pathways in biology and disease”, 19.-24.03.2014, Royal Dublin Society, Dublin, Ireland.

Schonauer, S., Raju, D. N., Körschen, H. G., and Wachten, D. Investigating the cross-talk between GBA1 and GBA2 in Gaucher disease. 06.11.2014, IHRS BioSoft Symposium, Forschungszentrum Jülich, Jülich, Germany.

Schonauer, S., Raju, D. N., Körschen, H. G., and Wachten, D. Investigating the cross-talk between GBA1 and GBA2 in Gaucher disease. Annual meeting of the “Bonner Forum Biomedizin”, 05.-06.02.2015, KSI, Bad Honnef, Germany.

Schonauer, S., Penno, A., Körschen, H. G., Thiele, C., and Wachten, D. Investigating the cross-talk between GBA1 and GBA2 in Gaucher disease. SphingoFOR123 Workshop on “Sphingolipids in infection and beyond”, 25.-26-06.2015, University of Würzburg, Würzburg, Germany.

Schonauer, S., Penno, A., Haberkant, P., Körschen, H. G., Raju, D. N., Zigdon, H., Thiele, C., Futerman, A. H., and Wachten, D. Investigating the cross-talk between GBA1 and GBA2 in Gaucher disease. “Cluster Science Days” of the “ImmunoSensation” Excellence Cluster, 02.-03.11.2015, Biomedizinischen Zentrum (BMZ), University Hospital, Bonn, Germany.

Schonauer, S., Penno, A., Haberkant, P., Körschen, H. G., Raju, D. N., Thiele, C., Zigdon, H., Futerman, A. H., and Wachten, D. Investigating the cross-talk between GBA1 and GBA2 in Gaucher disease. Gordon Research Conference on “Glycolipid and Sphingolipid Homeostasis and Function in Health and Disease”, 06.-11.03.2016, Renaissance Tuscany Il Ciocco, Lucca (Barga), Italy.

<u>Talks:</u>

Investigating the cross-talk between GBA1 and GBA2 in Gaucher disease. “Cluster Science Days” of the “ImmunoSensation” Excellence Cluster, 02.-03.11.2015, Biomedizinischen Zentrum (BMZ), University Hospital, Bonn, Germany.

Investigating the GBA1-dependent regulation of GBA2 activity in *Gaucher* disease. Annual meeting of the “Bonner Forum Biomedizin”, 18.-19.02.2016, Sportschule Hennef, Hennef, Germany.

Abstract

Glycosphingolipids (GSLs) are a large and heterogeneous class of lipids, whose function is equally versatile and complex. They consist of a membrane anchor, ceramide, and different kinds of sugar head groups. Glucosylceramide (GlcCer) is the simplest GSL and serves as a building block for the synthesis of more complex GSLs. GlcCer is degraded either in the lysosome by the acid beta-glucosidase GBA1 or by the non-lysosomal beta-glucosidase GBA2, which is associated with membranes at the Golgi and ER. It is not known whether their distinct localisation points towards a different cellular function. Accumulation of GlcCer due to the lack of GBA2 results in male infertility, whereas various mutations in the *GBA1* gene and loss of GBA1 activity cause the lipid-storage disorder *Gaucher* disease with different clinical subtypes. However, no genotype-phenotype correlation has been identified so far. The role of GBA2 in *Gaucher* disease pathology and its relationship to GBA1 is not well understood. My results reveal a GBA1-dependent down-regulation of GBA2 activity in patients suffering from *Gaucher* disease. I show that sphingosine, the cytotoxic metabolite accumulating in *Gaucher* cells through the action of GBA2, directly binds to GBA2 and inhibits its activity. I propose a negative feed-back loop that inhibits GBA2 activity in *Gaucher* cells through the action of sphingosine, preventing its further accumulation and cytotoxicity. My findings add a new chapter to the understanding of the complex molecular mechanism underlying *Gaucher* disease and the regulation of beta-glucosidase activity in general.

Zusammenfassung

Glycosphingolipide (GSL) stellen eine heterogene Lipidklasse dar, deren Funktion gleichermaßen vielseitig und komplex ist. Sie bestehen aus einem Membrananker, dem Ceramid, und verschiedenen Zucker-Kopfgruppen. Glucosylceramid (GlcCer) ist das einfachste GSL und dient als Baustein für die Synthese von komplexeren GSL. Der Abbau von GlcCer findet zum einen durch die saure beta-Glucosidase GBA1 im Lysosom statt, und zum anderen durch die nicht-lysosomale beta-Glucosidase GBA2, die mit Membranen von Golgi und ER assoziiert ist. GBA1 und GBA2 befinden sich in verschiedenen Bereichen der Zelle. Ob ihre jeweilige Lokalisation jedoch auf eine unterschiedliche Funktion auf zellulärer Ebene hindeutet, ist nicht bekannt. Die Anreicherung von GlcCer im Fall eines Verlusts von GBA2 führt zu männlicher Unfruchtbarkeit, wohingegen Mutationen im *GBA1*-Gen und der damit verbundene Verlust der GBA1 Aktivität das *Gaucher*-Syndrom, eine lysosomale Speicherkrankheit mit unterschiedlichen Ausprägungen, verursachen. Bis heute konnte keine Verbindung zwischen dem Genotyp und dem daraus resultierenden Phänotyp der Krankheit hergeleitet werden. Welche Rolle GBA2 beim *Gaucher*-Syndrom spielt und wie ihr Zusammenspiel mit GBA1 ist, ist nicht bekannt. In meiner Arbeit konnte ich zeigen, dass die GBA2 Aktivität in Patienten, die am *Gaucher*-Syndrom leiden, verringert ist. Durch meine Versuche fand ich heraus, dass Sphingosin, ein zytotoxischer Metabolit, der sich durch die Aktivität von GBA2 in *Gaucher* Zellen anreichert, direkt an GBA2 bindet und die Enzymaktivität inhibiert. Basierend auf diesen Ergebnissen habe ich ein Modell entwickelt, in dem eine negative Rückkopplung in *Gaucher* Zellen durch das von GBA2 produzierte Sphingosin die GBA2 direkt hemmt, wodurch die Anreicherung von zytotoxischen Mengen an Sphingosin verhindert wird. Erkenntnisse aus meinen Studien tragen deshalb zum Verständnis der komplexen Beschaffenheit des *Gaucher*-Syndroms und auch zur Regulierung von beta-Glucosidasen im Allgemeinen bei.

Index

List of abbreviations

°C	Degree celsius
4-MUG	4-methyl-umbelliferyl beta-D-glucopyranoside
A	Adenine
A	Ampere
Å	Ångström
Alas1	Aminolevulinic acid synthase 1
ANOVA	Analysis of variance
ApicSBDP	Azido-picolyl-sulfo-tetramethyl-BODIPY
APS	Ammonium persulfate
AR451	Marker and potent modulator for gamma-secretase
ASM	Acid sphingomyelinase
au	Arbitrary units
B	Beads
B2M	Beta-2-microglobulin
BCA	Bicinchoninic acid
BCECF	2',7'-bis-(2-carboxyethyl)-5-(and-6)-carboxyfluorescein
BDP	BODIPY/ boron-dipyrromethene
Bp	Base pair
BSA	Bovine serum albumin
Btn	Biotin
BU	Back-up
C	Cytosine

CBE	Conduritol B epoxide
cDNA	Complementary desoxyribonucleic acid
Cer	Ceramide
CerS	Ceramide synthase
CERT	Ceramide transfer protein
CHO	Chinese hamster ovary cell line
CHOP	CCAAT-enhancer-binding protein homologous protein
CM	Calcium chloride, magnesium chloride
cmc	Critical micelle concentration
CO_2	Carbon dioxide
CoA	Coenzyme A
CRISPR	Clustered Regularly Interspaced Short Palindromic Repeats
CV	Column volume
Da	Dalton
DAPI	4′,6-Diamidin-2-phenylindol
ddH_2O	Double-destilled water
DEPC	Diethylpyrocarbonate
DES	Desaturase
dk	Donkey
DMEM	Dulbecco's Modified Eagle Medium
DMSO	Dimethyl sulfoxide
DNA	Desoxyribonucleic acid
dNTP	Deoxynucleotide

DOPC	1,2-Dioleoyl-sn-glycero-3-phosphocholine
DTT	Dithiothreitol
E	Elution
E.Coli	*Escherichia Coli*
ECL	Enhanced chemical luminescence
EDTA	Ethylenediamintetraacetic acid
e.g.	*Exempli gratia*, for example
EMCCD	Electron multiplying charge-coupled device
ER	Endoplasmic reticulum
ERT	Enzyme replacement therapy
et al.	Et alii
F	Female
F12	Ham's F-12 Nutrient Mix
FA	Fatty acid
FAPP2	Four-phosphate-adaptor protein 2
FB1	Fumunisin B1
FCS	Fetal calf serum
FT	Flow-through
HEK293	Human embryonic kidney cells
HKG	Housekeeping gene
g	Gram
g	Gravitational force (9.81 m*s-2)
G	Guanine

G418	Geneticin
GalCer	Galactosylceramide
GalNacT	N-Acetylgalactosamine transferase
Gb3-S	Globotriaosylceramide synthase
GBA1	Acid beta-glucosidase
GBA2	Non-lysosomal beta-glucosidase
GBA3	Cytosolic beta-glucosidase
GC	Glucosylceramide
GD	*Gaucher* disease
GEM	Glycosphingolipid-enriched microdomains
GFP	Green fluorescent protein
GlcCer	Glucosylceramide
GlcCerS	Glucosylceramide synthase
GlcSph	Glucosylsphingosine
GLTP	Glycolipid transfer protein
GM1	Monosialotetrahexosylganglioside
GM2	Disialotetrahexosylganglioside
GM3	Trisialotetrahexosylganglioside
GM-95	GlcCerS-deficient mouse melanoma cell line
GOI	Gene of interest
GRP78	78 kDa glucose-regulated protein
GSL	Glycosphingolipid
gt	Goat

Gusb	Glucuronidase beta
h	Hour(s)
h	Human
HAP1	Human fibroblast-like cells
HA-tag	Hemagglutinin tag
HeLa	Immortalised cervical cancer cells originating from Henrietta Lacks
HEPES	2-(4-(2-hydroxyethyl)-1-piperazine)ethanesulfonic acid
hFB	Human fibroblast
HRP	Horseradish peroxidase
IC_{50}	Half maximal inhibitory concentration
IMDM	Iscove's Modified Dulbecco's Medium
In	Input
IPTG	Isopropyl beta-D-1-thiogalactopyranoside
IR	Infrared
IUPAC	International Union of Pure and Applied Chemistry
k	Kilo
K_i	Inhibition constant
KO	Knockout
KOD	*Thermococcus kodakaraensis*
KSA	3-ketosphinganine
l	Liter
L	Lysate
Lac	Lactose

LacCerS	Lactosylceramide synthase
LAMP1	Lysosomal-associated membrane protein 1
LB	Lysogeny broth
LED	Light-emitting diode
LIMP-2	Lysosomal integral protein
µ	Micro
M	Male
M	Molar
m	Milli
m	Mouse
MEB-4	Mouse melanoma control cell line
mEFB	Murine embryonal fibroblast
MEM	Minimum Essential Medium
MES	2-(N-morpholino)ethanesulfonic acid
min	Minute(s)
MNG	N-methyl-N'-nitro-N-nitrosoguanidine
mol	Mole
MOPS	3-(N-morpholino)propanesulfonic acid
mPIC	Mammalian protease-inhibitor cocktail
mRNA	Messenger ribonucleic acid
ms	Mouse
Mx1	Type I interferon inducible promoter
n	Nano

NADPH	Nicotinamide adenine dinucleotide phosphate
NB-DNJ	N-butyl-deoxynojirimycin
NP-C	*Niemann-Pick* type C
OD	Optical density
OptiMEM	Reduced Serum Medium
p	Pico
P	Pellet
pac	Photoactivatable and clickable
PAGE	Polyacrylamide-gel electrophoresis
PBS	Phosphate-buffered saline
PBS-T	Phosphate-buffered saline with Tween 20
PC	Phosphatidylcholine
PCR	Polymerase chain reaction
PDMP	1-phenyl-2-decanoylamino-3-morpholino-1-propanol
PEI	Polyethylenimine
PET	Primer efficiency test
PFA	Paraformaldehyde
pH	p[H+]
pH_e	Extracellular pH
pH_i	Intracellular pH
pic	Picolyl moiety
PLL	Poly-L-lysine
PNGase F	Peptide -*N*-Glycosidase F

PNS	Post-nuclear supernatant
Pre	Pre-incubation
PVDF	Polyvinylidene fluoride
Q-TOF	Quadrupole time-of-flight mass spectrometer
qPCR	Quantitative polymerase chain reaction
R	Ratio
rb	Rabbit
rfu	Relative fluorescence units
RNA	Ribonucleic acid
rpm	Rounds per minute
rt	Rat
RT	Room temperature (around 21 °C)
s	Second(s)
S	Supernatant
S1P	Sphingosine-1-phosphate
SD	Standard deviation
SDS	Sodium dodecyl sulfate
SGPL1	Sphingosine-1-phosphate lyase
SM	Sphingomyelin
SMS	Sphingomyelin synthase
Sph	Sphingosine
SPT	Serine palmitoyl transferase
SRT	Substrate reduction therapy

t	Time
T_A	Annealing temperature
TAG	Triacylglycerol
TBTA	Tris(benzyltriazolylmethyl)amine
TEMED	Tetramethylethylenediamine
Tfrc	Transferrin receptor
TLC	Thin layer chromatography
T_m	Melting temperature
Tris	2-amino-2-hydroxymethyl-propane-1,3-diol
UDP	Uridine diphosphate
UV	Ultra violet
v	Volume
V	Volt
w	Weight
W	Wash
WB	Western blot
WT	Wild-type
y	Year(s)

1 Introduction

1.1 Glycosphingolipids

Glycosphingolipids (GSLs) are a large and heterogeneous class of lipids, whose function is equally versatile and complex. Present in eukaryotes and some bacteria, GSLs consist of a membrane anchor, ceramide, and different kinds of sugar head groups attached via an O-glycosidic linkage (Merrill, 2002). To date, more than 60 different sphingoid bases and more than 300 different sugar chains have been identified in the field of GSLs.

1.1.1 GSL structure and synthesis

GSL synthesis starts with the condensation of serine and palmitoyl-CoA to 3-ketosphinganine, catalysed by the enzyme serine palmitoyl transferase (SPT) at the cytoplasmic side of the endoplasmic reticulum (ER) (Figure 1) (Braun&Snell, 1968; Mandon et al., 1992). In the next NADPH-dependent step, 3-ketosphinganine is reduced to sphinganine by 3-ketosphinganine reductase (KSA-reductase, Figure 1) (Stoffel et al., 1968) and sphinganine is subsequently acylated to dihydro-ceramide by ceramide synthase (CerS) (Rother et al., 1992). Ceramides possess various acyl chain lengths and, up to date, six different CerS have been identified (CerS 1-6) (Levy&Futerman, 2010). Each CerS shows a specificity for a particular acyl chain length used for N-acylation of the sphingoid base (Pewzner-Jung et al., 2006). Thus, just like the sphingoid bases, the fatty acids used for acylation of sphinganine can also vary in chain length, saturation, and hydroxylation and are mostly cell-type specific (Rosenthal, 1987). Therefore, the presence of certain ceramide species depends on the activity of a certain CerS. Besides the *de novo* synthesis of ceramide at the ER, ceramide can also be synthesised from sphingosine released from complex GSLs in the lysosomes, a mechanism also known as the salvage pathway (Hoekstra&Kok, 1992; Schwarzmann&Sandhoff, 1990; Tettamanti&Riboni, 1994; van Echten&Sandhoff, 1993). In both cases, ceramide synthesis relies on the action of CerS (Levy&Futerman, 2010).

Next, the *trans* desaturation of dihydro-ceramide at position C4 of the sphingoid base is carried out by a pair of desaturases (DES1 and DES2) on the cytoplasmic side of the ER, converting the sphinganine part to sphingosine (Figure 1) (Geeraert et al., 1997). Thus, free sphingosine, which is the common sphingoid backbone found in

GSLs, is not produced during GSL synthesis, but can be released from ceramide during GSL degradation. Sphingosine is the predominant sphingoid base in animals, which was first recognised by German biochemist Johann Thudichum in 1884, who described it as a substance “which is of an alkaloidal nature, and […] in commemoration of the many enigmas, which it presented to the inquirer” gave it the name “sphingosine” after the enigmatic Egyptian Sphinx (Thudichum, 1901). Thereafter, thousands of individual sphingolipids were discovered during the following century (Carter et al., 1947). Sphingosine is not only a precursor for higher-order glycosphingolipids, but also for glycerolipids (Figure 1). As previously mentioned, sphingosine is released from GSLs in the lysosome and then transported back to the ER, where it can be phosphorylated by sphingosine-1-phosphate (S1P) kinases to produce S1P (Spiegel&Milstien, 2003). S1P can be irreversibly cleaved by S1P lyase (SGPL1) to produce hexadecenal and phosphoethanolamine (Serra&Saba, 2010), of which hexadecenal enters the biosynthesis pathway for glycerolipids (Nakahara et al., 2012).

To produce more complex GSLs, ceramide is transported from the cytosolic leaflet of the ER membrane to the cytoplasmic side of the *trans* Golgi by ceramide transfer protein (CERT), which extracts ceramide from the ER membrane and targets it to the Golgi membrane via phosphatidylinositol-4-phosphate-rich domains (Hanada et al., 2003). Here, ceramide serves not only as a membrane anchor for more complex GSLs, but also as a precursor for sphingomyelin. The latter is synthesised by transfer of phosphorylcholine to the 1-hydroxyl group of ceramide in the luminal part of the Golgi (Figure 1) (Futerman et al., 1990). Sphingomyelin is present in basically all cell types with higher concentrations found in neuronal cells. It is incorporated in the plasma membrane and especially abundant in the myelin sheath that surrounds the axon of neurons (Ramstedt&Slotte, 2002).

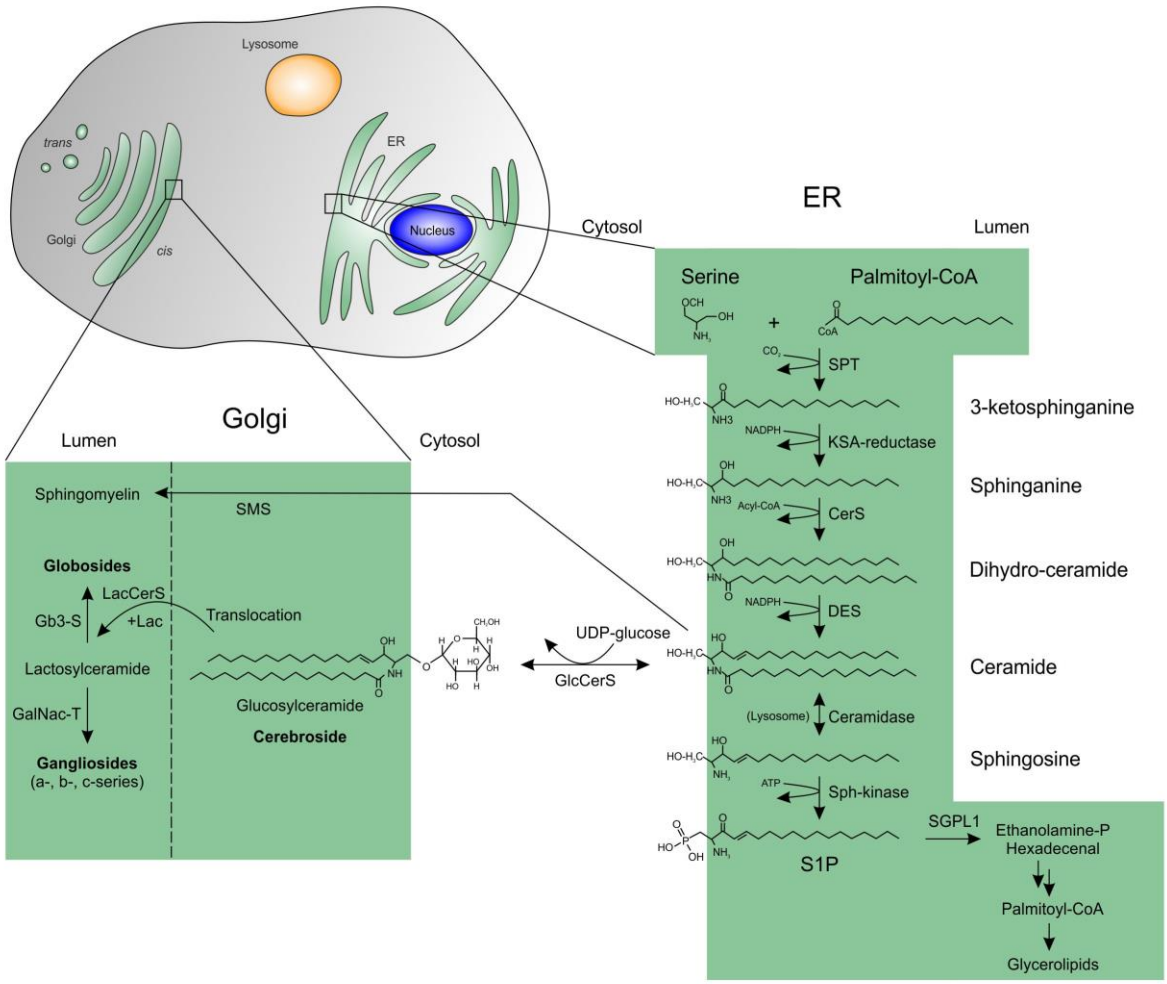

Figure 1: Synthesis of glycosphingolipids (GSLs). Early GSL synthesis takes place at the cytosolic side of the ER and is continued at both, the cytosolic and luminal side of the Golgi. Glucosylceramide (GlcCer) is the main precursor for more complex GSL such as the globosides and gangliosides. The single steps of GSL synthesis are described in the text. CoA: Coenzyme A, SPT: Serine palmitoyl transferase, KSA-Reductase: 3-ketosphinganine reductase, CerS: Ceramide synthase, DES: Desaturase, Sph-kinase: Sphingosine kinase, SGPL1: Sphingosine-1-phosphate lyase, Ethanolamine-P: Phosphoethanolamine, UDP-glucose: Uridine diphosphate glucose, LacCerS: Lactosylceramide synthase, Lac: Lactose, SMS: Sphingomyelin synthase, Gb3-S: Globotriaosylceramide synthase, GalNacT: N-Acetylgalactosamine transferase.

1.1.2 Glucosylceramide: The backbone of numerous glycolipids

The complex GSL family can be divided into three sub-classes: Cerebrosides, gangliosides, and globosides (Figure 1). Cerebrosides are the simplest form and are also called monoglycosylceramides because they have either galactose (galatosylcerebroside) or glucose (glucosylcerebroside) attached to the 1-hydroxy moiety of ceramide. GSLs based on galactosylceramide (GalCer) can be found in specialised cells such as neurons, where GalCer, just like sphingomyelin, is part of the

myelin sheath around the axon (Simons&van Meer, 1988). Glucosylceramide (GlcCer), however, is present in most eukaryotic cells and represents the major building block for more complex GSLs. GlcCer is synthesised by GlcCer synthase (GlcCerS), an enzyme that catalyses the formation of GlcCer from ceramide and UDP-glucose (Basu et al., 1968) at the cytoplasmic side of the *cis* and *medial* part of the Golgi (Schweizer et al., 1994). GlcCerS is a 38 kDa transmembrane protein that assembles to dimers or oligomers with the catalytic site facing the cytoplasm (Marks et al., 1999). Subsequently, more complex GSLs are synthesised in the Golgi lumen (Lannert et al., 1994). Thus, newly synthesised GlcCer has to translocate from the cytoplasmic side to the luminal part of the Golgi (Brade et al., 2000). It has been proposed that i) GlcCer reaches the lumen by either being transported back to the ER, where it is then flipped into the lumen via a rather non-specific phospholipid flippase (Chalat et al., 2012), or ii) through a yet unidentified transporter that flips GlcCer to the luminal side directly at the Golgi (D'Angelo et al., 2007). However, both mechanisms require the specific transport of GlcCer to the location sites of the proposed flippases, action that has been shown to rely on FAPP2 (four-phosphate-adaptor protein 2)-mediated transfer (D'Angelo et al., 2007).

Once GlcCer has reached the luminal side of the Golgi, sugar molecules are added stepwise to its glucose head group to produce higher-order GSLs. First, lactosylceramide synthase (LacCerS) beta links a lactose residue to the C4-hydroxyl group of glucose to produce LacCer (Figure 1) (Takizawa et al., 1999). N-acetylgalacto-saminyl-transferase then adds e.g. an N-acetylneuraminic acid residue to LacCer and during the following steps, gangliosides of the a-, b-, and c-series are synthesised (Figure 1). The term “gangliosides” generally describes all sialylated GSLs and was chosen by the German scientist Ernst Klenk, who isolated them from ganglion cells (Klenk, 1951). To date, more than 60 gangliosides are known, which mainly differ in the position and number of N-acetylneuraminic acid residues with the a-, b- and c-series having one, two, or three residues attached to the galactose residue of LacCer, respectively. GM3 (trisialotetrahexosylganglioside), for example, represents the simplest ganglioside of the a-series, which contains only one sialic acid residue. Here, “G” stands for “ganglioside”, “M” stands for one sialic acid residue (mono), and the number refers to the migration of GM3 on thin layer chromatography (TLC) (e.g. GM3 > GM2 > GM1) (according to the Svennerholm system, IUPAC-IUB Joint Commission on Biochemical Nomenclature 1997). Lastly, globosides contain more than one sugar

as a head group of ceramide and represent the major glycolipid in the human erythrocyte membrane (Klenk&Lauenstein, 1952). The sugars are a mix of N-acetylgalactosamine, D-glucose, and D-galactose.

1.1.3 Intracellular sorting, transport, and function of GSLs

After their synthesis is completed, GSLs are shuttled to the plasma membrane by vesicles that bud off from the Golgi membrane and fuse with the plasma membrane (Miller-Prodraza&Fishman, 1984). Via this process, the sugar moieties project into the extracellular space, whereas the ceramide part of GSLs is embedded into the outer leaflet of the plasma membrane (Varki, 1993). However, Metz and Radin discovered a small, soluble lipid transfer protein in 1980, which selectively transfers GSLs between intracellular membranes (Lin et al., 2000; Metz&Radin, 1980). Glycolipid transfer protein (GLTP) senses the carbohydrate head groups of GSLs on the membrane and forms a soluble complex, while the hydrophobic part of the lipid is incorporated into a cleft-like GLTP gate. GLTP transfers both, sphingoid- and glycerol-based glycolipids, but requires the first sugar head group to be beta-linked to the lipid part of the molecule (Brown&Mattjus, 2007). When GLTP is knocked-down, GlcCer transport to the plasma membrane is reduced by 50%, whereas GLTP over-expression leads to a two-fold increase in GlcCer transport (Halter et al., 2007). Thus, GLTP transports GSLs, in particular GlcCer, to the plasma membrane in a vesicle-independent manner (Halter et al., 2007; Warnock et al., 1994). This mechanism, however, requires a yet unidentified flippase or a transporter to actively translocate GlcCer (or GSLs) from the cytoplasmic side of the plasma membrane to the outer leaflet of the membrane.

Besides GLTP, FAPP2 is also known to transport GlcCer from the Golgi network to the plasma membrane (D'Angelo et al., 2007). Residues important for glycolipid transfer activity are conserved in FAPP2 and GLTP (Godi et al., 2004). Thus, GlcCer can either be transported to the plasma membrane through the vesicular pathway or by a cytosolic pathway involving glycolipid-transfer proteins like GLTP and FAPP2 (Sasaki, 1990; Warnock et al., 1994).

Once they have settled in the outer leaflet of the plasma membrane, GSLs exert a broad variety of functions. GSLs make up less than 5% of total membrane lipids in the plasma membrane of e.g. erythrocytes, but comprise more than 20% in the myelin sheath of neurons (Sako et al., 1987). Here, GSLs are not homogeneously distributed but rather cluster in so-called “lipid rafts”. The structure of lipid rafts is a topic of ongoing

debate, but it is widely recognised that they consist of sphingolipids like GSLs and SM, cholesterol, and certain proteins. GSLs can interact with each other side-by-side (*cis* interaction) to form clusters within one membrane leaflet, but they can also interact through their sugar head groups when facing another membrane (*trans* interaction) (Lofgren&Pascher, 1977). *Cis* interaction is also thought to lead to the formation of lipid raft-independent domains, so-called glycosphingolipid-enriched microdomains (GEMs), which assemble in absence of cholesterol and SM. GEMs are involved in cell adhesion and signal transduction (Iwabuchi et al., 1998), which is why GEMs have also been termed glycosynapses (Hakomori Si, 2002). Lectins, which are carbohydrate-binding proteins, recognise and bind to certain GSL structures, a process involved in cell adhesion (Varki, 1994). Furthermore, GSLs have been shown to function as receptors for microbial toxins and bacteria (Hakomori, 1981), where Jacewicz et al. showed that the globoside Gb3 is a receptor for shigatoxin on HeLa cells (Jacewicz et al., 1986), and the ganglioside GM3 has been shown to serve as a binding site for choleratoxin (Kuziemko et al., 1996). Additionally, many different GSLs are known to serve as infection sites for numerous bacteria (Karlsson, 1989). Besides serving as receptors, GSLs can also modulate the function of other receptor proteins (Sorice et al., 2001). GSLs, and gangliosides in particular, have been shown to interact with growth factor receptors, which in turn modulates cell growth, although the underlying mechanisms are not well understood. For example, N-glycosylation of the epidermal growth factor receptor keeps it in a certain confirmation that is essential for its interaction with GM3, which, in turn, is crucial for GM3-mediated suppression of the receptor (Wang et al., 2001). Thus, GSLs are involved in many, and most likely yet unidentified, mechanisms.

1.1.4 GSL degradation

GSL degradation mainly takes place in the endosomes and lysosomes of the cell but, in one case, can also occur at the cytosolic side of the *cis* Golgi and the ER. Sequential hydrolysis by lysosomal glycosidases releases sugars, sialic acids, fatty acids, and sphingoid bases, which are either further degraded or re-used within the salvage pathway (Schwarzmann&Sandhoff, 1990). Foreign and cellular cargo reaches the lysosome via endocytosis, phagocytosis, or direct transport (Figure 2). During endocytosis, cargo is internalised via a clathrin-dependent or –indepent mechanism (Mayor&Pagano, 2007) (Figure 2). In a first step, parts of the plasma membrane bud

off into the cytosol and then enter the endocytic vesicular pathway (Figure 2). Here, GSLs that were previously facing the extracellular space are now present in the luminal part of the endocytic vesicle (Figure 2). In the following steps, vesicles fuse with early endosomes and become intra-endosomal vesicles with the GSLs sitting in the outer membrane leaflet facing the lumen of the endosome (Figure 2). GSL digestion then starts during acidification of the early endosomes, which favours the activity of certain hydrolases (Maxfield&Yamashiro, 1987), whilst early endosomes become late endosomes. At this point, acid sphingomyelinase (ASM) releases e.g. ceramide from sphingomyelin (Schulze et al., 2009). In a final step, the remaining GSLs reach the lysosome for degradation. Since the lysosome is full of hydrolytic enzymes, its inner membrane (perimeter membrane) is protected from degradation by a thick glycocalix made out of the carbohydrate residues of integral and membrane-associated proteins (Peters&von Figura, 1994) (Figure 2). Thus, enzymes sitting in the perimeter membrane do not have access to lipids inside the lysosome. According to the current view, GSLs from former plasma membrane structures reach the lysosome as intra-lysosomal vesicles (Furst&Sandhoff, 1992), which also provide the platform for further degradation steps (Figure 2). With this orientation, GSLs are accessible to hydrolytic proteins like acid beta-glucosidase (GBA1) within the lumen of the lysosome.

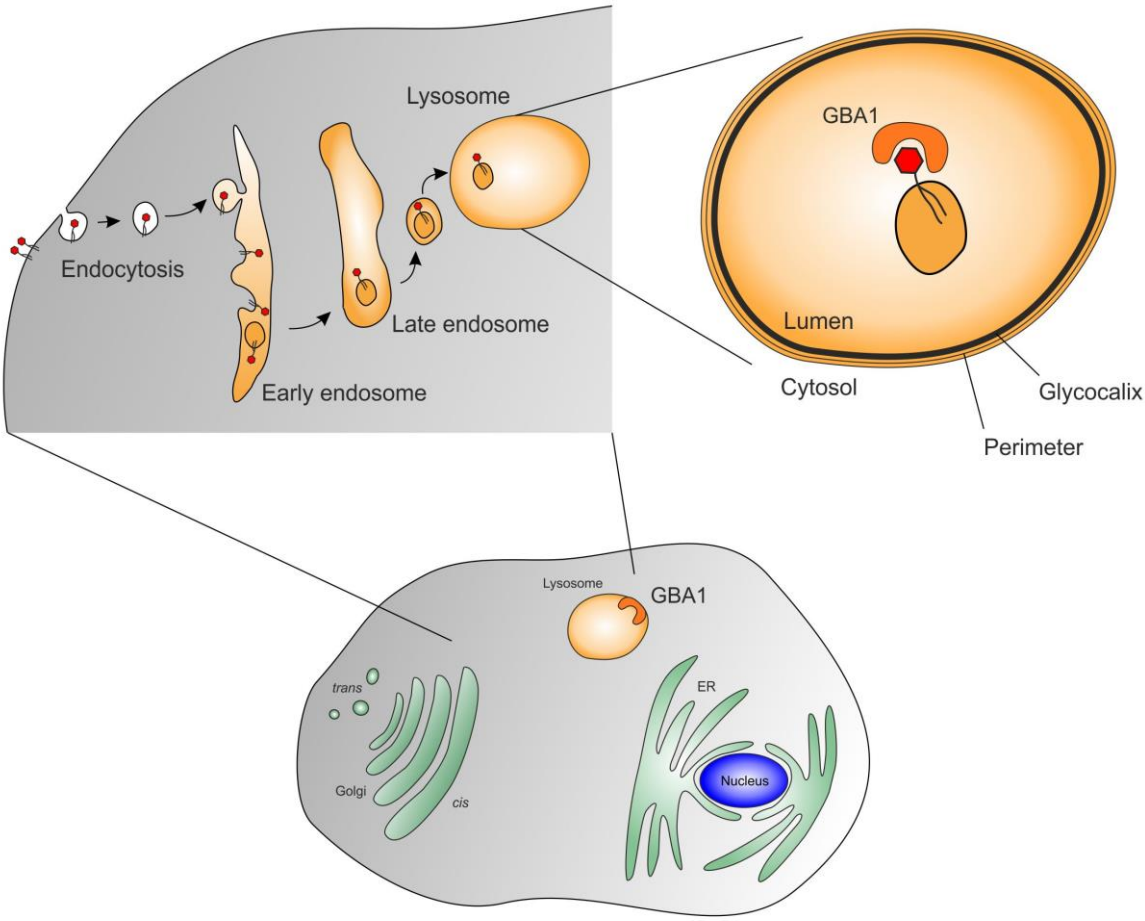

Figure 2: GSLs reach the lysosome via endocytosis. Parts of the plasma membrane bud off into the cytosol and then enter the endocytic vesicular pathway. Endocytic vesicles fuse with and enter early endosomes, which become late endosomes due to acidification. Endocytic vesicles reach the lysosome as intra-lysosomal vesicles, which provide a platform for hydrolases such as GBA1 (acid beta-glucosidase), which are involved in the step-wise break down of all kinds of GSLs.

1.1.4.1 Beta-glucosidases

Around 90% of mammalian GSLs are based on GlcCer (Lingwood, 2011). GlcCer is degraded by beta-glucosidases, which cleave the beta-glucosidic linkage of GlcCer to release D-glucose and ceramide (Brady et al., 1965). Degradation of GlcCer can take place in the lysosome by the acid beta-glucosidase GBA1, by the non-lysosomal beta-glucosidase GBA2, or by the cytosolic beta-glucosidase GBA3. In this study, GBA1 and GBA2 were examined in more detail.

1.1.4.1.1 GBA1

GBA1 is a peripheral membrane protein in the lysosome encoded by the *GBA1* gene (NM_000157, EC 3.2.1.45) (Figure 2, Figure 4). GBA1 is synthesised at the rough ER

and then enters the ER lumen for N-linked glycosylation at four asparagine residues (Berg-Fussman et al., 1993). After protein folding, GBA1 binds to the lysosomal integral protein LIMP-2, which subsequently targets GBA1 to the lysosome (Reczek et al., 2007). From here, the GBA1/LIMP-2 complex is shuttled to the Golgi, where GBA1 is further glycosylated. The molecular weight of GBA1 varies from 55 to 69 kDa, depending on the different states of glycosylation: GBA1 is synthesised as a 55 kDa polypeptide. By addition of high mannose-type oligosaccharide side chains in the Golgi, the molecular weight increases to 64 kDa and by addition of sialic acid residues, the protein finally reaches 69 kDa (Bergmann&Grabowski, 1989). Posttranslational modification and binding to LIMP-2 have both been proposed to be involved in targeting GBA1 to the lysosome (Van Weely et al., 1990) and keeping it stable within the lysosomal environment (Bergmann&Grabowski, 1989). Thus, the glycosylation state of GBA1 reflects its maturation, but not its potential activity (Van Weely et al., 1990). The activity of GBA1 depends on several factors with one of them being saposin C. The mechanism by which saposin C promotes GBA1 activity is not fully known yet, but a model proposes that the 9 kDa protein associates with both, GBA1 and the membrane, lifting GlcCer out of the membrane and making it accessible for GBA1 (Alattia et al., 2006). Absence of saposin C in humans impairs the function of GBA1 and leads to severe accumulation of the substrate, GlcCer, in the lysosome (Scriver, 1995). The enzyme itself possesses three domains, which are involved in substrate binding and hydrolysis: i) a catalytic site, which senses the beta-glucoside moiety (Grabowski et al., 1984), ii) an aglycon-binding site with specificity for acyl moieties, and iii) a domain that interacts with sphingosine derivatives (Grabowski et al., 1986). The most prominent inhibitor for GBA1 is conduritol B epoxide (CBE) (Grabowski et al., 1986). It binds covalently and, thus, irreversibly to the catalytic site of GBA1 and has been used solve the structure of GBA1 (Premkumar et al., 2005).

1.1.4.1.2 *Gaucher* disease – a lysosomal storage disorder

Mutations in the *GBA1* gene cause the most common lysosomal storage disorder in humans: *Gaucher* disease (Figure 3). The disease is named after Philippe Gaucher, who first described it in his doctoral thesis in 1882. The storage of non-defined molecules in tissues from *Gaucher* patients was recognised in 1907, whereas 17 years later, the accumulating material was characterised as cerebroside in accordance with the GSLs described earlier by Thudichum (Thudichum, 1901). The accumulating lipid

in *Gaucher* patients was first described as GlcCer in 1934 and, later on, located to the lysosome after discovery of the organelle by De Duve in 1955 (De Duve et al., 1955). Ten years later, Brady and co-workers described the enzyme deficiency and, thus, the molecular basis for the disease (Brady et al., 1965). Since then, around 200 different mutations in the *GBA1* gene have been described, which lead to loss of function of the enzyme and, thereby, to the accumulation of GlcCer in the lysosome (Grace et al., 1994; Scriver, 1995). *Gaucher* disease is an inherited autosomal recessive disorder with the most dramatic effect seen in tissue macrophages, which degrade red and white blood cells in the spleen (Figure 3a) (Pennelli et al., 1969). Macrophages lacking active GBA1 cannot break down the huge amount of membrane mass that they are facing and, thus, turn into "*Gaucher* cells", a pathologic hallmark of *Gaucher* disease. Presence of *Gaucher* cells in tissues like liver and spleen results in an up to 25-fold increase in organ size (organomegaly), a common symptom seen in *Gaucher* disease (Figure 3b) (Cox, 2001; Scriver, 1995).

Symptoms caused by malfunction of GBA1 can have a very early onset in life, but might also never manifest (Figure 3d). Due to its heterogeneous symptoms and phenotypes (Figure 3c), *Gaucher* disease has been classified into three major subtypes, namely type I, II, and III (Figure 3b, d). Type I *Gaucher* is the most common form of the disease, with patients being either not affected or showing symptoms like organomegaly of liver and spleen or defects in lung and bone marrow (Zimran et al., 1991). Type II patients represent the acute infantile neuronopathic form characterised by severe neurological defects and an early onset of the disease (Scriver, 1995). Patients suffering from type II *Gaucher* usually die within the first 2-3 years of life (Figure 3b, d) (Brady et al., 1993). Type III, the sub-acute form of the disease, involves symptoms of both, type I and II *Gaucher* disease, and, thus, represent an intermediate type (Erikson et al., 1997). It has been assumed that residual GBA1 activity might help to predict the severity of *Gaucher* disease (Scriver, 1995), but the progress of the disease even differs between patients carrying the same mutation (Meivar-Levy et al., 1994). Thus, no genotype-phenotype correlation has been established so far.

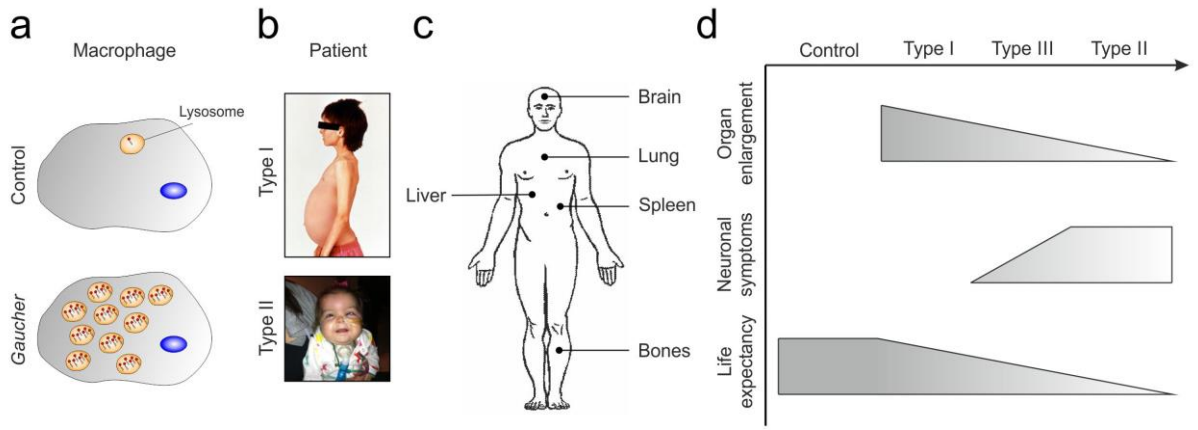

Figure 3: Gaucher disease. (a) GBA1 activity is lost in cells from *Gaucher* patients due to mutations in the human *GBA1* gene. In turn, the substrate of GBA1, GlcCer, accumulates in the lysosome. This effect is most dramatic in tissue macrophages, which break down e.g. red and white blood cells in the spleen. **(b)** Symptoms of *Gaucher* disease. Patients suffer from organomegaly of e.g. liver and spleen but, for yet unknown reasons, can also lead to severe neurological disorders. Top picture: 14-year old girl suffering from type I *Gaucher* disease and enlargement of liver and spleen, examined by Dr. R. Brady, National Institute of Neurological Disorders and Stroke. Bottom picture: Stella Grace, a girl diagnosed with type II *Gaucher* disease at 5 months of age suffering from severe neurological defects. **(c)** In general, symptoms have been described in brain, lung, liver, spleen, and in bone marrow. **(d)** *Gaucher* disease has been classified into three major subtypes: Type I, II, and III. Type I patients mainly show organ enlargement (also see **(b)**), whereas only type II and III patients suffer from neurological symptoms (also see **(b)**). Life expectancy, however, decreases with the severity and onset of the neurological defects.

It is not understood, how accumulation of GlcCer in the lysosomes causes cellular dysfunction. In particular, the fate of accumulating GlcCer has been a matter of debate during the past decades. It has been suggested that GlcCer might leave the lysosome and, thus, interfere with signalling pathways outside the lysosomes. Several papers have been published showing changes in phospholipid metabolism in neuronal *Gaucher* models (Bodennec et al., 2002) as well as in a CBE-induced macrophage model (Trajkovic-Bodennec et al., 2004). Furthermore, calcium homeostasis was altered in a neuronal *Gaucher* model (Korkotian et al., 1999) and in brain from type II *Gaucher* patients (Pelled et al., 2005). Both mechanisms, however, are associated with the ER, suggesting that GlcCer might recur at the ER. Furthermore, it remains unclear whether macrophage dysfunction underlies the different symptoms. Most likely, additional but yet unknown factors are involved in determining the fate of *Gaucher* patients (Vardi et al., 2016).

1.1.4.1.3 Enzyme replacement therapy (ERT)

Since *Gaucher* disease is a genetically inherited disorder, it cannot be cured (yet). Still, two different treatment strategies were developed during the past decades to reduce accumulation of GlcCer and diminish the symptoms. The enzyme replacement therapy (ERT), involves an active, recombinant form of GBA1 (imiglucerase) (Grabowski&Hopkin, 2003). Brady and Pentchev initially isolated GBA1 from human placenta and managed to isolate 9 mg active GBA1 within one year (Pentchev et al., 1973). Strikingly, intravenous administration of human placental GBA1 reduced the GlcCer accumulation in two *Gaucher* patients by 26% after 24 h (Brady et al., 1974). Today, mutated GBA1 in *Gaucher* patients is substituted by injection of recombinant GBA1 (imiglucerase) (Weinreb et al., 2002). Cerezyme (Genzyme Corporation, Cambridge, MA, USA) is produced and extracted from CHO cells heterologously expressing human GBA1 (Genzyme, Summary of Product Characteristics). Normally, bacteria are used for large-scale expression of proteins, but they are known to be incapable or at least less efficient in synthesising glycosylated proteins (Wacker et al., 2002). In 1970, work was published claiming that most (if not all) lysosomal proteins are glycoproteins (Goldstone&Koenig, 1973) and today it is known that acidic hydrolases like GBA1 reach the lysosome via a mannose 6-phosphate receptor-mediated pathway (Coutinho et al., 2012). In 1978, Stahl et al. found out that macrophages also bear a lectin moiety on their surface, which binds to terminal mannose residues with high affinity (Stahl et al., 1978). Thus, the mannose-type oligosaccharide side chains of GBA1 are used to target recombinant GBA1 to macrophages, from where the enzyme is then shuttled to the lysosome (Bergmann&Grabowski, 1989). Nevertheless, ERT requires the lifelong administration of Cerezyme, which costs around 200,000 $ per patient per year (Coutinho et al., 2016). Furthermore, recombinant enzymes do not cross the blood-brain barrier, rendering the treatment of type II *Gaucher* disease impossible. Thus, Cerezyme and ERT are used to treat type I and III *Gaucher* patients, reversing some of the symptoms, e.g. organomegaly of liver and spleen (Genzyme Corporation, Cambridge, MA, USA). Cerezyme was approved for use in the United States in 1994 and, later on, also approved in Europe in 1997 (Starzyk et al., 2007).

1.1.4.1.4 Substrate reduction therapy (SRT)

Twenty years ago, Radin proposed the substrate reduction therapy (SRT) using a drug that specifically inhibits GlcCerS to prevent the accumulation of GlcCer in *Gaucher* cells (Radin, 1996). At the same time, it was shown that the imino sugar N-butyl-deoxynojirimycin (NB-DNJ) is a potent inhibitor for GlcCerS in the low micro molar range (Platt et al., 1994). Inhibitors based on imino sugars structurally mimic the sugar head group of natural substrates, with the ring oxygen atom replaced by a nitrogen atom. This structure makes imino sugars potent inhibitors for hydrolases that recognise monosaccharide head groups and glucosyltransferases like GlcCerS that transfer single sugars to lipid backbones (Dwek et al., 2002). NB-DNJ was first studied in a mouse model in 1994 (Yamanaka et al., 1994) and then tested in a clinical study in 1998 in type I *Gaucher* patients (Aerts et al., 2006; Cox, 2001). Application of 100 mg NB-DNJ three times per day over a time period of one year significantly decreased the GlcCer accumulation in 28 adult type I *Gaucher* patients and improved liver and spleen size (Aerts et al., 2006). NB-DNJ was also tested in type II and III *Gaucher* patients, but did not improve neurological symptoms in these patients (Schiffmann et al., 2008). Today, NB-DNJ is sold by Actelion Pharmaceuticals (Basel, Switzerland) under the trade name Zavesca.

1.1.4.1.5 GBA1-deficient mouse models

Several GBA1-deficient mouse models are currently available, which are all used to study the underlying mechanisms in *Gaucher* disease. Chemical inhibition of GBA1 in mice has been shown to completely block GBA1 activity, resulting in accumulation of GlcCer in spleen, liver, and brain (Kanfer et al., 1975), accompanied by severe neurological defects (Stephens et al., 1978; Xu et al., 2008). The first genetic mouse model of *Gaucher* disease was generated by Tybulewicz et al., who created a null mutation, which resulted in a residual GBA1 activity of less than 4% (Tybulewicz et al., 1992). Sidransky et al. showed that these mice mimicked the symptoms seen in type II *Gaucher* patients, while also showing extremely decreased longevity due to trans-epidermal water loss caused by a skin barrier defect (Sidransky et al., 1992). To circumvent this problem, conditional GBA1-deficient mice have been generated. Enquist et al. expressed floxed GBA1 in an Mx1-Cre-loxP system, which allowed the Cre-mediated deletion of GBA1 upon treatment with polyinosinic-polycytidylic acid, which activates the Mx1 promotor (Enquist et al., 2006). The latter is administered after

birth so that the mice first develop normally before GBA1 is deleted. Overall, GBA1-deficient mice resemble the phenotypes seen in *Gaucher* disease patients, which makes them an ideal model to investigate this disorder.

1.1.4.1.6 GBA2

Besides GBA1, non-lysosomal beta-glucosidase GBA2 also cleaves GlcCer to D-glucose and ceramide (NM_020944.2, EC 3.2.1.45). GBA2 was first purified from human liver (Matern et al., 1997) and then cloned in 2001 (Matern et al., 2001). The enzyme is ubiquitously expressed, albeit at different levels (Matern et al., 2001; van Weely et al., 1993; Yildiz et al., 2006). GBA2 was first described as a beta-glucosidase with properties that differed from lysosomal GBA1 (Matern et al., 1992), that is insensitive to CBE, and is present in tissues such as brain and spleen (van Weely et al., 1993). GBA2 was characterised as a membrane-bound enzyme that is not located in the lysosomes, making it a candidate for extra-lysosomal GlcCer degradation. For a long time, GBA2 was thought to be a single pass transmembrane protein localised at the ER (Matern et al., 1992; Matern et al., 1997) or at the plasma membrane (Boot et al., 2007). We could recently show that GBA2 is not a transmembrane protein, but rather a protein tightly associated with membranes (Figure 4) (Körschen et al., 2013). Here, we could recover GBA2 in both, the soluble and membrane fraction of hypotonic protein lysates after ultracentrifugation, whereas hypotonic washes almost fully solubilised GBA2 that was attached to the membrane, proving that GBA2 is not a transmembrane protein. Furthermore, Boot et al. found that endogenous GBA2 was capable of cleaving the artificial substrate 4-methyl-umbelliferyl beta-D-glucopyranoside (4-MUG) supplied in the cell culture medium, which is why they concluded that the catalytic side of GBA2 must be in contact with the extracellular space (Boot et al., 2007). In contrast to that study, we could show that both ends of the enzyme were directly accessible from the cytosol, arguing against the finding that the catalytic side of GBA2 faces the extracellular space. Immunocytochemical stainings of heterologously expressed GBA2 and co-staining with organelle markers revealed that GBA2 localises to membranes at the cytosolic side of the *cis* Golgi and the ER (Körschen et al., 2013). Thus, GBA2 is localised in close proximity to GlcCerS and the synthesis pathway of its substrate, GlcCer (Schweizer et al., 1994).

In accordance with previous studies, our data showed that GBA2 is active at a less acidic pH compared to GBA1 and that it loses its activity in presence of detergents

(Körschen et al., 2013; Matern et al., 1997; van Weely et al., 1993). Furthermore, Matern et al. showed that GBA2 requires phospholipids to be active (Matern et al., 1997). In a later study, Boot et al. confirmed that the lipid environment is crucial for GBA2 activity since the enzyme loses its activity upon membrane solubilisation (Boot et al., 2007). Our studies revealed a similar scenario where GBA2 lost its activity in absence of membranes, but re-gained its activity in the presence of pure phosphatidylcholine liposomes (Körschen et al., 2013).

Besides their substrate specificity for GlcCer and artificial 4-MUG, GBA1 and GBA2 do not share any structural or sequence homology and clearly do not originate from the same ancestral gene. This is also reflected in several studies analysing the structurally different inhibitors for both enzymes. GBA1 shows maximal activity in presence of detergents, whereas GBA2 loses its activity, when its membrane surrounding is lost (Grabowski et al., 1986; van Weely et al., 1993). Nevertheless, GBA1 still exerts some remaining activity even under detergent-free conditions (Overkleeft et al., 1998; van Weely et al., 1993). Thus, the GBA2 activity has been determined in presence of CBE, the specific blocker for GBA1, in the past, to analyse the GBA2 activity independent from GBA1 (Grabowski et al., 1986). Since then, GBA2 has been described as the beta-glucosidase activity insensitive to up to 2.5 mM CBE under detergent-free conditions (Boot et al., 2007; Overkleeft et al., 1998). For a long time, CBE was thought to have no effect on the activity of GBA2, whereas Ridley et al. recently showed that CBE inhibits GBA2 in a concentration-dependent manner (Ridley et al., 2013). They determined the inhibition constant (K_i) of CBE towards both, GBA1 and GBA2, where the value for GBA2 was significantly higher, but still in the lower micro molar range (Ridley et al., 2013). Vice versa, GBA2, but not GBA1, is sensitive to the imino sugar NB-DNJ, the inhibitor for GlcCerS (Dwek et al., 2002; Ridley et al., 2013). We analysed the dose-response relationship of NB-DNJ and GBA2 in hypotonic tissue lysates from mouse liver, brain, and testis, demonstrating IC_{50} values in the low nanomolar range (20.9 ± 1.3 nM, 18.2 ± 0.3 nM, and 19.2 ± 0.4 nM, respectively) (Körschen et al., 2013). A daily dose of three times 100 mg of NB-DNJ/Zavesca during SRT to block GlcCerS, which results in low micromolar concentrations in blood plasma, prevents the accumulation of GlcCer (Aerts et al., 2006). The IC_{50} of NB-DNJ for GlcCerS is around 50 µM, which should partially inhibit GlcCerS to reduce the amount of GlcCer produced, but should still render it active enough to synthesise some GlcCer to maintain necessary GSL levels (Wennekes et al., 2010). On the other hand, recalling

the IC_{50} values of NB-DNJ for GBA2, treatment with NB-DNJ should completely inhibit GBA2 in *Gaucher* patients.

1.1.4.1.7 GBA2-associated diseases

For GBA2, no disease has been associated to the loss of GBA2 in humans so far. During the past few years, mutations in the *GBA2* gene have been reported in patients with hereditary spastic paraplegia or autosomal-recessive cerebellar ataxia with spasticity (Citterio et al., 2014; Hammer et al., 2013; Martin et al., 2013; Votsi et al., 2014). Here, homozygous mutations in GBA2 were found in affected patients, whereas additional but heterozygous mutations were also present in unaffected family members (Votsi et al., 2014). The group around van der Spoel recently analysed the GBA2 activity of the mutants found in those patients and showed that they were all inactive, suggesting that loss of GBA2 activity might indeed contribute to the symptoms of the reported diseases (Sultana et al., 2015). These findings are in line with data published by Martin et al., who knocked down GBA2 in zebrafish, resulting in defects of motor behaviour and axonal outgrowth of motor neurons, conditions that could be reversed with human wild-type mRNA, but not with RNA containing the mutated GBA2 sequence (Martin et al., 2013). Indeed, it had already been shown that the GBA2 activity increases during neuronal differentiation, suggesting an important role for GBA2 during neuron development (Aureli et al., 2012). Thus, even though GlcCer accumulates in both, GBA1- and GBA2-deficient models, the phenotypic outcome is completely different.

During the past few years, work from different groups has suggested that GBA2 contributes to the pathology of *Gaucher* disease. It has been proposed that GBA2 protein and mRNA expression in fibroblasts obtained from GBA1-deficient mice is increased (Yildiz et al., 2013). Furthermore, Burke et al. showed that the GBA2 activity is higher in GBA1-deficient mice and leucocytes from *Gaucher* patients compared to controls, supporting the data generated by Yildiz et al. (Burke et al., 2013). In contrast to these findings, we have demonstrated that the GBA2 activity is significantly reduced in embryonal fibroblasts from GBA1-deficient mice and dermal fibroblasts obtained from a type II *Gaucher* patient (Körschen et al., 2013). One year later, Mistry et al. proposed that in cells from *Gaucher* patients, both GlcCer and GlcSph spill-over from the lysosomes into the cytoplasm, thereby becoming a substrate for GBA2 (Mistry et al., 2014). In turn, GBA2 not only hydrolyses GlcCer to glucose and ceramide, but also

GlcSph to glucose and sphingosine (Mistry et al., 2014). Ceramide can be further broken down to sphingosine and a fatty acid through the action of the neutral ceramidase (Mistry et al., 2014). The net result is an accumulation of sphingosine in the cell. It has been proposed that sphingosine is the cytotoxic metabolite that causes some of the defects associated with *Gaucher* pathophysiology (Mistry et al., 2014). In fact, deletion of GBA2 rescued some of the defects associated with *Gaucher* pathophysiology by reducing the accumulation of sphingosine (Mistry et al., 2014).

1.1.4.1.8 GBA2-deficient mouse model

In 2006, the first GBA2-deficient mouse model was published, which showed significant accumulation of GlcCer in tissues with high GBA2 expression like brain, liver, and testis (Yildiz et al., 2006). Non-lysosomal accumulation of GlcCer mainly resulted in impaired male fertility (Yildiz et al., 2006) and delayed liver regeneration after partial hepatectomy (Gonzalez-Carmona et al., 2012). Previous to the generation of GBA2-deficient mice by Yildiz et al., pathology arising from the loss of active GBA2 has only been reported by studies applying pharmacology. In the past, van der Spoel et al. have shown that a final blood serum concentration of 57 µM NB-DNJ (Platt et al., 1997) caused impairment of spermatogenesis in male mice after administration for at least three weeks, an effect that was reversible when the treatment was stopped (van der Spoel et al., 2002). Thus, pharmacologic block of GBA2 resulted in the same phenotype as in GBA2-deficient male mice (Yildiz et al., 2006).

Interestingly, two men affected with Hereditary Spastic Paraplegia carrying mutations in the *GBA2* gene showed a bilateral testicular hypotrophy with their sperm displaying severe head abnormalities (Martin et al., 2013). However, other reports identified a patient carrying a homozygous nonsense mutations in the *GBA2* gene, who was the father of three children (Hammer et al., 2013). Furthermore, spermatogenesis remained unchanged in monkeys treated with NB-DNJ (van Weely et al., 1993) and healthy control patients, who orally took NB-DNJ/Zavesca for 6 weeks (Amory et al., 2007). Of note, 6 weeks equal 42 days of Zavesca uptake, whereas one full cycle of spermatogenesis in humans takes around 64 days to be completed (Clermont, 1972). Thus, the duration of the treatment might not have been long enough to allow a valid conclusion. However, we could recently show that accumulation of GlcCer alters cytoskeletal dynamics by augmenting actin polymerisation and promoting microtubule persistence in dermal fibroblasts and *Sertoli* cells from GBA2-deficient mice, which

leads to severe morphological defects during sperm development resulting in male infertility (Raju et al., 2015).

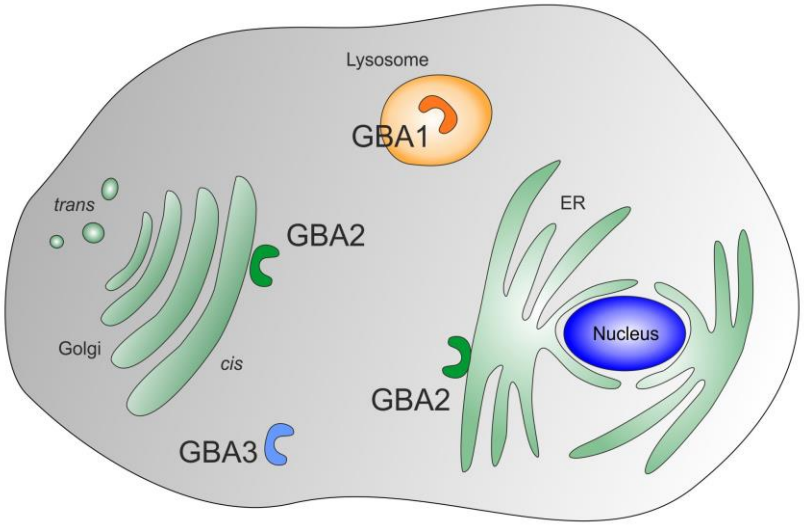

Figure 4: Beta-glucosidases. GBA1 is a soluble enzyme located inside the lysosome, whereas GBA2 is associated with membranes at the cytosolic side of the cis Golgi and the ER. GBA3 is located in the cytosol. GBA1: Acid beta-glucosidase, GBA2: Non-lysosomal beta-glucosidase, GBA3: Cytosolic beta-glucosidase.

1.2 Aim of the thesis

Although the non-lysosomal beta-glucosidase GBA2 has been well characterised during the past three decades, little is known about its interplay with GBA1 in controlling GlcCer homeostasis. We have shown that GBA2 activity is reduced in the absence of GBA1 (Körschen et al., 2013), whereas others have proposed the opposite effect (Burke et al., 2013; Mistry et al., 2014; Yildiz et al., 2013). Furthermore, the subcellular mechanisms causing the manifold phenotypes of *Gaucher* disease are not well understood. Thus, the aim of my PhD thesis is to investigate the molecular mechanisms underlying the regulation of GBA2 using *Gaucher* disease as a physiologically relevant model system.

2 Material and Methods

2.1 Material

Chemicals were purchased in p.A. quality from the following companies: AppliChem (Darmstadt), BioRad (Munich), Eppendorf (Hamburg), GE Healthcare Life Sciences (Munich), Invitrogen (Karlsruhe), Merck (Darmstadt), Nioline (London, UK), Pierce (Illinois, USA), Polysciences (Pennsylvania, USA), Qiagen (Hilden), Roth (Karlsruhe), Sigma (Steinheim), and Thermo Scientific (Waltham,USA). Enzymes and corresponding buffers were purchased from New England Biolabs (Frankfurt), Novagen (Darmstadt), and Roche (Mannheim). Oligonucleotides were purchased from Eurofins MWG Operon (Ebersberg). For the cultivation of bacterial cultures, media purchased from Roth (Karlsruhe) were used. Chemicals for use in mammalian cell culture were purchased from Invitrogen (Karlsruhe). Mammalian cell lines were purchased from the Coriell Institute (New Jersey, USA), the TeleThon Institutes (Italy), Horizon (Cambridge, UK), and ATCC (Virginia, USA). Cryo tubes were purchased from Greiner Bio-One (Kremsmünster, Österreich). Primary and secondary antibodies were purchased from Roche (Mannheim), Sigma (Steinheim), Novagen (Darmstadt), Millipore (Schwalbach), Abcam (Cambridge, UK), SantaCruz Biotechnology (Heidelberg), BD Transduction Laboratories (New Jersey, USA), LI-COR Biosciences (Nebraka, USA). Fluorescent alkynes were purchased from Dyomics (Jena). PVDF-membrane Immobilon P was purchased from Millipore (Schwalbach). Lipids were purchased from Avanti Polar Lipids (Alabama, USA), Sigma (Steinheim), and Matreya LLC (Pennsylvania, USA). Glass wool was purchased from Macherey Nagel (Düren).

All solutions were prepared using double-distilled water. If necessary, solutions were sterilised by autoclavation (20 min, 121 °C).

2.2 *Escherichia coli* culture

2.2.1 Bacterial strains and vectors

The *Escherichia coli* (*E.coli*) strain XL1-Blue (Bullock 1987, Stratagene, La Jolla, USA) was used to amplify plasmid DNA. The *E.coli* strain BL21 Codon Plus (DE3) RIPL (Jerpseth 1998, Agilent Technologies, Santa Clara, USA) was used for expression of pET21-mGBA2-His or pET21-hGLTP-His.

2.2.2 *E.coli* culture medium

For the preparation of LB-agar dishes, 15 g/l agar (Sigma) was added to LB-medium (Table 1). Both, medium and the medium-agar suspension, were autoclaved for 20 min at 121 °C and stored at RT. The medium-agar suspension was cooled down to around 50 °C and, if needed, antibiotics were added to the medium to a final concentration of 100 µg/ml (ampicillin) or 30 µg/ml (kanamycin), before pouring it into sterile agar dishes. Medium was stored at RT, agar plates at 4 °C.

Table 1: *E.coli* culture medium

LB (lysogeny broth) medium (Roth)
10 g/l Tryptone
5 g/l Yeast extract
5 g/l NaCl
pH 7.0 ± 0.2

2.2.3 Generation of competent *E.coli* cells

Competent *E.coli* cells were generated according to a modified protocol based on the $CaCl_2$ method (Mandel&Higa, 1970). The cells were cultured in 50 ml LB medium at 37 °C on a shaker until an optical density (OD) of 0.4 was reached, representing a cell number of approximately $2x10^8$ cells/ml. The OD was measured at 600 nm (OD_{600}). The culture was chilled on ice for 30 min and subsequently centrifuged for 10 min at 5,000 x g and 4 °C. The pellet was re-suspended in 1 ml cold 0.1 M $CaCl_2$ solution and brought to a final volume of 25 ml. After incubation on ice for 20 min, the cells were centrifuged again for 10 min at 5,000 x g and 4 °C, re-suspended in 1 ml cold 0.1 M $CaCl_2$ solution containing 25% glycerin, and brought to a final volume of 5 ml. Subsequently, the cells were incubated on ice for 2 h

before aliquots were prepared and stored at -80 °C for further use.

2.2.4 Retransformation

100 µl of competent *E.coli* cells (BL21 Codon Plus (DE3) RIPL, Stratagene) was thawed on ice and 50 ng DNA was added together with 5 µl 10x CM (Table 2) in a total

volume of 50 µl followed by incubation on ice for 20 min. Bacteria were incubated for 1 min at 42 °C, cooled down on ice for 10 min, and 200 µl LB medium was added. Bacteria were grown for 30 min at 37 °C in a shaking incubator. Afterwards, 100 µl of the suspension was streaked out on a LB plate and incubated over night at 37 °C.

Table 2: CM solution for bacteria retransformation

10x CM
100 mM $CaCl_2$
400 mM $MgCl_2$

2.2.5 Protein expression in *E.coli*

Overnight grown and transformed bacteria (2.2.4) were inoculated into 5 ml LB medium and incubated on a rotating shaker (New Brunswick Scientific, Edison, USA) at 37 °C for at least 8 h or overnight. For larger cultures, this pre-culture was used to inoculate 500 ml LB medium 1:500 without antibiotics. The culture was grown for around 3 h until an OD_{600} of ~0.545 was reached. Expression of the protein of interest was induced by induction with 1 mM isopropyl beta-D-1-thiogalactopyranoside (IPTG) and the culture was grown at 37 °C for 3 h or more. The OD_{600} was determined again and the culture was stored at 4 °C for further use.

2.2.6 Preparation of mGBA2-His expressed in bacteria for activity assays and Western blot analysis

30 ml of mGBA2-His *E.coli* cultures (2.2.5) were centrifuged for 10 min at 11,000 x g and 4 °C and the pellet was re-suspended in 4.8 ml hypotonic buffer (represents a 1:8 dilution of the initial volume, also see Figure 49). The cell suspension was sonicated by three pulses (20 s each) in ice-cold water (Branson Sonifier, also see 2.5.2) and 20 µl of the protein lysate were used per reaction if not otherwise stated.

2.3 Mammalian cell culture

2.3.1 Solutions and cell culture media

Cell culture media based on MEM, F12, and IMDM were incubated at 37 °C and 5% CO_2, media based on DMEM were kept at 37 °C and 7.5% CO_2 (Table 4). The pH of

PBS was set to 7.4, the buffer was autoclaved (20 min, 121 °C), and filled in sterile glass bottles under the hood.

Table 3: Phosphate-buffered saline (PBS) for the cell culture

PBS
137 mM NaCl
2.7 mM KCl
6.5 mM Na_2HPO_4
1.5 mM KH_2PO_4
pH 7.4

Table 4: Cell culture media

Coriell/TeleThon DH15 medium	Coriell/TeleThon M15 medium	HAP1 medium
DMEM	MEM/GlutaMAX	IMDM
15% FCS	15% FCS	10% FCS
100 mM Sodium pyruvate	100 mM Sodium pyruvate	70 IU/ml Penicillin
200 mM L-glutamine	200 mM L-glutamine	70 µg/ml Streptomycin
	1x Non-essential amino acids	
HEK #A3 M10 medium	HEK GBA1-KO DH10 medium	HeLa SL1P-KO/ mEFB DH10 medium
MEM	DMEM/GlutaMAX	DMEM
10% FCS	10% FCS	10% FCS
1x Non-essential amino acids	100 mM Sodium pyruvate	100 mM Sodium pyruvate
1 mg/ml G418	70 IU/ml Penicillin	200 mM L-glutamine
	70 µg/ml Streptomycin	70 IU/ml Penicillin
		70 µg/ml Streptomycin
Fibroblast growth medium	CHO mGBA1-HA/ mGBA2-HA stable cell line medium	Melanoma DH10 medium
DMEM/GlutaMAX	F12	DMEM
10% FCS	10% FCS	10% FCS
100 mM Sodium pyruvate	Opt.: 0.8 mg/ml G418	
200 mM L-glutamine	Opt.: 0.01 mg/ml Blasticidin	
70 IU/ml Penicillin		
70 µg/ml Streptomycin		

2.3.2 Transient transfection using polyethylenimine (PEI)

Cells were seeded out the day before transfection and grown to 90-95% confluency overnight (Table 14). DNA, OptiMEM, and polyethylenimine (PEI, Sigma) were mixed in a sterile tube according to Table 5 and incubated at RT for 10 min. Cell culture medium was removed from the dishes and replaced with starvation medium (normal cell culture medium containing only 2% FCS) according to Table 5. The PEI/DNA mix was then added to the cells and incubated overnight at 37 °C and normal CO_2 concentration for 1-3 days.

Table 5: Pipetting scheme for transient transfection

Dish	DNA (µg)	PEI (µg)	OptiMEM (µl)	Starvation medium (µl)
4-well	0.5	1	50	200
6-well	2.35	5	235	940
5 cm plate	4.5	10	470	1880
9 cm plate	8	18	846	3384

Table 6: Seeding cell numbers for PEI transfection per 9 cm dish

Cell line	Seeding cell # per 9 cm dish
HEK293	$2x10^6$
HeLa	$2x10^6$
HAP1	$2.5x10^6$

2.3.3 Plasmids used for transfection of mammalian cells

Table 7: Plasmids used for transfection

Plasmid	Expresses	Label	Concentration (µg/µl)	Date
pc6-QBImGBA1-HA-1	mGBA1-HA	Dr. W. Bönigk, Molecular Sensory Systems, caesar, Bonn, Germany	3.15	23/10/2012
pc3-mGBA2-HA-1	mGBA2-HA	Dr. W. Bönigk, Molecular Sensory Systems, caesar, Bonn, Germany	0.88	22/01/2015
pc3QBIGFP-HAmGBA2	mGBA2-HA	Dr. W. Bönigk, Molecular Sensory Systems, caesar, Bonn, Germany	5.58	07/07/2011
JAM3	JAM3	Dr. P. Haberkant, Proteomic Core Facility, EMBL Heidelberg, Heidelberg, Germany	1.045	15/04/2016

2.3.4 Generation of stable cell lines

Stable cell lines produced by H. G. Körschen were generated using the vectors pc3.1-mGBA2-HA or pc3.1-mGBA1-HA and the Neon100 µl electroporation kit by Invitrogen. The detailed protocol is published in (Körschen et al., 2013).

Stable HEK293 cell clone #A3 was generated by PEI transfection (2.3.2) using the vector pc3-mGBA2-HA-1 (W. Bönigk, 0.88 µg/µl from 22/01/2015). As a control, a second plate was transfected without DNA. On the next day, cells were split 1:10, 1:100, 1:1,000, and 1:10,000 to separate the cells and grow monoclonal colonies arising from one cell. On day three, G418 was added to a final concentration of 1.2 mg/ml in 9 ml culture medium per 9 cm dish to both, the transfected and the control plate. On day five, the G418 concentration was lowered to 1 mg/ml and colonies were selected under a light microscope. The single colonies were picked using the isolated rim of a 10 µl pipette tip, which was placed in sterile silicon and placed on the colony after the cells were washed with PBS. 50 µl trypsin (0.05% in DMEM) was added per ring and the cells were re-suspended in the solution after brief incubation on a 37 °C

heating plate. Each colony was transferred to 200 µl normal culture medium containing 1 mg/ml G418 in one well of a 96-well dish. The clones were scaled up to 5 cm dishes and stable expression of mGBA2 in the different clones was analysed by lysing the cells from one 5 cm dish in 60 µl hypotonic buffer and measuring the GBA2 activity compared to control samples using the fluorescence-based GBA activity assay (see 2.5.8). Back-ups were made from 9 cm dishes with at least $4x10^6$ cells per back-up.

2.3.5 Cell lines

2.3.5.1 Human dermal fibroblasts

Human dermal fibroblasts were obtained from the Coriell Institute and from the TeleThon Institutes (Filocamo et al., 2014).

Table 8: Human dermal fibroblast (hFB) cell lines

Cell line	Genotype	Producer	Catalogue #	Disease	Mutation	Patient	
						Sex	Age
hFB 1	Ctrl	Coriell	GM00024 C	-	-	M	30 y
hFB 2	Mutant GBA1	Coriell	GM00372 A	GD type I	84G ins, N370S	M	29 y
hFB 3	Mutant GBA1	Coriell	GM00852 A	GD type I	84G ins, N370S	M	20 y
hFB 4	Mutant GBA1	Coriell	GM00877 A	GD type II	L444P, L444P, A456P, V460V	M	1 y
hFB 5	Mutant GBA1	Coriell	GM00878	-	L444P, A456P, V460V	F	N/A
hFB 6	Mutant GBA1	Coriell	GM01607B	GD type I	N370S, V394L	M	30 y
hFB 7	Mutant GBA1	Coriell	GM04394	GD type I	L444P	M	1 y
hFB 8	Ctrl	Coriell	GM05399 A	-	-	M	1

hFB 9	Ctrl	Coriell	GM05757 C	-	-	M	7 y
hFB 10	Mutant GBA1	Coriell	GM08760	GD type II	L444P	M	1 y
hFB 11	Mutant GBA1	Coriell	GM10915 A	GD type I	L444P	M	7 y
hFB 12	Mutant GBA1	Coriell	GM20272 B	GD type III	L444P	M	N/A
hFB 14	Mutant GBA1	Coriell	GM01260	GD type II	L444P, P415R	F	11 m
hFB 15	Mutant GBA1	TeleThon	FFF0091977	GD type III	L444P, L444P	N/A	N/A
hFB 16	Mutant GBA1	TeleThon	FFF0491979	GD type III	L444P, L444P	N/A	N/A
hFB 17	Mutant GBA1	TeleThon	FFF1081981	GD type III	L444P, L444P	N/A	N/A
hFB 18	Mutant GBA1	TeleThon	FFF1161982	GD type II	L444P, R257Q	N/A	N/A
hFB 19	Mutant GBA1	TeleThon	FFF0181985	GD type II	L444P, R120W	N/A	N/A
hFB 20	Mutant GBA1	TeleThon	FFF0591990	GD type III	L444P, F213I	N/A	N/A
hFB 21	Mutant ASM	TeleThon	FFF040200	NP-A	N/A	N/A	N/A
hFB 22	Mutant ASM	TeleThon	FFF0771980	NP-A	N/A	N/A	N/A
hFB 23	Mutant ASM	TeleThon	FFF1142009	NP-A	N/A	N/A	N/A
hFB 24	Mutant ASM	TeleThon	FFF0202012	NP-B	N/A	N/A	N/A
hFB 25	Mutant ASM	TeleThon	FFF0681983	NP-B	N/A	N/A	N/A
hFB 26	Mutant ASM	TeleThon	FFF0752008	NP-B	N/A	N/A	N/A
hFB 27	Mutant NP-C	TeleThon	FFF0262000	NP-C	N/A	N/A	N/A

hFB 28	Mutant NP-C	TeleThon	FFF0522000	NP-C	N/A	N/A	N/A
hFB 29	Mutant NP-C	TeleThon	FFF0782006	NP-C	N/A	N/A	N/A

hFB: Human dermal fibroblast, GBA1: Acid beta-glucosidase, ASM: Acid sphingomyelinase, NP-C: *Niemann-Pick* type C, GD: *Gaucher* disease

2.3.5.2 Cells genetically modified using CRISPR/Cas9

2.3.5.2.1 Human fibroblast-like cells

Table 9: HAP1 cell lines

Cell line	Producer	Catalogue #	*GBA1* gene
HAP WT	Horizon	-	-
HAP1 GBA1-KO	Horizon	HZGHC002786c001	479 bp insertion in exon 6
HAP1 GBA1-KO	Horizon	HZGHC002786c010	1 bp insertion in exon 6
HAP1 GBA2-KO	Horizon	HZGHC004109c001	5 bp deletion in exon 1
HAP1 GBA2-KO	Horizon	HZGHC004109c011	1 bp insertion in exon 1

WT: Wild-type, GBA1: Acid beta-glucosidase, KO: Knockout

2.3.5.2.2 Human embryonic kidney cells (HEK293)

Table 10: HEK cell line

Cell line	Producer
HEK GBA1-KO	Gift from C. Yaacobi, Futerman lab, Weizmann Institute, Israel

HEK: Human embryonic kidney cells, GBA1: Acid beta-glucosidase, KO: Knockout

2.3.5.2.3 Cervical cancer cells (HeLa)

Table 11: HeLa cell line

Cell line	Producer	Genotype
Delta SGPL1 HeLa	Gift from M. Gerl, Biochemistry Center, Heidelberg University, Heidelberg, Germany (Gerl et al., 2016)	SGPL1-knockout

HeLa: Immortalised cervical cancer cells originating from Henrietta Lacks, SGPL1: Sphingosine-1-phosphate lyase, KO: Knockout

2.3.5.3 Murine embryonal fibroblasts

Table 12: Embryonal mouse fibroblast cell lines

Cell line	Genotype	Producer	Date
mEFB GBA1+/+ neu	Ctrl	Dr. Y. Yildiz, University Hospital Bonn, Bonn, Germany	N/A (BU: 06.06.2012)
mEFB GBA1 -/- alt	GBA1-KO	Dr. Y. Yildiz, University Hospital Bonn, Bonn, Germany	N/A
mEFB GBA1 ko -/-	GBA1-KO	Dr. Y. Yildiz, University Hospital Bonn, Bonn, Germany	N/A (BU: 15.10.2012)
mEFB GBA1 #E18 ko -/-	GBA1-KO	H. Angele, Molecular Sensory Systems, caesar, Bonn, Germany	30.06.2011

mEFB: Murine embryonal fibroblasts, Ctrl: Control, GBA1: Acid beta-glucosidase, +/+: Wild-type, -/-: Knockout, BU: Back-up.

2.3.5.3.1 Isolation of murine embryonal fibroblasts

Mouse embryos were dissected, the tail was cut off, and transferred to one well of a 6-well dish in 3 ml fibroblast growth medium (Table 4) under the cell culture hood. Dermal fibroblasts from the tails were isolated using collagenase digestion. Collagenase was prepared as a 50 mg/ml stock in pure DMEM/GlutaMAX and sterile filtered using a 0.45 µm mesh. 20 µl sterile collagenase solution was added per ml fibroblast growth medium to each well, swirled once, and the tails were cut into thin slices using a sterile blade. The pieces were incubated and digested for 3 h at 37 °C and 7.5% CO_2. The

supernatants were then transferred to a Falcon and pelleted at 600 x g for 5 min at RT. The pellet was re-suspended in 1 ml fibroblast growth medium, transferred to 2 ml medium in one well of a 6-well dish, and grown overnight at 37 °C and 7.5% CO_2. After 24 h, the cells were washed once with sterile PBS followed by addition of fresh medium. The cells were then grown to confluency for 2-3 days and scaled up to 9 cm dishes.

2.3.5.4 Melanoma cells

Table 13: Melanoma cell lines

Cell line	Species	Producer	Genotype
MEB-4	Mouse	Gift from Prof. C. Thiele, Biochemistry and Cell Biology of Lipids, LIMES, Bonn, Germany	Ctrl
GM-95	Mouse	Gift from Prof. C. Thiele, Biochemistry and Cell Biology of Lipids, LIMES, Bonn, Germany	GlcCerS-KO

Ctrl: Control, GlcCerS: glucosylceramide synthase, KO: Knockout

2.3.5.5 Stable cell lines

Table 14: Stable cell lines

Clone #	Cell type	Expresses	Producer	Resistance cassette
G4A11	CHO	mGBA2-HA	H. G. Körschen	G418
A8A11	CHO	mGBA2-HA	H. G. Körschen	G418
A8A6B5	CHO	mGBA1-HA mGBA2-HA	H. G. Körschen	G418, Blasticidin
A3	HEK293	mGBA2-HA	S. Schonauer	G418

2.3.6 Generation of cell culture back-ups

Cells were washed with PBS, trypsinised, and transferred to a falcon tube. Next, cells were pelleted for 5 min at 200 x g and RT and re-suspended in culture medium

containing 10% DMSO. Around 4-8x10^6 HAP1 cells, HEK293 cells, or CHO cells and at least 1x10^6 human dermal fibroblasts were frozen in 1 ml cryo tubes (Greiner) in a Mr. Frosty (Nunc) at -80 °C for 2-3 days before storage in liquid nitrogen.

2.3.7 Culturing of cell culture back-ups

To bring cells back into culture, 1 ml cell suspension was rapidly thawed at 37 °C (water bath) and transferred to 20 ml pre-warmed culture medium. The cells were pelleted for 5 min at 200 x g and RT, re-suspended in cell culture medium, and plated in normal culture medium in 9 cm dishes.

2.4 Molecular biology

2.4.1 qPCR primers

Table 15: Human qPCR primers

Gene	Primer numbers	Sequence (5‘-3‘)		
		Forward	Reverse	T_A (°C)
hGBA1	C1796/97	TGCCTATGCT GAGCACAAGT	GCTTCTGGGT CTGTCAGTAC	60/62
hGBA1	C1798/99	ACAGCCACAG CATCATCACG	AGGTCGTTCT TCTGACTGGC	62/62
hGBA2	C1800/01	CATATAGGCA TGGGCTTGAG	AGCTGCCAAC GACAGAACTG	60/62
hGBA2	C1802/03	CAGTTCTGTC GTTGGCAGCT	GAAGCTGATA GACAGTCCAG	62/60
hB2m	C1818/19	CGAGACATGT AAGCAGCATC	GCAACCTGCT CAGATACATC	60/60
hB2m	C1820/21	CGCTACTCTC TCTTTCTGGC	TTCACACGGC AGGCATACTC	62/62
hAlas1	C1822/23	GGACTTCTCG ACTTGAGTGC	GGGACTCGGG ATAAGAATGG	62/62
hAlas1	C1824/25	AGCTTCAGGA GGATGTGCAG	AGTTCTTCAG CAGTCCACTG	62/60

Table 16: Mouse qPCR primers

Gene	Primer numbers	Sequence (5‘-3‘)		
		Forward	Reverse	T_A (°C)
mGBA1	C1508/09	ATGACCAACG CTTGCTGCTA	GTGACTGTAC TGCATCCCTC	60/62
mGBA1	C1510/11	CCACCTACTC AGAAGCTGCT	TGTCTTCTTC TGGGAGGCTG	62/62
mGBA2	C1512/13	ATCTGCTTGG CTCACGAGTT	TGTCGATGAA AGGGGTCTTC	60/60
mGBA2	C1514/15	GAGAGGCCAG TTCTGTCGTT	AGGTGAGGGT GACATTCTGG	62/62
mGBA2	C1573/74	ATTCAGAGGA CTCTGGGCAG	TAGTGCCTCC TCCAATGCCA	62/62
mTfrc	C1520/21	GGGTCTAAGT CTACAGTGGC	GGCGACAGGA AGTGATACTC	62/62
mTfrc	C1522/23	ATGGTTCGTA CAGCAGCGGA	GCCACTGTAG ACTTAGACCC	62/62
mGusb	C1532/33	CCGTACGTGG ATGTTATCTG	CTCCTCACTG AACATGCGAG	60/62
mGusb	C1534/35	CTAGAGGTGA TGGAGGAGCT	GCTTTGGTGT GGGTGATCAG	62/62
mCHOP	C2187/88	TGAAGATGAG CGGGTGGCAG	GGTGGTGTAT GAAGATGCAC	64/60
mCHOP	C2189/90	ACCACCACAC CTGAAAGCAG	GACCTCCTGC AGATCCTCAT	62/62
mGRP78	C2195/96	CTTCGGTGCA GCAGGACATC	GTAACAACTG CATGGGTAAC	64/58
mGRP78	C2197/98	CTCTGGTGAT CAGGATACAG	TTTTGTTAGG GGTCGTTCAC	60/58

2.4.2 Polymerase chain reaction (PCR), testing of qPCR primers

To test whether primers designed for e.g. qPCR (2.4.6) amplify the sequence of interest, a conventional polymerase chain reaction (PCR) was performed (Thermocycler, SensoQuest). The PCR was done using the reaction mix shown in Table 17 and using the program shown in Table 18. For human and mouse primers (Table 15 and Table 16), cDNA obtained from a fibroblast cell line from a control patient (hFB 8, Table 8), or from a mouse wild-type testis was used.

Table 17: Pipetting scheme for PCR

Mix	Stock
0.5 µl KOD Hot Start polymerase (Novagen)	1 U/µl
3 µl KOD reaction buffer	10x
1 µl 1:5 diluted cDNA or 1:10 diluted cDNA (≙ 20-50 ng)	100 ng/µl from hFB 8 500 ng/µl from mouse testis
0.9 µl primer mix (≙ 0.3 µM each primer final)	10 µM each primer
3 µl dNTP mix	2 mM
1.2 µl $MgSO_4$	25 mM
ad 30 µl with ddH_2O	-

Table 18: PCR program

	Step	Temperature (°C)	Time (s)
I	Denaturation	95	80
II	Denaturation	95	30
III	Annealing	55	30
IV	Elongation (35x to II)	72	35
V	End	8	∞

2.4.3 Agarose-gel electrophoresis

DNA molecules were separated according to their size via agarose-gel electrophoresis. For the separation of DNA molecules of 75-200 base pairs (bp), gels containing 2% agarose (w/v) were used. Agarose was dissolved in 1x TAE buffer (Table 19) by boiling. Before pouring the gel, ethidium bromide (1 µg/ml) was added. 5 µl of the 30 µl PCR approach (Table 17) was diluted in 10x loading buffer (Table 19) and loaded on the gel. The 1 kb DNA ladder was used as size standard (Figure 5). Electrophoresis was carried out in 1x TAE buffer (Table 19) at a constant voltage of 120 V for 20 min. For gel analysis, the ethidium bromide stained DNA was visualised under UV light.

Table 19: Buffers used for agarose-gel electrophoresis

Loading buffer (10x)	TAE (50x)
10x TAE	2 M Tris/acetate, pH 7.5
50% glycerol	50 mM EDTA
0.25% Xylene caynol	

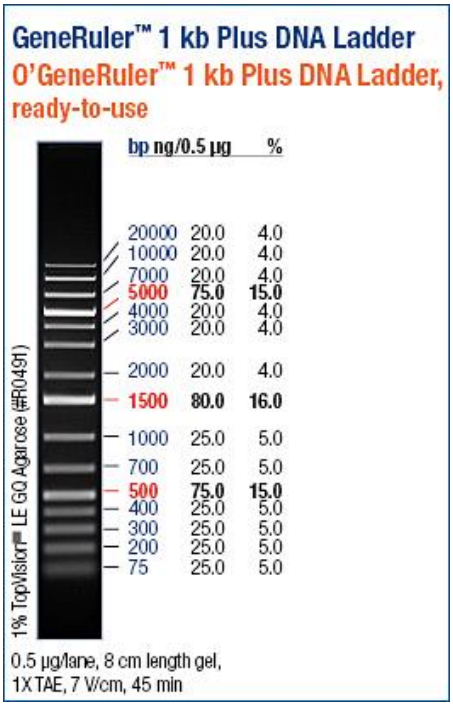

Figure 5: GeneRuler 1 kb Plus DNA Ladder.

2.4.4 SureClean protocol for DNA purification

PCR products (2.4.2) were purified using the SureClean kit (Bioline). The SureClean reagent was added 1:1 to the DNA solution and mixed thoroughly. After incubating for 10 min at RT, the DNA was centrifuged for 10 min at 14,000 x g and the DNA pellet was washed using 70% ethanol with a 2:1 volume of the starting sample. The mix was vortexed for 10 s and centrifuged for 10 min at 14,000 x g. The DNA pellet was air-dried for 5-10 min and re-suspended in ddH_2O.

2.4.5 Sending PCR products for sequencing

For sequencing, 7.5 µl purified DNA (2.4.4) were mixed 1:1 with ddH_2O. The corresponding forward primers were diluted to 2 pmol/µl in ddH_2O and 15 µl were sent. All PCR products had the predicted sequence (data not shown).

2.4.6 Analysis of mRNA expression

2.4.6.1 RNA isolation using the NucleoSpin RNA II kit

Cells in culture were washed once with sterile PBS and trypsinised at 37 °C. Cells were collected in a Falcon tube and pelleted for 5 min at 200 x g. Pellets were either directly subjected to mRNA extraction of pellets were frozen in liquid nitrogen and stored at -80 °C until further usage. Total RNA isolation was performed according to the manufacturer's instructions (NucleoSpin RNA II: Macherey & Nagel, Düren, Germany). A minimal RNA concentration of 0.25 µg/µl was required to reversely transcribe 2 µg RNA using the normal reaction volume of 20 µl during cDNA synthesis (see 2.4.6.4). Thus, RNA was eluted from the columns using only 40 µl RNase-free ddH_2O.

2.4.6.2 RNA isolation using Trizol

Tissues were dissected, weighted, and 1 ml Trizol (Thermo Fisher Scientific) was added per 50-100 mg. Tissues were homogenised using a Teflon douncer (IKA works), transferred to a 2 ml tube, and incubated for 5 min at RT. 200 µl chloroform were added per 1 ml Trizol and mixed for 15 s. After incubating for 2-3 min at RT, the sample was centrifuged for 15 min at 12,000 x g and 4 °C. The upper aqueous phase contained RNA, whereas proteins resided in the lower chloroform phase and DNA in the interphase. The upper phase was transferred to a new tube and 500 µl pure isopropanol were added per 1 ml Trizol. The solution was mixed and incubated for 10 min at RT. RNA was precipitated by centrifuging for 10 min at 12,000 x g and 4 °C.

The pellet was washed with 1 ml 75% ethanol (prepared in DEPC-treated ddH_2O) and briefly vortexed. After centrifuging for 5 min at 7,500 x g and 4 °C, the RNA pellet was air-dried for 5-10 min, re-suspended in 40 µl DEPC-treated ddH_2O, and incubated for 10 min at 55 °C. RNA concentration was measured using a spectrophotometer (see 2.4.6.3).

2.4.6.3 Quantification of nucleic acids

To determine the DNA or RNA concentration in a solution, 1.5 µl were analysed using the NanoDrop instrument (NanoDrop ND-1000). The concentration was measured using the following values:

dsDNA: 50 µg/ml at OD_{260}=1

RNA 40 µg/ml at OD_{260}=1

The ratio of the absorption at 260 nm and 280 nm provides information about the purity of the DNA/RNA and contaminations by e.g. proteins. The value should not be smaller than 1.8.

2.4.6.4 Reverse transcription of mRNA using the Superscript III kit

cDNA synthesis for qPCR analysis was performed according to the manufacturer's instructions (Superscript III: Thermo Fisher Scientific). For first strand synthesis, the mix shown in Table 20 was prepared:

Table 20: Pipetting scheme for reverse transcription (I)

Mix	Stock
2 µg RNA	-
1 µl random hexamers	50 µM
1 µl dNTP mix	10 mM each
ad 10 µl with RNase-free ddH_2O	-

The reaction mix was incubated at 65 °C for 5 min and chilled on ice for at least 1 min. Then, 9 µl of the 2x mix shown in Table 21 were added per reaction.

Table 21: Pipetting scheme for reverse transcription (II)

Mix	Stock
2 µl reaction buffer	10x
4 µl $MgCl_2$	25 mM
2 µl DTT	0.1 mM
1 µl RNase Out	1 U/µl

The reaction was mixed and incubated at 25 °C for 2 min before 1 U Superscript polymerase (1 U/µl, Invitrogen) was added. The reaction was incubated again at 25 °C for another 10 min, at 42 °C for 50 min, and at 70 °C for 15 min. The cDNA was stored at -20 °C.

2.4.6.5 Primer efficiency test (PET)

To reliably analyse the data obtained from qPCR, a primer efficiency test (PET) was performed. Here, the normal qPCR program (Table 23) was performed on a serial dilution (1:1, 1:5, 1:10, 1:50, 1:100, and 1:1,000) of the template (e.g. cDNA from human dermal fibroblasts) using the different primer pairs. In a perfect PCR cycle, the amount of DNA should double and the primer efficiency would be 100%. The PET was performed for two primer pairs per GOI (hGBA1, hGBA2) and HEK (hB2m, hAlas1) in duplets. The slope obtained from plotting the individual C_T values against the logarithm of the cDNA dilutions was used to calculate the primer efficiency (E = 10-1/slope). Primers used for qPCR showed at least 90% and maximal 105% efficiency (Table 57 and Table 60). For qPCR experiments, two master mixes were prepared (Table 22) and the PCR was performed using the program shown in Table 23.

Table 22: Pipetting scheme for qPCR mixes I and II

Mix I	Mix II
1 µl of a 5 µM dilution of each primer of one primer pair	1 µl of diluted cDNA
12.5 µl SYBR Green Supermix (Biorad)	10.5 µl ddH_2O

Table 23: qPCR program

Cycle	Step	Step	Temperature (°C)	Time (s)
1	I	Denaturation	95	180
2	I	Denaturation	95	10
	II	Annealing	59	30
	III	Elongation (45x to 2)	72	30
3	I	Denaturation	95	60
4	I	Melt curve	55	60
5	I		55	30

2.4.6.6 Quantitative real-time PCR (qPCR)

qPCR was performed for the GOIs hGBA1 and hGBA2, and the HKGs hB2m and hAlas1 and human dermal fibroblast samples as templates (see Table 8, Table 55). Furthermore, qPCR was performed for mGBA2 and the HKGs mTfrc and mGusb on brain samples from control and CBE-treated mice as templates (see Figure 25a, Table 58). The reactions were set up in triplets for each gene and each template. Additionally, a non-template control was set up for each primer pair. All qRT-PCR experiments were performed in the BioRad I-cycler with an IQ5 optical system. Data was analysed using the BioRad IQ5 optical system software and calculated according to the delta-delta-CT method (Biorad Bulletin). After running the cycles, a melt-curve analysis was performed to detect non-specifically amplified products. mRNA expression-levels for all samples were normalised to the mean of the individual HKGs.

Table 24: cDNA dilutions for qPCR

Sample	cDNA dilution
hFBs	1:7
Mouse brain	1:10

2.5 Protein biochemistry

2.5.1 Antibodies for immunostainings

2.5.1.1 Primary antibodies

The generation of monoclonal rat antibodies against different epitopes of mGBA2 is described in Körschen et al. 2013. Polyclonal antibodies were generated against an mGBA2 fusion protein carrying an N-terminal His-tag expressed and purified from *E.coli* strain BL21 Codon Plus (DE3) RIPL.

Table 25: Monoclonal primary antibodies

Antibody	Species	Producer	Catalogue #	Dilution		Weight (kDa)
				WB	ICC	
GBA2-3H8	rt	H. G. Körschen	-	1:20	-	~120
GBA2-4A12	rt	H. G. Körschen	-	1:20	-	~120
GBA2-5A8/1	rt	H. G. Körschen	-	1:20	-	~120
GBA2-8G4	rt	H. G. Körschen	-	1:20	-	~120
GBA2-4F8	rt	H. G. Körschen	-	1:20	-	~120
GBA2-4D7	rt	H. G. Körschen	-	1:20	-	~120
GBA2-12F8	rt	H. G. Körschen	-	1:20	-	~120
GBA2-2H1	rt	H. G. Körschen	-	1:20	-	~120
GBA2-2F8	rt	H. G. Körschen	-	1:20	-	~120
GBA2-5A8/4	rt	H. G. Körschen	-	1:20	-	~120
GBA2-4A12/2F8 mix	rt	H. G. Körschen	-	1:50 each	-	~120
HA-Tag	rt	Roche	11867431001	1:5,000	-	-
Beta-Tubulin	ms	Sigma	TUB 2.1	1:1,000	-	55
His-Tag	ms	Novagen	70796-3	1:1,000		-

GFP	ms	Millipore	MAB3580	1:5,000-10,000	-	30
GM130	ms	BD Transduction Laboratories	Clone 35, 610822	-	1:100	130

rt: Rat, ms: Mouse

Table 26: Polyclonal primary antibodies

Antibody	Species	Producer	Catalogue #	Dilution		Weight (kDa)
				WB	ICC	
Calnexin	rb	Sigma	C4731	1:40,000 (tissue)	-	90
				1:5,000-10,000 (cells)	-	90
GBA1	rb	Sigma	G4171	1:1,000	-	55-69
GBA1-3kb	rb	H. G. Körschen	-	1:5,000	-	55-69
GFP	rb	Abcam	ab6556	1:5,000	-	-
GBA2	rb	Y. Yildiz	-			~120
GBA2-4kb	rb	H. G. Körschen	-	1:1,000-5,000	-	~120
GBA2-5kb	rb	H. G. Körschen	-	1:1,000-5,000	-	~120
GBA2-4kb/5kb mix	rb	H. G. Körschen	-	1:5,000 each	-	~120
LAMP1	rb	Abcam	ab24170	1:1,000	1:200	120
GLTP	gt	Santa Cruz	N-17	1:500	-	25

kb: Körschen, Bonn, rb: Rabbit, gt: Goat

2.5.1.2 Secondary antibodies

Table 27: Secondary antibodies

Antibody	Producer	Catalogue #	Dilution	
			WB	ICC
dk α gt IRDye680	LI-COR Biosciences	926-32224	1:20,000	-
dk α ms IRDye680LT	LI-COR Biosciences	926-68022	1:20,000	-
dk α ms IRDye800CW	LI-COR Biosciences	926-32212	1:20,000	-
dk α rb IRDye680	LI-COR Biosciences	926-32223	1:20,000	-
dk α rb IRDye800CW	LI-COR Biosciences	926-32213	1:20,000	-
gt α rt IRDye680	LI-COR Biosciences	926-32229	1:20,000	-
gt α rt IRDye800CW	LI-COR Biosciences	926-32219	1:20,000	-
d α ms Cy3	Dianova	715-165-151	-	1:500
d α rb A647	Dianova	711-605-152	-	1:400
ms α rt IgG_{2b} HRP	Gift from E. Kremmer	-	1:1,000	-
gt α rt HRP	Dianova	112-035-068	1:5,000	-
ms α rt kappa HRP	Gift from E. Kremmer	-	1:1,000	-

dk: Donkey, gt: Goat, ms: Mouse, rb: Rabbit, rt: Rat, HRP: Horseradish peroxidase

2.5.2 Protein preparation

All steps were performed at 4 °C in the presence of mammalian protease inhibitor cocktail (mPIC, Sigma Aldrich). Tissues were homogenised in 10 ml/g wet weight of the organ of hypotonic buffer (Table 28) using an Ultra-thurrax (IKA) and three pulses (20 s each) of sonification in ice-cold water (Branson Sonifier). Tissue suspensions (total lysate) were subjected to low speed centrifugation for 20 min at 1,000 x g. The supernatant (PNS, post-nuclear supernatant) was used for activity assays (also see

Körschen 2013). Cultured cells were washed once with PBS and harvested using 1 ml of 0.5 g/l EDTA in PBS (pH 7.4) per 9 cm cell culture dish and cells were pelleted for 5 min at 600 x g and 4 °C. Afterwards, the pellets were directly lysed in hypotonic buffer, sonicated (see above), and used for activity assays or Western blot analysis. If the lysates were left on ice for some time, they were briefly sonicated again to maintain the homogeneous suspension. The protein concentration was estimated using either the Bradford assay (2.5.2.1) or the bicinchoninic acid (BCA) test (2.5.2.2).

Table 28: Hypotonic buffer

Hypotonic buffer
10 mM HEPES/NaOH, pH. 7.4
0.5 mM EDTA
1:500 mPIC
in ddH_2O

2.5.2.1 Bradford assay

The Bradford assay makes use of an absorbance shift of the dye Coomassie Brilliant Blue G-250 (Bradford reagent, Biorad) due to protein binding. Upon protein binding, the red form of the dye shifts to a blue form, which can be detected by measuring the absorbance at 595 nm. The increase of absorbance at 595 nm is proportional to the amount of bound dye, and, thus, represents a measure for the protein concentration. The Bradford reagent was diluted 1:5 in ddH_2O and the shift in absorbance was measured in 5 µl of the (diluted) protein suspension in 1 ml diluted Bradford reagent in a disposable plastic cuvette at the spectrophotometer (Hitachi U-1900) and compared to a blank sample. The optical density (OD) at 595 nm was determined in an absorbance range from 0.005 to 0.15, at higher values the protein suspension was diluted and measured again.

2.5.2.2 The bicinchoninic acid (BCA) test

The bicinchoninic acid (BCA) test kit (Pierce) is based on the reduction of Cu^{2+} to Cu^{+} in alkaline solution and in the presence of protein, where the amount of reduced Cu^{+} ions directly correlates with the amount of protein present. The Cu^{+} ions react with the bicinchoninic acid in aqueous solution with a high absorption at 562 nm. The BCA

solution was prepared by mixing of solutions A and B from the kit in a ratio of 50:1. Dilutions of the samples to be analysed and a serial dilution of a BSA reference (10 µl) were prepared in a 96-well plate and mixed with 190 µl BCA solution. After incubating for 30 min at 37 °C, the absorption of all samples was measured at 570 nm in the Packrad Fusion Instrument plate reader. The protein concentration was calculated using the linear regression of the BSA standard.

2.5.2.3 Deglycosylation of proteins

Glycosylated proteins were de-glycosylated for e.g. Western blot analysis using PNGase F from NEB (Table 29, Table 30). 20 µg total protein were mixed with denaturing buffer and incubated at RT for 10 min. Then, G7 buffer, NP-40, and PNGase F were added and the approach was incubated at 37 °C for at least 2 h. Afterwards, 4x SDS sample buffer was added and the proteins were either loaded to polyacrylamide gel or stored at -20 °C until further usage.

Table 29: Deglycosylation approach

Deglycosylation approach	Stock
20 µg total protein	-
ad 22.5 µl with ddH_2O	-
2.5 µl denaturing buffer	10x
3 µl G7 buffer	10x
3 µl NP-40	10% (w/v)
1 µl PNGase F (NEB)	1 U/µl

Table 30: Buffers used for deglycosylation

Denaturing buffer (10x)	G7 buffer (10x)
0.5% (w/v) SDS	50 mM sodium phosphate buffer,
1% (w/v) beta-mercaptoethanol	pH 7.5

2.5.3 Studying the interaction between GBA2 and pacSphingosine

2.5.3.1 In vitro

Delta SGPL1 HeLa cells (Table 11) heterologously expressing mGBA1, mGBA2, and GFP (2.3.2 and 1.1.1), or JAM3 were harvested (2.5.2) and lysed in 200 µl of 100 mM HEPES/KOH (pH 7.4) + mPIC per 9 cm dish by sonication (2.5.2). The protein concentration was determined via Bradford assay (2.5.2.1). Samples were incubated directly with 6 µM pacSphingosine (pacSph) or AR451 (Table 31) for 1 h at RT. Lipids and binding proteins were photo cross-linked by irradiation with UV light (LED lamp, 1.25 mA) for 7 minutes with minimal distance between the lamp and the top of the tube. During irradiation, the protein lysate was mixed by inversion every two minutes. 50 µg of total protein were filled up to 21 µl sample volume with 100 mM HEPES/KOH (pH 7.4) and 4 µl of a 25x concentrated click-reaction mix (Table 32) were added (final 1x). Samples were clicked at 37 °C for 1 h before the sample volume was increased to 27 µl with 100 mM HEPES/KOH (pH 7.4) and 9 µl 4x SDS sample buffer were added. All samples were loaded to a 10% polyacrylamide gel (Table 34) and subjected to SDS-polyacrylamide gel electrophoresis (SDS-PAGE) and Western blot analysis (2.5.4 and 2.5.5) or stored at -20 °C until further use. Western blots were immunostained (2.5.5.2) using the primary antibodies against HA (Roche, Table 25) and GFP (Abcam, Table 26) and species specific IR800-coupled secondary antibodies (Table 27).

Table 31: Photoactivatable and clickable lipids

Lipid	Stock	Source
pacSphingosine (pacSph)	25 mM in EtOH	Dr. P. Haberkant, Proteomic Core Facility, EMBL Heidelberg, Heidelberg, Germany
AR451	24 mM in DMSO	Dr. A. Rennhack, Molecular Sensory Systems, caesar, Bonn, Germany

Table 32: Click-reaction mix for pac lipids

Click-reaction mix for pac lipids (1x)	Click-reaction mix for pac lipids (25x)	Stock
1 mM $CuSO_4$	25 mM	200 mM in ddH_2O
0.1 mM TBTA	2.5 mM	25 mM in DMSO
25 µM Azido-DY-654 (Dyomics)	0.625 mM	1 mM in ddH_2O
1 mM Ascorbic acid	25 mM	100 mM in ddH_2O

2.5.3.2 In vivo

Interaction of GBA2 and pacSph *in vivo* was performed as described in 2.5.3.1, but delta SGPL1 HeLa cells (Table 11) heterologously expressing mGBA1, mGBA2, and GFP (2.3.2 and 1.1.1), or JAM3 were incubated with normal culture medium containing 10% de-lipidated FCS (Gift from Prof. C. Thiele) instead of the one normally used and 6 µM pacSph or AR451 in 5 ml total volume per 9 cm dish. The cells were incubated at 37 °C for 1 h before harvesting, cell lysis, and UV irradiation (see 2.5.3.1).

2.5.4 SDS-PAGE

2.5.4.1 Self-casted polyacrylamide gels

The separation of proteins prepared for Western blot analysis was accomplished by denaturing SDS-PAGE following the modified protocol by Laemmli (Laemmli, 1970). Electrophoresis was carried out using a minigel chamber (Biometra). The polyacrylamide concentration of the separating gel was varied from 7.5-15%, depending on the size of the protein of interest, while 5% polyacrylamide stacking gels were used in all experiments. The gel composition is summarised in Table 34. Protein samples were mixed with 4x SDS-sample buffer (final 1x, Table 33) and heated to 98 °C for 5 min prior to loading onto polyacrylamide gel. The pre-stained maker VI (Applichem, Figure 6) was used as a protein standard. For electrophoretic separation, SDS running buffer (final 1x, Table 33) was used. For protein separation, currents of 15 mA were applied during the stacking gel phase, whereas currents were raised to 25 mA as soon as the samples traversed the border of the stacking to separating gel.

Table 33: Buffers used for SDS-PAGE

SDS-sample buffer (4x)	SDS running buffer (10x)
200 mM Tris/HCl, pH 6.8	250 mM Tris
0.04% Bromophenol blue	1.92 M Glycine
4% beta-Mercaptoethanol	1% SDS
8% SDS	
50% glycerine	

Table 34 Pipetting scheme for polyacrylamide gels

	Stacking gel (5%)	Separating gel (7.5-15%)
1.5 M Tris/HCl, pH 6.8/8.8	0.5 ml (pH 6.8)	1.5 ml (pH 8.8)
10% SDS	20 µl	60 µl
10% APS	40 µl	40 µl
TEMED	2.5 µl	4.5 µl
Acrylamide	340 µl	1.5 – 3.0 ml
ddH_2O	1.12 ml	2.92 – 1.42 ml

2.5.4.2 Gradient polyacrylamide gels (Invitrogen)

The separation of proteins prepared for Western blot analysis on gradient polyacrylamide gels (Invitrogen) was accomplished using the XCell SureLock Mini-Gel System (Invitrogen). The polyacrylamide concentration of the separating gel is a gradient ranging from e.g. 4-12%, which provides a better separation of the proteins. 1.0 mm tick gradient gels with 15 slots were used. As described in 2.5.4.1, protein samples were mixed with 4x SDS-sample buffer (final 1x, Table 33) and heated to 98 °C for 5 min prior to loading onto polyacrylamide gel. The pre-stained maker VI (Applichem, Figure 6) was used as a protein standard. For electrophoretic separation, NuPAGE MOPS running buffer was used (final 1x, Table 35). SDS-PAGE was performed for 1-1.5 h at 180 V and 120 mA per gel.

Table 35: NuPAGE MOPS running buffer for SDS-PAGE

NuPAGE MOPS running buffer (20x)
50 mM MOPS
50 mM Tris base
0.1% SDS
1 mM EDTA
pH 7.7

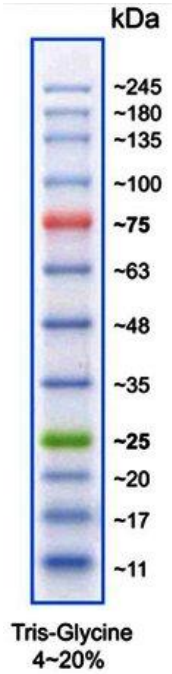

Figure 6: Protein standard used for SDS-PAGE

2.5.5 Western blot analysis

2.5.5.1 Immobilisation of proteins on PVDF membranes

For immunostainings of proteins separated by SDS-PAGE (2.5.4), the proteins were transferred to PVDF membranes (Immobilon FL for fluorescently-labelled secondary antibodies and Immobilon P for HRP-conjugates secondary antibodies, Millipore, Table 27) using the Western blot technique modified from Towbin et al. 1997. The protein transfer was performed in a semi-dry procedure using a blotting chamber (Roth). The transfer time was set to 40 min at 2.4 mA/cm^2/membrane using 8x9 cm membranes.

After blotting, membranes were briefly re-hydrated in methanol and subjected to immunostaining.

2.5.5.2 Immunostaining of immobilised proteins

For the immunological detection of protein on PVDF membranes, sets of primary and secondary antibodies were used (Table 25 to Table 27). Immunostainings were carried out in three steps (Table 36): First, the membrane was blocked with blocking buffer (Table 37) to saturate non-specific binding sites for antibody binding. In a second step, the membrane was incubated with primary antibody, suitable for binding the protein of interest on the membrane. In a third step, a corresponding secondary antibody was added for detection of the antibody-antigen complex. The secondary antibody is species specific, as it is directed against a constant region of the primary antibody. Furthermore, the secondary antibody is conjugated with a fluorophore, IRDye680 or IRDye800 (Table 27), which emits light at 694 or 794 nm when exited with light of 680 nm or 778 nm, respectively (LI-COR Biosciences). Membranes probed with fluorescently labelled secondary antibodies were analysed using the Odyssey Imaging System (LI-COR). Quantification of the Western blots was done using ImageJ (version 1.46m).

Immunological detection of proteins on PVDF membranes using horseradish peroxidase (HRP)-coupled secondary antibodies was carried out as described above, whereas non-specific binding sites were blocked using milk-powder. The secondary antibodies were conjugated with HRP, which enables the detection of the antibody-antigen complex using the enhanced chemiluminescence (ECL) solution (Sigma).

Table 36: Immunostaining of immobilised proteins

Working step	Incubation time	Solution
Membrane blocking	30 min (RT)	Blocking buffer
Primary antibody incubation	60 min (RT) or overnight (4 °C)	Primary antibody in blocking buffer
Wash	2x 10 min (RT)	PBS-T
Secondary antibody incubation	60 min (RT)	Secondary antibody in blocking buffer
Wash	2x 10 min (RT)	PBS-T
Wash	1x 10 min	PBS

Table 37: Buffers used for immunostaining of immobilised proteins

PBS washing buffer (pH 7.4)	PBS-T washing buffer (pH 7.4)
130 mM NaCl	130 mM NaCl
7 mM Na_2HPO_4	7 mM Na_2HPO_4
3 mM NaH_2PO_4	3 mM NaH_2PO_4
	0.05% Tween 20
Western blot blocking buffer for fluorophore-coupled secondary antibodies	Western blot blocking buffer for HRP-coupled secondary antibodies
1:1 PBS-T/Blok (Millipore)	2.5% milk powder in PBS-T

2.5.6 GlcCer column

The amount of the tip of a scoop of dried GlcCer column resin was equilibrated with 1 ml sterile-filtered PBS (pH 7.4) (= 10x column volume, CV) in a normal tube by centrifugation at 500 x g and 4 °C for 5 min. The resin was then incubated with 100 µl protein lysate or 100 µl of 0.35 µM purified GLTP (also see

Table ***39***) in PBS end-over-end at 4 °C overnight. On the next day, the sample was centrifuged at 500 x g and 4 °C for 5 min (supernatant = non-bound proteins) and the resin was washed 4x with 500 µl lysis buffer or PBS supplemented with 1% Triton X-100. During each washing step, the resin was centrifuged at 500 x g and 4 °C for 5 min. Bound proteins were eluted by incubation with 1 CV of lysis buffer or PBS containing 2% SDS end-over end at RT for 10-30 min. The resin was then centrifuged at 14,000 x g and RT for 5 min and the supernanant containing the eluted proteins was transferred to a fresh tube. The GlcCer resin was washed with PBS and air-dried with an open lid. Dry resin was stored at -20 °C until further use.

2.5.7 Immunocytochemistry (ICC)

2.5.7.1 Preparation of glass coverslips for ICC

For immunocytochemical experiments, $4x10^4$ cells (human dermal fibroblasts) were seeded on poly-L-lysine (PLL) coated 13 mm glass coverslips. The glass slides were distributed to a 24-well plate and covered with 500 µl of 0.1 mg/ml PLL. After incubation at RT for 45 min, PLL was removed and the glass slides were washed twice with PBS.

2.5.7.2 GLTP-mediated transfer of clickGlcCer

2.5.7.2.1 Preparation of clickGlcCer/DOPC liposomes by extrusion

Liposomes were prepared according to the manufacturer's protocol (Avanti Polar Lipids). The desired amounts of lipids (Table 38, DOPC: 1,2-Dioleoyl-sn-glycero-3-phosphocholine) were mixed in a 2 ml glass vial and vortexed. The solvents were evaporated under a constant nitrogen flow while rolling the glass vial to obtain a lipid film. Afterwards, residual solvents were evaporated for another 30 min. The minimal volume to produce a lipid film is 50 µl. Dried lipids were re-suspended in the desired amount of buffer (e.g. PBS) and vortexed for 1.5 min. The suspension now contained giant multilamellar vesicles and looked milky. Unilamellar vesicles were produced by five consecutive freeze-thaw cycles, where the samples were frozen in liquid nitrogen and immediately thawed in a water bath at 37 °C. The Mini-Extruder from Avanti Polar Lipids was assembled according to the manufacturer's protocol (Figure 7) and the membranes were pre-wetted with 500 µl PBS in 1 ml Hamilton syringes. 400 nm pore Whatman filters were used to produce liposomes with a diameter of 400 nm. The lipid suspension containing unilamellar vesicles was then sucked up by one of the two syringes and passed through the membrane into the second syringe 13 times. During

this procedure, the suspension got more transparent. Lipids were stored at 4 °C until further use for up to one week.

Table 38: Lipids used for liposomes

Lipid	Stock	Company	Catalogue #
clickGlcCer	1 mg/ml in chloroform/methanol	Gift from Prof. C. Thiele, Biochemistry and Cell Biology of Lipids, LIMES, Bonn, Germany	-
DOPC	20 mg/ml in chloroform	Avanti Polar Lipids	850375c

DOPC: 1,2-Dioleoyl-sn-glycero-3-phosphocholine

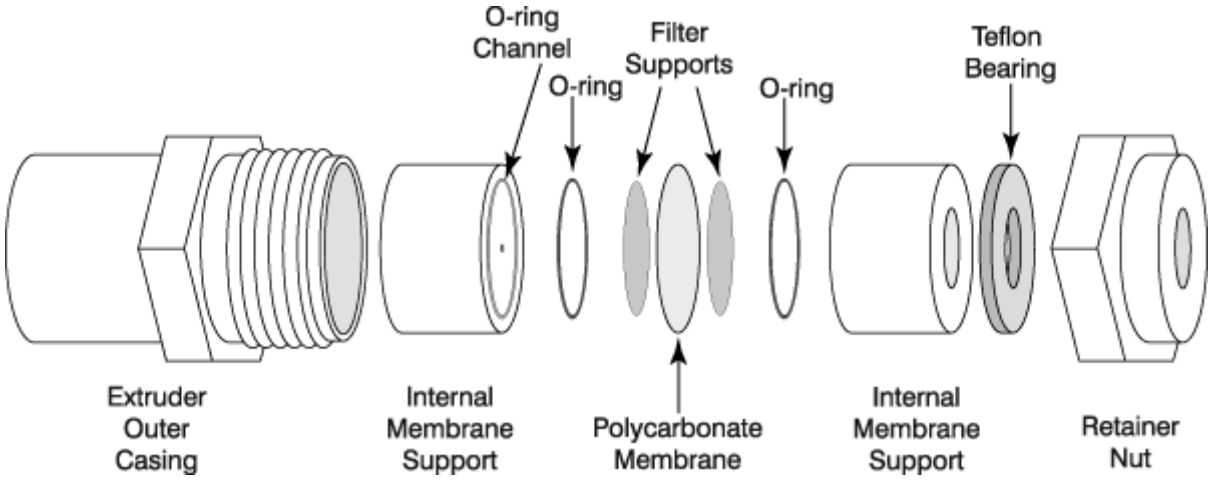

Figure 7: Assembly scheme of the Mini-Extruder by Avanti Polar Lipids.

2.5.7.2.2 Feeding of cells with clickGlcCer/DOPC liposomes

Human dermal fibroblasts seeded on PLL-coverslips for immunocytochemical analysis (2.5.7.4) or seeded on the plastic surface of the culture dish (2.6.2) from control and type I *Gaucher* patients were pulsed with 200 µl DOPC liposomes containing either 0 or 10 mol% clickGlcCer (2.5.7.2.1) for 1 h or 24 h (Table 39). Cells pulsed for 1 h were subsequently chased for 23 h. Afterwards, lipids were extracted, clicked to 3-azido-7-hydroxycoumarin, and analysed by TLC (2.6.2) or fixed for immunocytochemical staining (2.5.7.3 following).

Table 39: ClickGlcCer feeding approach

GLTP-mediated clickGlcCer transfer approach/well	Stock	Source
18 µM hGLTP-His	66.6 µM	Plasmid: AG Lang, Limes Institute, University of Bonn,Germany published in Lauria et al. 2013
1:2.5 dilution of liposomes	-	
ad 200 µl with PBS	-	

2.5.7.3 Fixation of cells for ICC

In preparation for immunocytochemical stainings, cells were fixed on PLL-coated glass coverslips (2.5.7.1). After removal of the cell culture medium and washing with PBS, cells were fixed in 300 µl of 4% paraformaldehyde (PFA) in PBS at RT for 10 min. Afterwards, cells were washed 3x with PBS and directly subjected to immunocytochemical stainings or stored in 700 µl PBS containing 0.05% sodium azide at 4 °C.

2.5.7.4 Immunocytochemical staining

Fixed cells (2.5.7.3) were washed with PBS, with 155 mM ammonium acetate, and, again, with PBS. Non-specific binding sites were blocked with ICC blocking buffer suitable for click chemistry (Table 40) at RT for 30 min. The primary antibody was diluted in ICC blocking buffer and added to the cells for 1 h at RT, followed by washing 3x with PBS. The secondary antibody was also diluted in ICC blocking buffer and the coverslips were placed upside-down on 35 µl droplets of secondary antibody solution for 1 h at RT in the dark. The cells were washed once with PBS and subjected to click chemistry (2.5.7.5).

Table 40: ICC blocking buffer suitable for click chemistry

ICC blocking buffer for click chemistry
1% (w/v) Cold water fish gelatine
0.01% (w/v) Saponine
in PBS

2.5.7.5 Click chemistry for ICC

Fixed cells (2.5.7.3) were washed once with 100 mM HEPES/KOH (pH 7.4) and 0.01% Saponine. The click-reaction mix (Table 41) was prepared, distributed to the wells, and the plate was pre-warmed to 43 °C in a water bath. 10 µl of 100 mM Cu(I)TFB in acetonitrile were directly added to each well, the plate was swirled once, and the mix was incubated at 43 °C for 1 h. Afterwards, cells were washed with 100 mM HEPES/KOH (pH 7.4) and PBS. AP3Btn or APpic2Btn (see Figure 72a) were detected by placing the coverslips upside-down on 35 µl droplets of a detection mix (Table 41) at RT for 1 h in the dark. Afterwards, cells were washed twice with PBS and mounted using mounting medium (Polysciences) and incubated at RT for 1 h and stored at 4 °C until further use. Pictures were taken on a confocal microscope (Olympus FV1000).

Table 41: Click-reaction mix and detection mix for cells

Click-reaction mix/coverslip	Stock	Detection mix/coverslip	Stock
800 µl 100 mM HEPES/KOH, pH 7.4	-	40 µl 100 mM HEPES/KOH, pH 7.4	-
0.01% (w/v) Saponine	-	1 µl Streptavidin-Alexa488	1 mg/ml in ddH_2O
12.5 µM AP3Btn	10 mM in DMSO		
12.5 µM APpic2Btn	10 mM in DMSO		
10 µM ApicSBDP	10 mM in DMSO		

HEPES: 4-(2-hydroxyethyl)-1-piperazineethanesulfonic acid

2.5.8 Fluorometric measurements

2.5.8.1 Measuring principle of the Fluostar plate reader

Fluorescence measurements of protein suspensions in multiwall plates were carried out using the fluorescence plate-reader Fluostar Omega (BMG Labtech). For the measurements, black 384-well plates with a glass bottom were used. In the Fluostar, the multi-well plate is moved past a detector head, which records the fluorescence of each well individually.

2.5.8.2 Fluorescence-based GBA activity assay

The assay has been performed as described previously (Körschen et al., 2013). The GBA activity in hypotonic protein lysates (2.5.2) was analysed by cleavage of 4-MUG in real-time in a Fluostar Omega reader (BMG Labtech) at 29 °C using the filter pair 355 nm/460 nm for excitation and emission, respectively. The assay reactions were prepared on a 96-well plate, left) of which 4x 25 µl were transferred to a 384-well plate (Greiner) for analysis of quadruples. The assays were performed in the plate mode. Each well contained 20 - 100 µg of total protein. To discriminate between GBA1 and GBA2 activity, 25 µM CBE (conduritol B epoxide, Sigma Aldrich), an inhibitor for GBA1, or 8.2 µM NB-DNJ (N-butyldeoxynojirimycin, Sigma Aldrich), an inhibitor for GBA2, were included. The pH of the protein lysates and the 4-MUG solution were adjusted by diluting with McIlvaine buffer (Table 42). Analysis of GBA activity was initiated by adding 5 µl of 4-MUG (10 mM), resulting in a final concentration of 1.67 mM. The hydrolysis of 4-MUG was monitored and recorded as a change of relative fluorescence units (rfu) per minute. Per genotype, tissues or cells from at least three animals were analysed if not otherwise stated.

Table 42: Pipetting scheme for GBA activity assay

Assay approach per well (96-well plate)	Assay approach per well (384-well plate)	McIllvaine buffer
90 µl pH buffer	25 µl approach from 96-well plate	0.1 M citric acid
20 µl protein sample	(25 µM CBE final and 8.3 µM NB-DNJ final)	0.2 M Na_2HPO_4
20 µl hypotonic buffer	5 µl 10 mM 4-MUG	
or: 10 µl of either/each 390 µM CBE and/or 130 µM NB-DNJ		

For each plate, the fluorescence was analysed for 150 cycles with the first 50 cycles applying 2 flashes per well and the last 100 cycles applying 10 flashes per well (Table 43). Fluorescence was recorded from the top of each well. The gain was set to 800. Beta-glucosidase activity was expressed as the increase in fluorescence from cycle 50 – 100 in rfu/min (slope).

Table 43: Fluostar plate mode settings for beta-glucosidase activity assays

Kinetic window	1	2
No. of cycles	50	100
Cycle time (s)	50	80
No. of flashes per well	2	10

2.5.9 Treatment of cells with CBE or NB-DNJ

For treatment of cells with CBE or NB-DNJ, cells were seeded out the day before transfection (HEK293, 2.3.2) or the day before treatment (CHO, CHO #G4A11, hFBs) (Table 44). CBE or NB-DNJ were diluted to 25 µM or 2 µM in 9 ml normal culture medium per 9 cm plate, respectively. Cells were incubated with the blockers at 37 °C for 2 d before analysing the beta-glucosidase activity (2.5.8.2).

Table 44: Cell numbers seeded for CBE and NB-DNJ treatment

Cell line	Cell number per 9 cm dish
HEK293	$2x10^6$
CHO	$5x10^5$
CHO #G4A11	$5x10^5$
hFB	$2x10^6$

2.5.10 Treatment of cells with Fumunisin B1

For treatment of human dermal fibroblasts with Fumunisin B1 (FB1), cells were seeded out the day before treatment (Table 45). According to Merrill et al., the IC_{50} of FB1 for CerS is around 0.1 µM (Merrill et al., 1993b). Cells were incubated with 5 µM FB1 in 9 ml normal culture medium per 9 cm plate. Cells were incubated at 37 °C for 2 d before analysing the beta-glucosidase activity (2.5.8.2).

Table 45: Cell numbers seeded for Fumunisin B1 treatment

Cell line	Cell number per 9 cm dish
hFB	$2x10^6$

2.5.11 Lipid-BSA complexes

2.5.11.1 Preparation of lipid-BSA complexes by sonication

A 4 mg/ml BSA solution was prepared from a 1 M BSA stock in PBS (pH 7.4). The lipid stocks (Table 46) were diluted in the 4 mg/ml BSA solution to the desired concentration. Lipid-BSA complexes were produced by sonicating for 2 min (Branson Sonifier), resulting in a milky suspension. No precipitate was visible.

Table 46: Lipids used for analysis

Lipid	Stock (mM) in DMSO	Company	Catalogue #
Sphingosine	66.3	Sigma	1802
Sphinganine	66.3	Avanti Polar Lipids	860498P

FTY720	29.07	Sigma	SML0700
Sphingosine-1-phosphate	20	Avanti Polar Lipids	860492P
Ceramide	8.83	Matreya LLC	1832
Glucosylceramide	6.16	Matreya LLC	1057
Carnitine	31.25	Avanti Polar Lipids	870851P

2.5.11.2 Treatment of cells with lipid-BSA complexes

Cells were seeded out the day before treatment with sphingoid bases. The lipid-BSA complexes were diluted in 9 ml cell culture medium containing only 1% FCS in the desired concentration per 9 cm dish and incubated at 37 °C for 4.5 h. Afterwards, cells were harvested (2.5.2) und subjected to the beta-glucosidase activity assay (2.5.8.2).

Table 47: Cell numbers seeded for lipid-BSA treatment

Cell line	Cell number per 9 cm dish
CHO #A8A11	$3x10^6$
mEF	$1.2x10^6$

2.5.11.3 Treatment of protein lysates with lipid-BSA complexes

Hypotonic lysates from CHO cells or bacterial cells expressing mGBA1-HA and mGBA2-HA or mGBA2-His, respectively, were prepared in tubes (Table 48) and incubated with a serial dilution of 10x concentrated stocks (1x final) of lipid-BSA complexes at RT for 1 h prior to analysis of beta-glucosidase activity (2.5.8.2).

Table 48: Pipetting scheme for assay with lipid-BSA complexes

Assay approach per tube	Assay approach per well (96-well plate)	Assay approach per well (384-well plate)
72 µl hypotonic protein lysate	90 µl pH buffer	25 µl approach from 96-well plate
8 µl 10x concentrated lipid-BSA stock	20 µl protein sample containing lipid-BSA complexes	(25 µM CBE final and 8.3 µM NB-DNJ final)

	11 µl of lipid-BSA complex stocks 9 µl 433 µM CBE (30 µM final) or 144 µM NB-DNJ (10 µM final) ad 130 µl with hypotonic buffer	5 µl 10 mM 4-MUG

2.5.11.4 Fluorometric pH measurements

2.5.11.4.1 Cell preparation

To study the intracellular pH, human dermal fibroblasts from control and type I *Gaucher* patients (hFB 9 and hFB 11, respectively, Table 8) were trypsinised, harvested, counted, and $3x10^4$ – $7.3x10^4$ cells/50 µl were washed twice with PBS and re-suspended in 450 µl TYH buffer containing 5 mM HEPES/NaOH, pH 7.4 (Table 49).

2.5.11.4.2 Buffers and solutions for BCECF measurements

TYH buffers were prepared according to Table 49 and the osmolarity was determined in a 50 µl buffer sample after the pH was adjusted using a cryoscopic osmometer (Osmomat 030, Gonotec). The osmolarity of all buffers should be around 290 – 310 mOsmol. From the two strongly buffered TYH buffers of pH 6.2 (50 mM MES) and 6.8 (50 mM HEPES), five different buffers were prepared with pH values ranging from 6.18 – 7.75 (pH 6.18 and 6.48: MES, pH 6.81, 7.56, and 7.76: HEPES) by titration with NaOH. To determine the final pH value (pH_e) in each well, the weakly buffered TYH buffer (5 mM HEPES, pH 7.4) was mixed with each of the five strongly buffered TYH buffers in a ratio of 1:5 and the pH was determined using a pH-meter (Table 50).

Table 49: TYH buffer

TYH buffer	5 mM HEPES	50 mM HEPES	50 mM MES	Stock
NaCl	137.5 mM	97.5 mM	97.5 mM	5 M
KCl	0.75 mM	0.75 mM	0.75 mM	1 M
$CaCl_2$	2 mM	2 mM	2 mM	1 M
KH_2PO_4	1.2 mM	1.2 mM	1.2 mM	200 mM

$MgSO_4$	1 mM	1 mM	1 mM	1 M
Glucose	5.6 mM	5.6 mM	5.6 mM	-
HEPES/MES	5 mM	50 mM	50 mM	-
Sodium pyruvate	0.5 mM	0.5 mM	0.5 mM	-
L-Lactate	10 MM	10 MM	10 MM	-
	pH 7.4 /w NaOH	pH 6.8	pH 6.2	

Table 50: pH values of pH_e buffers

pH of pH_e buffer before mixing	pH of pH_e buffer after mixing
6.18	6.24
6.48	6.52
6.81	6.79
7.56	7.55
7.76	7.75

2.5.11.4.3 Loading of cells with BCECF

Cells were loaded with BCECF-AM according to Table 51 and incubated at RT in the dark for 10 min. Afterwards, remaining BCECF-AM was removed by washing twice with TYH buffer (5 mM HEPES, pH 7.4) and centrifuging at 700 x g for 5 min.

Table 51: Pipetting scheme for BCECF loading

BCECF loading	Stock
Cell suspension ($3x10^4$ – $7.3x10^4$ cells/50 µl)	-
0.05% Pluronic	10% (w/v)
10 µM BCECF-AM	2 mM
3 mM Probenizid	300 mM

2.5.11.4.4 Determining the intracellular pH in human dermal fibroblasts

One well of a 96-well flat bottom plate (Greiner) contained 50 µl cell suspension with $3x10^4$ – $7.3x10^4$ cells. To lyse the cells, Triton X-100 was prepared as a 6-fold stock solution (0.3% Triton X-100, 0.5% final) in five TYH ("pH_e") buffers with different pH values (pH 6.18 to 7.76) according to Table 50 and Table 52. First, the baseline was measured at 29 °C with an excitation wavelength of 440-10 nm and 485 nm for two cycles and the emission was detected at 520 nm. Next, 250 µl lysis/pH_e buffer (Table 52) were added and the change in BCECF fluorescence was measured over eight cycles (Table 53). To determine pH_i in fibroblasts from control and type I *Gaucher* patients (2.5.11.4.1), the "null-point" method was applied. The method is described in detail in passage 3.8.

Table 52: Buffers used for BCECF measurements

Lysis/pH_e buffer	Stock
TYH buffer (50 mM HEPES or MES, pH 6.32 – 7.73)	-
0.3% (w/v) Triton X-100	5%

Table 53: Fluostar plate mode settings for BCECF measurements

No. of cycles	10
Cycle time (s)	55
No. of flashes per well	100

2.5.12 Ultracentrifugation of protein lysates

To separate proteins into a membrane-bound and soluble fraction, hypotonic protein lysates (2.5.2) were transferred into plastic centrifugation vials suited for the TLA 100 rotor of Optima XP Ultracentrifuge (Beckman Coulter) and ultracentrifuged for 30 min at 70,000 rpm and 4 °C. Supernatants were transferred to new tubes, whereas the pellets were solubilised in the initial amount of hypotonic buffer or a reduced volume to concentrate the samples. Solubilised pellets were also transferred to new tubes and sonicated (Branson Sonifier) until the sample appeared homogenous. The presence

of GBA2 was analysed either by Western blot (2.5.5) or by the fluorescence-based GBA activity assay (2.5.8.2).

2.6 Lipid analysis

2.6.1 Non-fluorescent lipid analysis using thin layer chromatography

2.6.1.1 General glycosphingolipid extraction from cells

Per sample, cells from 6-8 confluent 9 cm dishes were harvested as previously described in 2.5.2., frozen in liquid nitrogen, and stored at -80 °C until further usage. Then, cells were thawed on ice, re-suspended in 1 ml ddH_2O and sonicated 3x for 30 sec in ice-cold water using a Branson Sonifier. The protein concentration was determined by a BCA test (2.5.2.2). 2 ml methanol were added, and the mix was vortexed and sonicated in a water bath for 2 min. Lipids were extracted by adding 2 ml methanol and 3 ml “ExMi” (chloroform/methanol/ddH_2O in a ratio of 10:5:1, v/v/v) and shaking in a 37 °C waterbath overnight. On the next day, the samples were centrifuged at 2,000 rpm for 10 min and the supernatant containing the lipids was filtered through a 230 mm long Pasteur glass pipette filled with glass fibre wool (Macherey-Nagel). The flow-through containing the extracted lipids was collected in a new tube. The pellet was re-suspended in 2 ml chloroform/methanol in a ratio of 1:1 (v/v), vortexed, sonicated for 5 min, and also filtered through the glass wool. Both flow-throughs containing the extracted lipids were pooled and transferred to a new tube.

2.6.1.2 General glycosphingolipid extraction from mouse tissues

To isolate lipids from spleens of control, GBA2-deficient and GBA1/GBA2-deficient mice, the wet weight of all tissues was determined before freezing and lyophilisation. All following steps were carried out in glass tubes. 1 ml ddH_2O was added per tissue for homogenisation using a Teflon douncer. The glass vials were then covered with a filter paper and subjected to lyophilisation for three days. Next, the dry weight of the samples was determined. The dried tissue powder was then solubilised in 1 ml ddH_2O, vortexed, and lipid extraction was carried out three times on three consecutive days: (i) 4 ml methanol and 3 ml “ExMi” (chloroform/methanol/ddH_2O in a ratio of 10:5:1, v/v/v), (ii) 5 ml chloroform/methanol in a ratio of 1:1 (v/v), or (iii) 5 ml chloroform/methanol in a ratio of 2:1 (v/v) were added and lipids were extracted by shaking in a 37 °C waterbath overnight. On the next day, the samples were centrifuged at maximal speed for 5 min and the supernatant containing the lipids was filtered

through a 230 mm long Pasteur glass pipette filled with glass fibre wool (Macherey-Nagel). The flow-through containing the extracted lipids was collected in a new tube and the solvents were evaporated under a constant stream of nitrogen.

2.6.1.3 Alkaline hydrolysis of phospholipids

Phospholipids were removed by alkaline hydrolysis with 4 M NaOH (125 µM final) in a shaking water bath at 37 °C for 2 h. The reaction was terminated by addition of 10 µl glacial acid and the liquids were evaporated using nitrogen.

2.6.1.4 Reversed-phase chromatography

Salts were removed using RP-18 columns (reversed phase material with 18 C atoms side-chains). Here, dried lipids were re-suspended in 1 ml 300 mM aqueous ammonium acetate by vortexing and directly loaded to the columns. Remaining lipids were washed off of the tube by addition of 1 ml 200 mM ammonium acetate in methanol/ddH_2O in a ratio of 1:1 (v/v) and also applied to the column. Salts and other water-soluble substances were washed from the column by addition of 6 ml ddH_2O, whereas lipids were extracted by adding 600 µl methanol and, subsequently, 8x1 ml chloroform/methanol in a ratio of 1:1 (v/v) to the column. The elution was collected in a new tube.

2.6.1.5 Thin layer chromatography and general lipid visualisation

For cell samples, lipids corresponding to 1-2 mg total protein and for mouse spleen samples, lipids corresponding to 15 mg dry weight were applied to pre-washed silica gel 60 plates (stationary phase, Merck, Darmstadt, Germany) and analysed by thin layer chromatography (TLC) using $CHCl_3$/MeOH/ddH_2O in a ratio of 70:30:5 (v/v/v) as liquid phase. After chromatography, lipids were visualised using a mixture of $CuSO_4$-pentahydrate and phosphoric acid and were baked at 180 °C (Yao 1985). To determine the amount of GlcCer present, the signal intensity of a serial dilution of purified galactosylceramide (galactose is a C-4 epimer of glucose) was analysed using a Densitometer and compared to the GlcCer signals.

2.6.2 Fluorescent clickGlcCer lipid analysis using thin layer chromatography

Besides visualisation of clickGlcCer in human dermal fibroblasts (2.5.7.5), the fate of clickGlcCer was also studied by TLC. As previously described in 2.5.7.1, $4x10^4$ cells were seeded per well on a 24-well plate directly to the plastic surface. After pulsing

and chasing of clickGlcCer, cells were washed once with PBS to remove residual clickGlcCer. 1 ml methanol/chloroform in a ratio of 5:1 was applied to the cells and the culture dish was swirled once before the solvent was transferred to a 1.5 ml (safe-lock) Eppendorf tube (method also described in Thiele et al. (Thiele et al., 2012)). The solvent/lipid mix was centrifuged at full speed and RT for 2 min, resulting in sedimentation of a whitish protein pellet from the solution. The supernatant containing the lipids was transferred to a 2 ml (safe-lock) Eppendorf tube and 350 µl chloroform and 400 µl ddH_2O were added. Everything was mixed vigorously by hand and centrifuged at full speed and RT for 2 min to achieve phase separation. The lower chloroform phase containing the lipids was transferred to a new 1.5 ml (safe-lock) Eppendorf tube and the solvent was evaporated using a speed-vac centrifuge. Lipids were re-suspended in 40 µl chloroform, vortexed for 5 min, and sonicated in a water bath for 5 min. After incubating at RT for 15 min, 20 µl of the lipids were transferred to a new 1.5 ml Eppendorf tube, while the remaining 20 µl were frozen to -20 °C. 30 µl click-reaction mix (Table 54) were added per sample, briefly spun down, and incubated for 2-3 h at 43 °C. As size standard, alkyne derivatives of ceramide, glucosylceramide, sphinganine, triacylglycerol, diacylglycerol, and palmitate were also clicked using the same click-reaction mix. The TLC chamber was pre-incubated with the first mobile phase (chloroform/methanol/ddH_2O in a ratio of 65/25/4) for at least 30 min whilst 30 µl of the 50 µl of each sample were applied onto a silica gel 60 plate (stationary phase, 20x20 cm, Millipore) with a glass capillary. The click-reacted standards were diluted 1:10 in chloroform and around 10 µl were loaded (clickable standards were synthesised by Prof. C. Thiele, Biochemistry and Cell Biology of Lipids, LIMES, Bonn, Germany) (Thiele et al., 2012). TLC was performed in the first mobile phase up to a height of 12 cm (~30 min). Then, the silica plate was placed to a second TLC chamber and run chromatography was performed in a second mobile phase (hexane/ethyl acetate in a ratio of 1:1) until the solvent had reached the top of the plate (~40 min). TLCs were shortly soaked in 4% (v/v) *N,N*,-diisopropylethylamine in hexane before fluorescent images of the TLC plates were acquired using a 420 nm LED (Roithner Lasertechnik, Vienna, Austria) filtered through a coloured glass filter (HEBO V01, Hebo Spezialglas) for excitation and an EMCCD camera (Rolera-MGi Plus Fast 1394, Q-imaging), equipped with a 494/20 (channel for detection of the coumarin signal) and 572/28 (channel for detection and correction of background fluorescence) bandpass emission filters.

Table 54: Click-reaction mix for extracted alkynes

Click-reaction mix for extracted alkynes
850 µl Ethanol
250 µl of 10 mM [acetonitrile]$_4$ $CuBF_4$ in acetonitrile
10 µl of 44.5 mM (2 mg/ml) 3-azido-7-hydroxycoumarin in ethanol

2.6.3 Fluorescent alkyne lipid analysis using thin layer chromatography

This method has been described in great detail in Thiele et al. (Thiele et al., 2012). Briefly, lipids were extracted by methanol/chloroform in a ratio of 4:1. Dried lipids were re-dissolved in chloroform and 30 µl click-reaction mix (Table 54) was added. The click reaction was performed at 43 °C for 3 h. The click-reacted lipids were applied to TLC silica plates and separated in solvent 1 (chloroform/methanol/H_2O/acetic acid 65/25/4/1, $^2/_3$ of the plate) and subsequently in solvent 2 (hexane/ethyl acetate 1/1, whole plate). TLC analysis was performed as previously described in 2.6.2).

2.6.4 Extraction and quantification of sphingolipids using mass spectrometry

2.6.4.1 Isolation of lipids from fibroblasts for mass spectrometry

Human dermal fibroblasts were harvested as previously described in 2.5.2, frozen in liquid nitrogen, and stored at -80 °C until further usage. Cell samples were thawed on ice, lysed in hypotonic buffer as previously described in 2.5.2, and the protein concentration was determined by BCA test (2.5.2.2).

Further isolation of lipids was performed by Dr. Katharina vom Dorp, Institute of Molecular Physiology and Biotechnology of Plants, University of Bonn, Bonn, Germany.

500 µl chloroform/methanol/formic acid in a ratio of 1:1:0.1 (v/v/v) and 50 µl of internal standard mix (“Sphingomix”, personal communication with Dr. K. vom Dorp) were added per sample and mixed thoroughly. 250 µl of 1 M KCl/0.2 M H3PO4 were added, samples were vortexed, and centrifuges at 5,000 rpm for 3 min to obtain phase separation. The lower phase containing the lipids was transferred to a fresh glass vial and the remaining samples were re-extracted by again adding 500 µl of chloroform/methanol in a ratio of 2:1 (v/v). Samples were vortexed, centrifuged at

5,000 rpm for 3 min and the lower phase was transferred to the glass vial and combined with the previous extract. Solvents were evaporated under air flow and lipids were re-suspended in 500 µl of pure chloroform by vortexing.

2.6.4.2 Lipid purification using silica columns for mass spectrometry

Lipid purification was performed by Dr. Katharina vom Dorp, Institute of Molecular Physiology and Biotechnology of Plants, University of Bonn, Bonn, Germany.

Small silica columns (Strata-1-Silica, 55 µM, 70 Å containing 100 mg silica) were equilibrated by flushing with pure chloroform for three times. Afterwards, samples dissolved in pure chloroform were applied and non-polar lipids were eluted with three column volumes (CV) of pure chloroform. Medium-polar sphingolipids (LCBs, ceramides, hexosylceramides) were eluted with 3 CV of acetone/isopropanol in a ratio of 1:1 (v/v). Very polar sphingolipids (e.g. sphingomyelin) were eluted with 3 CV of pure methanol. The acetone/isopropanol fraction was dried under air flow and dissolved in 100 µl of Q-TOF solvent (chloroform/methanol/300 mM ammonium acetate in a ratio of 300:665:35, v/v/v) and subjected to mass spec analysis. Mass spec analysis was carried out as previously described in Ginkel et al. (Ginkel et al., 2012) and Raju et al. (Raju et al., 2015).

2.7 Animals

GBA1-deficient mice were generated as described in Enquist et al. (Enquist et al., 2006). Mice deficient for GBA2 were generated as mentioned in Yildiz et al. (Yildiz et al., 2006). All experiments performed with animals were in accordance with the relevant guidelines and regulations.

2.7.1 Injection mice with CBE

The injection of eight days old 6OlaHsd mice with 25 – 100 mg CBE/kg/day for 10 days was carried out in the lab of Prof. T. Futerman (Weizman Institute, Israel) as previously described in Klein et al. (Klein et al., 2016). Brains were dissected, frozen, and sent to our lab for further analysis.

2.7.2 Statistics

Data presented in this study represent the mean value with standard deviation from at least three independent experiments. Differences between samples were analysed

using Student's t-test or the analysis of variance (ANOVA) and the OriginPro software version 9.0. The N number represents the amount of animals or different cell lines if not stated otherwise.

3 Results

3.1 Assay to measure GBA1 and GBA2 activity

Studying the function of two enzymes that are ubiquitously expressed (Brady et al., 1965; Yildiz et al., 2006) and share the same substrate requires an assay that allows to discriminate between the activity of lysosomal GBA1 and non-lysosomal GBA2. In Körschen et al., we published an activity assay that allows to individually measure the activity of GBA1 and GBA2 using an artificial, water-soluble and GlcCer-like substrate called 4-Methylumbelliferyl beta-D-glucopyranoside or, in short 4-MUG (also see 2.5.8.2) (Körschen et al., 2013). In this assay, we made use of the differential activity of GBA1 and GBA2 at different pH values, which allows to distinguish between the two activities (Figure 8). GBA2 activity is sensitive to detergents (Körschen et al., 2013). Thus, pH profiles of the total beta-glucosidase activity were measured in hypotonic mouse tissue lysates. To further delineate the two activities, the assay was performed in the presence and absence of 25 µM CBE, a specific blocker for GBA1, and 8.3 µM NB-DNJ, a specific blocker for GBA2 (Ridley et al., 2013). Addition of NB-DNJ demonstrated that GBA1 represents the predominant beta-glucosidase activity at acidic pH values with a maximum at pH 4.25 (Figure 8, orange). Vice versa, addition of CBE revealed that GBA2 is active at rather neutral pH values with a maximum at pH 5.25 (Figure 8, green). Addition of both, CBE and NB-DNJ, completely blocked any beta-glucosidase activity. However, although the individual activities were highest at the particular pH optima, the remaining activity of the other enzyme at these values was still evident (Figure 8). Thus, the assay was performed at the pH optimum for each enzyme and in the presence of the specific blockers. Based on these results, we defined the activity of GBA1 as the CBE-blockable activity at pH 4 and the activity of GBA2 as the NB-DNJ-blockable activity at pH 6 (Figure 8).

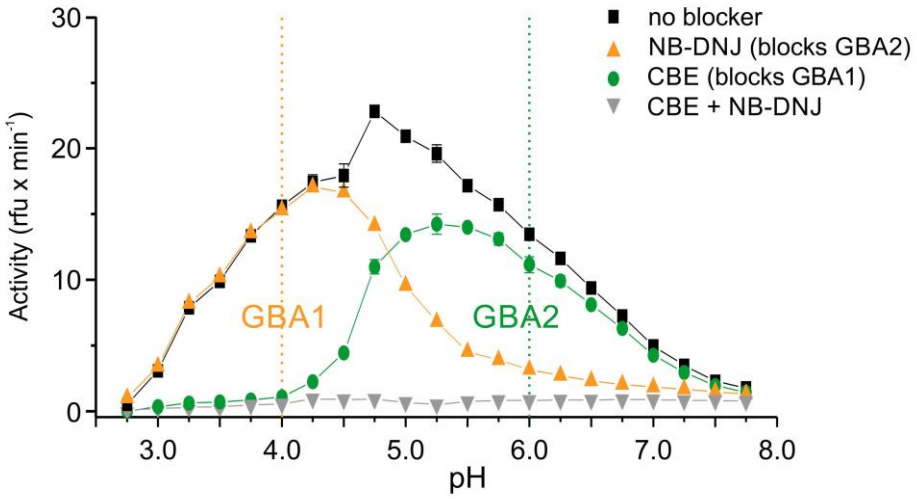

Figure 8: Beta-glucosidase activity in hypotonic mouse tissue lysates at different pH values. The beta-glucosidase activity was measured at different pH values using 1.67 mM 4-MUG. In the presence of 8.3 µM NB-DNJ, the GBA2-specific blocker, GBA1 activity was maximal at pH 4.25, whereas in presence of 25 µM CBE, the GBA1-specific blocker, GBA2 activity was maximal at pH 5.25. Thus, GBA1 activity was measured at pH 4 and GBA2 activity was determined at pH 6 in further assays. Data published in Körschen et al. 2013. CBE: Conduritol B epoxide, NB-DNJ: N-butyl-deoxynojirimycin, 4-MUG: 4-Methylumbelliferyl beta-D-glucopyranoside. Data are presented as mean ± SD. Representative plot of quadruples for n = 3 experiments.

3.2 GBA2 activity is reduced in embryonal fibroblasts from GBA1-deficient mice

GBA1 and GBA2 both are ubiquitously expressed and cleave the same substrate, GlcCer (Brady et al., 1965; Yildiz et al., 2006). The question arises why a cell expresses two enzymes that are spatially separated, while hydrolysing the same substrate? What is their specific function? Is their function mutually exclusive or do they interact with each other? The simplest way to address this question is to analyse the expression and activity of one enzyme in absence of the other.

First, the GBA2 activity was analysed in GBA1-deficient murine embryonal fibroblasts (Enquist et al., 2006; Körschen et al., 2013) (Figure 9a, b). GBA1 activity was absent, but, surprisingly, the GBA2 activity was also reduced to around 53% of the control (Figure 9a, b). Next, the reverse experiment was performed by analysing the GBA1 activity in hypotonic brain lysates from GBA2-deficient mice (Figure 9c, d). However, loss of GBA2 did not affect the activity of GBA1 (Figure 9c).

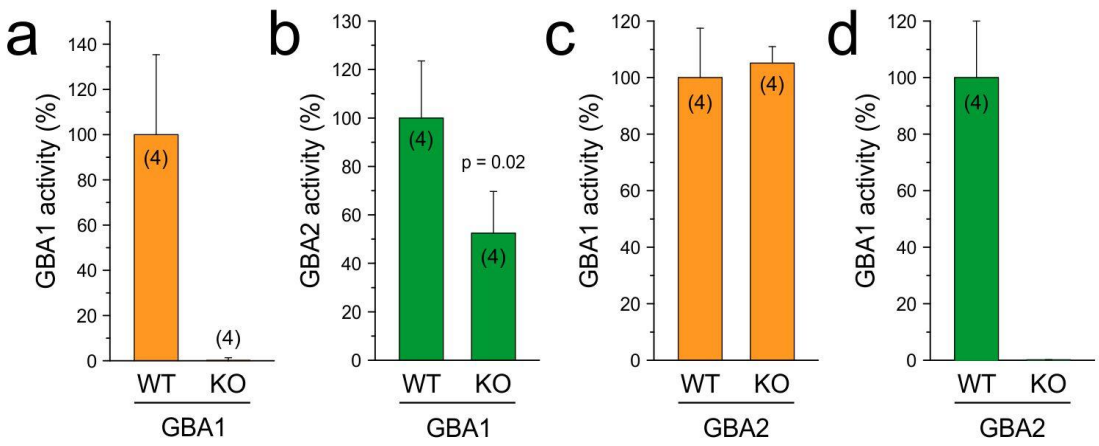

Figure 9: GBA2 activity is reduced in embryonal fibroblasts from GBA1-deficient mice. Analysis of the GBA1 and GBA2 activity in hypotonic lysates of wild-type (WT) and GBA1-deficient (knock-out, KO) embryonal fibroblasts in presence of 1.67 mM 4-MUG. **(a)** GBA1 activity was absent in hypotonic lysates of GBA1-deficient mouse embryonal fibroblasts compared to control cells. **(b)** GBA2 activity was reduced to 53% of control values in GBA1-deficient fibroblasts. **(c)** Vice versa, GBA1 activity remained unchanged in hypotonic brain lysates from GBA2-deficient mice **(d),** which lacked any GBA2 activity. 4-MUG: 4-Methylumbelliferyl beta-D-glucopyranoside. Data are presented as mean + SD. N numbers are indicated in brackets. The p value was determined using One-way ANOVA.

3.3 GBA2 activity is reduced in fibroblasts from *Gaucher* patients

GBA1-deficient mice represent the animal model for the most common lipid storage disorder in humans termed *Gaucher* disease (Farfel-Becker et al., 2011) (also see 1.1.4.1.2). To date, there is no genotype-phenotype relation for *Gaucher* disease. As previously mentioned, the variety of symptoms has been used to classify the disease into type I, II, and III *Gaucher* disease, where type I patients mainly show an enlargement of liver and spleen, type II patients are characterized by an early onset of the disease together with severe neurological defects, and type III patients show moderate neurological symptoms compared to type II patients (Grabowski, 2001). Thus, additional factors seem to determine the fate of a patient carrying a mutation in the *GBA1* gene (Vardi et al., 2016).

Since the GBA2 activity was reduced in embryonal fibroblasts from GBA1-deficient mice, we wondered whether GBA2 might be one of those “additional factors” that play a role in *Gaucher* disease. Thus, the GBA1 and GBA2 expression and activity were analysed in more detail using dermal fibroblasts from *Gaucher* patients with different mutations in the *GBA1* gene and different phenotypes of the disease (Figure 12 - Figure 14).

First, a protocol to analyse the mRNA expression in dermal fibroblasts from *Gaucher* patients, with various genetic backgrounds and phenotypes, and control patients was established using quantitative real-time PCR (qPCR). There are several DNA-binding dyes available for quantitative real-time polymerase chain reaction (qPCR). Here, SYBR Green was used (Biorad).

Amplicons for qPCR were designed on cDNA with a length of 75-200 base pairs (bp) since fragments shorter than 75 bp cannot be distinguished from primer dimers in the reaction and amplicons longer than 200 bp are amplified less efficiently (Real-Time PCR Applications Guide, Biorad) (Table 56). The template sequences did not contain repeats of more than four bases and the overall GC content was 50-60%. Most importantly, amplicons that span an intron were chosen to avoid the amplification of contaminating genomic DNA.

Primers for qPCR were 20 nucleotides (nt) long, had a GC content of 50-60% (Table 15), and have a similiar melting temperature (T_M) (between 50-65 °C). Repeats of Gs and Cs longer than three bases and repeats of matching bases (e.g. AA and TT) were avoided. The specificity of the primers and the amplicon was checked using the Basic Local Alignment Search Tool (BLAST, http://blast.ncbi.nlm.nih.gov/) or BLAT (http://genome.ucsc.edu/cgi-bin/hgBlat) because some DNA sequences appear multiple times in the genome, especially when they are rather short. To normalise the expression levels of the genes of interest (GOIs, GBA1 and GBA2, Table 55), suitable housekeeping genes (HKGs) were selected (hB2m and hAlas1, Table 55). A housekeeper is a reference gene, whose expression level is constant across all tested samples. Normally, genes that are commonly expressed and maintain basic cellular functions are used. The same rules for amplicon and primer design were applied when choosing suitable HKGs. As a reference, one highly expressed HKG and one with rather low expression was chosen.

Table 55: Human genes of interest (GOIs) and housekeeping genes (HKGs) chosen for qPCR analysis

Gene	Gene product	Reference
hGBA1	Acid beta-glucosidase	NM_0010057
hGBA2	Non-lysosomal beta-glucosidase	NM_020944

hB2m	Beta-2-microglobulin	NM_004048
hAlas1	Aminolevulinic acid synthase 1	NM_199166

Table 56: Amplicon sizes of human primer pairs selected for qPCR

Gene	Primer pair	Expected amplicon size (bp)
hGBA1	C1796/97	249
hGBA1	C1798/99	244
hGBA2	C1800/01	185
hGBA2	C1802/03	220
hB2m	C1818/19	216
hB2m	C1820/21	277
hAlas1	C1822/23	135
hAlas1	C1824/25	123

bp: Base pairs

To test whether primers designed for qPCR amplify the sequence of interest, a conventional polymerase chain reaction (PCR) was performed (2.4.2). For human primers (Table 15), cDNA obtained from a fibroblast cell line from a control patient (hFB 8, Table 8) was used. All amplicons (Figure 10) had the expected sizes (Table 56), whereas primer pairs C1798/99, C1802/03, and C1824/25 showed additional PCR products (Figure 10).

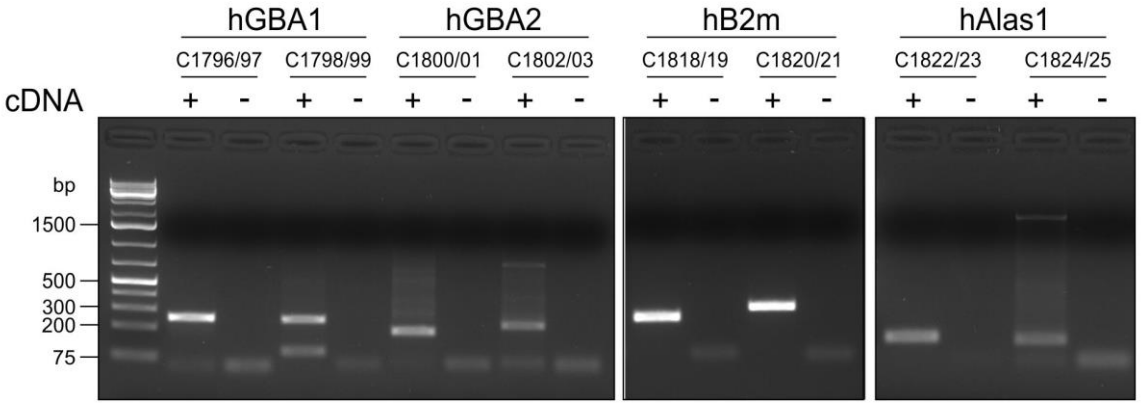

Figure 10: Analysis of the amplicons of human qPCR primers and control cDNA from human dermal fibroblast line hFB 8. 5 µl of the PCR approach were loaded to a 2% agarose gel and the fragments were analysed under a UV lamp. All human amplicons had the expected sizes, whereas human primer pairs C1798/99, C1802/03, and C1824/25 showed additional PCR products. bp: base pairs.

To reliably analyse the data obtained from qPCR, a primer efficiency test (PET) was performed (2.4.6.5). In a perfect PCR cycle, the amount of DNA should double and the primer efficiency would be 100%. The PET was performed for two primer pairs per GOI (hGBA1, hGBA2) and HEK (hB2m, hAlas1) in duplets. The slope obtained from plotting the individual C_T values (the PCR cycle at which the fluorescent signal reaches the threshold line) against the logarithm of the cDNA dilutions was used to calculate the primer efficiency (E = 10-1/slope). Primers used for qPCR showed at least 90% and maximal 105% efficiency (Table 57 and Table 60).

Exemplarily, the C_T values of hGBA2 primer pair C1800/01 were plotted against the logarithm of the cDNA dilution in Figure 11. Here, the primer efficiency is 103% (Table 57). Based on these results and those obtained from the remaining primer pairs, the following human primers were used for subsequent experiments: hGBA1: C1798/99, hGBA2: C1800/01, hB2m: C1818/19, and hAlas1: C1824/25. The PCR products generated by these primer pairs were send for sequencing and, thus, verified to be the right amplicons (data not shown).

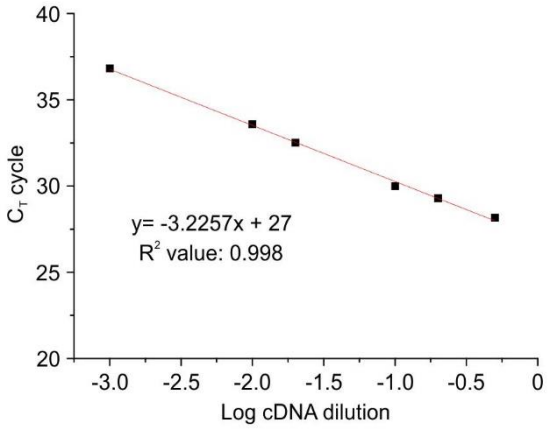

Figure 11: Primer efficiency test. The C_T values of hGBA2 primer pair C1800/01 were plotted against the logarithm of the different cDNA dilutions.

Table 57: Human qPCR primer efficiencies

Gene	Primer numbers	Slope	R^2 value	Efficiency (%)
hGBA1	C1796/97	-3.0654	0.9993	112
hGBA1	C1798/99	-3.1823	0.9971	106
hGBA2	C1800/01	-3.2557	0.998	103
hGBA2	C1802/03	-2.5901	0.9869	143
hB2m	C1818/19	-3.5344	0.9973	92
hB2m	C1820/21	-3.5809	0.9965	90
hAlas1	C1822/23	-3.4814	0.9978	94
hAlas1	C1824/25	-3.3301	0.9992	100

qPCR was performed for the GOIs hGBA1 and hGBA2, and the HKGs hB2m and hAlas1 and human dermal fibroblast samples as templates (see Table 8, Table 55, 2.4.6.6). For both, GBA1 and GBA2, there was no difference between the relative mRNA expression in control and *Gaucher* fibroblasts (Figure 12).

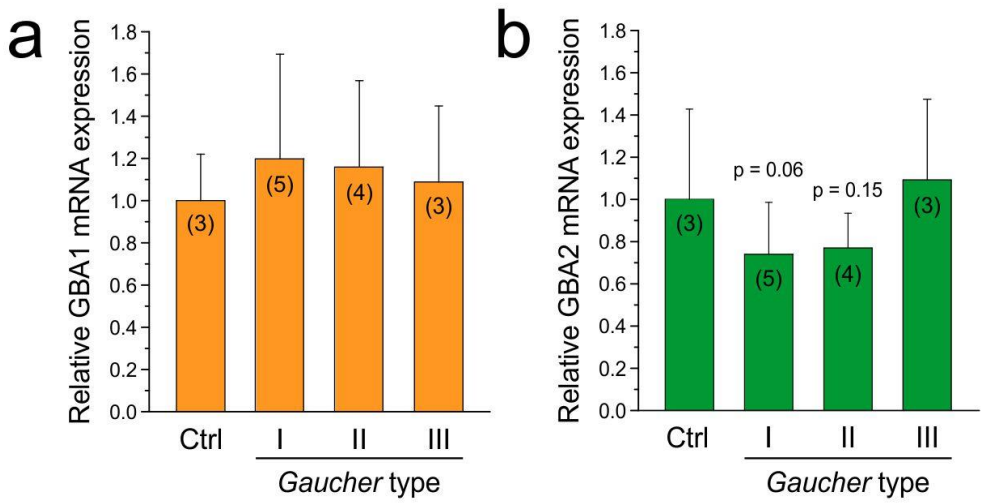

Figure 12: GBA1 and GBA2 mRNA expression in dermal fibroblasts from *Gaucher* patients. Analysis of GBA1 and GBA2 mRNA levels in control (Ctrl) and *Gaucher* fibroblasts using qPCR. Neither **(a)** GBA1 nor **(b)** GBA2 mRNA expression were changed between control and *Gaucher* fibroblasts. Data are presented as mean + SD; the different types of *Gaucher* disease are indicated. N numbers are indicated in brackets.

Secondly, the GBA1 and GBA2 protein expression was analysed in dermal fibroblasts from *Gaucher* and control patients by Western blot analysis (Figure 13). GBA1 expression was significantly reduced in *Gaucher* fibroblasts with the lowest expression in type II samples (Figure 13b). However, GBA2 protein expression remained unchanged in control and *Gaucher* fibroblasts (Figure 13c).

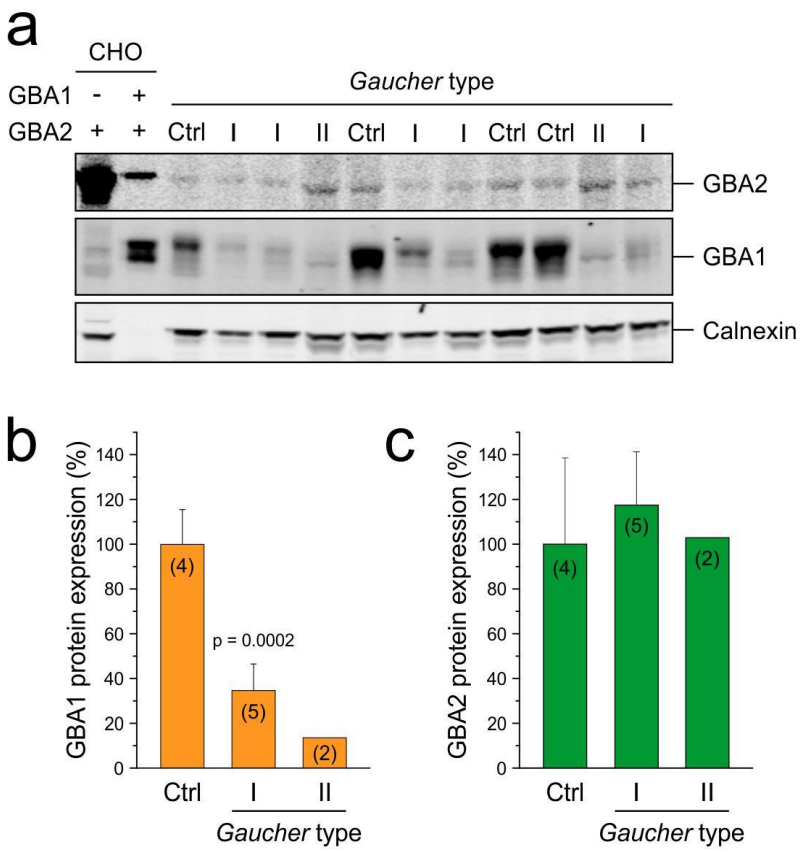

Figure 13: Western blot analysis of GBA1 and GBA2 protein expression in dermal fibroblasts from *Gaucher* and control patients. Hypotonic protein lysates from control (Ctrl) and *Gaucher* fibroblasts were labelled using antibodies against GBA1 (Sigma) and GBA2 (monoclonal antibody mix 2F8/4A12). CHO cells stably over-expressing mGBA1-HA and/or mGBA2-HA were used as positive controls. Calnexin was used as a loading control. **(a)** GBA1 expression was significantly reduced in *Gaucher* fibroblasts with the lowest expression in type II samples. GBA2 protein expression remained unchanged in control and *Gaucher* fibroblasts. **(b)** Quantification of GBA1 protein levels normalised to calnexin. **(c)** same as **(b)** for GBA2. Data are presented as mean + SD. The different types of *Gaucher* disease are indicated. N numbers are shown in brackets. The p value was determined using One-way ANOVA.

Finally, the GBA1 and GBA2 activity was analysed in *Gaucher* and control fibroblasts using our activity assay (Figure 14). GBA1 activity was barely detectable in all patient fibroblast lines, with remaining activities of 8%, 2.6%, and 5.6% for type I, II, and III, respectively (Figure 14a). Interestingly, GBA2 activity was also reduced to around 60% in all *Gaucher* types compared to the controls (Figure 14b). Thus, these data underline the finding from GBA1-deficient fibroblasts. However, since the GBA2 activity was evenly reduced in type I, II, and III patients, GBA2 does not play a role in genotype-phenotype correlation of *Gaucher* disease.

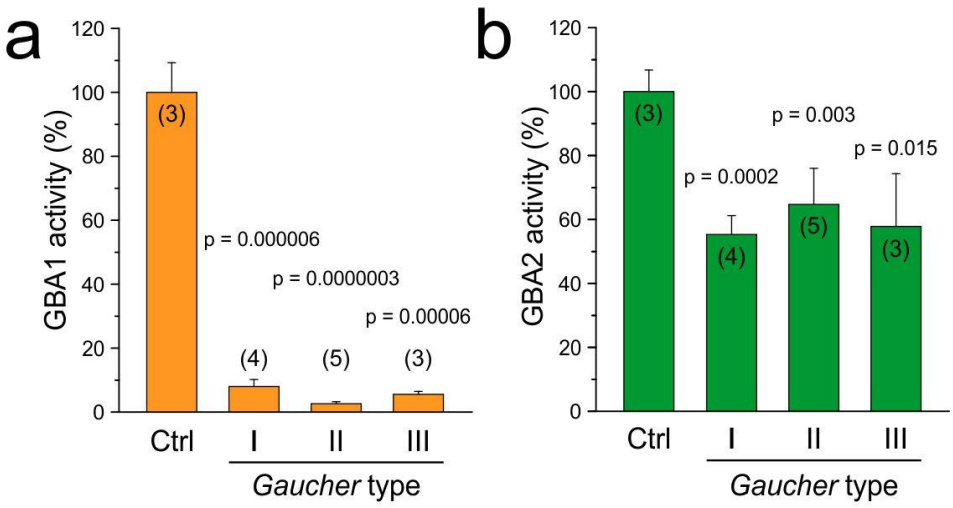

Figure 14: GBA1 and GBA2 activity in Gaucher and control fibroblasts. Analysis of the GBA1 and GBA2 activity in hypotonic lysates of control (Ctrl) and Gaucher fibroblasts in presence of 1.67 mM 4-MUG. **(a)** GBA1 activity was barely detectable in all patient fibroblast lines, with remaining activities of 8%, 2.6%, and 5.6% for type I, II, and III, respectively. **(b)** The GBA2 activity was also reduced to around 60% in all Gaucher types compared to the controls. 4-MUG: 4-Methylumbelliferyl beta-D-glucopyranoside. Data are presented as mean + SD. The different types of Gaucher disease are indicated. N numbers are shown in brackets. P values were determined using One-way ANOVA.

3.4 GBA2 activity is reduced in CRISPR/Cas9-generated GBA1-deficient cells

3.4.1 GBA2 activity in control and GBA1-deficient HAP1 cells

To analyse the GBA1-dependent regulation of GBA2 activity in more detail, independent from secondary effects that might occur in patient samples, GBA1 and GBA2 activity were also studied in human fibroblast-like cells, where GBA1 or GBA2 was deleted via CRISPR/Cas9 (Figure 15). The first GBA1-deficient HAP1 cell line (HZGHC002786c001, abbreviated #001) contains a 479 bp insertion in exon 6 of the *GBA1* gene and the second GBA1-deficient HAP1 cell line (HZGHC002786c010, abbreviated #010) contains a 1 bp insertion in exon 6, both resulting in a frame shift and, therefore, in gene silencing. GBA1 activity was completely absent in both GBA1-deficient HAP1 cell lines compared to the control (Figure 15a). In fact, the GBA2 activity was again decreased to around 64% and 71%, respectively (Figure 15b). The experiment was also performed vice versa by analysing the GBA1 activity in GBA2-deficient HAP1 cells (Figure 15c, d). In the first GBA2-deficient HAP1 cell line (HZGHC004109c001, abbreviated #001), 5 bp were deleted in exon 1 of the human *GBA2* gene, whereas the second GBA2-deficient HAP1 cell line (HZGHC004109c011,

abbreviated #011) contains a 1 bp insertion in exon 1, both resulting in a frameshift and, therefore, in gene silencing. Similar to the results obtained from brain lysates from GBA2-deficient mice (Figure 9c), GBA1 activity remained unchanged in control and GBA2-deficient HAP1 cells (Figure 15c).

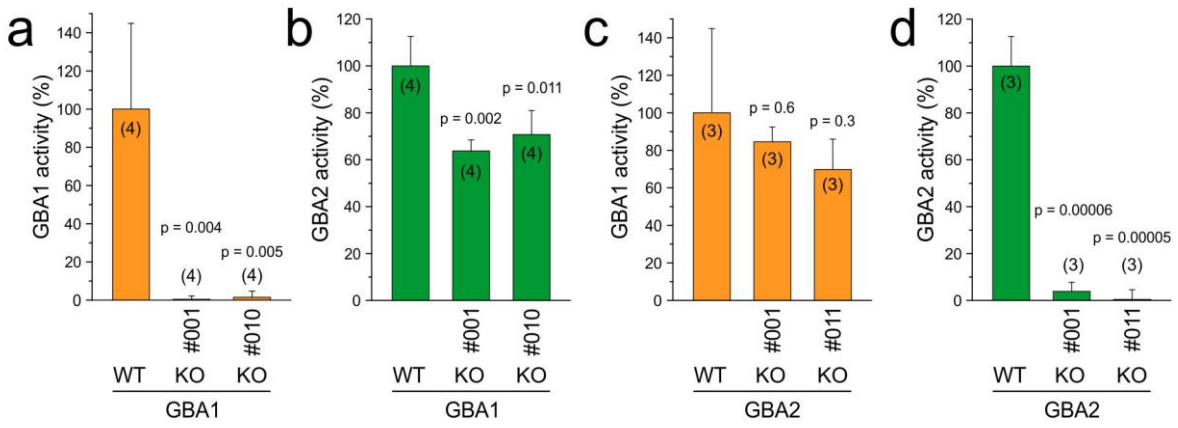

Figure 15: GBA1 and GBA2 activity in CRISPR/Cas9-generated GBA1-deficient HAP1 cells. Analysis of the GBA1 and GBA2 activity in hypotonic lysates of control (Ctrl) and CRISPR/Cas9-generated HAP1 cells deficient for GBA1 in presence of 1.67 mM 4-MUG. **(a)** GBA1 activity was absent in both GBA1-deficient HAP1 cell lines compared to the control. **(b)** GBA2 activity was decreased to around 64% and 71% compared to control cells, respectively. **(c)** Vice versa, GBA1 activity remained unchanged in control and GBA2-deficient HAP1 cells **(d),** showing no GBA2 activity. GBA1-deficient HAP1 cell lines: HZGHC002786c001 and HZGHC002786c010, GBA2-deficient cell lines: HZGHC004109c001 and HZGHC004109c011. 4-MUG: 4-Methylumbelliferyl beta-D-glucopyranoside. Data are presented as mean + SD. N numbers are indicated in brackets. P values were determined using One-way ANOVA.

3.4.2 GBA2 activity in control and GBA1-deficient HEK293 cells

Lastly, the GBA1-dependent regulation of GBA2 activity was also verified in HEK293 cells, a widely used human-derived cell model (Graham et al., 1977). I compared the GBA1 and GBA2 activity in control cells and HEK293 cells deficient for GBA1, generated by the CRISPR/Cas9 system (obtained from C. Yaacobi, Futerman lab, Weizmann Institute, Israel). Again, the GBA2 activity was reduced to around 37% of the control (Figure 16).

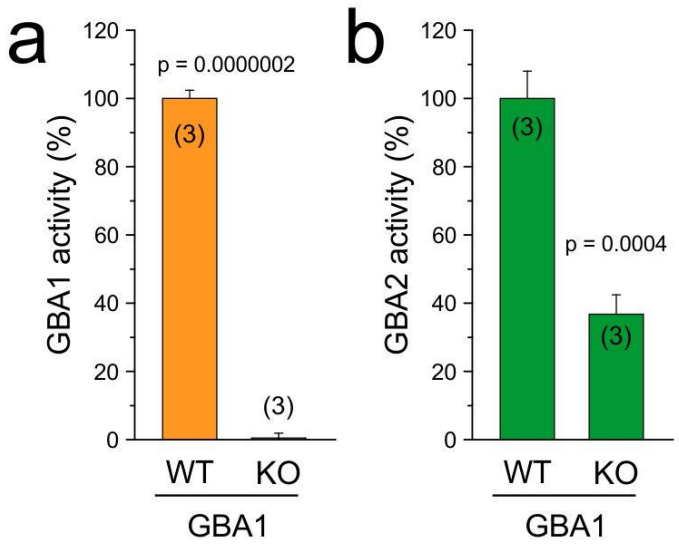

Figure 16: GBA1 and GBA2 activity in CRISPR/Cas9-generated GBA1-deficient HEK293 cells. Analysis of the GBA1 and GBA2 activity in hypotonic lysates of wild-type (WT) and CRISPR/Cas9-generated HEK293 cells deficient for GBA1 (knockout, KO) in presence of 1.67 mM 4-MUG. **(a)** GBA1 activity was absent in GBA1-deficient HEK293 cells compared to the control, **(b)** resulting in a reduced GBA2 activity of only 37%. 4-MUG: 4-Methylumbelliferyl beta-D-glucopyranoside. Data are presented as mean + SD. N numbers are indicated in brackets. P values were determined using One-way ANOVA.

3.5 GBA2 activity depends on GBA1 activity

3.5.1 GBA2 activity is reduced in CBE-treated cells

To get a more mechanistic insight, we analysed whether it is the loss of GBA1 expression and/or activity that reduces GBA2 activity. Here, a pharmacologic approach was applied. CBE inhibits GBA1 with an IC_{50} value of 2.7 ± 0.3 µM in hypotonic testis lysates, while GBA2 activity is reduced at higher CBE concentrations (starting at around 100 µM) (Körschen et al., 2013) (Figure 17a). Vice versa, NB-DNJ inhibits GBA2 with an IC_{50} value of 19.2 ± 0.4 nM without blocking GBA1 activity (Körschen et al., 2013) (Figure 17b).

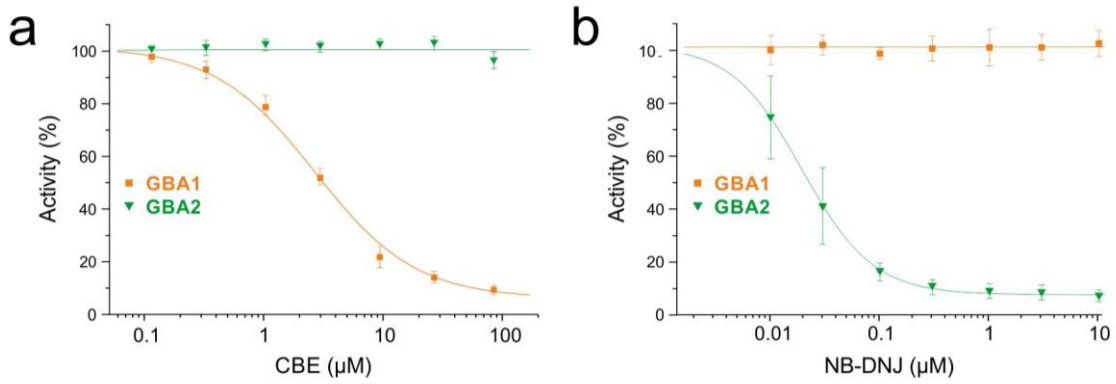

Figure 17: Dose-response relationship of CBE and NB-DNJ for GBA1 and GBA2 activity in hypotonic testis lysates. Analysis of the GBA1 and GBA2 activity in hypotonic testis lysates from control mice in the presence of 0.1-100 µM CBE or 0.01-10 µM NB-DNJ and 1.67 mM 4-MUG. **(a)** CBE inhibits GBA1 with an IC_{50} value of 2.7 ± 0.3 µM in hypotonic testis lysates, while GBA2 activity is reduced at higher CBE concentrations. **(b)** NB-DNJ inhibits GBA2 with an IC_{50} value of 19.2 ± 0.4 nM without blocking GBA1 activity. Data published in Körschen et al., 2013. CBE: Conduritol B epoxide, NB-DNJ: N-butyl-deoxynojirimycin, 4-MUG: 4-Methylumbelliferyl beta-D-glucopyranoside. Data are presented as mean ± SD. Representative plots of quadruples for n = 3 experiments.

To block GBA1 activity without affecting GBA2 activity, control fibroblasts were treated with 25 µM CBE for 48 h (Figure 18a, b). As shown in Figure 18a, GBA1 activity was dramatically reduced in CBE-treated cells compared to the non-treated controls (Figure 18a). In line with the findings from *Gaucher* and GBA1-deficient fibroblasts, GBA2 activity in CBE-treated cells was reduced to about 39% of the activity in non-treated control cells (Figure 18b). These results demonstrate that blocking GBA1 activity is sufficient to reduce GBA2 activity.

This experimental paradigm was also tested in CHO control cells (Figure 18c, d) and cells stably over-expressing mGBA2 (#G4A11) (Figure 18e, f). Incubation with 25 µM CBE for 48 h completely abolished the endogenous GBA1 activity in CHO cells (Figure 18c, e). In line with the previous findings, the endogenous and over-expressed GBA2 activity was decreased to around 45% and 36% compared to non-treated controls, respectively (Figure 18d, f).

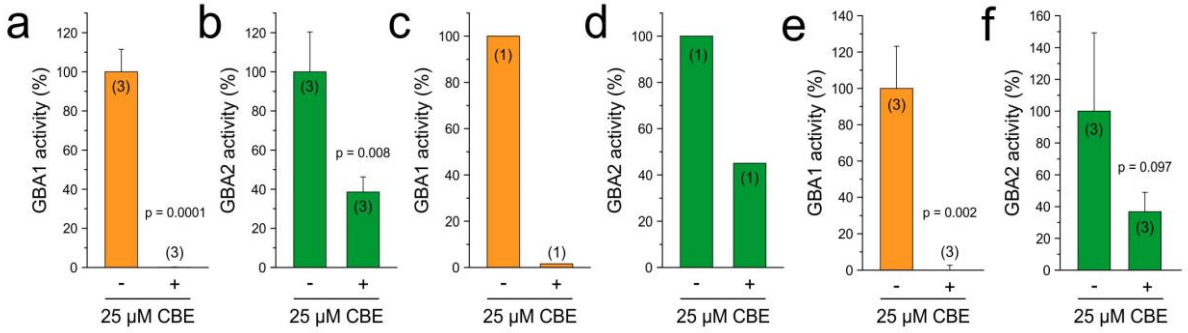

Figure 18: GBA2 activity in human fibroblasts and CHO cells treated with 25 µM CBE. Human dermal fibroblasts and CHO cells were treated with 25 µM CBE for 48 h to block GBA1 activity. Beta-glucosidase activities were analysed in hypotonic cell lysates in presence of 1.67 mM 4-MUG. **(a)** GBA1 activity was dramatically reduced in CBE-treated fibroblasts compared to the non-treated cells. **(b)** GBA2 activity in CBE-treated cells was reduced to about 39% of the activity in non-treated control cells. **(c)** + **(d)** and **(e)** + **(f)** same as **(a)** + **(b)** in CHO control cells and CHO cells stably over-expressing mGBA2. The GBA2 activity was reduced to around 45% and 36% compared to non-treated controls, respectively. CBE: Conduritol B epoxide, 4-MUG: 4-Methylumbelliferyl beta-D-glucopyranoside. Data are presented as mean + SD. N numbers are indicated in brackets. P values were determined using One-way ANOVA.

As a control, the experiment was performed vice versa in CHO cells stably over-expressing mGBA2 (#G4A11) and blocking its activity with 2 µM NB-DNJ for 48 h (Figure 19). Whereas the activity of GBA2 was completely abolished in NB-DNJ-treated cells (Figure 19b), GBA1 activity remained unchanged (Figure 19a).

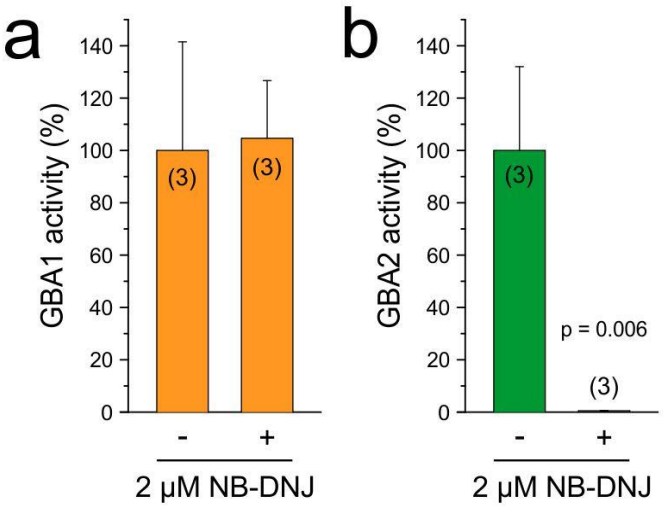

Figure 19: GBA1 activity in CHO cells stably over-expressing mGBA2 treated with 2 µM NB-DNJ. CHO cells stably over-expressing mGBA2 were treated with 2 µM NB-DNJ for 48 h to block GBA2 activity. The subsequent effect on the GBA1 and GBA2 activity was analysed in hypotonic cell lysates in presence of 1.67 mM 4-MUG. **(a)** GBA1 activity remained unchanged in cells treated with 2 µM NB-

DNJ **(d)** in absence of GBA2 activity. NB-DNJ: N-butyl-deoxynojirimycin, 4-MUG: 4-Methylumbelliferyl beta-D-glucopyranoside. Data are presented as mean + SD. N numbers are indicated in brackets. The p value was determined using One-way ANOVA.

To verify whether the pharmacological block of GBA1 activity does not affect GBA1 protein expression, Western blot analysis was performed. The GBA1-specific antibody recognises the human, but not the hamster protein. Thus, the cell model was switched from CHO to HEK293 cells. HEK293 cells transiently over-expressing mGBA2 and endogenously expressing GBA1 were incubated with 25 µM CBE for 48 h and, again, CBE treatment reduced GBA2 activity to about 46% of the activity in non-treated control cells (Figure 20b). The experiments were also performed vice versa in HEK293 cells over-expressing mGBA2 by blocking GBA2 activity with 2 µM NB-DNJ for 48 h before assessing the GBA1 and GBA2 activity (Figure 20c, d). GBA2 activity was absent in NB-DNJ-treated cells (Figure 20d), whereas GBA1 activity remained unchanged (Figure 20c). Similar to what has been observed for the other systems, GBA1 and GBA2 protein expression was not different between treated and non-treated cells (Figure 20e-h).

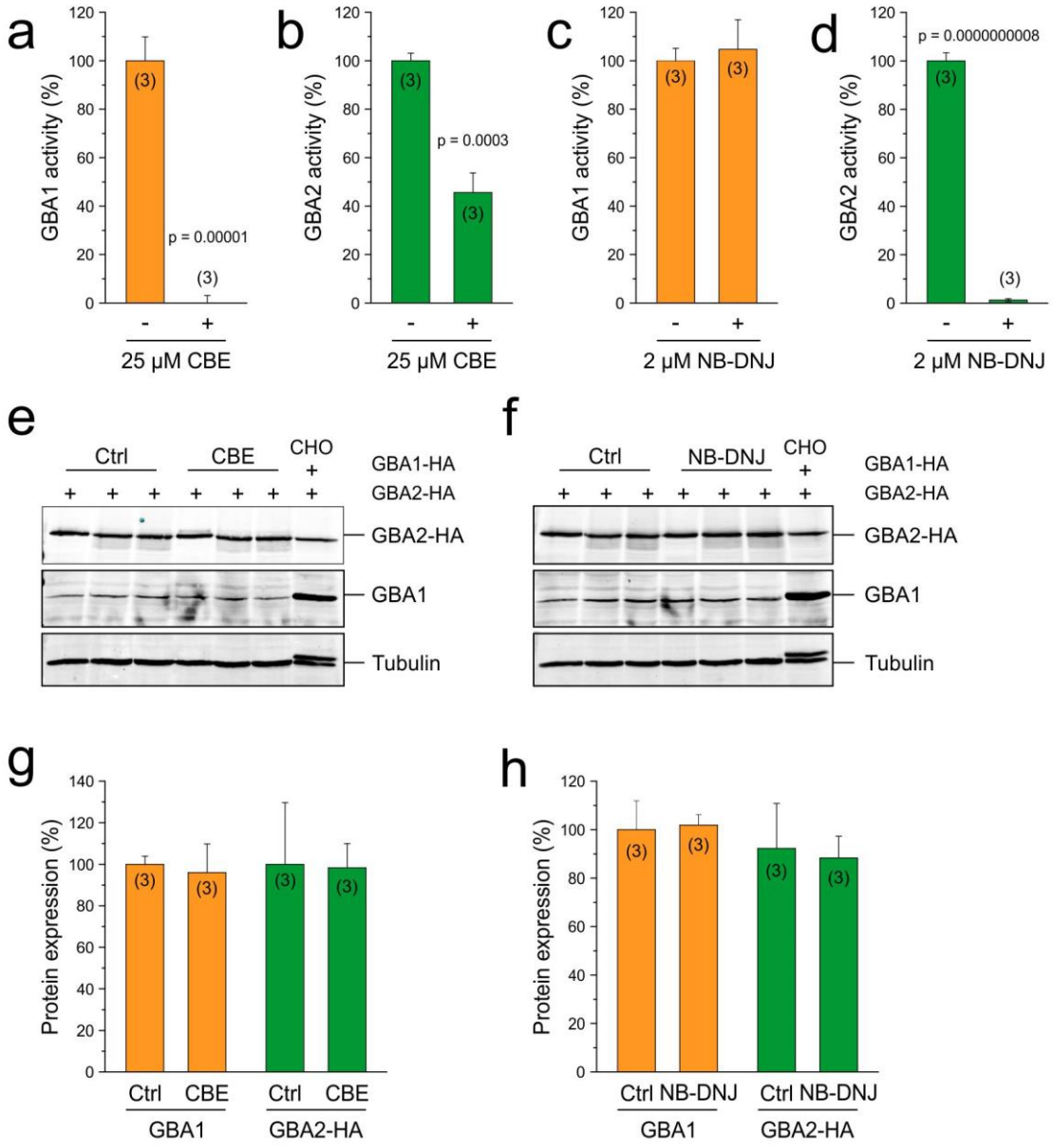

Figure 20: Analysis of the GBA1 and GBA2 activity and protein expression in HEK293 cells transiently over-expressing mGBA2 treated with CBE or NB-DNJ. HEK293 cells transiently over-expressing mGBA2 were treated with either 25 µM CBE or 2 µM NB-DNJ for 48 h to block GBA1 or GBA2, respectively. Beta-glucosidase activities were analysed in hypotonic cell lysates in the presence of 1.67 mM 4-MUG and protein expression was analysed by Western blot using antibodies against GBA1 (Sigma) and GBA2 (anti-HA, Sigma). CHO cells stably over-expressing mGBA1-HA and mGBA2-HA were used as positive controls. Tubulin was used as a loading control. **(a)** Endogenous GBA1 activity was blocked in with the presence of 25 µM CBE. **(b)** GBA2 activity in CBE-treated cells was reduced to around 46% of the activity in non-treated cells (Ctrl). Vice versa, **(c)** GBA1 activity remained unchanged in cells treated with 2 µM NB-DNJ **(d)** in absence of GBA2 activity. **(e)** GBA1 and GBA2 protein expression was not different between CBE-treated and non-treated cells. **(f)** Same as **(e)** for NB-DNJ treated and non-treated cells. **(g)** Quantification of GBA1 and GBA2 protein levels in CBE-treated and control cells normalised to tubulin. **(h)** Same as **(g)** for NB-DNJ-treated and control cells. CBE:

Conduritol B epoxide, NB-DNJ: N-butyl-deoxynojirimycin, 4-MUG: 4-Methylumbelliferyl beta-D-glucopyranoside. Data are presented as mean + SD. N numbers are indicated in brackets. P values were determined using Student's t-test.

To rule out that CBE directly inhibits GBA2 activity, embryonic fibroblasts from GBA1-deficient mice were incubated with 25 µM CBE for 48 h (Figure 21), which allows to measure CBE-dependent effects on GBA2 activity independent of GBA1. The activity of GBA2 remained the same in both, CBE-treated and control GBA1-deficient cells (Figure 21b). Thus, these results reveal that GBA1 activity regulates GBA2 activity, but not vice versa, and that the regulation occurs on the activity level independent of changes in protein expression.

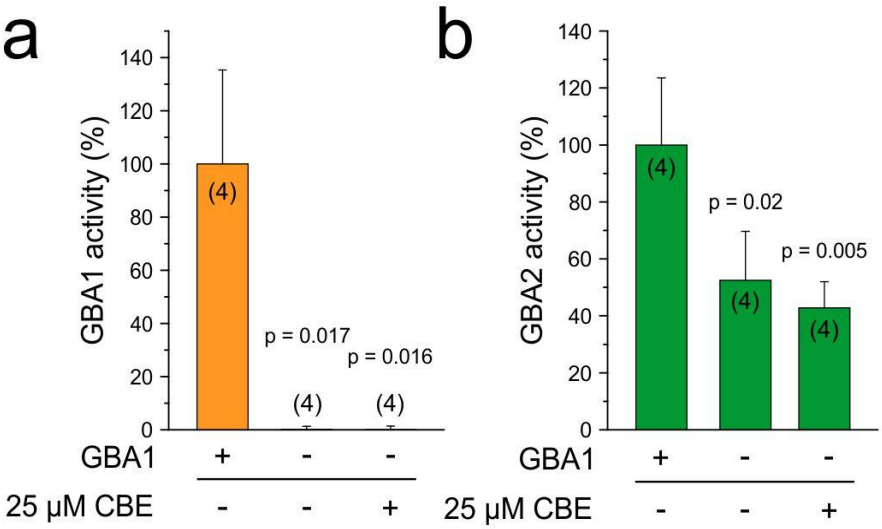

Figure 21: GBA2 activity in GBA1-deficient mouse embryonal fibroblasts treated with CBE. GBA1-deficient embryonal mouse fibroblasts were treated with 25 µM CBE for 48 h. Beta-glucosidase activity was analysed in hypotonic cell lysates in presence of 1.67 mM 4-MUG. **(a)** GBA1-deficient embryonal fibroblasts did not show any GBA1 activity. **(b)** The activity of GBA2 remained the same in both, CBE-treated and control GBA1-deficient cells. CBE: Conduritol B epoxide, 4-MUG: 4-Methylumbelliferyl beta-D-glucopyranoside. Data are presented as mean + SD. N numbers are indicated in brackets. P values were determined using One-way ANOVA.

To understand the underlying mechanism in more detail, the time course of the GBA1-dependent regulation of GBA2 activity was analysed in human dermal fibroblasts and CHO cells stably over-expressing mGBA2 (#G4A11) (Figure 22). GBA1 activity was blocked with 25 µM CBE for 10 min up to 48 h before analysing GBA1 and GBA2 activity (Figure 22). A significant reduction of GBA1 activity was observed after 3 h of CBE-treatment in both cell lines; GBA1 was maximally blocked after 3 h in human

dermal fibroblasts (Figure 22a) and after 24 h in CHO cells expressing mGBA2 (Figure 22b). Interestingly, GBA2 activity was only reduced when GBA1 activity was fully blocked (Figure 22). This result suggests that the GBA2 activity directly responds to GBA1-dependent changes in the cell, e.g. the accumulation of its substrate, GlcCer, in the lysosomes or changes of downstream metabolites in the cytoplasm.

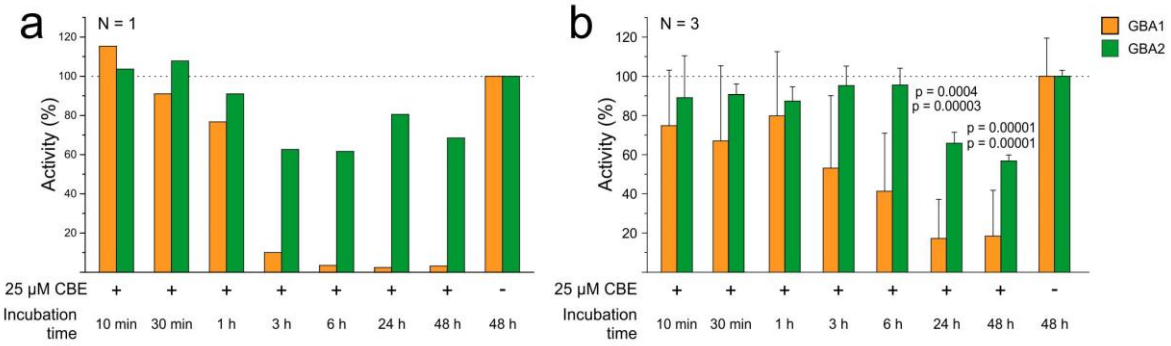

Figure 22: Time course of the GBA1-dependent regulation of GBA2 activity in human dermal fibroblasts and CHO cells stably over-expressing mGBA2. Fibroblasts and CHO cells stably over-expressing mGBA2 were incubated with 25 µM CBE for 10 min up to 48 h. Beta-glucosidase activity was analysed in hypotonic cell lysates in presence of 1.67 mM 4-MUG. **(a)** GBA1 was maximally blocked after 3 h in human dermal fibroblasts. GBA2 activity was only reduced when GBA1 activity was fully blocked. **(b)** as in **(a)** for CHO cells stably over-expressing mGBA2. GBA1 was maximally blocked after 24 h in CHO cells expressing mGBA2. Again, an effect on GBA2 was only visible when GBA1 activity was almost completely absent. CBE: Conduritol B epoxide, 4-MUG: 4-Methylumbelliferyl beta-D-glucopyranoside. Data are presented as mean + SD. N numbers are indicated. P values were determined using Student's t-test.

3.6 GBA1-dependent regulation of GBA2 activity also occurs *in vivo* in a pharmacologic *Gaucher* mouse model

The injection of CBE into wild-type mice represents an approved pharmacologic approach to evoke the *Gaucher* phenotype *in vivo* in a mouse model (Kanfer et al., 1975; Vardi et al., 2016). This model was used to analyse whether the GBA1-dependent regulation of GBA2 activity also occurs *in vivo* (Figure 23). Eight days old 6OlaHsd mice were injected intra-peritoneally with 25 – 100 mg CBE/kg/day for 10 days. After the treatment, mice were sacrificed and the brains dissected. First, beta-glucosidase activity was determined in hypotonic brain lysates from CBE-treated and control mice. GBA1 activity was blocked at all tested CBE concentrations (Figure 23a). In line with our earlier findings, GBA2 activity was also reduced to around 80% at all CBE concentrations tested (Figure 23b). As shown above and by others, at high

concentrations, CBE also inhibits the activity of GBA2 (Figure 17a) (Körschen et al., 2013; Ridley et al., 2013). The final concentration of CBE in the brain for the different treatments is difficult to estimate. However, the reduction of GBA2 activity was similar at all doses of CBE tested (Figure 23b), arguing against a direct inhibition by CBE, but rather favouring a GBA1-dependent effect.

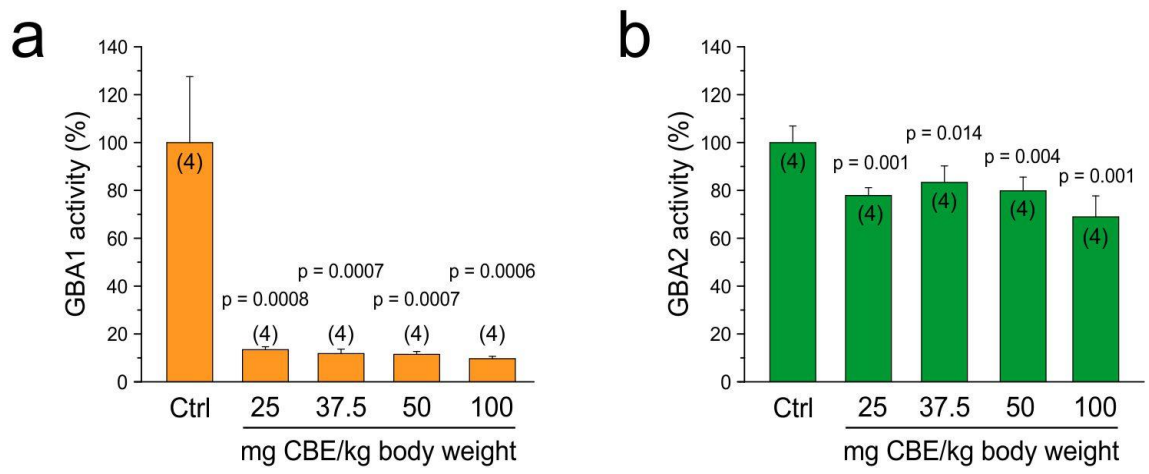

Figure 23: GBA1 and GBA2 activity in CBE-treated mice. Eight days old 6OlaHsd mice were injected intra-peritoneally with 25 – 100 mg CBE/kg/day for 10 days. Beta-glucosidase activity was analysed in hypotonic brain lysates in presence of 1.67 mM 4-MUG. **(a)** GBA1 activity was blocked at all tested CBE concentrations. **(b)** GBA2 activity was also reduced to around 80% at all CBE concentrations tested. CBE: Conduritol B epoxide, 4-MUG: 4-Methylumbelliferyl beta-D-glucopyranoside. Data are presented as mean + SD. N numbers are indicated in brackets. P values were determined using One-way ANOVA.

To verify in this *in vivo* model that the regulation occurs on the activity, and not on the expression level, the GBA2 mRNA and protein expression was analysed (Figure 23c-f). First, a protocol to analyse the mRNA expression in mouse brains treated with different amounts of CBE was established as previously described in passage 3.3 using qPCR. Besides the GOI (mGBA2), mTfrc and mGusb were selected as suitable HKGs) (Table 58).

Table 58: Mouse genes of interest (GOIs) and housekeeping genes (HKGs) chosen for qPCR analysis

Gene	Gene product	Reference
mGBA2	Non-lysosomal beta-glucosidase	NM_172692
mTfrc	Transferrin receptor	NM_011638
mGusb	Glucuronidase beta	NM_010368

Table 59: Amplicon sizes of mouse primer pairs selected for qPCR

Gene	Primer pair	Expected amplicon size (bp)
mGBA1	C1508/09	251
mGBA1	C1510/11	169
mGBA2	C1512/13	157
mGBA2	C1514/15	251
mTfrc	C1520/21	159
mTfrc	C1522/23	169
mGusb	C1532/33	201
mGusb	C1534/35	137

bp: base pairs

To test whether primers designed for qPCR amplify the sequence of interest, a conventional polymerase chain reaction (PCR) was performed (2.4.2). For mouse primers (Table 16), cDNA obtained from a mouse wild-type testis was used. All amplicons (Figure 24) had the expected sizes (Table 59), but some of the primer pairs showed a slight DNA contamination in the H_2O control and mGusb pair C1534/35 showed an additional band.

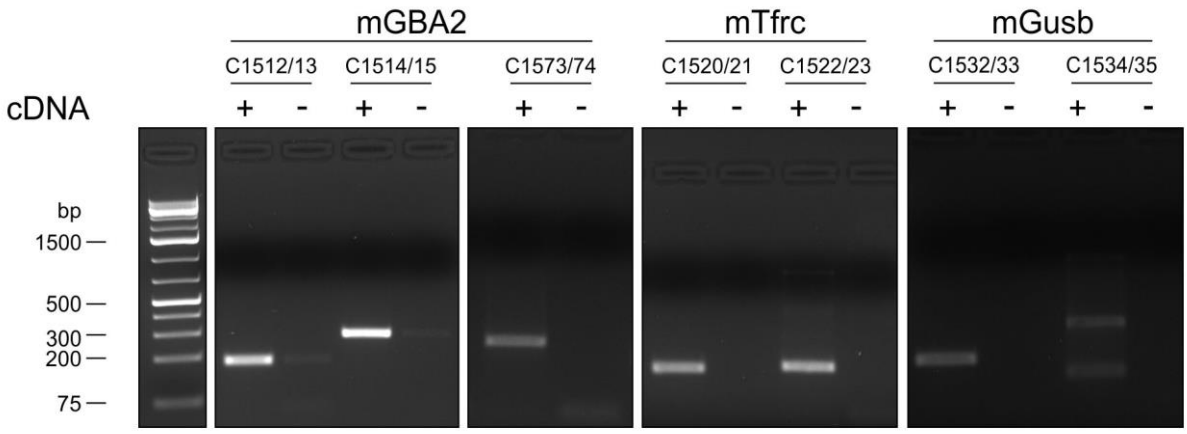

Figure 24: Analysis of the amplicons of mouse qPCR primers and control cDNA from mouse wild-type testis. 5 µl of the PCR approach were loaded to a 2% agarose gel and the fragments were analysed under a UV lamp. All amplicons had the expected sizes, but some of the primer pairs showed a slight DNA contamination in the H_2O control and mGusb pair C1534/35 showed an additional band. bp: base pairs.

To reliably analyse the data obtained from qPCR, a primer efficiency test (PET) was performed (2.4.6.5). Based on these results, the following mouse primers were used for subsequent experiments: mGBA2: C1573/74, mTfrc: C1522/23, and mGusb: CC1532/33 (Table 60). The PCR products generated by these primer pairs were send for sequencing and, thus, verified to be the right amplicons (data not shown).

Table 60: Mouse qPCR primer efficiencies

Gene	Primer numbers	Slope	R^2 value	Efficiency (%)
mGBA2	C1512/13	-3.2545	0.9954	103
mGBA2	C1514/15	-3.466	0.9995	94
mTfrc	C1520/21	-3.2077	0.9995	105
mTfrc	C1522/23	-3.2583	0.9999	103
mGusb	C1532/33	-3.4448	0.9987	95
mGusb	C1534/35	-3.0089	0.9948	115

qPCR was performed for the GOI mGBA2 and the HKGs mTfrc and mGusb and CBE-treated mouse brains as templates (see Table 58, 2.4.6.6). GBA2 mRNA expression was significantly reduced in brain treated with 25 mg CBE/kg/day and 100 mg

CBE/kg/day (Figure 25a). However, this did not result in a change in protein expression, as shown by Western blot analysis (Figure 25b, c). Here, both, GBA1 and GBA2, were similarly expressed in all tested samples (Figure 25d-g). Thus, the GBA1-dependent regulation of GBA2 activity occurs not only *in vitro*, but also *in vivo*.

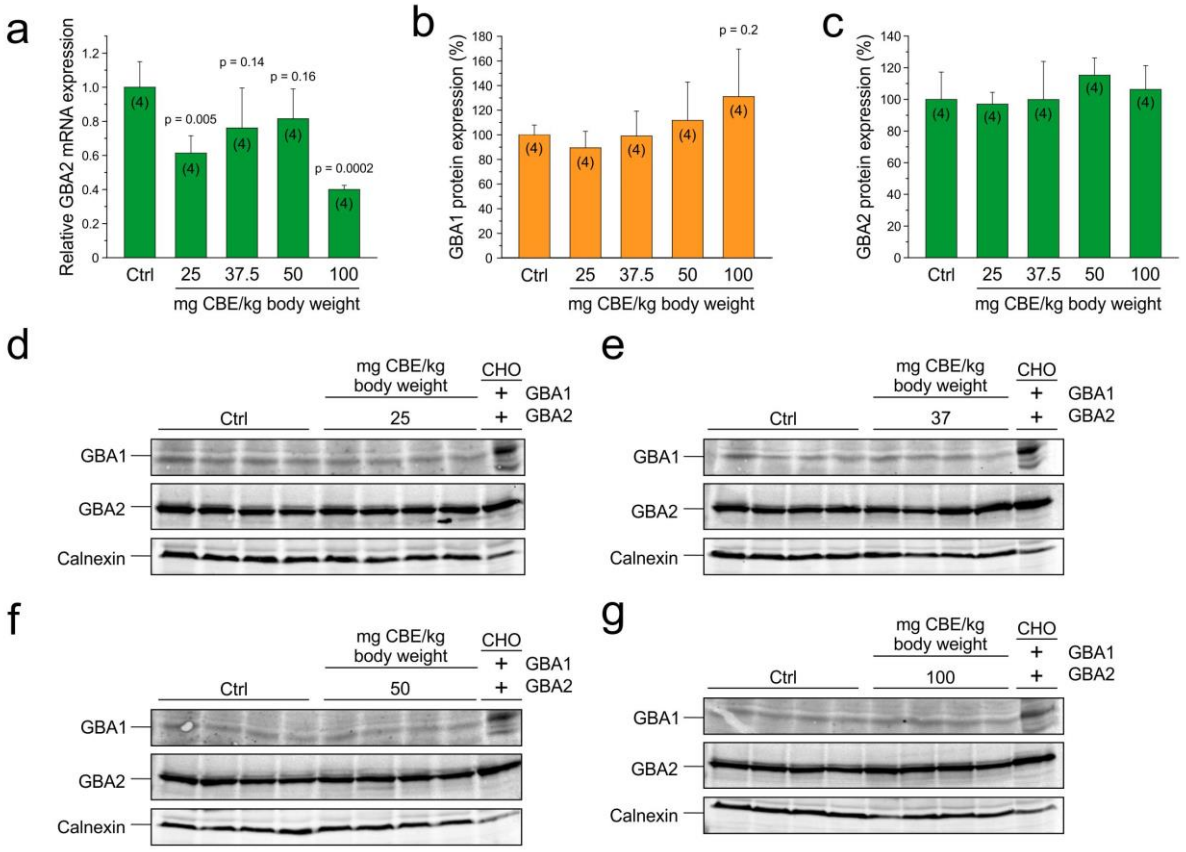

Figure 25: GBA2 mRNA expression and GBA1 and GBA2 protein expression in CBE-treated mice. Eight days old 6OlaHsd mice were injected intra-peritoneally with 25 – 100 mg CBE/kg/day for 10 days. RNA was extracted from brain tissue and analysed using qPCR. Protein expression was analysed in hypotonic brain lysates by Western blot using antibodies against GBA1 (Sigma) and GBA2 (polyclonal 4/5 kb mix from rabbit, non-published). CHO cells stably over-expressing mGBA1-HA and mGBA2-HA were used as positive controls. Calnexin was used as a loading control. **(a)** GBA2 mRNA expression was significantly reduced in brains treated with 25 mg CBE/kg/day and 100 mg CBE/kg/day. **(b)** Quantification of GBA1 protein levels in CBE-treated and control mice normalised to calnexin. **(c)** As in **(b)** for GBA2. **(d) – (g)** Blots showing that GBA1 and GBA2 protein expression was similar in CBE-treated and control mice treated with 25 – 100 mg CBE/kg/day. CBE: Conduritol B epoxide, 4-MUG: 4-

Methylumbelliferyl beta-D-glucopyranoside. Data are presented as mean + SD. N numbers are indicated in brackets. The p value was determined using One-way ANOVA.

3.7 Analysing the affinity of GBA2 for 4-MUG

Loss of GBA1 activity results in a severe accumulation of GlcCer in the lysosomes (Brady et al., 1965). The GBA1-dependent regulation of GBA2 activity occurs only on the activity level (see Figure 9 and Figure 14). I wondered whether GBA2 in lysates from GBA1-deficient cells might be occupied cleaving the increased amount of endogenously accumulated GlcCer rather than the artificial substrate 4-MUG that is used in the assay. This would be (falsely) visible as reduced GBA2 activity in the assay. Matern and colleagues have previously studied the affinity of GBA2 for 4-MUG, albeit in a different assay system, and found a K_m value of 210 µM (Matern et al., 1997). The affinity of GBA2 for its natural substrate, however, has not been published so far.

3.7.1 Analysis of GlcCer levels in control and *Gaucher* fibroblasts by thin layer chromatography

To compare the amount of endogenous GlcCer and artificial substrate (4-MUG) present in the assay, the amount of GlcCer in dermal fibroblasts from control and *Gaucher* patients was analysed by TLC. First, lipids were isolated from spleens of control, GBA2-deficient, and GBA1/GBA2-deficient mice to establish a protocol for GSL extraction from samples that show rather high GlcCer levels (Figure 26). To determine the amount of GlcCer present, the signal intensity of a serial dilution of purified galactosylceramide (galactose is a C-4 epimer of glucose) was analysed and compared to the GlcCer bands (Figure 26b). Wild-type spleen contained 0.03 µg GlcCer/mg wet weight, whereas the GlcCer levels was slightly elevated to 0.14 µg/mg wet weight in spleens from GBA2-deficient mice and strongly increased to 1.38 µg GlcCer/mg wet weight in GBA1/GBA2-deficient mice (Figure 26b, also published in Yildiz et al. (Yildiz et al., 2013).

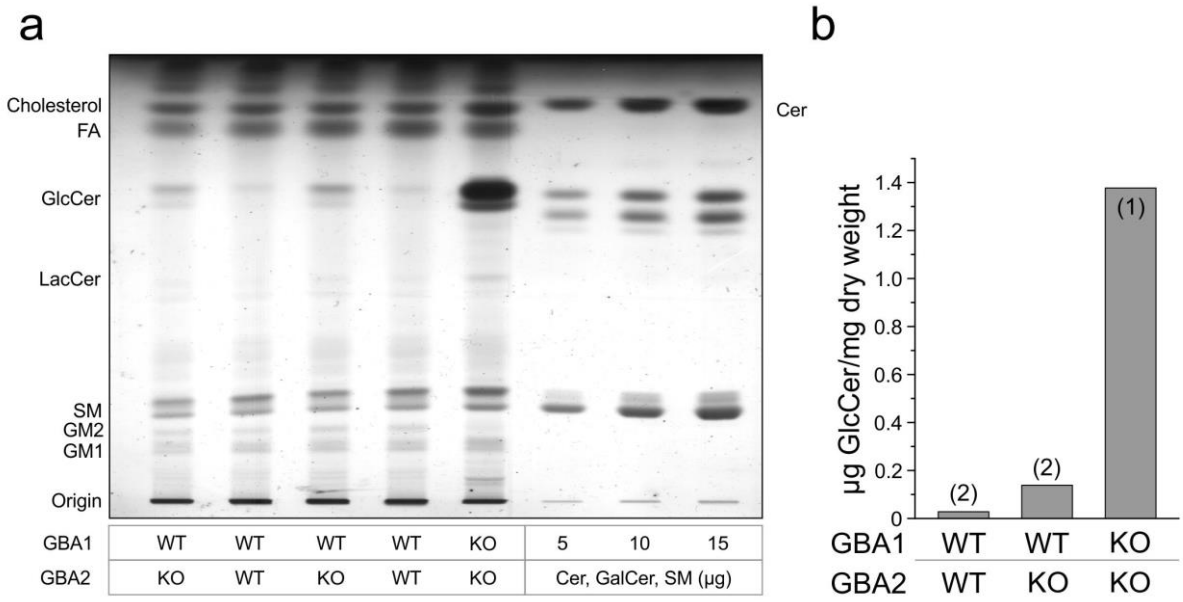

Figure 26: GlcCer levels in spleen from wild-type, GBA2-deficient, and GBA1/GBA2-deficient mice. (a) TLC of GSLs extracted from mouse spleen with different genetic backgrounds, showing accumulation of GlcCer in GBA2-deficient and GBA1/GBA2-deficient tissues compared to the wild-type (WT) control. **(b)** Quantification of endogenous GlcCer levels by comparing the signal intensity to purified GalCer. GSL: Glycosphingolipids, FA: Fatty acid, GlcCer: Glucosylceramide, LacCer: Lactosylceramide, SM: Sphingomyelin, GM1/2: monosialic ganglioside 1/2, Cer: ceramide, GalCer: Galactosylceramide, WT: Wild-type, KO: Knockout. Data are presented as mean values. N numbers are indicated in brackets.

Next, fibroblast samples from control and *Gaucher* patients were collected and lipids were extracted. Fibroblasts from control patients contained 1.26 µg GlcCer per mg protein, whereas GlcCer levels were slightly increased in type I and III fibroblasts to 2.26 µg/mg protein and 1.7 µg/mg protein, respectively (Figure 27b). GlcCer levels in type II fibroblasts were comparable to the controls (1.21 µg/mg protein). Fuller et al. have also analysed GlcCer levels in cultured dermal fibroblasts from control and different *Gaucher* patients one week and six weeks post-confluency and found GlcCer levels to be increased in cells derived from both, type I and type II patients (Fuller 2008). Control fibroblasts contained 0.5 nmol/mg total protein, whereas type I fibroblasts contained 1.2 nmol/mg protein and type II fibroblasts contained 3.5 nmol/mg protein (Fuller et al., 2008). My results showed that control fibroblasts contained 1.26 µg GlcCer per mg protein, which, considering that GlcCer has an average molecular weight of 785 g/mol, resembles 1.61 nmol/mg protein, which, even though it is double the amount of what has been measured by Fuller and co-workers, still is in the same range. Thus, based on my results and those obtained by others, GlcCer also accumulates in dermal fibroblasts from *Gaucher* patients.

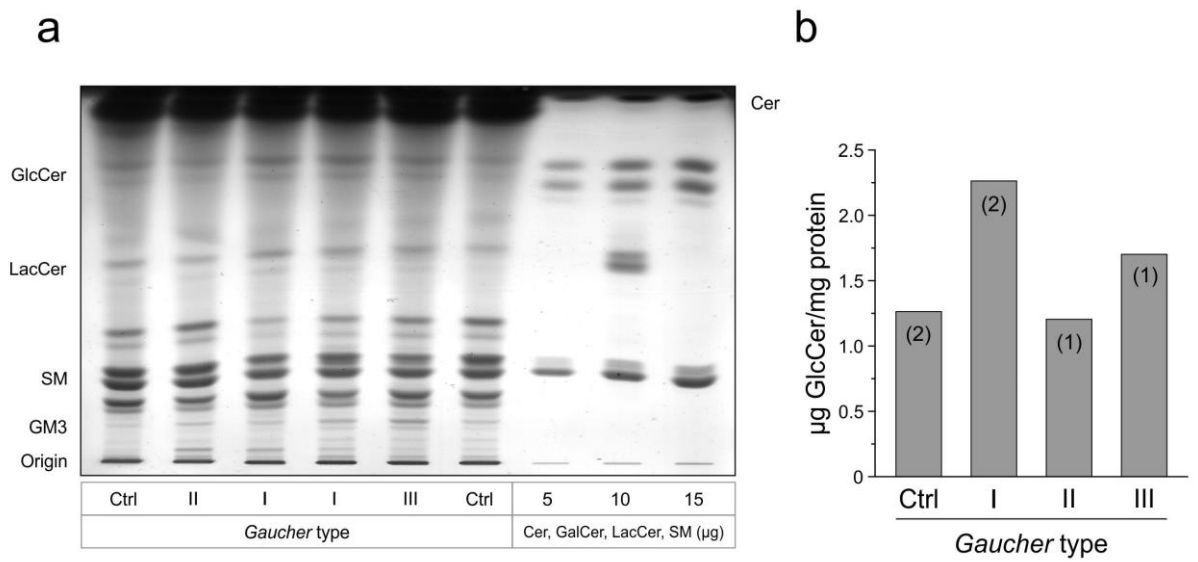

Figure 27: GlcCer levels in fibroblasts from control and *Gaucher* patients. (a) TLC of GSLs extracted from control (Ctrl) and *Gaucher* fibroblasts showing no pronounced accumulation of GlcCer in *Gaucher* cells. Control cells contained 1.26 µg GlcCer/mg protein, type I fibroblasts 2.26 µg/mg protein, type II fibroblasts 1.21 µg/mg protein, and type III fibroblasts 1.7 µg/mg protein. **(b)** Quantification of endogenous GlcCer levels by comparing the signal intensity to purified GalCer. GSL: Glycosphingolipids, GlcCer: Glucosylceramide, LacCer: Lactosylceramide, SM: Sphingomyelin, GM3: monosialic ganglioside 3, Cer: ceramide, GalCer: Galactosylceramide. The different *Gaucher* types are indicated. Data are presented as mean values. N numbers are shown in brackets.

3.7.2 Analysis of GlcCer levels in control and *Gaucher* fibroblasts by mass spectrometry

To validate these results, the amount of GlcCer in dermal fibroblasts from control and *Gaucher* patients was analysed by mass spectrometry (Figure 28). In total, fibroblasts from *Gaucher* patients contain 3.4 ± 0.4 pmol GlcCer/µg protein and control fibroblasts 2.6 ± 1.1 pmol GlcCer/µg protein (Figure 28). The molecular weight of GlcCer is 785 g/mol. Thus, 2.6 pmol GlcCer/µg protein equal 2.041 ng GlcCer/µg protein. Quantification of TLC control band intensities resulted in 1.26 µg GlcCer per mg protein (see above), which equals 1.26 ng GlcCer/µg protein. Thus, quantification of GlcCer levels by mass spectrometry resulted in a 1.6-fold higher value compared to TLC analysis. Given the fact that mass spectrometric analysis is a lot more sensitive, I used the latter value for further calculations.

Generally, 75 µg of hypotonic protein lysates are used for each reaction when analysing the GBA2 activity. This would result in a total amount of 195-255 pmol endogenous GlcCer (control and *Gaucher* samples, respectively) present in each

reaction. In comparison, 50 nmol 4-MUG is used per reaction, which is around 196-fold more than the amount of endogenous GlcCer present. Thus, it is unlikely that the assay underestimates the GBA2 activity.

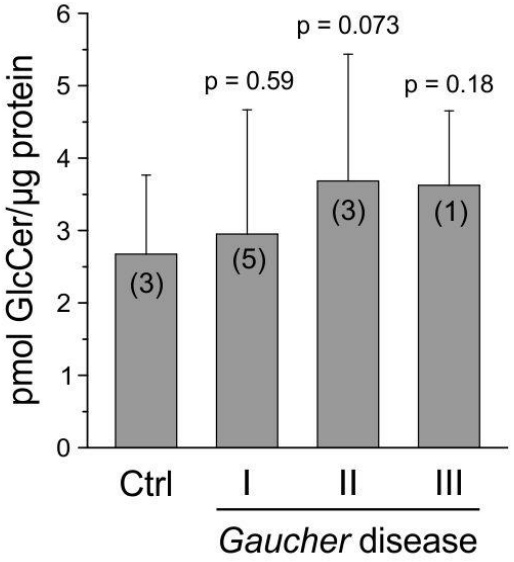

Figure 28: GlcCer levels in Gaucher and control fibroblasts. Mass spectrometric analysis of GlcCer levels normalised to the amount of protein per sample. GlcCer levels were slightly albeit not significantly increased in type II *Gaucher* fibroblasts and slightly lower in type III cells compared to the controls (Ctrl). Control cells contained 2.6 ± 1.1 pmol GlcCer/µg protein and *Gaucher* cells contained in total 3.4 ± 0.4 pmol GlcCer/µg protein. The different *Gaucher* types are indicated. Data are presented as mean + SD. N numbers are shown in brackets. P values were determined using One-way ANOVA.

3.7.3 Determining the K_m value of GBA2 from control and GBA1-deficient cells for 4-MUG

To experimentally verify this conclusion, GBA2 activity for 4-MUG was measured in GBA1-deficient HEK293 and control cells using a serial dilution of the artificial substrate (Figure 29). GBA2 activity reached a maximum at around 600 µM 4-MUG (Figure 29), using 75 µg of hypotonic protein lysates from either HEK293 control or GBA1-deficient cells. A further increase in substrate concentration did not cause an increase in the reaction rate as there was no more enzyme available to react with the substrate. In the assay, 4-MUG is present at a final concentration of 1.67 mM, which is around 2.8-fold more than the substrate concentration, at which maximal GBA2 activity was reached. Thus, the assay is performed under saturating conditions. Control cells showed a maximal reaction activity (V_{max}) of 1.03 ± 0.58 rfu/min, whereas the maximal GBA2 activity in GBA1-deficient cells was only 0.43 ± 0.17 rfu/min,

underlining the GBA1-dependent effect on GBA2 activity (compare Figure 14). The Michaelis constant K_m is the substrate concentration, at which the reaction rate is half of V_{max} (IUPAC. Compendium of Chemical Terminology). Under saturating conditions, K_m is a measure for the affinity of an enzyme for its substrate (IUPAC. Compendium of Chemical Terminology). The K_m determined for GBA2 in control cells was 60.25 ± 28.64 µM, whereas the K_m in GBA1-deficient cells was slightly, albeit not significantly, increased to 76.58 ± 23.43 µM. The K_m value for GBA2 has already been determined by Matern and colleagues, albeit in a different assay system, with GBA2 showing a K_m value of 210 µM towards 4-MUG, which is 3-fold higher than the value that I obtained (Matern et al., 1997). However, the fact that GBA2 in GBA1-deficient cells does not reach the same activity as in control cells, even with very high concentrations of 4-MUG, indicates that endogenous GlcCer in GBA1-deficient cell lysates is not extensively occupying or competing for the active site of GBA2 and, therefore, does not hinder 4-MUG from entering the catalytic site. These data verify that there is indeed a GBA1-dependent regulation of GBA2 activity that is not imposed by design of the assay, but due to changes in pathways downstream of GBA1.

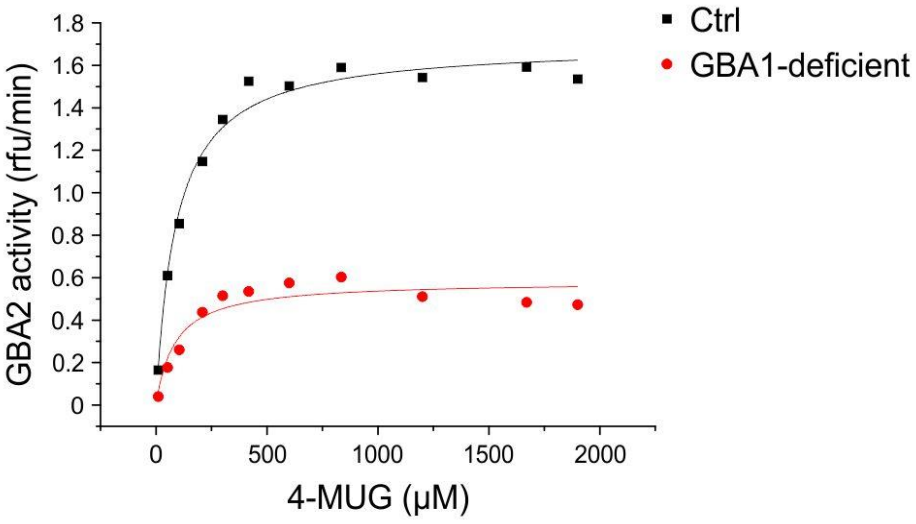

Figure 29: Activity of GBA2 from control and GBA1-deficient HEK293 cell lysates towards 4-MUG. Analysis of the GBA2 activity in hypotonic lysates of HEK293 control (Ctrl) or GBA1-deficient cells and using a serial dilution of 4-MUG. GBA2 activity reached a maximum at 600 µM 4-MUG when 75 µg of hypotonic protein lysates from either cell line were used. Control cells showed a V_{max} of 1.03 ± 0.58 rfu/min, whereas the maximal GBA2 activity in GBA1-deficient cells was only 0.43 ± 0.17 rfu/min. The K_m for GBA2 in control cells was 60.25 ± 28.64 µM, whereas the K_m in GBA1-deficient cells was slightly increased to 76.58 ± 23.43 µM. 4-MUG: 4-Methylumbelliferyl beta-D-glucopyranoside. Representative plot for n = 3 experiments.

3.7.4 A tool to search for new GlcCer-binding proteins

GlcCer accumulates in both, GBA1-deficient and GBA2-deficient cells (Rosenberg&Chargaff, 1958; Yildiz et al., 2006). Besides changing the lipid composition of certain membranes and, thus, changing their structure and/or curvature, accumulation of GlcCer could also affect the function of GlcCer-binding proteins, which, in turn, could affect yet unknown downstream mechanisms. To date, only three GlcCer-binding proteins have been identified, with two of them being GLTP and FAPP2 (Godi et al., 2004; Metz&Radin, 1980).

To learn more about the mechanisms involved downstream of GlcCer, we developed an assay to search for new GlcCer-binding proteins (collaboration with Dr. A. Rennhack, caesar, and Dr. G Schwarzmann, University of Bonn) (also see 2.5.6). A non-cleavable GlcCer-derivative was synthesised that carries an S-glycosidic linkage instead of an O-glycosidic linkage, which renders GlcCer in its normal steric conformation, but cannot be cleaved by glucocerebrosidases (Figure 30a). The GlcCer derivative was coupled to a NHS-Tentagel and the GlcCer-coupled beads were incubated with protein lysates to allow batch purification of possible binding proteins. Finally, the elute will be analysed by mass spectrometry to identify the purified proteins (Figure 30b). I tested the specificity of the GlcCer beads by incubating them with purified and hGLTP (Figure 30c, d, see 3.15.1). The empty NHS-Tentagel matrix as well as the one coupled to GlcCer were incubated with 100 µl 0.35 µM hGLTP before washing with PBS to remove non-bound protein (Figure 30c, d). Bound protein was eluted from the column using 2% SDS in PBS and analysed by Western blot using a specific anti-GLTP antibody (Figure 30c, d). As visible in Figure 30c, hGLTP did not bind to the empty column material and was fully recovered in the flow-through. In contrast, fewer hGLTP was found in the flow-through of the GlcCer-column and hGLTP was recovered in the elution fraction (E, Figure 30d). Thus, this systems serves as a valid tool to search for yet unknown GlcCer-binding partners. Due to time limitations, the experiment was followed up during my PhD.

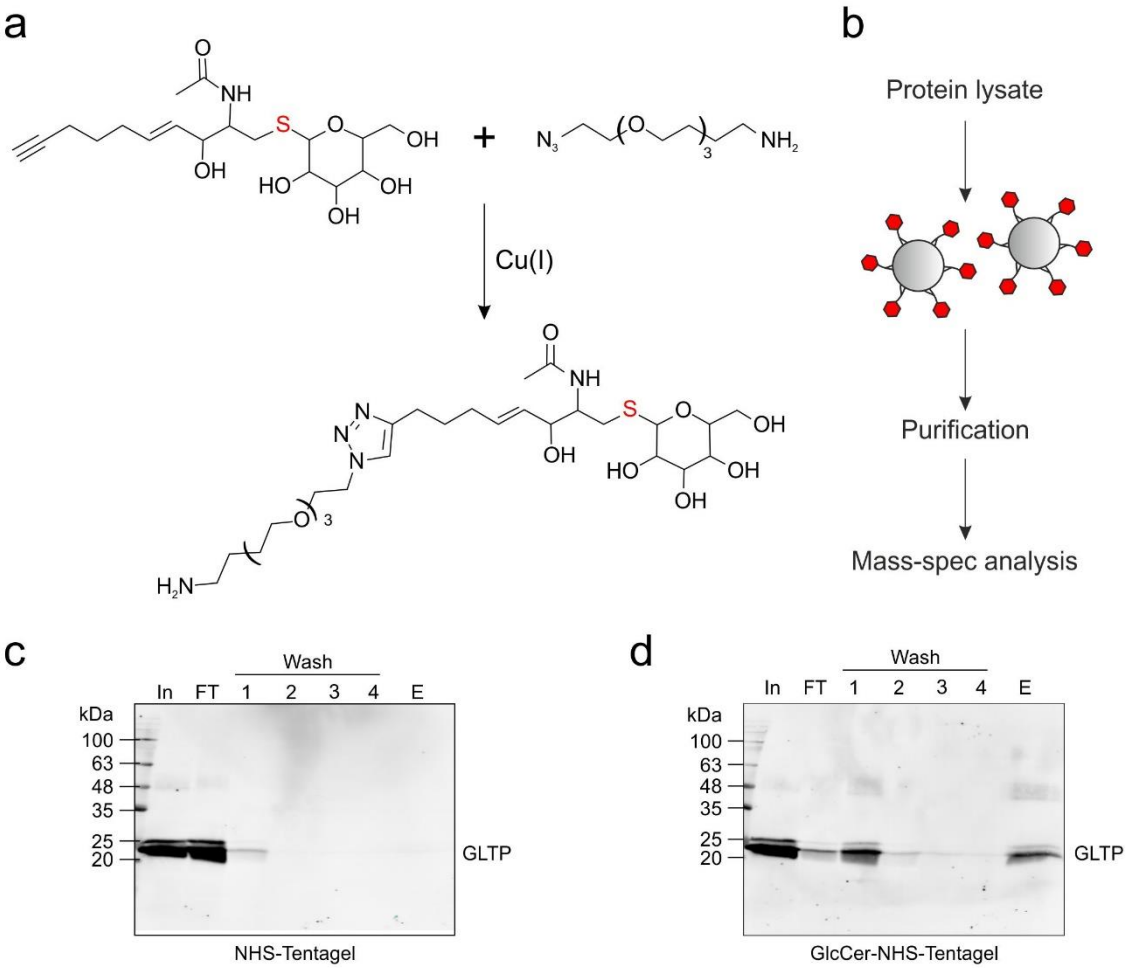

Figure 30: A tool to search for new GlcCer-binding proteins. (a) A non-cleavable GlcCer-derivative was synthesised to allow purification of GlcCer-binding proteins. The GlcCer derivative carries an S-glycosidic linkage instead of an O-glycosidic linkage, which renders GlcCer in its normal steric conformation, but cannot be cleaved by beta-glucosidases. **(b)** The GlcCer derivative was coupled to a NHS-Tentagel and the GlcCer-coupled beads can be incubated with a protein lysate to allow batch purification of possible binding proteins. **(c)** The normal NHS-Tentagel matrix as well as **(d)** the GlcCer-coupled one were incubated with 100 µl 0.35 µM GLTP before washing with PBS to remove non-bound protein. Bound protein was eluted from the column using 2% SDS in PBS and analysed by Western blot GLTP-specific antibody (Santa Cruz). GLTP did not bind to the pure column material but was recovered in the elution fraction of the GlcCer-column. In: Input, FT: Flow-through, E: Elution, GlcCer: Glucosylceramide, GLTP: Glycolipid transfer protein.

3.8 Analysing the intracellular pH in GBA1-deficient and control cells

GBA2 activity is sensitive to the environmental pH. Thus, I determined the intracellular pH (pH_i) in both, control and *Gaucher* fibroblasts, using BCECF to study whether a change in the cytoplasmic pH in GBA1-deficient cells might be responsible for the reduction in GBA2 activity. BCECF (2',7'-Bis-(2-Carboxyethyl)-5-(and-6)-

Carboxyfluorescein, Invitrogen) is a molecule commonly used to measure changes in the cytosolic pH in cells. BCECF is a fluorescein derivative that emits (em) light at 590 nm when excited (ex) at 490 nm in a pH-dependent manner: the fluorescence intensity increases with increasing pH. Furthermore, BCECF allows to do ratiometric measurements because the emission at 590 nm is independent of the surrounding pH when excited at 440 nm (isosbestic point) (Figure 31). In fact, the ratio [($440_{ex}520_{em}$)/($485_{ex}520_{em}$)] is independent from both, the amount of BCECF taken up by a cell and the total number of cells and with a pKa value of 6.98, it can be used to calibrate the intracellular pH. Fibroblasts were loaded with BCECF-AM, the acetoxymethyl ester form of BCECF, which is non-fluorescent, but membrane permeable. When BCECF-AM enters the cytosol of cells, cytosolic esterases convert it to its membrane impermeable, but fluorescent form (Gallo, 2001).

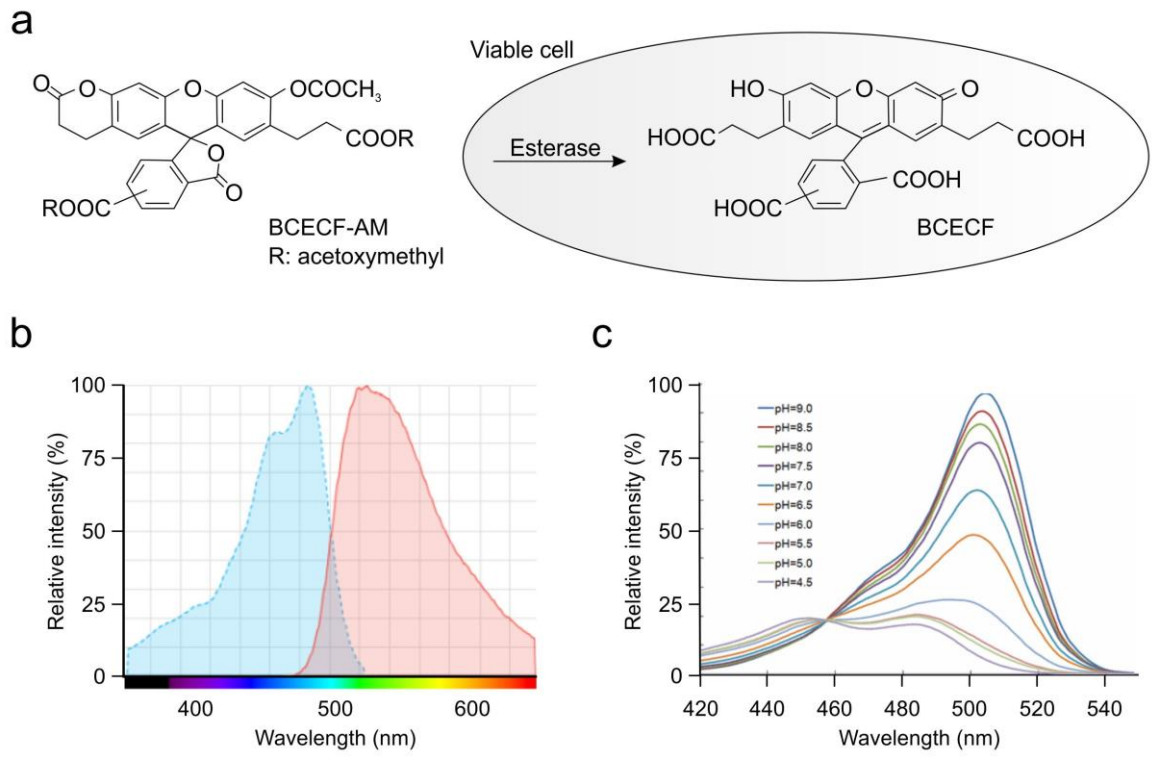

Figure 31: The pH indicator BCECF. (a) Chemical structure of BCECF. Fibroblasts were loaded with non-fluorescent but membrane permeable BCECF-AM. When BCECF-AM enters the cytosol of cells, cytosolic esterases convert it to its membrane impermeable, but fluorescent form. **(b)** Excitation- (blue) and emission- (red) spectra of BCECF. **(c)** Relative fluorescence intensity of BCECF in dependence of the pH (4.5 – 9.0). Excitation at 490 nm, emission at 520 nm. The isosbestic point is at 439 nm. BCECF: 2',7'-Bis-(2-Carboxyethyl)-5-(and-6)-Carboxyfluorescein. AM: Acetoxymethyl. Modified according to www.lifetechnologies.com.

The BCECF fluorescence was calibrated by releasing BCECF from the cells into strongly buffered TYH buffers of different pH values ("null-point" method). BCECF will change its fluorescence according to the difference of pH_i and the pH of the extracellular solution (pH_e). Only if $pH_i = pH_e$, no change is observed. This calibration is performed using several extracellular solutions of different pH values to generate a calibration curve, which can be used to calculate the apparent pH_i.

Lysing the cells and releasing BCECF from the cytosol into the extracellular buffer requires addition of a detergent (Rink et al., 1982). To lyse the cells, Triton X-100 was first diluted in TYH buffer of pH 8.0, with a final concentration of 0.01-0.5%. The ratio $(440_{ex}520_{em})/(485_{ex}520_{em})$ was plotted over time (Figure 32). Addition of all tested Triton X-100 concentrations immediately lysed the cells, resulting in the release of BCECF and an increase in fluorescence, showing that pH_e was higher than pH_i (Figure 32). Control experiments verified that the addition of Triton X-100 itself does not evoke a change in pH and, thus, a change in fluorescence (Dr. D. Fusshöller, Molecular Sensory Systems, caesar, Bonn, non-published data). Thus, a final concentration of 0.05% Triton X-100 was used to lyse cells in further experiments.

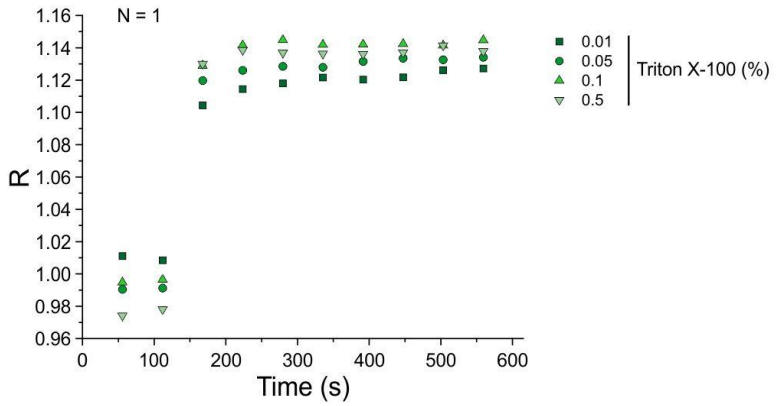

Figure 32: Changes in BCECF fluorescence upon Triton X100-induced lysis of control fibroblasts. Changes in BCECF fluorescence in control fibroblasts plotted as the ratio R (440ex520em)/(485ex520em) over time, recorded in the Fluostar before and after injection of Triton X-100. Addition of all tested Triton X-100 concentrations immediately lysed the cells, resulting in the release of BCECF and in a change in fluorescence. A final concentration of 0.05% Triton X-100 was used to lyse cells in further experiments. The N number is indicated.

To determine pH_i in fibroblasts from control and type I *Gaucher* patients, the "null-point" method was applied. Cells were loaded with BCECF-AM and kept in TYH buffer containing 5 mM HEPES at pH 7.4 in a 96-well plate. TYH buffers containing either

50 mM HEPES or 50 mM MES were prepared and checked to have a final pH of 6.24, 6.52, 6.79, 7.55, and 7.75 when mixed with 5 mM HEPES TYH buffer of pH 7.4 in a ratio of 5:1. After measuring the BCECF baseline, TYH buffers containing Triton X-100 were added to the cells and a change in fluorescence was observed over time (Figure 33). The ratio [($440_{ex}520_{em}$)/($485_{ex}520_{em}$)] was normalised to the baseline fluorescence and plotted over time (Figure 33a, c). Here, ratios below 0 indicate that pH_i is more acidic than pH_e and traces above 0 that pH_i is more basic than pH_e (Figure 33a, c). The "pH-null point" is the pH_e, at which no change in ΔR/R occurs because pH_i and pH_e are equal. Applying a liner fit to the ΔR values for each pH_e results in a "pH-null point" of 7.04 ± 0.32 (crossing point x axis) in control fibroblasts and 7.08 ± 0.32 in *Gaucher* fibroblasts (Figure 33b, d), which is similar to the pH_i of 7.2 in HEK293 cells (Sell 2014). Thus, there is no difference in pH_i between fibroblasts from control and *Gaucher* patients.

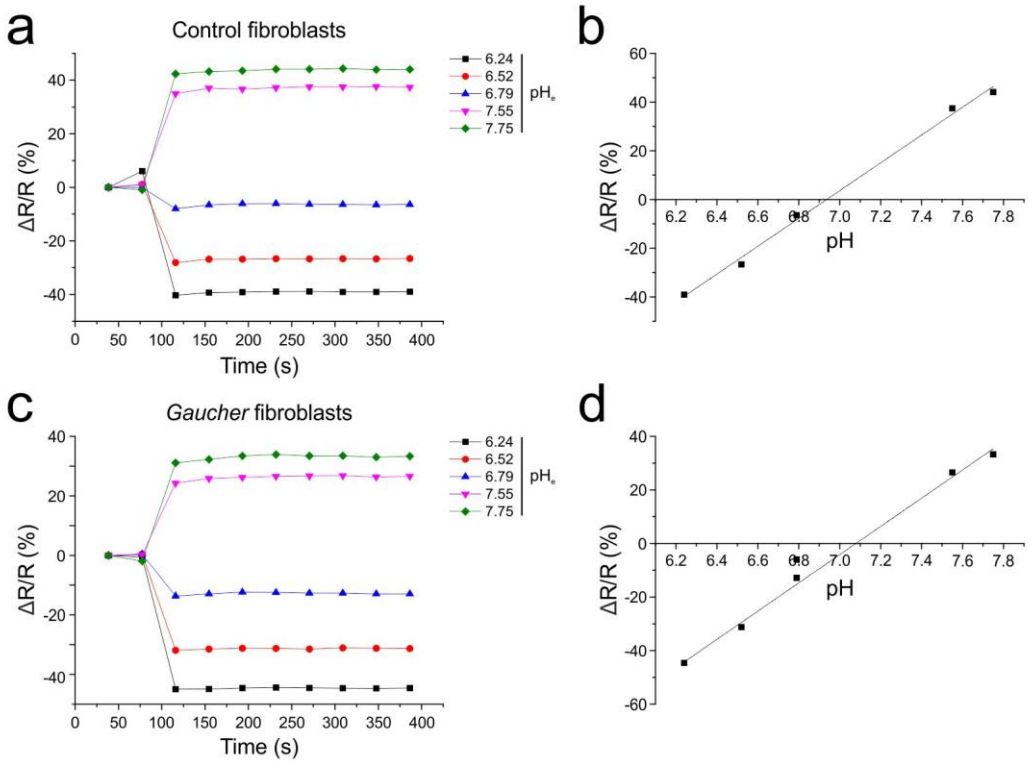

Figure 33: Null-point calibration of pH_i in control and *Gaucher* fibroblasts. pH_i was determined by a "null-point" calibration using BCECF fluorescence, as explained in the text. Representative fluorescence changes of ΔR/R (%) of BCECF recorded in **(a)** control and **(c)** *Gaucher* fibroblast suspensions in the Fluostar. 50 µl of pH-buffered TYH (50 mM HEPES or MES) supplemented with 0.05% Triton X-100 was injected in 250 µl pH-buffered (5 mM HEPES, pH 7.4) fibroblast suspension, resulting in a defined pH_e. The mean ΔR/R after 294, 336, and 378 s (3 data points) was determined for **(b)** control and **(d)** *Gaucher* fibroblasts and plotted against the pH values. A linear fit yielded a ΔR/R =

0 at pH_e = 7.04 ± 0.32 in **(b)** control fibroblasts and **(d)** 7.08 ± 0.32 in *Gaucher* fibroblasts. R: Ratio, s: Seconds. Representative plots for n = 3 experiments.

3.9 Determining the pH optimum of GBA2 in GBA1-deficient and control cells

To test whether a change in the pH optimum for GBA2 activity underlies the reduction of GBA2 activity in GBA1-deficient cells, a pH profile of GBA2 activity was measured from pH 3.5 to pH 7.0 in embryonal fibroblasts from GBA1-deficient and control mice (Figure 34). The highest GBA2 activity in embryonal fibroblasts from control mice was measured at pH 5.5, which is slightly more basic than the optimal pH value determined in liver lysates of control mice (pH 5.25, see Figure 8). However, the highest GBA2 activity in lysates of GBA1-deficient embryonal fibroblasts was measured at pH 5.25, which is slightly more acidic than pH 5.5 (control cells), but not dramatically different (Figure 34). This in in line with findings from other groups, who have determined a pH optimum for GBA2 in human fibroblasts of 5.8 (Aureli et al., 2009; Aureli et al., 2016).

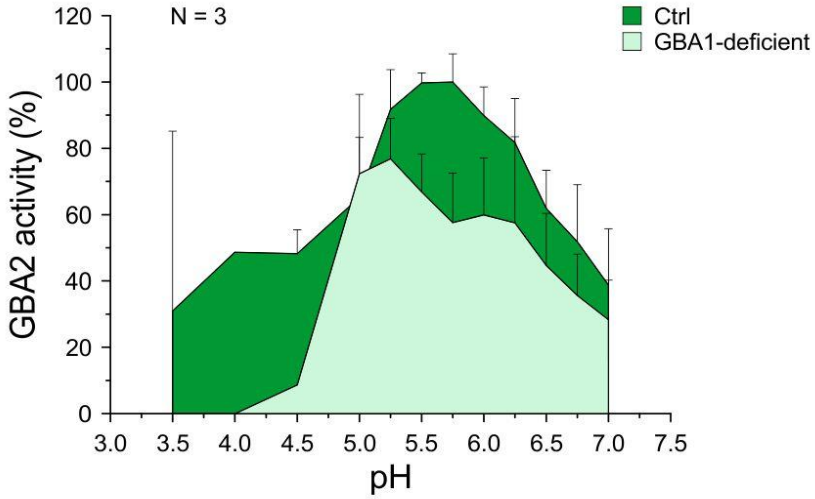

Figure 34: pH optimum of GBA2 activity in embryonal fibroblasts from control and GBA1-deficient mice. Analysis of the GBA2 activity in hypotonic lysates of control and GBA1-deficient mouse embryonal fibroblasts at a pH ranging from 3.5 – 7.0 in presence of 1.67 mM 4-MUG. The highest GBA2 activity in embryonal fibroblasts from control mice was measured at pH 5.5, whereas the highest GBA2 activity in lysates of GBA1-deficient embryonal fibroblasts was measured at pH 5.25. 4-MUG: 4-Methylumbelliferyl beta-D-glucopyranoside. Data are presented as mean + SD. The N number is indicated.

3.10 Rescuing GBA2 activity in GBA1-deficient cells

Since the activity of GBA2 seems to be directly correlated to the activity of GBA1, I tested whether GBA2 activity could be restored by over-expressing mGBA1 in GBA1-

deficient cells. HAP1 GBA1-deficient cells were transfected with mGBA1 and analysed two days after transfection. Transfection resulted in over-expression of GBA1 (Figure 35a), and GBA1 activity of 0.45 rfu/min (Figure 35b). However, the slight increase in GBA1 activity did not increase the activity of GBA2 (Figure 35c).

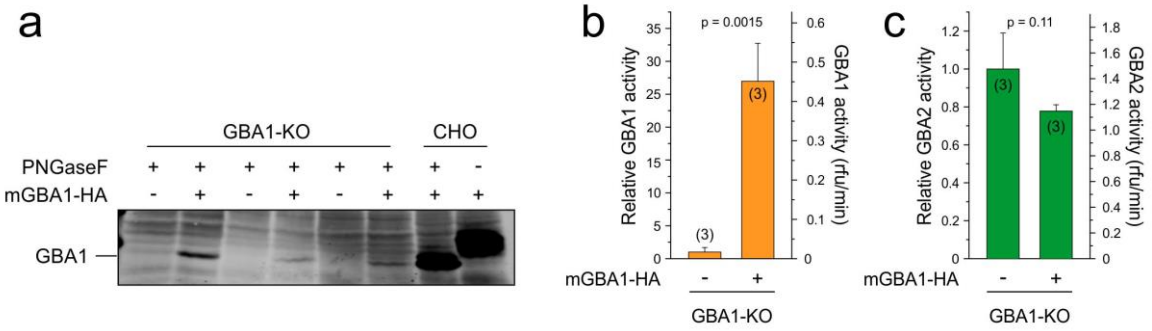

Figure 35: GBA1 and GBA2 protein expression and activity in HAP1 cells deficient for GBA1 transiently transfected with mGBA1. Analysis of total (endogenous and heterologous) GBA1 protein expression in HAP1 GBA1-deficient cell lysates after deglycosylation using PNGaseF by Western blot using a GBA1-specific antibody (Sigma). CHO cells stably over-expressing mGBA1-HA were used as a positive control. GBA1 and GBA2 activity were analysed in hypotonic cell lysates in presence of 1.67 mM 4-MUG. **(a)** GBA1-HA protein expression was visible in GBA1-deficient HAP1 cells after transfection. **(b)** Transfection with mGBA1 resulted in GBA1 activity of 0.45 rfu/min. **(c)** The GBA2 activity remained unchanged in GBA1-deficient HAP1 cells transfected with mGBA1 compared to the controls. PNGaseF: Peptide-N-Glycosidase F (NEB), KO: Knock-out, 4-MUG: 4-Methylumbelliferyl beta-D-glucopyranoside. Data are presented as mean + SD. N numbers are shown in brackets. P values were determined using One-way ANOVA.

3.11 GBA1 and GBA2 activity in dermal fibroblasts from *Niemann-Pick* patients

Niemann-Pick disease also belongs to the group of lysosomal storage disorders (Vanier&Millat, 2003). The disease is classified into three major categories (Crocker, 1961), although there is no clear genotype-phenotype correlation, similar to what has been shown for *Gaucher* disease. *Niemann-Pick* type A and B (NP-A and –B) result from a deficiency in acid sphingomyelinase, an enzyme that is encoded by the *SMPD1* gene in humans (Schuchman, 2010). Acid sphingomyelinase resides in the lysosomes and breaks down sphingomyelin to ceramide and phosphocholine (Schuchman, 2010). Thus, in case of NP-A and –B, sphingomyelin accumulates to harmful quantities in the lysosomes, causing enlargement of liver and spleen (mainly type B) or severe neurological defects (mainly type A) (Crocker, 1961). Mutations in *NPC1* or *NPC2* cause the third form of *Niemann-Pick* disease, namely type C (NP-C) (Pentchev et al., 1994). The proteins encoded by these genes are essential for the export of cholesterol

from the lysosomes (Sleat et al., 2004). Therefore, NP-C is now considered a cellular lipid trafficking disorder that mainly, but not only, involves cholesterol (Pentchev et al., 1994). As for NP-A and –B, the age of onset of the disease is extremely heterogeneous and so is the variety of symptoms: patients suffering from the disease show visceral involvement of liver and spleen, and also neurologic manifestations (Vanier, 2010).

A recent study by Marques and co-workers proposed that the activity of GBA2 is increased in the brain of NP-C mice (Marques et al., 2015). To reduce the GBA2 activity back to normal control levels, they either bred NP-C mice to GBA2-deficient mice to create double knockout mice or treated NP-C mice with a brain-permeable inhibitor for GBA2 to block its activity. Interestingly, reduction of GBA2 activity significantly improved the motor coordination and lifespan of these NP-C mice, while cholesterol mis-trafficking was still observed (Marques et al., 2015). Based on their data, Marques and co-workers concluded that GBA2 might be a therapeutic target in *Niemann-Pick* disease type C.

To learn more about the regulation of GBA2 in *Niemann-Pick* disease, the GBA1 and GBA2 activity was analysed in dermal fibroblasts obtained from NP-A, -B, and –C patients and compared to control fibroblasts (Figure 36). The GBA1 activity in NP-A and –B fibroblasts was variable, with GBA1 being slightly more active in some of the tested cell lines (Figure 36a). GBA2, however, remained constant in all tested NP-A and –B samples (Figure 36b). Interestingly, the GBA1 activity was significantly reduced to around 10% and 12% in two of the three tested NP-C samples (Figure 36a). Vanier *et al.* already published work in 1983 showing that a reduction in GBA1 activity is a secondary effect in NP-C cells, resulting in accumulation of GlcCer up to levels seen in *Gaucher* samples (Vanier, 1983). Interestingly, the GBA2 activity in these cell lines was also reduced to 48% (Figure 36b). As seen above (Figure 22), GBA2 activity was only significantly reduced when GBA1 activity was almost fully absent (Figure 36b). However, my results do not confirm the data obtained by Marques and co-workers. Their data were generated using different methods and different samples (mouse brain *versus* dermal fibroblasts from *Niemann-Pick* patients). To be able to fully compare the two data sets, I would have to analyse the GBA1 and GBA2 activity in brains from NP-C and control mice with our assay.

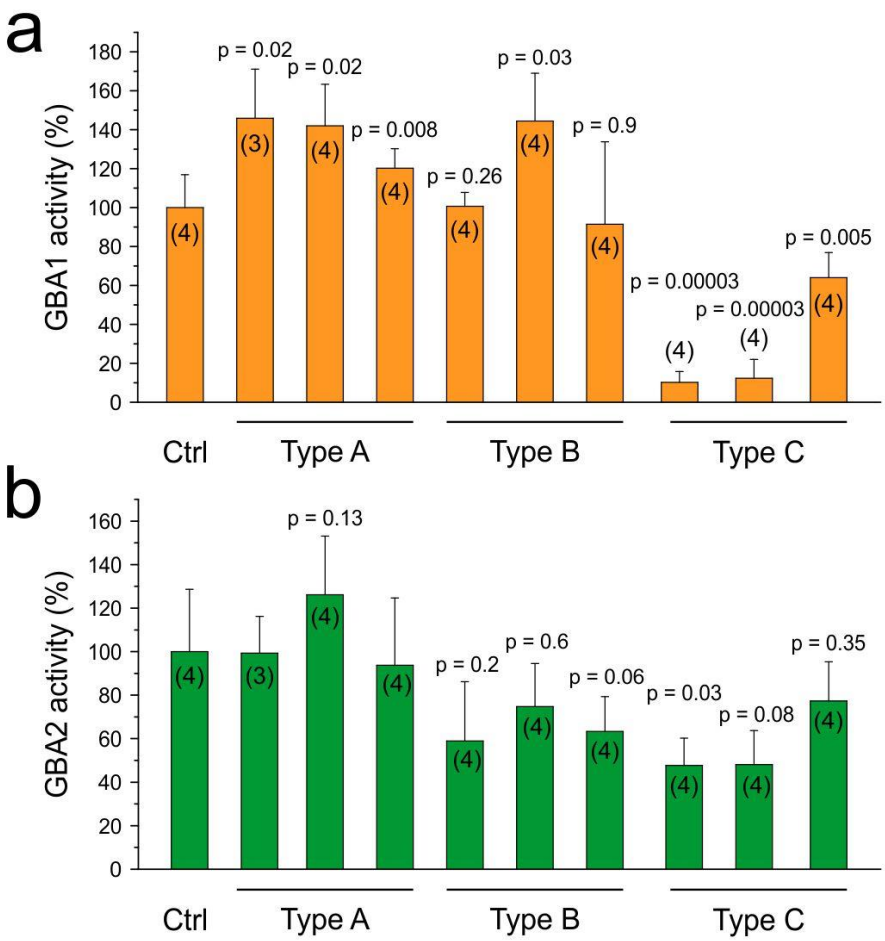

Figure 36: GBA1 and GBA2 activity in dermal fibroblasts from control and Niemann-Pick disease patients. Analysis of beta-glucosidase activity in hypotonic lysates of control fibroblasts and cells carrying mutations in either the SMPD1 gene or the *NPC1/2* gene, resulting in Niemann-Pick disease type A, B, or C, in presence of 1.67 mM 4-MUG **(a)** The GBA1 activity was very heterogeneous in NP-A and –B cells and significantly reduced in NP-C cells. **(b)** The GBA2 activity was comparable to control values in NP-A and –B cells but reduced to 48% and 77% in NP-C cells. 4-MUG: 4-Methylumbelliferyl beta-D-glucopyranoside. Data are presented as mean + SD. N numbers are indicated in brackets. P values were determined using One-way ANOVA.

3.12 GBA2 activity is not dependent on the availability of GlcCer

In GBA1-deficient cells, GlcCer accumulates and the GBA2 activity is reduced. In turn, I wondered if a reduction in GlcCer levels would also affect the beta-glucosidase activity. In this scenario, GBA1 and GBA2 could work as “sensors” for GlcCer in the cell. The easiest way to study this hypothesis is to analyse the GBA1 and GBA2 activity in cells that lack GlcCer. As previously mentioned, ceramides are synthesised at the cytosolic side of the ER and have various acyl chain lengths, which are specific to one of the six CerS, which catalyse their transfer to sphinganine/sphingosine

(Levy&Futerman, 2010). Therefore, the presence of certain ceramide species depends on the activity of a certain CerS. In general, lack of ceramide also leads to lack of GlcCer. GlcCer, however, is synthesised by GlcCerS at the cytoplasmic side of the *cis* and *medial* part of the Golgi (Basu et al., 1968; Schweizer et al., 1994).

3.12.1 GBA1 and GBA2 activity in tissues from CerS2-deficient mice

To study this hypothesis, GBA1 and GBA2 activity was analysed in brain, testis, and liver from ceramide synthase 2 (CerS2)-deficient mice (Imgrund et al., 2009). CerS2 tissue expression is quite broad with major expression in liver, kidney, and bone marrow and moderate expression in brain and testis (Levy&Futerman, 2010). Whilst GBA1 is ubiquitously expressed amongst all tissues (Brady et al., 1965), GBA2 shows highest expression in brain, liver, and testis (Yildiz et al., 2006). Thus, the latter three organs were chosen for activity and expression analysis (Figure 37). GBA1 activity was similar in brain, testis, and liver from CerS2-deficient and control mice (Figure 37a). In CerS2-deficient liver, GBA2 was slightly less active compared to control livers (Figure 37b). Furthermore, GBA2 activity was similar in brain and testis from CerS2-deficient mice and control brain (Figure 37b). As a control experiment, GBA2 protein expression was verified in CerS2-deficient tissues by Western blot analysis and, as expected from the assay results, GBA2 was similarly expressed in all tissues from both genotypes (Figure 37c-i). Thus, lack of a certain ceramide species does not affect the activity of GBA1 or GBA2.

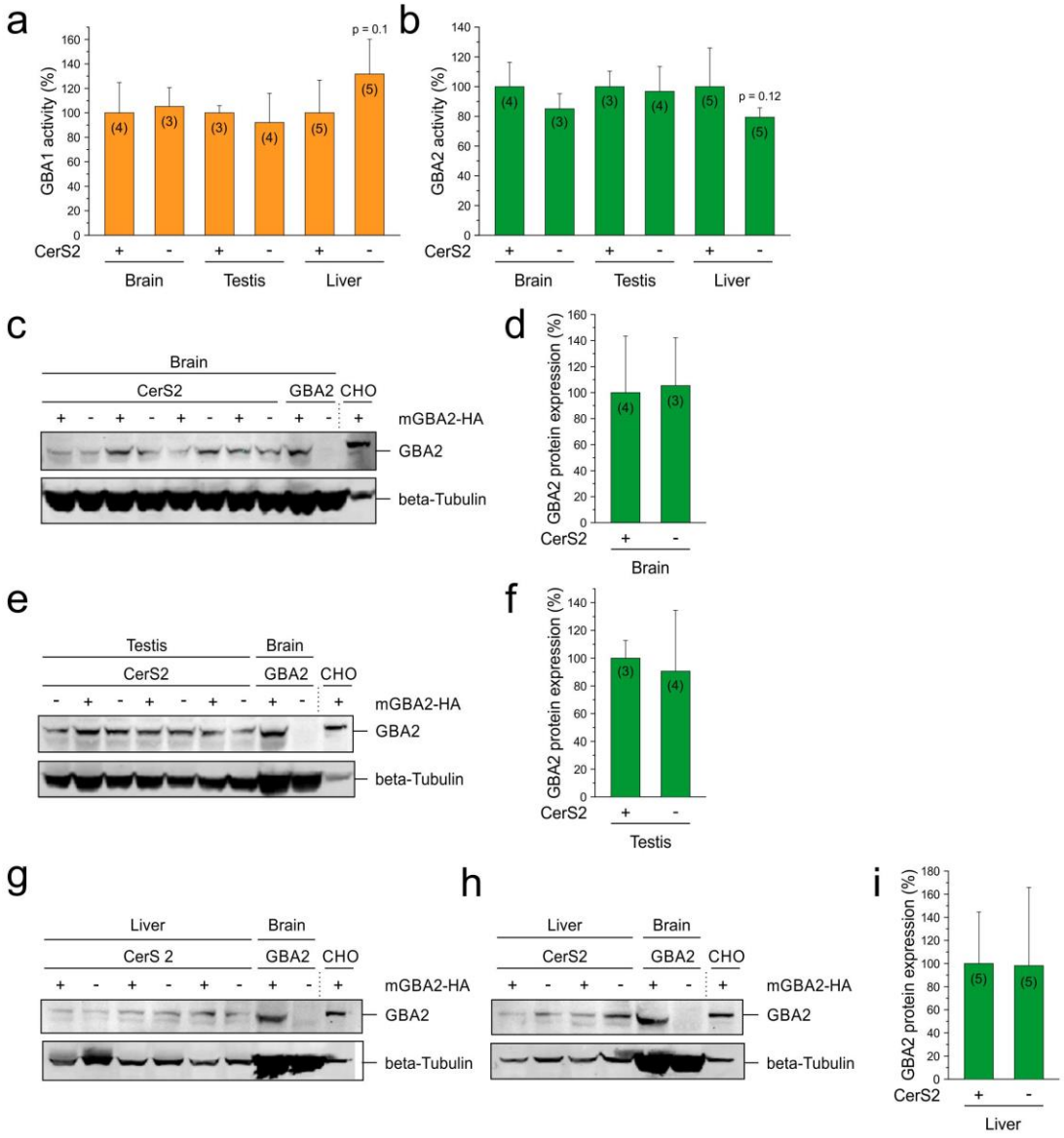

Figure 37: GBA1 and GBA2 activity and protein expression in tissues from CerS2-deficient mice. Analysis of GBA1 and GBA2 activity in hypotonic lysates of control and CerS2-deficient mice in presence of 1.67 mM 4-MUG. GBA2 protein expression was analysed in hypotonic lysates by Western blot using a GBA2-specific antibody (clone 2F8, rat, Körschen et al. 2013). Tubulin was used as loading control. **(a)** GBA1 activity was similar in brain, testis, and liver from CerS2-deficient and control mice. **(b)** GBA2 was slightly but not significantly less active in CerS2-deficient liver and remained unchanged in brain and testis. **(c)** GBA2 protein expression was similar in hypotonic brain lysates from control and CerS2-deficient mice. **(d)** Quantification of GBA2 protein expression in brain from control and CerS2-deficient mice normalised to Tubulin. **(e)** + **(f)** and **(g)** - **(i)** as **(c)** + **(d)** for testis and liver lysates. CerS2: Ceramide synthase 2, 4-MUG: 4-Methylumbelliferyl beta-D-glucopyranoside. Data are presented as mean + SD. N numbers are indicated in brackets. P values were determined using One-way ANOVA.

3.12.2 GBA1 and GBA2 activity in cells treated with Fumonisin B1

As previously mentioned, there are six CerS known, with each isoform showing a specificity for a particular acyl chain-length. To block ceramide synthesis, a pharmacologic approach was applied that blocks all six CerS at once by using Fumonisin B1 (FB1) (Figure 38). FB1 is produced by several species of *Fusarium* molds (Marasas, 2001) and inhibits N-acylation of both, sphingosine and sphinganine, during ceramide synthesis (Merrill et al., 1993a; Merrill et al., 1993b; Merrill&Wang, 1992). Merrill and co-workers demonstrated that around 50% of CerS activity is blocked by 75 nM FB1 in mouse brain microsomes (Merrill et al., 1993a). Thus, dermal fibroblasts from control patients were incubated with 5 µM FB1 for 48 h to fully block CerS activity (Figure 38). Cells were harvested and hypotonic protein lysates were split in two fractions, with one sample maintaining the initial concentration of 5 µM FB1 in the lysate (Figure 38). However, GBA1 and GBA2 activity in FB1-treated cells was similar to control cells (Figure 38). Thus, these data confirm my previous results (see Figure 37), underlining that the absence of ceramide does not affect GBA1 and GBA2 activity.

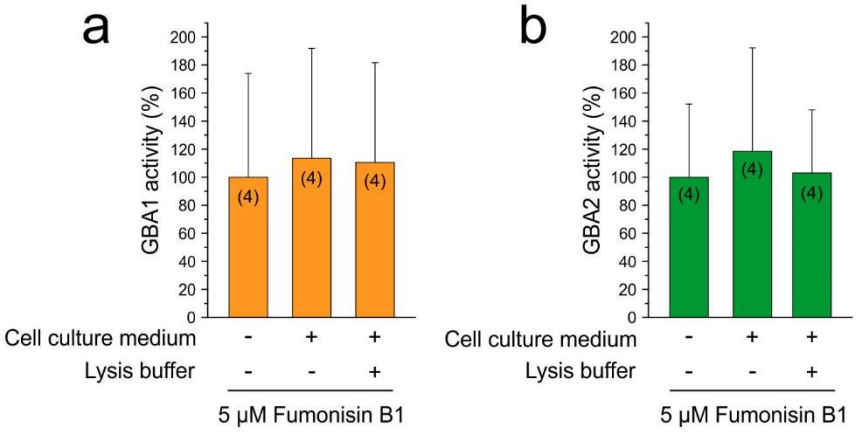

Figure 38: GBA1 and GBA2 activity in human dermal fibroblasts treated with Fumonisin B1. Analysis of GBA1 and GBA2 activity in hypotonic lysates of human dermal fibroblasts treated with 5 µM Fumonisin B1 to block CerS activity compared to control cells in presence of 1.67 mM 4-MUG. **(a)** GBA1 and **(b)** GBA2 activity remained unchanged in cells treated with 5 µM Fumonisin B1. 4-MUG: 4-Methylumbelliferyl beta-D-glucopyranoside. Data are presented as mean + SD. N numbers are indicated in brackets.

3.12.3 GBA1 and GBA2 activity in cells deficient for GlcCerS

Furthermore, I analysed the activity of GBA1 and GBA2 in cells that do not express GlcCerS, termed GM-95 cells, and thereby, lack any glycosphingolipids (Ichikawa et

al., 1994). GM-95 cells, formerly known as MEB-4 cells (Nozue et al., 1988), were generated from a mouse B16 melanoma cell line (termed MEB-4 cells) by N-methyl-N'-nitro-N-nitrosoguanidine (MNG) mutagenesis (Nozue et al., 1988). MNG adds alkyl groups to O6 of guanine and O4 of thymine, causing mutations between GC and AT (Merck Index, 11th Edition, 6017). These changes are not detected by the DNA mismatch repair–system, resulting in mutations that may cause gene silencing (Merck Index, 11th Edition, 6017). According to Ichikawa and co-workers, GM-95 cells do not express an active form of ceramide glucosyltransferase (Ichikawa et al., 1994), meaning these cells do not synthesise any glycosphingolipids, whereas ceramide levels are normal. Compared to the parental cell line (MEB-4), GM-95 cells show an elongated and fibroblast-like morphology, while exhibiting longer proliferation times (Ichikawa et al., 1994). According to my previous hypothesis, GBA1 activity might be reduced in these cells due to the lack of total GlcCer and could then also evoke the same effect on GBA2 activity that I had previously seen in *Gaucher* fibroblasts. But, again, GBA2 could also work as an independent "sensor" for GlcCer at the Golgi, meaning that lack of GlcCer in GM-95 cells could also have a GBA1-independent effect on GBA2.

The GBA1 and GBA2 activity was studied in GlcCer-deficient (GM-95) and control (MEB-4) cells to analyse whether the absence of GlcCer affects the activity of either beta-glucosidase (Figure 39). Surprisingly, neither GBA1 nor GBA2 activity were significantly changed between both cell lines (Figure 39). Thus, the absence of GlcCer has no effect on the regulation of GBA1 and GBA2. Of note, this result does not rule out that increased levels of GlcCer affect GBA1 or GBA2 activity.

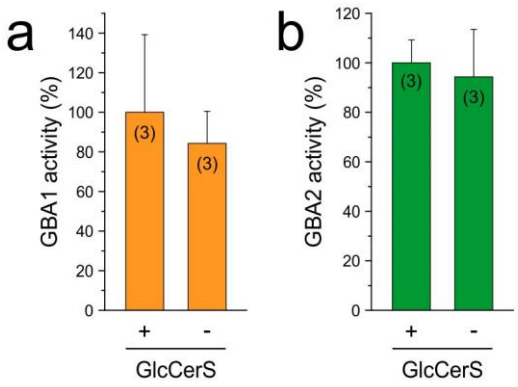

Figure 39: GBA1 and GBA2 activity in GlcCerS-deficient cells. Analysis of GBA1 and GBA2 activity in hypotonic lysates of control (MEB-4) and GlcCerS-deficient (GM-95) mouse melanoma cells in

presence of 1.67 mM 4-MUG. Both, GBA1 **(a)** and GBA2 **(b)** activity, remained unchanged in the absence of GlcCer. GlcCerS: glucosylceramide synthase, 4-MUG: 4-Methylumbelliferyl beta-D-glucopyranoside. Data are presented as mean + SD. N numbers are indicated in brackets.

3.13 The effect of sphingoid bases on GBA2 activity

3.13.1 Sphingosine inhibits GBA2 activity

Deficiency of GBA1 in *Gaucher* patients causes the accumulation of not only GlcCer, but also glucosylsphingosine (GlcSph) (Ferraz et al., 2016). As previously mentioned, it has been proposed that in cells from *Gaucher* patients, both, GlcCer and GlcSph, spill-over from the lysosomes into the cytoplasm, thereby becoming a substrate for GBA2 (Mistry et al., 2014). This increase of a GBA2-dependent break down of GlcCer would lead to an accumulation of cytotoxic sphingosine in the cell, which has been proposed to cause some of the defects associated with *Gaucher* pathophysiology (Mistry et al., 2014). In favour of this hypothesis, deletion of GBA2 rescued some of the defects associated with *Gaucher* pathophysiology (Mistry et al., 2014).

I hypothesised that cells, accumulating GlcCer and GlcSph in the lysosomes due to a loss of GBA1 activity, have developed a mechanism, whereby GBA2 activity is diminished to avoid accumulation of the cytotoxic metabolite sphingosine. The simplest scenario that could be envisioned would be a regulation of GBA2 activity by sphingosine. To test this hypothesis, I analysed if the GBA2 activity is sensitive to sphingosine.

CHO cells stably over-expressing mGBA2 were incubated with 20 µM sphingosine for 4.5 h and the GBA1 and GBA2 activity was measured (Figure 40a). Surprisingly, both, GBA1 and GBA2 activity, were significantly reduced to around 26% and 42% of the non-treated samples, respectively (Figure 40b, c). In *Gaucher* disease patients, this effect only applies to GBA2 as GBA1 is not active (see Figure 14). However, the experimental set up in CHO cells does not allow to conclude whether both, GBA1 and GBA2, are sensitive to sphingosine because a down-regulation of GBA1 activity by sphingosine would be sufficient to reduce GBA2 activity, without sphingosine having a direct effect on GBA2. Arguing against this is the short incubation time with sphingosine (4.5 h). In previous experiments using CBE, GBA1 activity was significantly reduced after 3 h and GBA2 activity was only reduced when GBA1 was almost completely blocked for several hours (see Figure 22). Thus, an incubation time of only 4.5 h might not be sufficient to reduce GBA2 activity via GBA1. However, one has to keep in mind

that CBE and sphingosine might possess different properties when entering a cell (e.g. trafficking time to the lysosomes) and their mechanism of action on GBA1 are, most likely, also completely different.

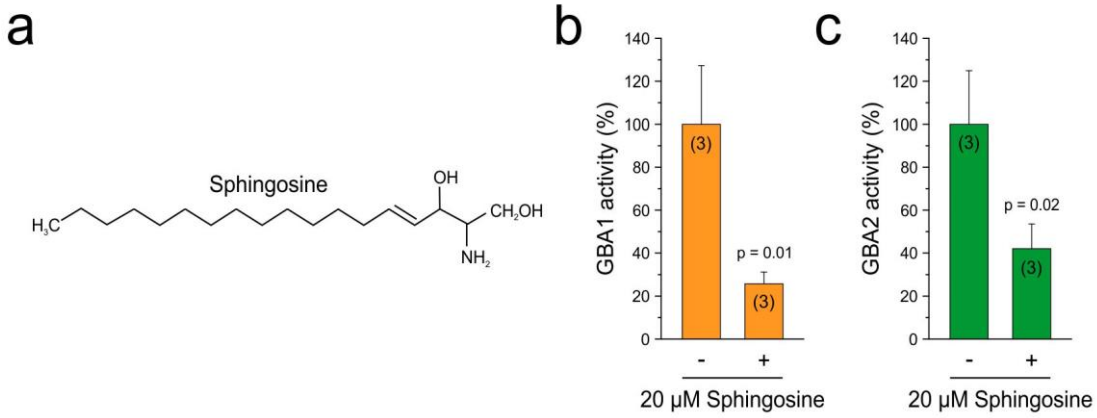

Figure 40: GBA1 and GBA2 activity in CHO cells stably over-expressing mGBA2 treated with 20 µM sphingosine. Analysis of GBA1 and GBA2 activity in hypotonic lysates of CHO cells stably over-expressing mGBA2 treated with 20 µM sphingosine compared to control cells in presence of 1.67 mM 4-MUG. **(a)** Structure of sphingosine. **(b)** GBA1 and **(c)** GBA2 activity were significantly reduced to around 26% and 42% of the non-treated samples, respectively. 4-MUG: 4-Methylumbelliferyl beta-D-glucopyranoside. Data are presented as mean + SD. N numbers are indicated in brackets. P values were determined using One-way ANOVA.

To tackle this problem, embryonal fibroblasts from GBA1-deficient mice were incubated with 20 µM sphingosine for 4.5 h to study the effect of sphingosine on GBA2 in a GBA1-independent manner (Figure 41). As seen in Figure 41, incubation with 20 µM sphingosine reduced the GBA2 activity in control cells to around 62% compared to the non-treated samples. Interestingly, sphingosine further reduced the GBA2 activity in GBA1-deficient cells to only 6% compared to 14% in the non-treated GBA1-deficient samples (Figure 41). Thus, GBA1 and GBA2 are both sensitive to sphingosine.

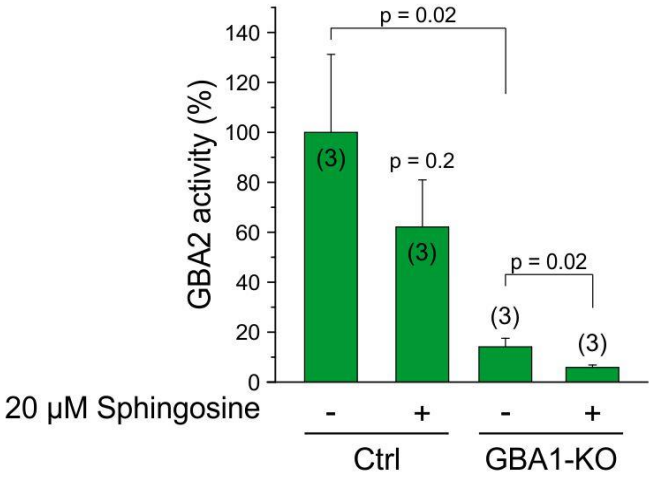

Figure 41: GBA2 activity in control and GBA1-deficient mouse embryonal fibroblasts treated with 20 µM sphingosine. Analysis of the GBA2 activity in hypotonic lysates of GBA1-deficient mouse embryonal fibroblasts treated with 20 µM sphingosine compared to control (Ctrl) cells in presence of 1.67 mM 4-MUG. Incubation with 20 µM sphingosine reduced the GBA2 activity in control cells to around 62% and to only 6% compared to 14% in GBA1-deficient samples. 4-MUG: 4-Methylumbelliferyl beta-D-glucopyranoside. Data are presented as mean + SD. N numbers are indicated in brackets. P values were determined using One-way ANOVA.

3.13.2 GBA2 is also sensitive to sphinganine

Sphinganine differs from sphingosine by one double bond in the alkyl chain (Figure 42a). To test whether sphinganine, the saturated form of this sphingoid base, also exhibits an inhibitory effect, experiments were repeated in CHO cells stably over-expressing mGBA2 using 20 µM sphinganine (Figure 42). Again, both enzymes were less active after incubation with sphinganine, albeit the effect was stronger for GBA1 (Figure 42b). In summary, GBA1 and GBA2 are both sensitive to sphingosine and sphinganine, suggesting that the steric dimension of the sphingoid alkyl chain is irrelevant for the inhibitory effect.

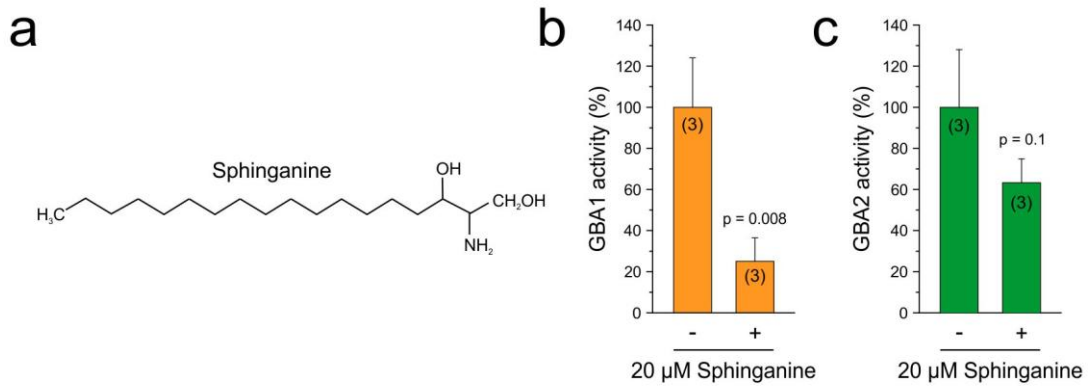

Figure 42: GBA1 and GBA2 activity in CHO cells stably over-expressing mGBA2 treated with 20 µM sphinganine. Analysis of GBA1 and GBA2 activity in hypotonic lysates of CHO cells stably over-expressing mGBA2 treated with 20 µM sphinganine compared to control cells in presence of 1.67 mM 4-MUG. **(a)** Structure of sphinganine. **(b)** GBA1 and **(c)** GBA2 activity were significantly reduced to around 26% and 63% of the non-treated samples, respectively. 4-MUG: 4-Methylumbelliferyl beta-D-glucopyranoside. Data are presented as mean + SD. N numbers are indicated in brackets. P values were determined using One-way ANOVA.

3.13.3 Sphingosine reduces the GBA2 activity in protein lysates from different mouse tissues

Next, I tested whether the inhibitory effect of sphingosine on GBA2 is direct or involves a signalling cascade that requires an intact cell. I analysed GBA1 and GBA2 activity in hypotonic protein lysates from murine brain after incubation with 20 µM sphingosine for 1.5 h and compared the results to non-treated control lysates (Figure 43). GBA1 activity remained unchanged after incubation with sphingosine, whereas the GBA2 activity was slightly, but significantly, reduced to 81% (Figure 43). These data again support the idea that sphingosine blocks GBA2 directly and independent from GBA1.

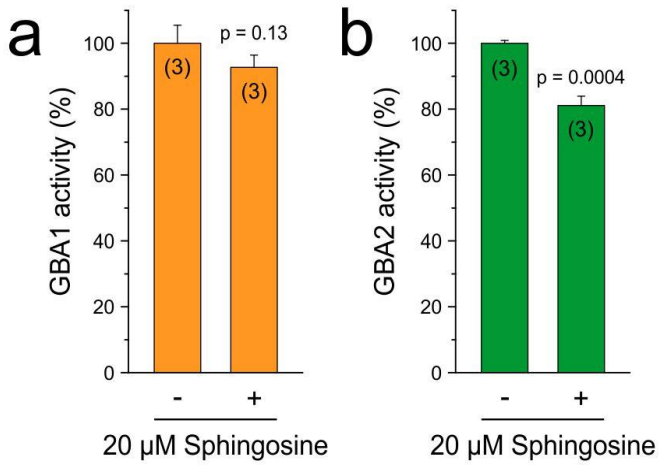

Figure 43: GBA1 and GBA2 activity in control brain lysates incubated with 20 µM sphingosine. Analysis of GBA1 and GBA2 activity in hypotonic brain lysates from control mice incubated with 20 µM sphingosine compared to control lysates in presence of 1.67 mM 4-MUG. **(a)** The GBA1 activity remained unchanged after incubation with sphingosine, whereas the **(b)** GBA2 activity was slightly, but significantly, reduced to 81% compared to the controls. 4-MUG: 4-Methylumbelliferyl beta-D-glucopyranoside. Data are presented as mean + SD. N numbers are indicated in brackets. P values were determined using One-way ANOVA.

To validate these results, I made use of the different localisations of GBA1 and GBA2. Microsomes originate from ER membranes and contain GBA2, but not GBA1 (Körschen et al., 2013). Microsomes can be separated from other cellular organelles by differential centrifugation: Nuclei and cellular debris are sedimented at rather low g-forces (low speed centrifugation, e.g. 1,000 x g), while soluble enzymes and organelles like mitochondria and the ER (microsomes) remain in the supernatant. After high speed centrifugation (e.g. 15,000 x g), organelles are separated from the soluble lysate fraction. Finally, microsomes are sedimented at around 80,000 x g (ultracentrifugation) (Claude, 1946). Microsomes were prepared from brain and liver of GBA2-deficient and control mice (Figure 44) (Optima MAX-XP Ultracentrifuge, Beckman Coulter).

The different steps of the microsomal preparation from liver were verified by Western blot analysis using an anti-GBA2 antibody and an organelle marker for the ER, calnexin (Figure 44b). Both, GBA2-deficient and control microsomal samples, were strongly positive for calnexin, demonstrating that the enrichment worked. The anti-GBA2 antibody also labelled a band in the microsomal fraction of the control but not in the GBA2-deficient sample, demonstrating that GBA2 was enriched in this fraction (Figure 44b). GBA2 was also present in the supernatant after ultracentrifugation, although this fraction was negative for calnexin, underlining the finding that GBA2 is only membrane-

associated (Figure 44b) (Körschen et al., 2013). To verify the absence of lysosomes and, thereby, GBA1 in the microsomal fraction, I also stained with an anti-GBA1 antibody (Figure 44b). GBA1 is highly glycosylated (Bergmann&Grabowski, 1989), making it difficult to detect defined protein bands on the Western blot without de-glycosylation of the protein. Thus, bands labelled by the anti-GBA1 antibody were not very defined and rather cloudy (Figure 44b).

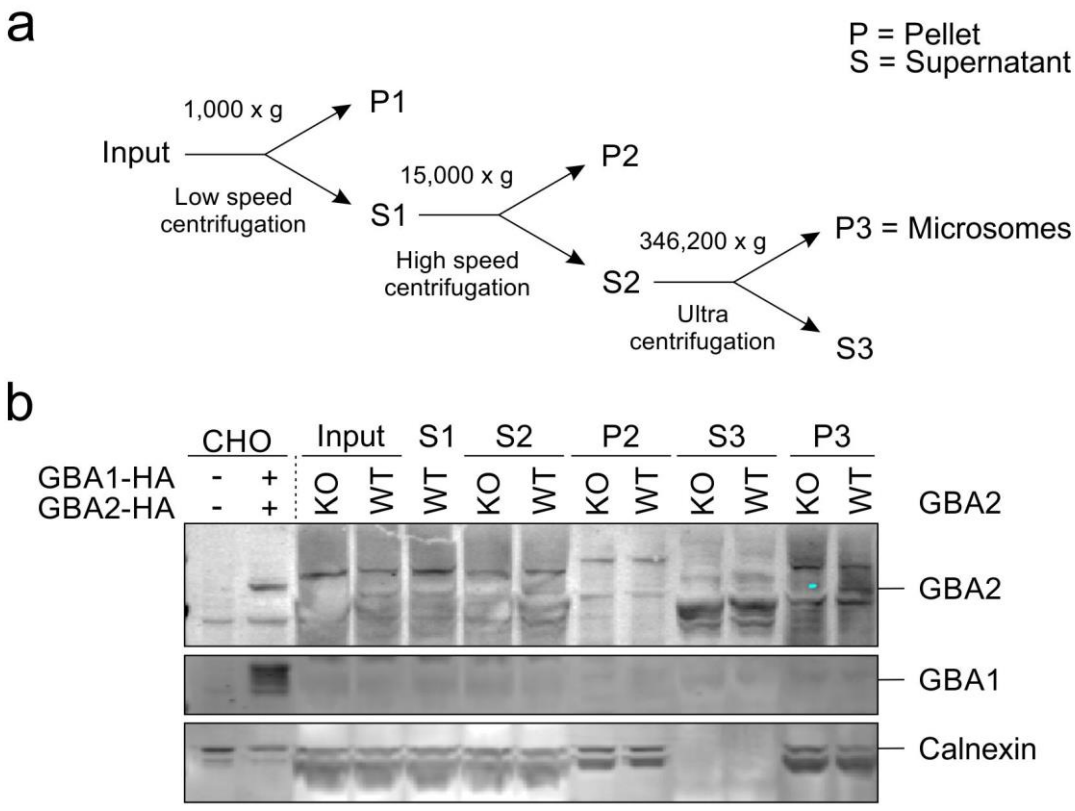

Figure 44: Preparation of microsomes from mouse liver. Purification of microsomes from a hypotonic lysate of a mouse liver by differential centrifugation. **(a)** Flow-chart of microsome preparation. **(b)** The single fractions were analysed for the presence of GBA1 and GBA2 by Western blot using specific antibodies against GBA1 (Sigma) or GBA2 (mix of monoclonal antibody clones 4A12 and 2F8 from rat, Körschen et al. 2013). The ER-resident protein calnexin was used to verify the presence of ER membranes. GBA2 was enriched in the microsomal fraction/P3 of the control mouse together with calnexin. P: Pellet, S: Supernatant, WT: Wild-type, KO: Knockout.

To further verify the preparation, I also analysed the beta-glucosidase activity in the input and pellet fractions (Figure 45). The main activity for both, GBA1 and GBA2, was detected in the first pellet fraction, indicating that most of the protein was lost during the first step. Accordingly, the GBA2 activity recovered in the last pellet fractions was rather low compared to the input (Figure 45b). Unfortunately, there was activity

detectable at both pH values in the microsomal fraction, indicating that GBA1 was still present in the pellet fraction after ultracentrifugation (Figure 45a).

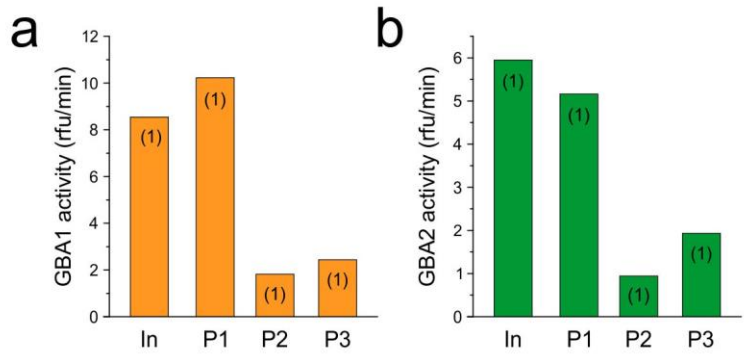

Figure 45: GBA1 and GBA2 activity in different fractions from hypotonic mouse liver lysates after differential centrifugation. Analysis of GBA1 and GBA2 activity in hypotonic liver lysates from control mice in presence of 1.67 mM 4-MUG. **(a)** Most of GBA1 and **(b)** GBA2 remained in the first pellet fraction, indicating that most of the protein was lost during the first step. The GBA2 activity recovered in the last pellet fractions was rather low compared to the input. The separation of GBA2 from GBA1 did not work. 4-MUG: 4-Methylumbelliferyl beta-D-glucopyranoside. N numbers are indicated in brackets.

Thus, I tested the same approach using hypotonic lysates of a mouse brain (Figure 46). In brain lysates, the absolute GBA2 activity is much higher than the activity of GBA1 (Figure 46). However, also here, most of GBA1 and GBA2 seem to be lost after the first centrifugation, which resulted in very little beta-glucosidase activity in the last pellet fraction (Figure 46). As seen for liver (Figure 45), GBA1 activity was detectable in the microsomal fraction (Figure 46a), albeit the activity of GBA2 in the microsomal fraction was significantly higher than the GBA1 activity (38 rfu/min *versus* 6.5 rfu/min) (Figure 46).

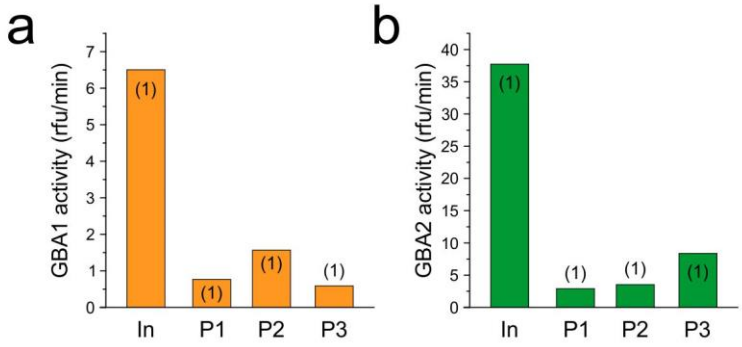

Figure 46: GBA1 and GBA2 activity in different fractions from hypotonic mouse brain lysates after differential centrifugation. Analysis of GBA1 and GBA2 activity in hypotonic liver lysates from control mice in presence of 1.67 mM 4-MUG. **(a)** Most of GBA1 and **(b)** GBA2 seems to remain in the first supernatant, resulting in very little GBA2 activity in the microsomal/P3 pellet fraction. The separation

of GBA2 from GBA1 did not work. 4-MUG: 4-Methylumbelliferyl beta-D-glucopyranoside. N numbers are indicated in brackets.

3.14 Sphingosine directly inhibits GBA2

3.14.1 Expression of mGBA2-His in bacteria

To finally reveal whether sphingosine exerts a direct effect on GBA2, I switched to a prokaryotic system and expressed mGBA2 in *E.coli* BL21 CodonPlus DE3 RIPL, which contain the DE3 bacteriophage lambda lysogen and, thus, carry the *lacI* gene together with its promotor (binding site for RNA polymerase), the lac operon, and the gene for T7 RNA polymerase under control of lacUV5 promoter (Figure 47) (Agilent Technologies). The *lacI* gene encodes the lac repressor. Under normal conditions, the lac repressor is constantly expressed and binds to the operator between the lacUV5 promoter and the gene for T7 RNA polymerase. Thus, T7 RNA polymerase is not expressed. The lac operon itself consists of its promoter, the operator, and the coding sequence of the *lacZ* gene, encoding the beta-galactosidase that cleaves lactose. Bacteria were transformed with a pET21 vector containing the coding sequence of mGBA2-His under control of the T7 promotor (EMD Biosciences). Thus, it is only expressed after addition of isopropyl beta-D-1-thiogalactopyranoside (IPTG), a molecular mimic of allolactose that binds to the lac repressor. Binding of the lac repressor to IPTG prevents it from further occupying the operator and, thus, activates expression of the T7 RNA polymerase, which can then bind to its promoter (T7 promoter) and initiate the transcription of mGBA2-His.

Figure 47: The *lac* operon. Schematic drawing of the *lac* operon containing the *lacI* gene and its promoter and the *lac* operon and its promoter and operator. The single functions are described in the text.

I followed mGBA2 expression in the bacterial lysates by analysing the GBA2 protein expression and activity in hypotonic lysates before and after addition of 1 mM IPTG (Figure 48). mGBA2-His expression was only observed after IPTG induction (Figure 48a, c). Furthermore, NB-DNJ-blockable beta-glucosidase activity at pH 6 was only measured in the IPTG-induced sample, demonstrating that these bacteria contain no endogenous GBA2 activity (Figure 48c). Of note, the bacteria also lack beta-

glucosidase activity at pH 4, demonstrating that they also lack endogenous GBA1 activity (Figure 48b).

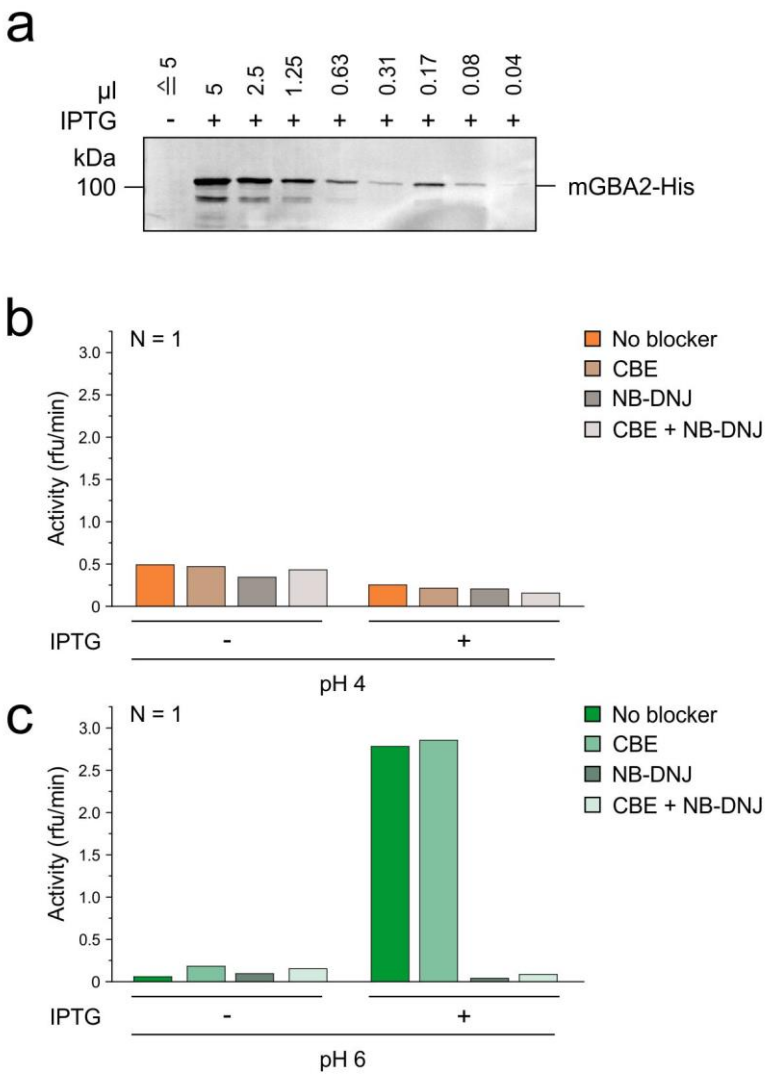

Figure 48: Expression of mGBA2 in *E. coli*. Bacteria of the *E.coli* strain BL21 CodonPlus DE3 RIPL were transformed with a pET21 vector containing mGBA2-His under the control of the T7 promotor. Induction of mGBA2 expression by addition of 1 mM IPTG was followed by Western blot using an anti-His antibody (Novagen). Beta-glucosidase activity was analysed at pH 4 and pH 6 before and after addition of IPTG in presence of 1.67 mM 4-MUG. **(a)** mGBA2-His was only detectable after IPTG induction. **(b)** There was no beta-glucosidase activity detectable at pH 4 in the bacteria culture before and after induction with IPTG. **(c)** NB-DNJ-blockable beta-glucosidase activity was only measurable at pH 6 in the IPTG-induced bacteria culture. IPTG: Isopropyl beta-D-1-thiogalactopyranoside, 4-MUG: 4-Methylumbelliferyl beta-D-glucopyranoside. N numbers are indicated.

The bacterial lysate was very viscous and difficult to pipet, which is why I made a serial dilution of the lysate to identify a dilution that was easy to pipet and showed a prominent GBA2 activity (Figure 49). Here, the 1:8 diluted sample had the smallest variation when

assayed as quadruples with an activity of 2.9 rfu/min (Figure 49). Thus, all experiments with bacterial lysates expressing mGBA2 were carried out in 1:8 diluted samples.

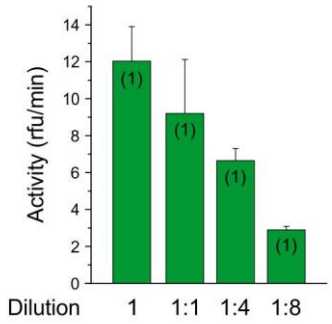

Figure 49: GBA2 activity in a serial dilution of hypotonic bacterial lysates over-expressing mGBA2. The GBA2 activity in a serial dilution of bacterial lysates was analysed in presence of 1.67 mM 4-MUG. The 1:8 diluted sample had the smallest variation with an activity of 2.9 rfu/min and was used for further experiments. 4-MUG: 4-Methylumbelliferyl beta-D-glucopyranoside. Data are presented as mean of quadruples + SD. N numbers are indicated in brackets.

To determine the amount of active GBA2 in the bacterial lysates, the total GBA2 activity in the lysates was correlated with the amount of GBA2 protein present. The latter was determined by Western blot analysis using an anti-GFP antibody and, as a reference, a purified GFP-fusion protein with a known protein concentration (Figure 50a). GFP-tagged mGBA2 was expressed in CHO cells and the activity of over-expressed GBA2 was analysed in these lysates. Here, 40 µg total lysate showed an endogenous activity of 0.5 ± 0.1 rfu/min and a total activity of 2.45 ± 0.14 rfu/min, resulting in an activity of 1.94 rfu/min for the over-expressed GBA2 protein (Figure 50c). I analysed the signal intensity of GFP-mGBA2 by Western blot using an anti-GFP antibody and compared the signal to the reference protein (Figure 50a, b). Here, e.g. 5 µg total protein from the CHO cell lysate corresponded to 7563 arbitrary units according to the anti-GFP antibody staining. By plotting a standard curve of the reference protein, I correlated the total amount of GFP/mGBA2 with the total amount of the reference protein (Figure 50b). Thus, 5 µg total protein from the CHO cell lysate contained 30.51 ng heterologously expressed mGBA2, which represents 244.08 ng GBA2 in 40 µg total protein and a GBA2 activity of 1.94 rfu/min (Figure 50c). I used 20 µl of a 1:8 diluted bacterial lysate over-expressing mGBA2-His to generate each data point in the following experiments (see Figure 51 following). Since 20 µl of this sample showed a GBA2 activity of 2.9 rfu/min (see Figure 49), it contained 359.31 ng GBA2.

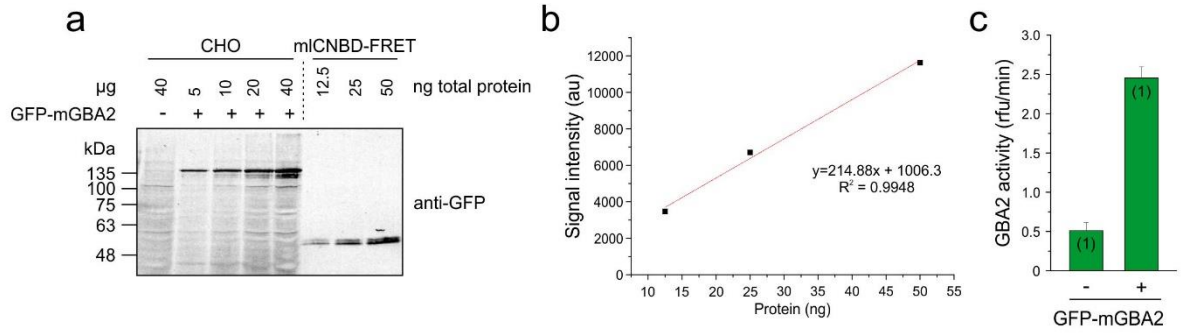

Figure 50: Determining the absolute amount of active GBA2 in bacterial lysates. GFP-tagged mGBA2 was expressed in CHO cells and analysed by Western blot using a GFP-specific antibody (Abcam). The activity of GBA2 was determined in GFP-mGBA2-transfected CHO cells in presence of 8.3 µM NB-DNJ and compared to the non-transfected control in presence of 1.67 mM 4-MUG. **(a)** 5 µg total protein from the CHO cell lysate had a GFP signal intensity of 7563 arbitrary units. **(b)** Plotting a standard curve of the reference protein revealed that 5 µg total protein from the CHO cell lysate contained 30.51 ng heterologously expressed mGBA2. **(c)** 40 µg total CHO lysate possessed a heterologous GBA2 activity of 1.94 rfu/min, which represented 244.08 ng GBA2. R^2 value: coefficient of determination, 4-MUG: 4-Methylumbelliferyl beta-D-glucopyranoside, au: Arbitrary units. Data are presented as mean of quadruples + SD. N numbers are indicated in brackets.

I first analysed the dose-response relationship of the beta-glucosidase activity to NB-DNJ (Figure 51). The IC_{50} for NB-DNJ in bacterial lysates over-expressing mGBA2 was 14.51 ± 2.7 nM, which is similar to the IC_{50} values previously determined in hypotonic lysates of mouse brain, liver, and testis (18.2 ± 0.3 nM, 20.9 ± 1.3 nM, and 19.2 ± 0.4 nM, respectively) (Körschen et al., 2013). Furthermore, the IC_{50} did not significantly change in the presence of 25 µM CBE (13.64 ± 3.4 nM, Figure 51b), demonstrating that the beta-glucosidase activity in the bacterial lysates was solely due to GBA2 (also compare Figure 48).

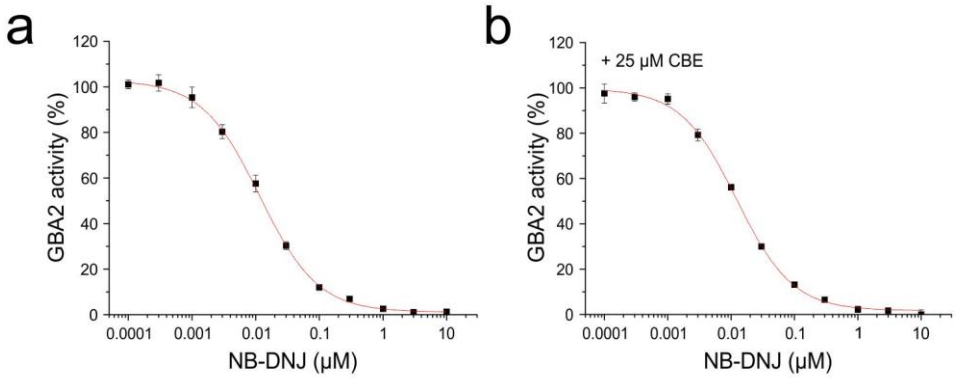

Figure 51: Dose-response relationship of GBA2 to NB-DNJ. Analysis of the GBA2 activity in bacterial lysates over-expressing mGBA2 in presence of a serial NB-DNJ dilution and 1.67 mM 4-MUG. Data

were normalised to a non-treated control. **(a)** The IC_{50} for NB-DNJ in bacterial lysates over-expressing mGBA2 was 14.51 ± 2.7 nM. **(b)** The IC_{50} for NB-DNJ in presence of 25 µM CBE was 13.64 ± 3.4 nM. NB-DNJ: N-butyl-deoxynojirimycin, CBE: Conduritol B epoxide, 4-MUG: 4-Methylumbelliferyl beta-D-glucopyranoside. Data are presented as mean of quadruples ± SD. Representative plot for n = 3 experiments.

3.14.2 Sphingoid bases directly inhibit GBA2 activity

I then assayed the dose-response relationship of GBA2 for sphingosine in bacterial lysates. Sphingosine reduced the GBA2 activity with an IC_{50} of 25.04 ± 0.2 µM (Figure 52). In summary, these results demonstrate that sphingosine directly inhibits GBA2 (Figure 52).

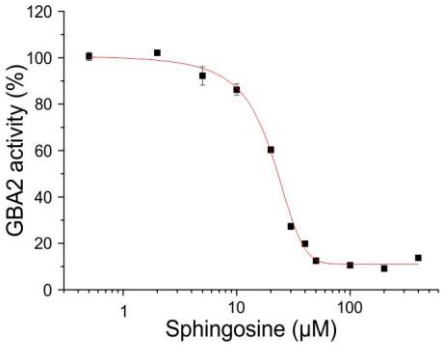

Figure 52: Dose-response relationship of GBA2 to sphingosine. Analysis of the GBA2 activity in bacterial lysates over-expressing mGBA2 in presence of sphingosine and 1.67 mM 4-MUG. Data were normalised to a non-treated control. The IC_{50} for sphingosine in bacterial lysates over-expressing mGBA2 was 25.04 ± 0.2 µM. 4-MUG: 4-Methylumbelliferyl beta-D-glucopyranoside. Data are presented as mean of quadruples ± SD. Representative plot for n = 3 experiments.

I could already show that sphinganine, the saturated derivative of sphingosine, affects the GBA2 activity when incubated with CHO cells stably over-expressing mGBA2 (see Figure 42). Thus, I also wanted to test whether sphinganine has the same effect on GBA2 in bacterial lysates and analysed the dose-response relationship of sphinganine for GBA2 over-expressed in bacteria (Figure 53). In accordance with my previous results, sphinganine inhibited GBA2 with an IC_{50} of 30.56 ± 4.47 µM, suggesting that the steric dimension of the sphingoid alkyl chain is irrelevant for the inhibitory effect.

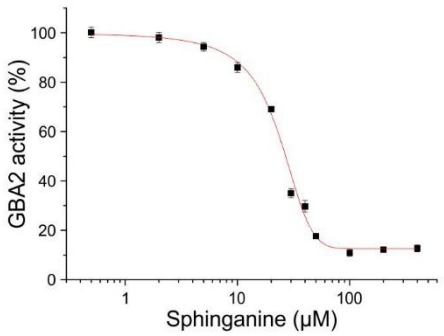

Figure 53: Dose-response relationship of GBA2 to sphinganine. Analysis of the GBA2 activity in bacterial lysates over-expressing mGBA2 in presence of a serial dilution of sphinganine and 1.67 mM 4-MUG at pH 6. Data were normalised to a non-treated control. The IC_{50} for sphinganine in bacterial lysates over-expressing mGBA2 was 30.56 ± 4.47 µM. Representative plot for n = 3 experiments, data are presented as mean of quadruples ± SD.

In the cell, sphingosine can be phosphorylated by sphingosine kinases to sphingosine-1-phosphate (S1P), a sphingoid messenger that controls multiple signalling pathways (Spiegel&Milstien, 2003). S1P is structurally similar to sphingosine, but additionally bears a phosphate head group (Figure 54a). I analysed whether GBA2 is also sensitive to S1P by determining the dose-response relationship of S1P for GBA2 over-expressed in bacteria. Sphingosine-1-phosphate did not inhibit GBA2 activity, suggesting that the presence of a phosphate group disturbs the inhibition of GBA2 (Figure 54b).

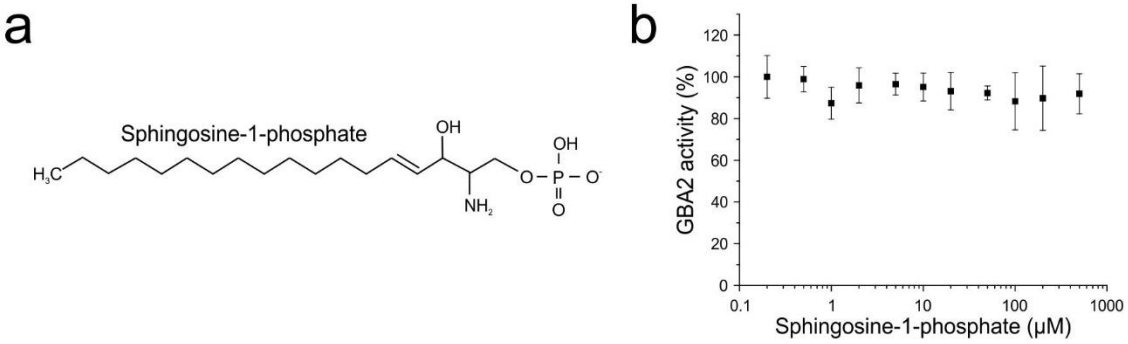

Figure 54: Dose-response relationship of GBA2 to sphingosine-1-phosphate. Analysis of GBA2 activity in bacterial lysates over-expressing mGBA2 in the presence of sphingosine-1-phosphate and 1.67 mM 4-MUG. Data were normalised to a non-treated control. **(a)** Structure of sphingosine-1-phosphate. **(b)** Sphingosine-1-phosphate had no effect on GBA2 activity. 4-MUG: 4-Methylumbelliferyl beta-D-glucopyranoside. Data are presented as mean of quadruples ± SD. Representative plot for n = 3 experiments.

Fingolimod, or FTY720, is derived from myriocin (ISP-1), a metabolite of the fungus *Isaria sinclairii,* and is a manufactured analogue of sphingosine, approved for the treatment of Multiple Sclerosis (Figure 55a) (Kappos et al., 2010). Just like sphingosine (2-amino-1.3-dihydroxy-4-trans-octadecen), FTY720 (2-amino-2-[2-(4-octylphenyl)-ethyl]) propane-1,3-diol) is also substituted with an amine at C2 and carries two hydroxyl groups in the head region. Other than sphingosine, FTY720 carries an octylphenyl group in its carbon tail, while sphingosine itself only bears a double bond at C4 (compare Figure 40a and Figure 55a). *In vivo*, FTY720 is phosphorylated to form FTY720-phosphate, which resembles naturally occurring S1P and also binds to S1P-surface receptors of cells (Brinkmann et al., 2002; Chun&Hartung, 2010), demonstrating that FTY720 behaves like natural sphingosine. To test whether FTY720 blocks GBA2 activity, I analysed the dose-response relationship of FTY720 for GBA2 over-expressed in bacteria (Figure 55b). GBA2 activity was also inhibited by FTY720 with a slightly lower IC_{50} value of 18.6 ± 0.44 µM. Thus, GBA2 activity is sensitive to sphingoid bases, but without any head group attached to C1 (like e.g. S1P).

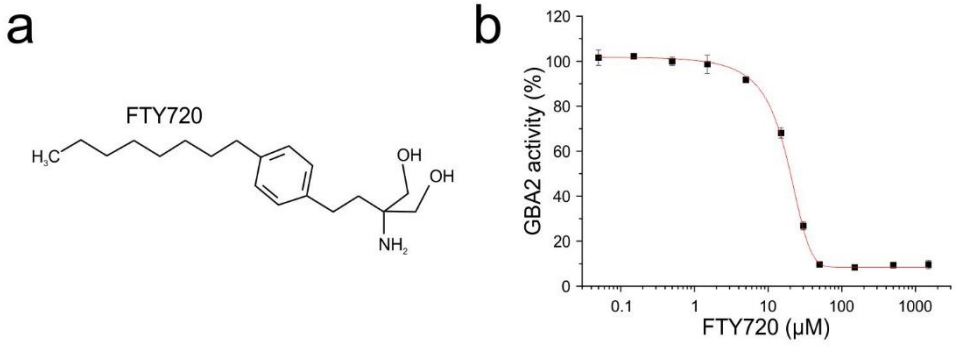

Figure 55: Dose-response relationship of GBA2 to FTY720. Analysis of the GBA2 activity in bacterial lysates over-expressing mGBA2 in presence of FTY720 and 1.67 mM 4-MUG. Data were normalised to a non-treated control. **(a)** Structure of FTY720. **(b)** The IC_{50} for FTY720 in bacterial lysates over-expressing mGBA2 was 18.6 ± 0.44 µM. 4-MUG: 4-Methylumbelliferyl beta-D-glucopyranoside. Data are presented as mean of quadruples ± SD. Representative plot for n = 3 experiments.

In a cellular system, change in ceramide levels did not affect GBA2 activity (see Figure 37 - Figure 39). Nevertheless, ceramide is composed of sphingosine coupled to a fatty acid via an amide bond without any head group (Figure 56a). I revisited the effect of ceramide on GBA2 activity by using GBA2 over-expressed in bacteria. Cell lysates were incubated with C18 ceramide and the activity of GBA2 was analysed. However, ceramide did not block GBA2 activity (Figure 56b). Thus, GBA2 seems to be only

sensitive to sphingoid bases (sphingosine, sphinganine, FTY720) and not to higher order derivatives (ceramide).

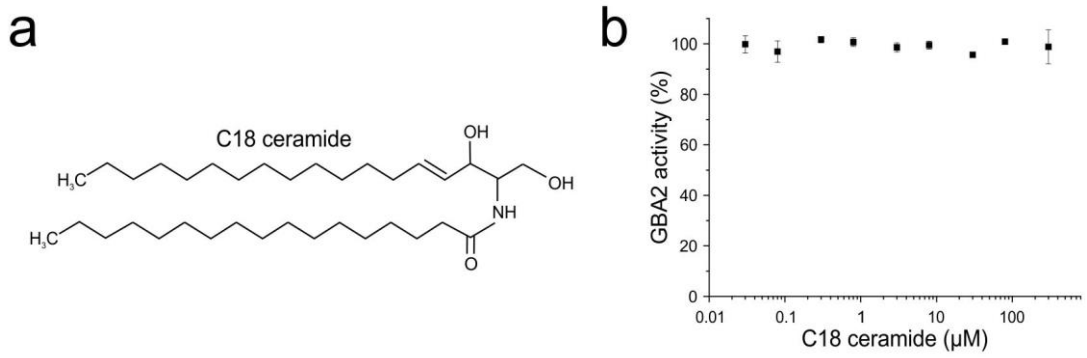

Figure 56: Dose-response relationship of GBA2 to C18 ceramide. Analysis of the GBA2 activity in bacterial lysates over-expressing mGBA2 in presence of C18 ceramide and 1.67 mM 4-MUG. Data were normalised to a non-treated control. **(a)** Structure of C18 ceramide. **(b)** C18 ceramide had no effect on GBA2 activity. 4-MUG: 4-Methylumbelliferyl beta-D-glucopyranoside. Data are presented as mean of quadruples ± SD. Representative plot for n = 3 experiments.

3.14.3 Sphingosine does not quench the fluorescence of 4-Methylumbelliferone

In our beta-glucosidase activity assay, I determine the beta-glucosidase activity according to the increase in fluorescence over time (see Figure 8) (Körschen et al., 2013), when 4-MUG is cleaved to beta-D-glucose and 4-Methylumbelliferone (4-MU) (Figure 57a). 4-MU is highly fluorescent at 365 nm excitation and emits light at 445 nm (The Merck Index, 12th ed., Entry# 4903). To test whether the addition of sphingosine (or other sphingoid bases) quenches the fluorescence of 4-MU, I tested the 4-MU fluorescence in the presence of 0-400 µM sphingosine (Figure 57b). The fluorescence increased in a dose-dependent manner and there was no difference in the presence or absence of sphingosine (Figure 57b). Thus, sphingosine did not quench the fluorescence of the cleavage-product of 4-MUG.

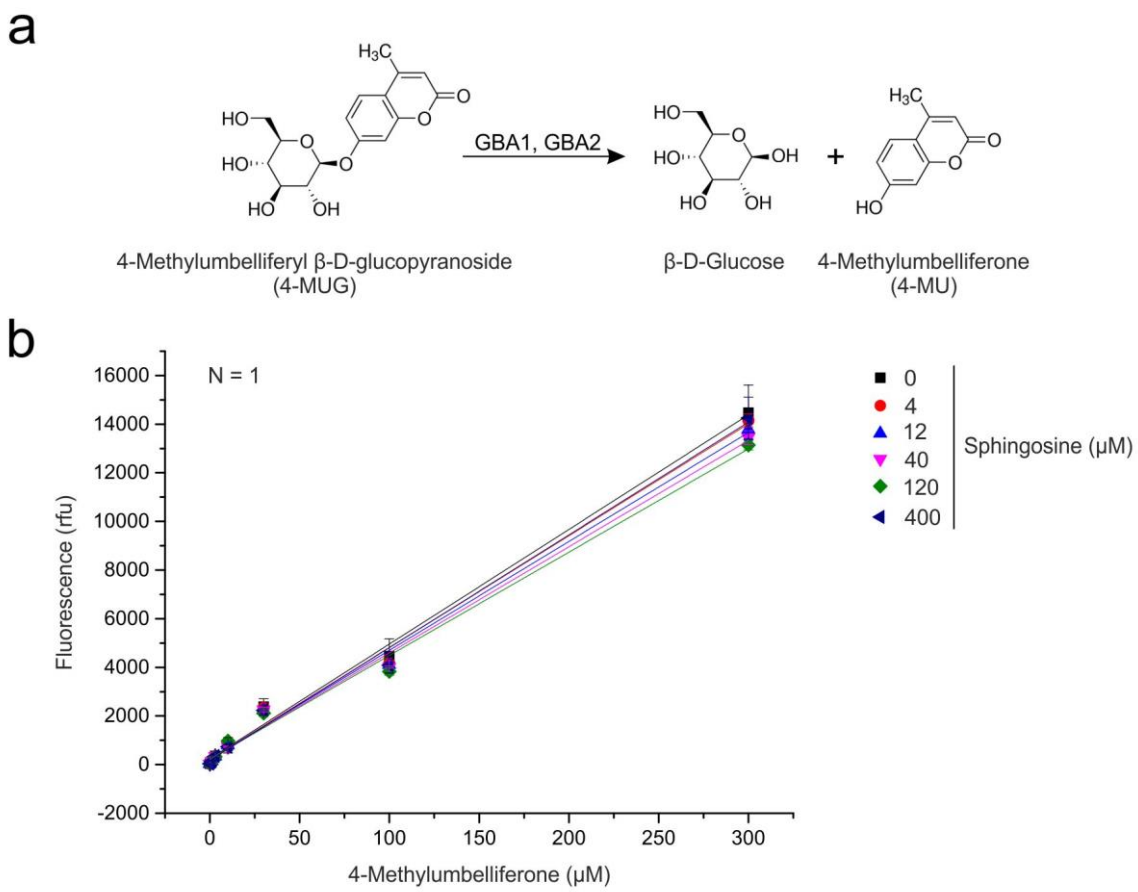

Figure 57: 4-MU fluorescence in presence of sphingosine. Analysis of the fluorescence of 4-MU in presence of sphingosine. **(a)** GBA1 and GBA2 cleave 4-MUG to β-D-glucose and 4-MU. **(b)** The fluorescence of 4-MU increased in a dose-dependent manner and there was no difference in the presence or absence of sphingosine. 4-MUG: 4-Methylumbelliferyl beta-D-glucopyranoside, 4-MU: 4-Methylumbelliferone. Data are presented as mean of quadruples ± SD. The N number is indicated.

3.14.4 The sphingosine-dependent inhibition of GBA2 is reversible and rather non-competitive

To further characterise the sphingosine-dependent block of GBA2 activity, I tested whether the block is reversible (Figure 58). Three samples of hypotonic lysates of bacteria expressing mGBA2 were pre-incubated with either 25 µM sphingosine to evoke a half-maximal block of GBA2 activity (two samples) or with DMSO as a control (one sample) (see Figure 58a). Then, all samples were diluted 1:6.5, resulting in a final sphingosine concentration of 3.85 µM. In a control sample, the initial sphingosine concentration of 25 µM was maintained by re-addition of sphingosine (Figure 58a). 25 µM sphingosine reduced the GBA2 activity to 50% of the control (DMSO) sample, whereas almost full GBA2 activity was recovered when sphingosine was diluted to 3.85 µM (Figure 58b). These results indicate that sphingosine reversibly blocks GBA2

activity. In parallel, hypotonic lysates of bacteria expressing mGBA2 were also pre-incubated with either 14 nM NB-DNJ or PBS to follow the reversible inhibition of GBA2 by NB-DNJ (Ridley et al., 2013) (Figure 58c). In the presence of 14 nM NB-DNJ, the GBA2 activity was reduced to 33%, whereas dilution to 2.15 nM NB-DNJ recovered the GBA2 activity to 56% of the control (Figure 58c).

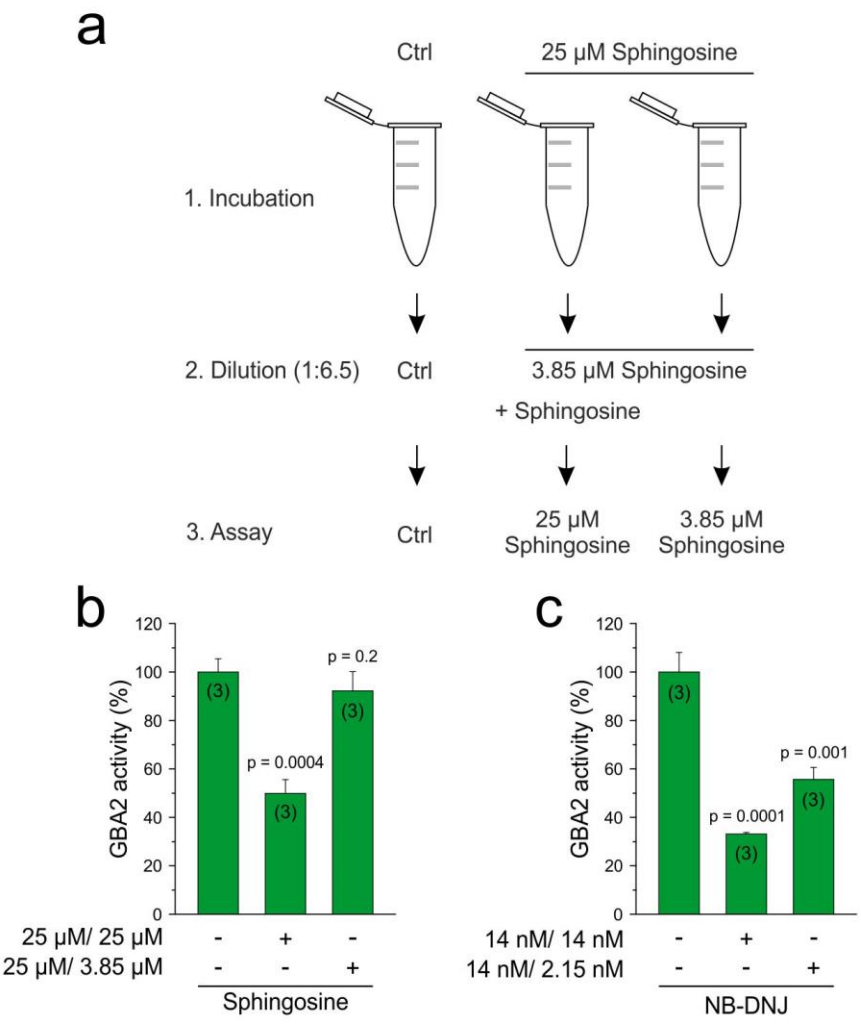

Figure 58: Sphingosine reversibly inhibits GBA2. Analysis of the GBA2 activity in bacterial lysates over-expressing mGBA2 in presence of 25 µM sphingosine or 14 nM NB-DNJ diluted 1:6.5 in hypotonic buffer with or without maintaining the concentration of sphingosine or NB-DNJ in presence of 1.67 mM 4-MUG. Data were normalised to the non-treated control (Ctrl). **(a)** Flow-chart of the experiment. **(b)** The GBA2 activity was recovered in lysates after diluting 25 µM sphingosine down to 3.85 µM, demonstrating that the block is reversible. **(c)** Dilution of NB-DNJ, the reversible blocker for GBA2, also results in recovery of GBA2 activity. NB-DNJ: N-butyl-deoxynojirimycin, 4-MUG: 4-Methylumbelliferyl beta-D-glucopyranoside. Data are presented as mean + SD. N numbers are indicated in brackets. P values were determined using One-way ANOVA.

To characterise the type of reversible inhibition, I incubated bacterial lysates over-expressing mGBA2 with 25 µM sphingosine and competed the inhibitory effect by adding increasing amounts of 4-MUG (Figure 59). Data were analysed according to Michaelis-Menten. In the presence of sphingosine, the GBA2 activity (V_{max}) was reduced to about 50% of the control activity (3.53 ± 0.13 rfu/min *versus* 1.93 ± 0.13 rfu/min), indicating a non-competitive inhibition of sphingosine for GBA2. However, the K_m value was shifted towards higher concentrations (171.03 ± 13.83 µM *versus* 303.97 ± 44.30 µM), which does not resemble the classic non-competitive inhibition model. Thus, my data suggest that the inhibition of GBA2 by sphingosine follows the rules of mixed inhibition, where the inhibitor can bind to an allosteric site of the enzyme if it has not bound its substrate yet, as well as to the enzyme-substrate complex. In this case, the K_m value is increased, which resembles a lower affinity of the enzyme for its substrate, and V_{max} is decreased.

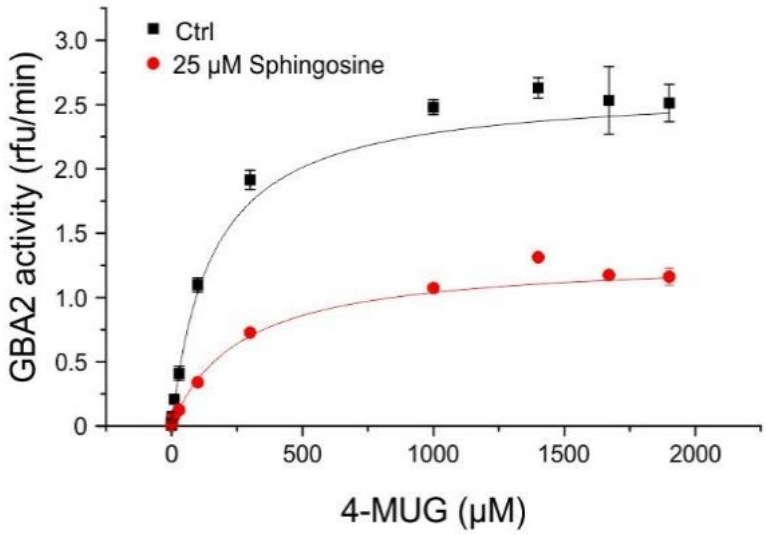

Figure 59: GBA2 activity in presence of 25 µM sphingosine and a serial dilution of 4-MUG. Analysis of the GBA2 activity in bacterial lysates over-expressing mGBA2 in presence of 25 µM sphingosine and an increasing amount of 4-MUG. Data were normalised to the non-treated control and compared to DMSO-treated samples. V_{max} of GBA2 was reduced to about 50% in presence of 25 µM sphingosine of the control activity (3.53 ± 0.13 rfu/min *versus* 1.93 ± 0.13 rfu/min). The K_m value was shifted from 171.03 ± 13.83 µM to 303.97 ± 44.30 µM in the presence of sphingosine. 4-MUG: 4-Methylumbelliferyl beta-D-glucopyranoside. Data are presented as mean of quadruples ± SD. Representative plot for n = 3 experiments,

Since 4-MUG is not the natural substrate for GBA2, I also tested whether GlcCer and sphingosine compete for the same binding site. Again, bacterial lysates over-expressing GBA2 were incubated with 25 µM sphingosine and then assayed in the

presence of increasing amounts of GlcCer (Figure 60) with a final 4-MUG concentration of 1.67 mM. As seen in the previous experiment, increasing amounts of GlcCer, just as 4-MUG, did not reverse the inhibitory effect of sphingosine (Figure 60). Of note, the GBA2 activity in both samples decreased when high concentrations of GlcCer were reached (Figure 60). Since there was no precipitate visible in both samples, the remaining pool of active GBA2 most likely started to rather cleave the natural substrate instead of 4-MUG, which in this assay appears as a reduction in fluorescence and, thereby, looks like a decrease in overall activity (Figure 60). In conclusion, these data strengthen the result that sphingosine binds an allosteric site evoking a mixed inhibition of GBA2.

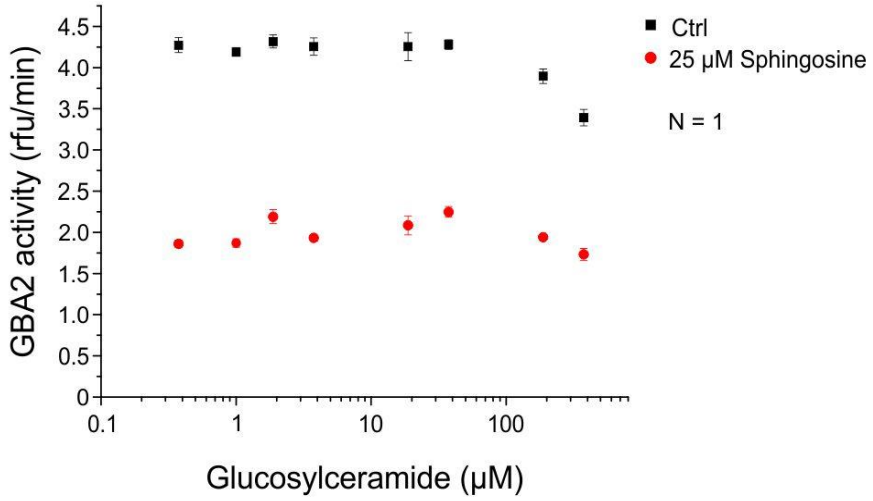

Figure 60: GBA2 activity in presence of 25 µM sphingosine and a serial dilution of GlcCer. Analysis of the GBA2 activity in bacterial lysates over-expressing mGBA2 in presence of 25 µM sphingosine and C18 GlcCer in presence of 1.67 mM 4-MUG. GlcCer did not reverse the sphingosine-dependent effect. At high GlcCer concentrations, GBA2 seemed to rather cleave natural GlcCer compared to 4-MUG, resulting in a decrease in fluorescence. 4-MUG: 4-Methylumbelliferyl beta-D-glucopyranoside. Data are presented as mean of quadruples ± SD. The N number is indicated.

3.14.5 GBA1 is sensitive to sphingosine and sphinganine

Since both, sphingosine and sphinganine, had an inhibitory effect on GBA1 when incubated with cells (Figure 40 and Figure 42), I also tested whether both sphingoid bases would exhibit a direct effect on the activity of GBA1. Thus, I analysed the dose-response relationship of both lipids on the GBA1 activity using hypotonic cell lysates from CHO cells stably over-expressing mGBA1 (#A8A6B5) (Figure 61). Sphingosine inhibited GBA1 with an IC_{50} value of 15.81 ± 1.3 µM and sphinganine inhibited showed

the same effect with an IC_{50} value of 37.63 ± 4.4 µM (Figure 61). Of note, neither sphingosine nor sphinganine evoked a full block of GBA1 activity even at high concentrations (Figure 61). Thus, GBA1 was probably not fully accessible for the sphingoid bases in the lysate even though the enzyme seemed to still be accessible for the substrate 4-MUG resulting in remaining activity/fluorescence (Figure 61).

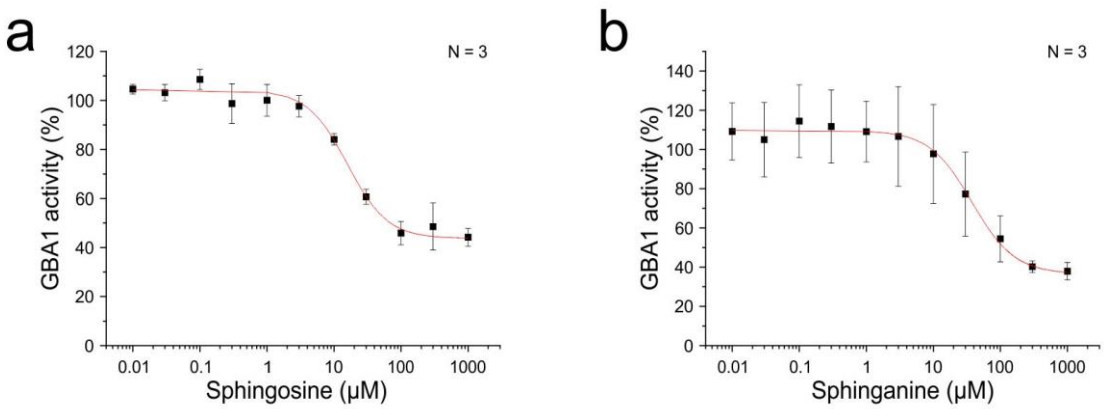

Figure 61: Dose-response relationship of GBA1 to sphingosine and sphinganine. Analysis of the GBA1 activity in lysates from CHO cells stably over-expressing mGBA1 in presence of a serial dilution of sphingosine or sphinganine and 1.67 mM 4-MUG at pH 4. Data were normalised to a non-treated control. The IC_{50} for **(a)** sphingosine and **(b)** sphinganine in CHO cell lysates over-expressing mGBA2 was 15.81 ± 1.3 µM and 37.63 ± 4.4 µM, respectively. 4-MUG: 4-Methylumbelliferyl beta-D-glucopyranoside. Data are presented as mean ± SD. N numbers are indicated.

3.14.6 Intracellular sphingosine levels are not increased in *Gaucher* fibroblasts

To analyse whether intracellular sphingosine levels are indeed altered in GBA1-deficient cells, dermal fibroblasts from control and *Gaucher* patients were analysed by mass spectrometry (Figure 62). Sphingosine levels were not significantly increased in *Gaucher* fibroblasts with 1.32 ± 0.81 pmol/µg protein in type I samples, 2.23 ± 2.28 pmol/µg protein in type II samples, and 1.2 ± 0.51 pmol/µg protein in type III samples compared to 1.41 ± 0.61 pmol/µg protein in control cells (Figure 62a). Sphinganine levels showed a similar distribution with 5.72 ± 2.1 pmol/µg protein in control cells and 5.05 ± 3.12 in type I, 7.72 ± 6.1 in type II, and 4.53 ± 2.62 pmol/µg protein in type III *Gaucher* fibroblasts (Figure 62b). Thus, neither sphingosine nor sphinganine levels were significantly changed in fibroblasts from *Gaucher* patients.

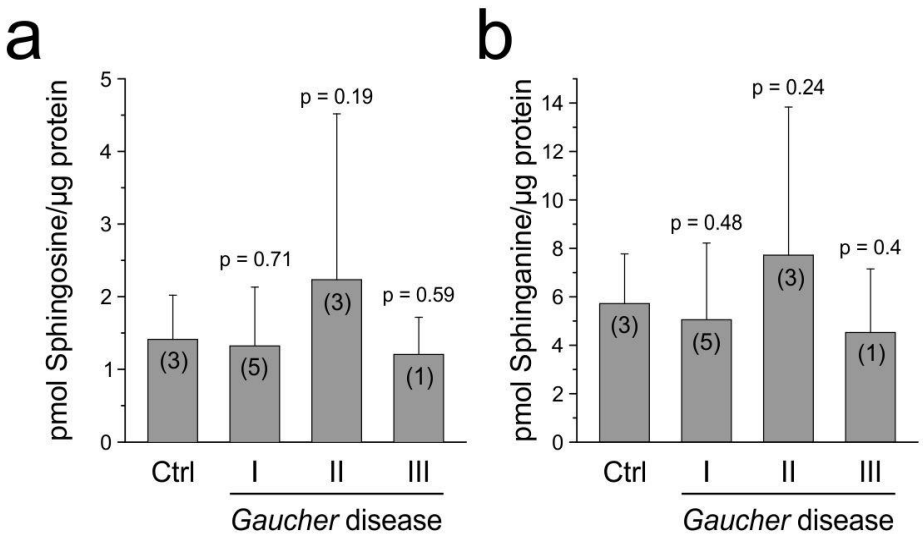

Figure 62: Sphingosine and sphinganine levels in *Gaucher* and control fibroblasts. Mass spectrometric analysis of sphinganine and sphingosine levels normalised to the amount of protein per sample. **(a)** Sphingosine levels were not significantly increased in all three *Gaucher* types with type II cells showing the highest sphingosine amount. Control (Ctrl) cells contained 1.41 ± 0.61 pmol sphingosine/µg protein and *Gaucher* cells contained in total 1.2 – 2.23 pmol sphingosine/µg protein. **(b)** As for **(a)** with sphinganine control values of 5.72 ± 2.1 pmol per µg protein and *Gaucher* cells containing 4.53 – 7.72 pmol sphinganine/µg protein. The different *Gaucher* types are indicated. Data are presented as mean + SD. N numbers are shown in brackets. P values were determined using One-way ANOVA.

3.15 Analysing ER stress in dermal fibroblasts from GBA2-deficient mice

In *Gaucher* disease, the human *GBA1* gene is prone to mutations, which comprise missense mutations and, thereby, premature termination of the gene, splice site mutations, and deletions (Hruska et al., 2008). GBA1 is synthesised on polyribosomes at the ER (Erickson et al., 1985). The pre-mature GBA1 undergoes N-linked glycosylation at four specific glycosylation sites, after which the enzyme is then subjected to ER quality control. In case the protein is correctly folded, GBA1 is transported to the Golgi, where its N-glycan moieties are further modified. In a last step, GBA1 is shuttled to the lysosomes. This process does not take place in *Gaucher* cells, because mutant GBA1 is not properly folded. In 2008, work was published showing that mRNA expression levels of GRP78 are slightly increased in fibroblasts from *Gaucher* disease type I and II patients as well as in *Niemann-Pick* type C patients (Wei et al., 2008). Furthermore, GRP78 and CHOP mRNA levels were increased in dermal fibroblasts derived from *Gaucher* disease patients, carrying different mutations in the *GBA1* gene (Maor et al., 2013). In contrast to these findings, Farfel-Becker et al. did not see any change in GRP78 and CHOP mRNA expression in both, cell culture

models and animal-derived cells of neuronopathic *Gaucher* disease (Farfel-Becker et al., 2009). However, both, GRP78 and CHOP, are so-called ER stress marker genes for a mechanism called unfolded protein response (UPR), which is activated by accumulation of misfolded protein in the ER (Cao&Kaufman, 2012). Thus, UPR prevents the accumulation of unfolded proteins by activating e.g. chaperones to increase the protein-folding capacity or the degradation of proteins through ER-associated protein degradation (ERAD) (Kaufman, 2002). Activation of UPR can be monitored by analysing the expression of e.g. GRP78 and CHOP (Walter&Ron, 2011). The 78 kDa glucose-regulated protein GRP78 is an ER chaperone and key regulator of ER stress transducers. Under normal conditions, the kinases IRE1 and PERK as well as the transcription factor ATF6 are bound to GRP78, which keeps them in an inactive state (Rutkowski&Kaufman, 2004). During ER stress, all three proteins are released from GRP78 and activated, which in turn stimulates UPR (Bertolotti et al., 2000; Ye et al., 2000). ATF6 subsequently gets processed, enters the nucleus, and activates UPR target genes like GRP78 (Ye et al., 2000). Thus, GRP78 is an ER chaperone with anti-apoptotic properties that controls and regulates UPR (Lee, 2005). Thus, mRNA expression of the GRP78 gene is commonly used as a biological marker for UPR and, thus, ER stress.

On the other hand, expression of the transcription factor CHOP (CCAAT-enhancer-binding protein homologous protein) is associated with ER stress-induced apoptosis (Oyadomari&Mori, 2004). CHOP is expressed at very low levels, but activation of IRE1, PERK, and ATF6 stimulate CHOP mRNA expression, promoting its translocation from the cytosol to the nucleus (Ron&Habener, 1992). Over-expression of CHOP leads to apoptosis in several cell lines and CHOP-deficient mice are less prone to ER stress (Oyadomari&Mori, 2004). Thus, CHOP is a key player for the induction of apoptosis.

My previous studies have shown that the GBA1 and GBA2 mRNA expression remains unchanged in dermal fibroblasts derived from *Gaucher* patients with different phenotypes (Figure 12). Still, the GBA2 activity is reduced in these and other cells in a GBA1-dependent manner (Figure 14). We have shown that GBA2 localises to both, the cytoplasmic side of the *cis* Golgi and the ER (Körschen et al., 2013). Thus, a change in GBA2 activity might directly affect ER membrane properties, leading to ER stress. Thus, I wondered whether a change in GBA2 activity might generate ER stress. Because the severity of the GBA1-dependent effect on GBA2 activity varied between

samples, I analysed the mRNA levels of GRP78 and CHOP in mouse dermal fibroblasts from control and GBA2-deficient mice using qPCR (Yildiz et al., 2006). First, a protocol to analyse the mRNA expression in mouse fibroblasts was established as previously described in passage 3.3 using qPCR. Besides the GOIs (mCHOP and mGRP78, Table 61 and Table 62), the previously established HKGs were used (3.6).

Table 61: Mouse genes of interest (GOIs) chosen for ER stress qPCR analysis

Gene	Gene product	Reference
mCHOP	CCAAT-enhancer-binding protein homologous protein	NM_007837
mGRP78	78 kDa glucose-regulated protein	NM_0011634

Table 62: Amplicon sizes of mouse primer pairs selected for ER stress qPCR

Gene	Primer pair	Expected amplicon size (bp)
mCHOP	C2187/88	93
mCHOP	C2189/90	124
mGRP78	C2195/96	196
mGRP78	C2197/98	208

bp: Base pairs

To test whether primers designed for qPCR amplify the sequence of interest, a conventional polymerase chain reaction (PCR) was performed (2.4.2). For mouse primers (Table 16), cDNA obtained from mouse wild-type fibroblasts was used. All amplicons (Figure 63) had the expected sizes (Table 62).

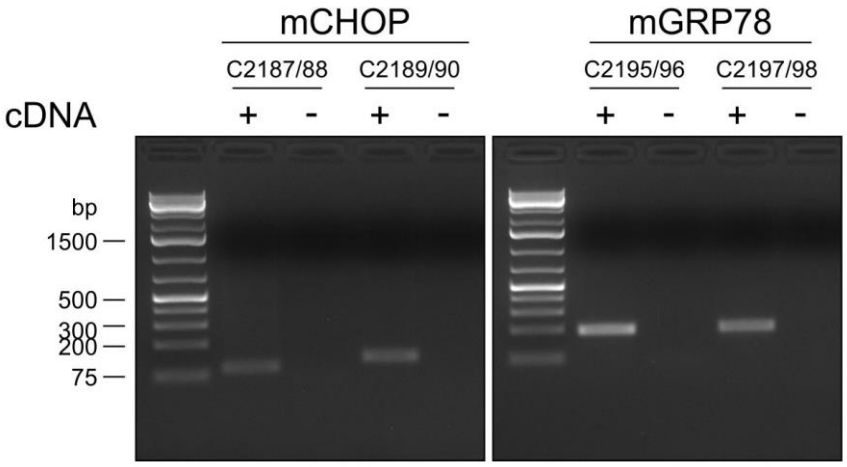

Figure 63: Analysis of the amplicons of mouse ER stress qPCR primers and control cDNA from mouse wild-type fibroblasts. 5 µl of the PCR approach were loaded to a 2% agarose gel and the fragments were analysed under a UV lamp. All amplicons had the expected sizes. bp: base pairs.

To reliably analyse the data obtained from qPCR, a primer efficiency test (PET) was performed (2.4.6.5). Based on these results, the following mouse primers were used for subsequent experiments: mCHOP: C2189/90 and mGRP78: C2197/98 (Table 63). The PCR products generated by these primer pairs were send for sequencing and, thus, verified to be the right amplicons (data not shown).

Table 63: Mouse ER stress qPCR primer efficiencies

Gene	Primer numbers	Slope	R^2 value	Efficiency (%)
mCHOP	C2187/88	-3.245	0.9988	103.3
mCHOP	C2189/90	-3.2648	0.9986	102.4
mGRP78	C2195/96	-3.5847	0.998	90.1
mGRP78	C2197/98	-3.4489	0.9986	95.0

However, mRNA expression levels of GRP78 and CHOP were similar between control and GBA2-deficient fibroblasts (Figure 64). Thus, there is no evidence for ER stress in absence of GBA2.

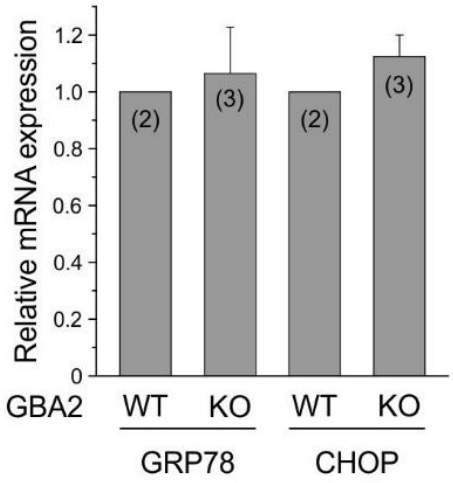

Figure 64: Analysis of ER stress markers in GBA2-deficient mouse dermal fibroblasts. mRNA expression of the ER stress markers GRP78 and CHOP was analysed in control and GBA2-deficient dermal fibroblasts by qPCR. Neither GRP78 nor CHOP were altered in GBA2-deficient samples. ER: Endoplasmic reticulum, GRP78: 78 kDa glucose-regulated protein, CHOP: CCAAT-enhancer-binding protein homologous protein. Data are presented as mean + SD. N numbers are indicated in brackets.

3.15.1 Studying the subcellular distribution of GlcCer

Even though the mass spectrometric analysis of sphingosine levels in dermal fibroblasts from *Gaucher* and control patients did not reveal any difference (Figure 62a), I wondered whether a local increase in cytoplasmic sphingosine levels could occur in GBA1-deficient cells. To date and to my knowledge, there is no fluorescent probe available that allows to visualise the subcellular localisation of sphingosine. Thus, I tackled this problem via a different approach: As previously mentioned, loss of GBA1 in *Gaucher* patients leads to the accumulation of GlcCer and GlcSph (Ferraz et al., 2016). Both lipids have been proposed to spill-over from the lysosome into the cytoplasm, where they become a substrate for GBA2 and Sph is released from both, GlcCer (via Cer and a neutral ceramidase) and GlcSph (Mistry et al., 2014). This scenario requires GlcCer (and GlcSph) to co-localise with GBA2. Thus, I established a protocol to visualise GlcCer in the cell. Here, immunocytochemistry is a common technique that uses a specific primary antibody, which is visualised by binding of a fluorescently conjugated secondary antibody. The (sub-) cellular localisation of the labelled protein can then be studied by using a fluorescence microscope. Antibodies have not only been generated against proteins, but also against certain lipids. An polyclonal anti-GlcCer antibody from rabbit is commercially available (RAS_0010, Glycobiotech) and its specificity for GlcCer has been tested *in vitro* by TLC

immunostainings and *in vivo* by immunohistochemical stainings of human epidermis (Brade et al., 2000). The antibody did neither react with other glycosphingolipids nor with ceramide, suggesting that the beta-glycosidic linkage between ceramide and glucose (head group) represents the epitope (Brade et al., 2000). Furthermore, the antibody has been used to demonstrate that GlcCer is localised within lamellar bodies and at the *trans* Golgi network in the stratum granulosum of human forearm skin biopsies (Vielhaber et al., 2001). In absence of FAPP2, GlcCer localises to the *cis* Golgi (D'Angelo et al., 2007).

To study the localisation of GlcCer in the cell, I established an immunogold labelling protocol for ultrathin sections for transmission electron microscopy (TEM) in collaboration with the Electron Microscopy and Analysis (EMA) facility at research center caesar (Bonn). The immunostaining protocol was established using control and GlcCerS-deficient cells, which do not synthesise GlcCer. In fact, immunogold labelling of GlcCer was present in control but not in GlcCerS-deficient cells (D'Angelo et al., 2007). Thus, I tried to reproduce the visualisation of GlcCer in control and GlcCerS-deficient cells using our experimental set up. First, the detection of 1.4 nm Nanogold particles was verified using a transmission electron microscope (Figure 65). Individual gold particles were visible (arrows, Figure 65a), but were too small to be properly identified at a lower magnification mode. Therefore, the size of the gold particles was enhanced for 3 min using a gold-enhancement kit (Nanoprobes) (Figure 65b). After 3 min, the particle size was around 18 nm, which, however, was too large for proper labelling. In further experiments, the enhancement time was reduced to 1 min.

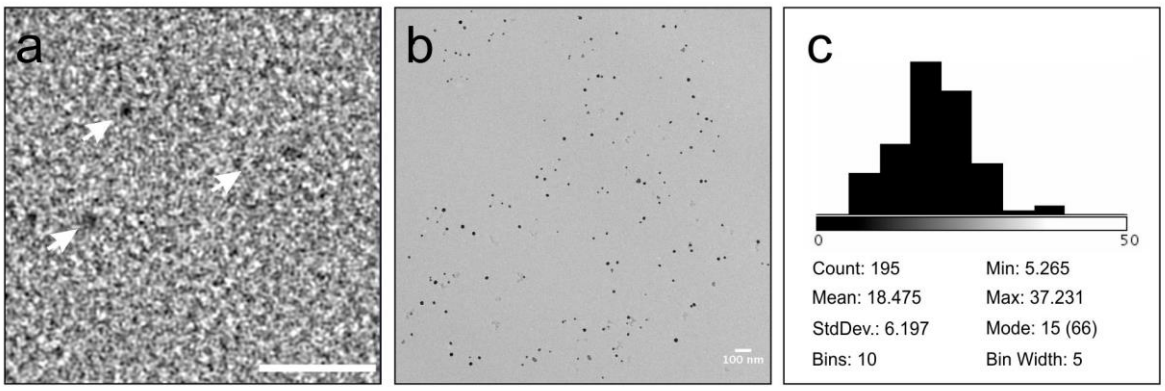

Figure 65: Detection of Nanogold particles. (a) Detection limit of pure 1.4 nm Nanogold. Micrograph of 1.4 nm gold particles (Nanoprobes, USA) on a continuous carbon film. Individual gold nanoparticles

are visible (arrows) but too small for proper identification at lower magnifications. Magnification: 100,000, scale bar: 20 nm. **(b)** Detection limit of 1.4 nm Nanogold after enhancement. 1.4 nm gold particles were enhanced with a gold-enhancement kit (both Nanoprobes). The particle size was large enough for easy detection but slightly too large for proper labelling. Enhancement time: 3 min. For further experiments, enhancement time was reduced to 1 min. Magnification: 20,000, scale bar: 100 nm. **(c)** Particle size distribution after enhancement of **(b)**. Mean particle size is 18 (±6) nm.

Sections of GlcCerS-deficient and control cells were immuno-labelled using the anti-GlcCer antibody according to the protocol presented in Vielhaber et al. (Vielhaber et al., 2001). Signals in control cells were mainly present in the nucleus (Figure 66a). In GlcCerS-deficient cells, the gold labels were evenly distributed over the section, representing the background signal (Figure 66c).

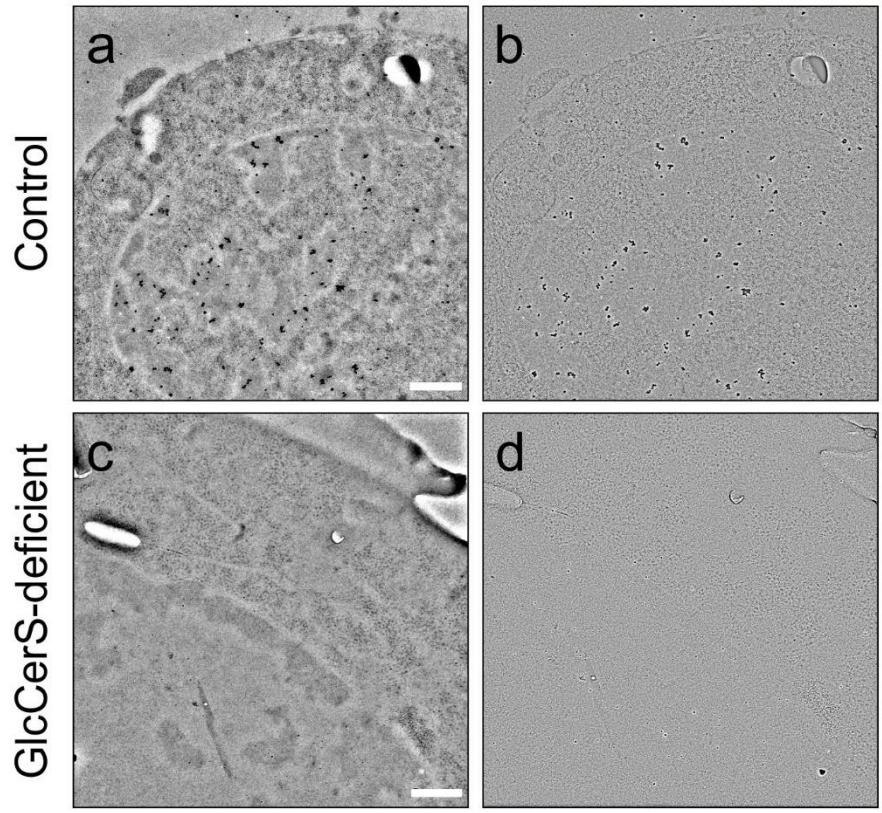

Figure 66: Immuno-labelling of GlcCerS-deficient and control cells using the anti-GlcCer antiserum. The cells were labelled according to Vielhaber et al. 2001. **(a)** Micrograph of section of control cells. Labelling accumulated mainly in the nucleus. **(b)** High-pass filtered version of **(a)** to visually enhance the gold particles. Scale bar: 200 nm. **(c)** Micrograph of a section of GlcCerS-deficient cells. The particles were evenly distributed representing the background. Scale bar: 200 nm. **(b)** High-pass filtered version of **(a)** to visually enhance the gold particles.

In further experiments, the protocol was modified to block non-specific nuclear epitopes and suppress the background (Figure 67) by blocking with EDTA.

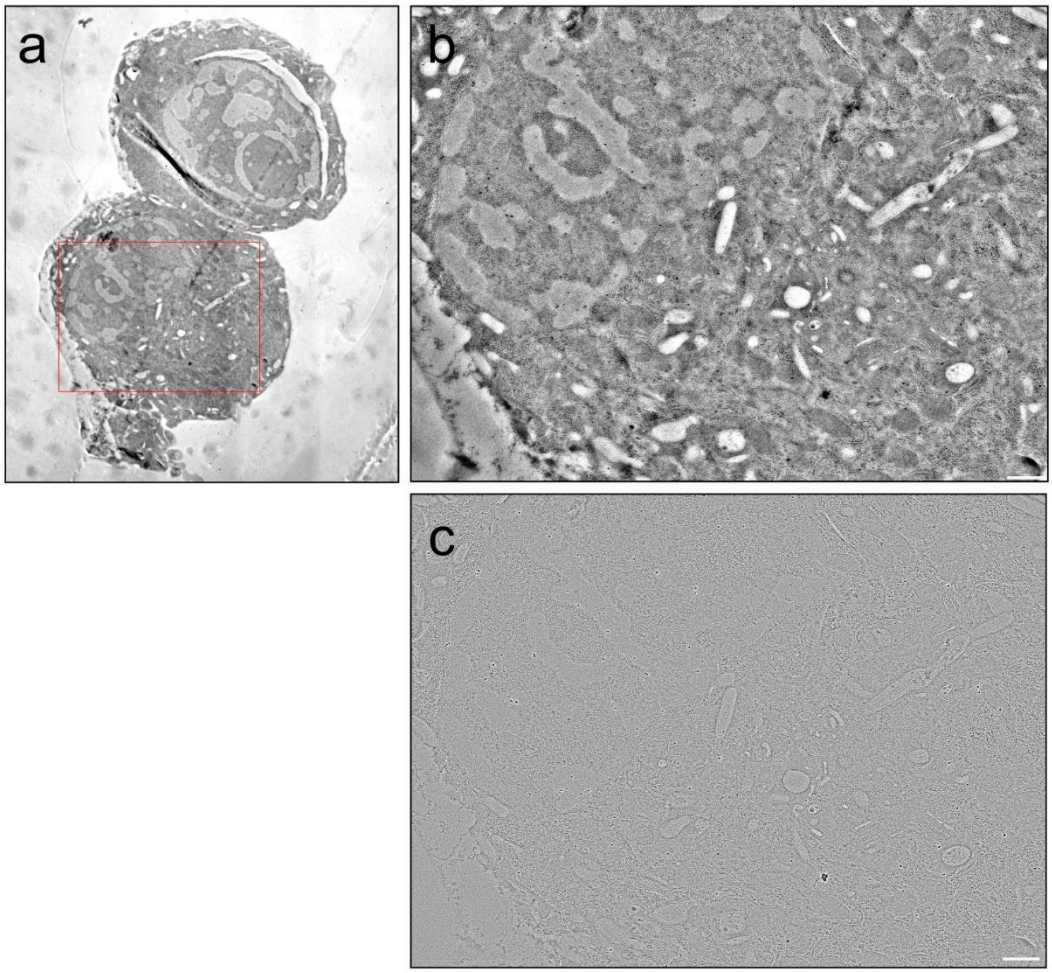

Figure 67: Immunogold labelling of sections of control cells using the anti-GlcCer antiserum after histone blocking. (a) Multi image map of two control cells. Image processing using IMOD. Histones in nucleus were blocked using EDTA. **(b)** Magnified view (red frame in navigator image) of the nucleus region. Binding of gold particles to the histones was successfully reduced by blocking with EDTA. Magnification: 10,000, scale bar: 500 nm. **(c)** High-pass filtered version of **(b)** to visually enhance the gold particles.

To further improve the immunogold staining, the protocol presented by Vielhaber and co-workers was slightly modified. Instead of 3% normal goat serum in PBS, a blocking solution containing BSA was used (Aurion). To reduce non-specific binding, the primary antibody was diluted to 1:400 and was incubated at 4 °C overnight. Washing steps were carried out using 0.1% BSA in PBS containing 20 mM NaCl (pH 7.4). Finally, the samples were pre-fixed using 2.5% glutaraldehyde in PBS containing 20 mM NaCl (pH 7.4) before enhancement of the gold particles using the gold-

enhancement kit (Nanoprobes). The result of immunostaining improvements are shown in Figure 68: Unfortunately, there was no specific labelling of the anti-GlcCer antibody in the Golgi or ER region.

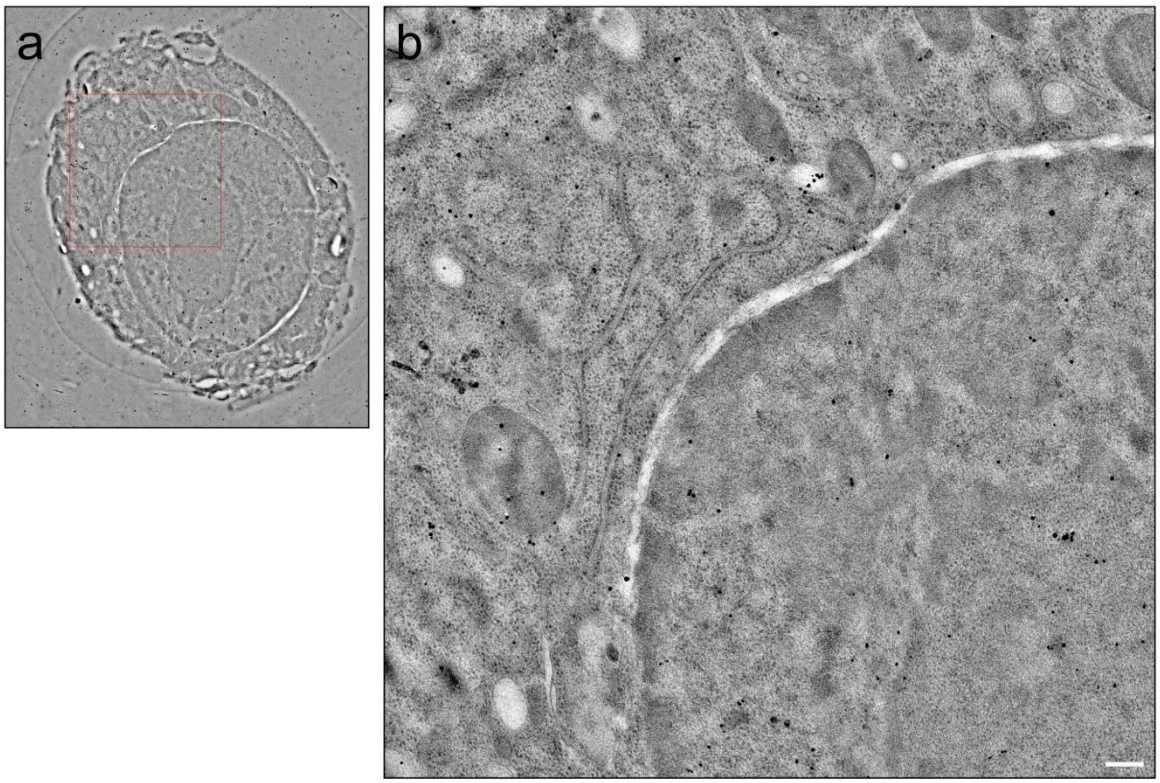

Figure 68: Immunogold labelling of sections of control cells using the anti-GlcCer antiserum after protocol modification. (a) Multi image map of a control cell. Image processing using IMOD. **(b)** Magnified view (red frame in navigator image) of the nucleus region. There was no specific GlcCer-labelling in the Golgi or ER region of the cell. Magnification: 10,000, scale bar: 500 nm.

To finally reveal whether the anti-GlcCer antiserum detects GlcCer at all, DOPC liposomes of 100 nm and 800 nm diameter containing GlcCer were prepared and handled as described above. There was no specific labelling of liposome membranes containing GlcCer, showing that the anti-GlcCer antibody does not recognise GlcCer in membranes.

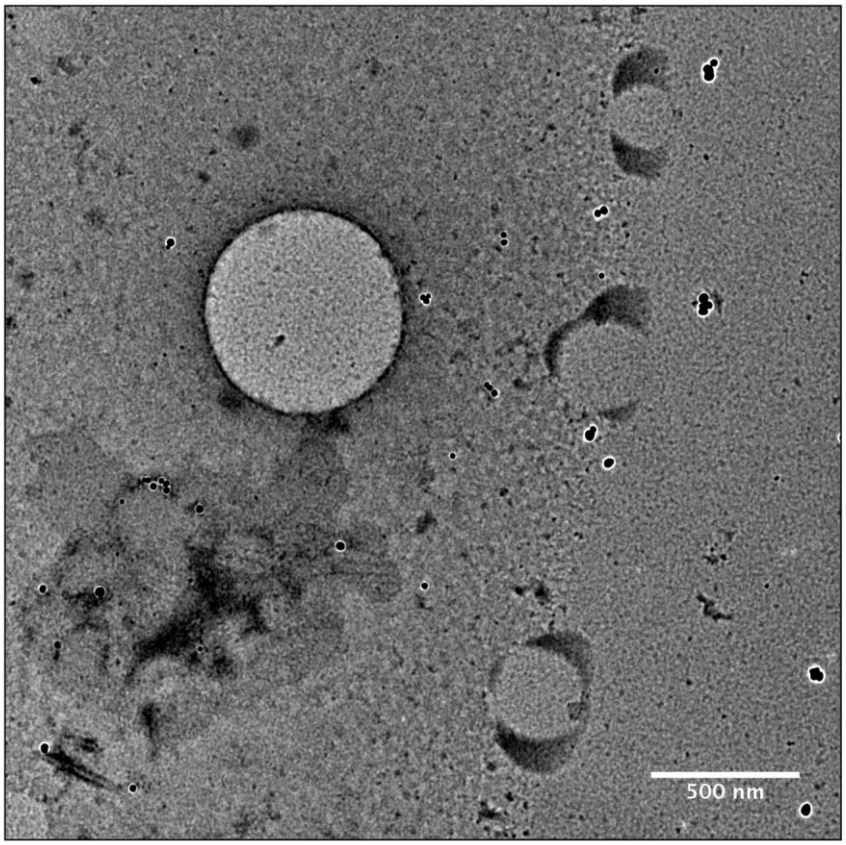

Figure 69: GlcCer/DOPC-liposomes after labelling with the anti-GlcCer antiserum. Size-enhanced gold particles are distributed over the grid. There was no specific labelling of liposome membranes containing GlcCer. Magnification: 8,000, scale bar: 500 nm.

Thus, a different strategy was developed (Figure 70). Recently, it has been shown that GLTP was sufficient to transfer GM1 from artificial donor liposomes to increase glycolipid levels at native membranes (Lauria et al., 2013). I adapted this approach and established a protocol to feed dermal fibroblasts with a clickable GlcCer derivative (clickGlcCer), carrying a terminal alkyne group at the fatty acid residue (Prof. C. Thiele, non-published) (Figure 70b, c), and compared the subcellular distribution of (click) GlcCer between control and *Gaucher* fibroblasts (Figure 71 and following). Cells constantly internalise material such as ligands, plasma membrane proteins, and lipids via endocytosis (Grant&Donaldson, 2009). In fact, it has been estimated that cells internalise material equivalent to their cell surface about one to five times per hour (Steinman et al., 1983). Upon endocytosis, cargo is usually transported to the early endosomes, where material is sorted. From here, the material is either forwarded to the *trans* Golgi network, recycled and brought back to the plasma membrane, or shuttled to late endosomes and, finally, to the lysosomes for degradation

(Grant&Donaldson, 2009). Thus, after being transferred from extracellular liposomal membranes to the outer leaflet of the plasma membrane via GLTP, clickGlcCer should enter the endosomal pathway and would, eventually, end up in the liposomes of control and *Gaucher* fibroblasts (Deduve, 1964). As GBA1 is almost inactive in the latter, clickGlcCer, similar to endogenous GlcCer, should not be degraded and, thus, accumulate in the lysosomes. If accumulating GlcCer indeed spills over from the lysosomes in GBA1-deficient cells, it should then be possible to visualise this process via clickGlcCer.

To establish the protocol using dermal fibroblasts, I first tested whether cells take up clickGlcCer via the aforementioned approach and metabolise it to glucose and ceramide, which would be further broken down by an acid ceramidase to release sphingosine and the fatty acid carrying the alkyne group (compare Figure 70) (Gatt, 1963). In immunocytochemical stainings, a labelled fatty acid would not be distinguishable from labelled GlcCer, producing a misleading result. In GBA1-deficient cells, acid ceramidase could also release the fatty acid from GlcCer to produce GlcSph. Thus, pulse and chase times had to be carefully examined to ensure the presence of clickGlcCer.

Control human dermal fibroblasts were seeded on glass coverslips coated with poly-L-lysine. His-tagged human GLTP (hGLTP-His) was expressed in bacteria and purified using the ÄKTA chromatography system from GE Healthcare (Lauria et al., 2013). The cells were incubated with 10 µM hGLTP and DOPC (1,2-Dioleoyl-sn-glycero-3-phosphocholine) liposomes containing 0 mol%, 1 mol%, 5 mol%, or 10 mol% clickGlcCer diluted 1:2.5 in sterile PBS (Figure 70a). Cells were pulsed for 10 min and the lipids were chased for either 30 minutes or overnight at 37 °C. Then, the total lipids were either extracted for TLC analysis or the cells were fixed using 4% PFA in PBS for immunocytochemistry (Labelling for immunocytochemistry: Figure 70b, labelling for TLC: Figure 70c). As a control, cells were also fed with 5 µM clickSphinganine. Extracted lipids were clicked to 3-azido-7-hydroxycoumarin in presence of Cu(I)TFB at 43 °C for 2 h (Figure 70c). 3-azido-7-hydroxycoumarin is a fluorescent organic chemical compound that can be clicked to an alkyne group and is then excited by light of 404 nm and emits light at 480 nm (Sivakumar et al., 2004). Thus, clickable lipids can be visualised after TLC simply at 404 nm. ClickGlcCer in fixed and permeabilised cells was clicked to azido biotin (AP3Btn or APpic2Btn, Figure 72a) at 37 °C for 1 h and

biotin was then detected via a fluorophore-labelled streptavidin to visualise ectopic GlcCer in the cells (Figure 70b).

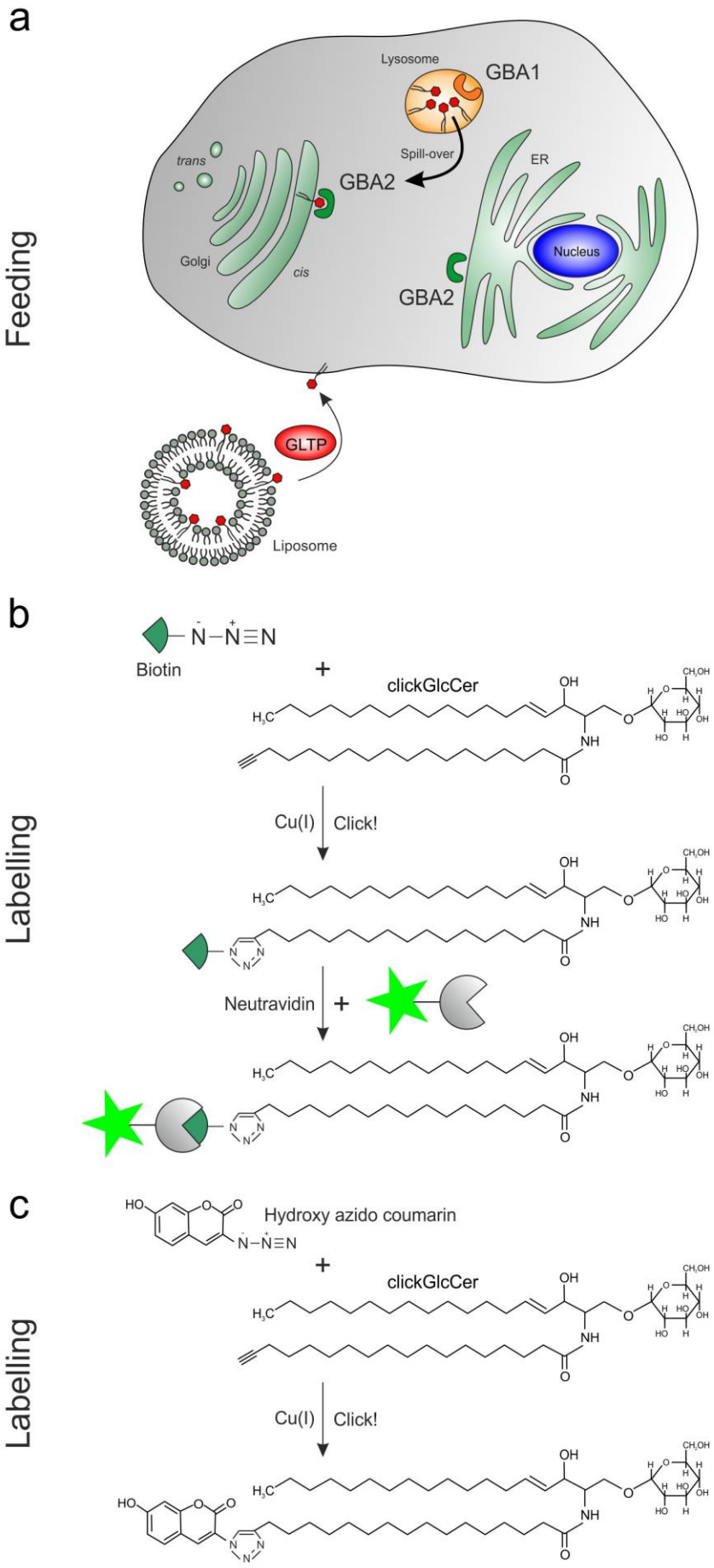
a
Feeding
Lysosome
GBA1
Spill-over
ER
trans
GBA2
Golgi
cis
Nucleus
GBA2
GLTP
Liposome
b
Labelling
Biotin
clickGlcCer
Cu(I)
Click!
Neutravidin
c
Labelling
Hydroxy azido coumarin
clickGlcCer
Cu(I)
Click!

Figure 70: Visualisation of GlcCer in the cell. Schematic drawing of the experiment described in the text. **(a)** GLTP-mediated transfer of clickGlcCer from DOPC liposomes to the outer leaflet of the plasma membrane of cells. **(b)** Visualisation of clickGlcCer in cells fixed with PFA via azido biotin (AP3Btn or APpic2Btn, Figure 72a) and detection via a fluorophore-labelled streptavidin. **(c)** Visualisation of clickGlcCer via 3-azido-7-hydroxycoumarin and excitation at 404 nm after thin layer chromatography (TLC). GLTP: glycolipid transfer protein, DOPC: 1,2-Dioleoyl-sn-glycero-3-phosphocholine, ER: Endoplasmic reticulum, Cu: Copper.

Incubation with different amounts of clickGlcCer showed a clear dose-dependent signal on the TLC plate with no signal in the control lanes and stronger signals in the 10 mol% sample (Figure 71a). Overall, chasing for 30 minutes resulted in better signals than incubation overnight, even though no additional coumarin-labelled bands became visible, suggesting that clickGlcCer did not get metabolised (Figure 71a). I also compared the signal intensity between cells that were incubated with liposomes containing 5 mol% clickGlcCer produced by an extruder (E, Figure 71a, upper pictures, Figure 71b) or by sonication (S, Figure 71a, bottom pictures, Figure 71b). An extruder produces rather large, unilamellar vesicles by repetitive extrusion through a membrane of a defined size (Avanti Polar Lipids). Here, liposomes with a diameter of 400 nm were produced. In comparison, sonication of lipid suspensions generates small unilamellar vesicles with diameters from 15 to 50 nm (Avanti Polar Lipids). As displayed in Figure 71a, the amount of clickGlcCer present in control fibroblasts after a 30 minutes chase was significantly higher when cells were pulsed with 5 mol% liposomes produced by sonication compared to extrusion. It has already been shown that the fusion rate constant of liposomes depends on liposome size, with smaller liposomes fusing more easily with other membranes (Bentz&Duzgunes, 1985). Thus, these findings are reflected in Figure 71a, where smaller liposomes (sonication) resulted in a stronger signal than larger liposomes (extrusion). Nevertheless, when clickGlcCer/DOPC liposomes fuse with the plasma membrane, clickGlcCer gets incorporated into both, the intracellular and extracellular membrane leaflet. ClickGlcCer sitting in the inner leaflet of the plasma membrane becomes accessible to e.g. glycolipid transfer proteins like GLTP and FAPP2, because it faces the cytoplasm when present in the “outer” leaflet of emerging endosomes. With this orientation, clickGlcCer would not reach the lumen of the lysosome, since GSLs show very slow spontaneous trans-bilayer movement due to their large polar head group (Buton et al., 2002). Thus, I decided to prepare rather large (400 nm) liposomes that are less likely to fuse with the plasma

membrane of cells and favour the transfer of clickGlcCer to the outer leaflet of the plasma membrane via GLTP (Lauria et al., 2013).

Even though the experiment and the presence of clickGlcCer per se was verified by TLC analysis (Figure 71a), there was no difference in fluorescence intensity of streptavidin-Alexa488 between cells pulsed with clickGlcCer and the negative control (Figure 71b). The click reaction between clickGlcCer and biotin-azide as well as the detection of the latter by streptavidin-Alexa488, however, seemed to work, since there was a clear fluorescent signal visible in cells pulsed with 5 µM clickSphinganine (Figure 71b). This result suggests that the feeding and clicking of clickGlcCer itself works, but that there was a subsequent problem during detection of the biotinylated (AP3Btn) clickGlcCer, probably due to a still rather low abundance of the lipid in the cells after feeding.

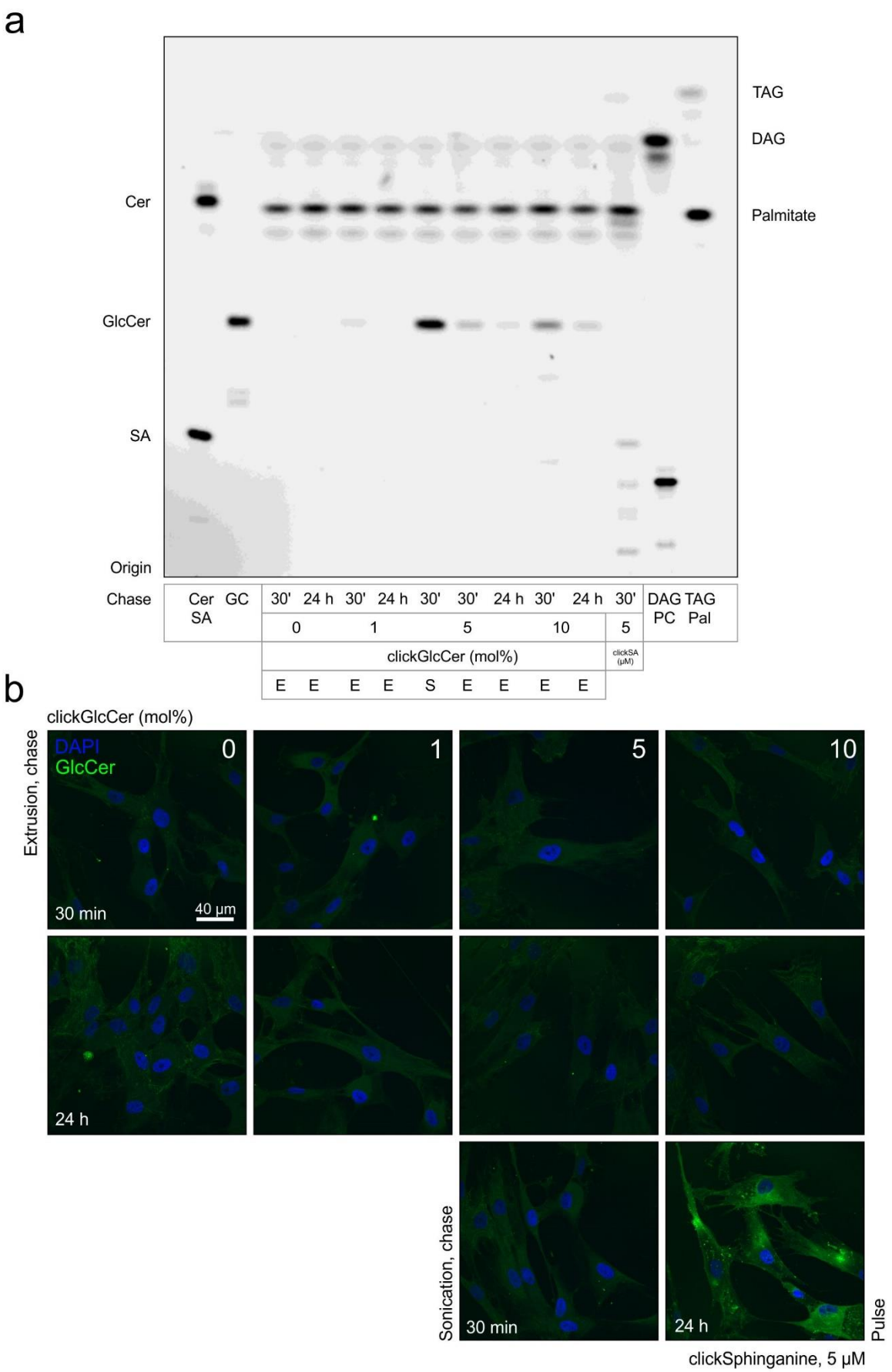
a
TAG
DAG
Palmitate
Cer
GlcCer
SA
Origin
Chase
Cer GC
SA
30' 24 h 30' 24 h 30' 30' 24 h 30' 24 h 30'
DAG TAG
PC Pal
0 1 5 10 5
clickGlcCer (mol%)
clickSA (µM)
E E E E S E E E E
b
clickGlcCer (mol%)
Extrusion, chase
DAPI
GlcCer
0
1
5
10
30 min
40 µm
24 h
Sonication, chase
30 min
24 h
Pulse
clickSphinganine, 5 µM

Figure 71: Analysis of clickGlcCer feeding by TLC and microscopy. Control fibroblasts were incubated with 10 µM hGLTP and DOPC liposomes containing no, 1, 5, or 10 mol% clickGlcCer to facilitate GLTP-mediated transfer of click-GlcCer to the plasma membrane. Cells were pulsed with clickGlcCer for 10 minutes and the lipid was then chased for either 30 minutes or 24 h. Lipids extracted from the cells were clicked to 3-azido-7-hydroxycoumarin and analysed by thin layer chromatography (TLC) at 404 nm. Cells for microscopy were fixed using 4% PFA in PBS, clicked to azido biotin (AP3Btn), and detected via a streptavidin coupled to Alexa488 to visualise ectopic GlcCer (green) in the cells. **(a)** TLC analysis of clickGlcCer fed to control fibroblasts. Chasing for 30 minutes resulted in better signals than incubation for 24 h and in dose-dependent band pattern for clickGlcCer. Comparison of liposomes containing 5 mol% produced by extrusion or sonication resulted in a stronger signal coming from sonicated liposomes. **(b)** There was no difference in fluorescence intensity of streptavidin-Alexa488 between cells pulsed with clickGlcCer and the negative control. Incubation with 5 µM clickSphinganine resulted in a clear fluorescent signal. Blue channel: DAPI. GlcCer: Glucosylceramide, TAG: Triacylglycerol, SM: Sphingomyelin, PC: Phosphatidylcholine, DOPC: 1,2-Dioleoyl-sn-glycero-3-phosphocholine, GLTP: Glycolipid transfer protein. Scale bars are indicated.

To solve this problem, I first tested a more sensitive azido-biotin (APpic2Btn, Figure 72a) (Gaebler et al., 2016), carrying a picolyl moiety, which chelates copper, the catalyst for the click reaction, and, thereby increases the detection sensitivity (Gaebler et al., 2016). Additionally, I also tested two different catalysts for the click reaction, (Cu(I)TFB and $CuSO_4$/TBTA) (Figure 72b). Control dermal fibroblasts were pulsed with either 10 mol% clickGlcCer/DOPC liposomes diluted 1:2.5 in PBS together with 18 µM hGLTP for 15 min and chased for 1 h or with 5 µM clickSphinganine for 1 h (Figure 72b). After fixation, cells were clicked to either AP3Btn or APpic2Btn in the presence of Cu(I)TFB or $CuSO_4$/TBTA and visualised using streptavidin-Alexa488 (Figure 72b). AP3Btn showed strong signals in cells pulsed with 10 mol% clickGlcCer and clicked in presence of $CuSO_4$/TBTA, but the signal was even more pronounced using APpic2Btn (Figure 72b). The overall fluorescence in both, cells pulsed with clickGlcCer or clickSphinganine, was very strong, but samples clicked in presence of $CuSO_4$/TBTA generally showed more background than cells clicked in presence of Cu(I)TFB (Figure 72b). Since samples clicked to APpic2Btn in presence of Cu(I)TFB displayed nice results, I chose this combination for further experiments (Figure 72b).

a

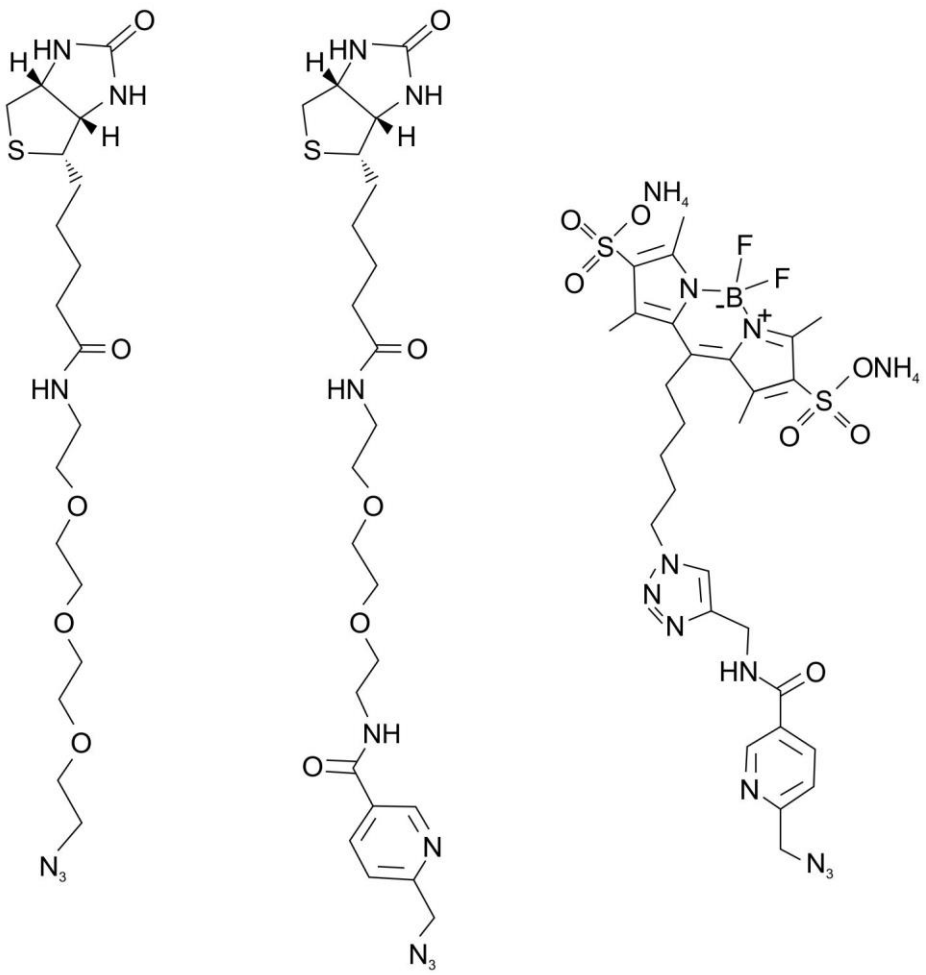
AP3Btn
APpic2Btn
ApicSBDP

b

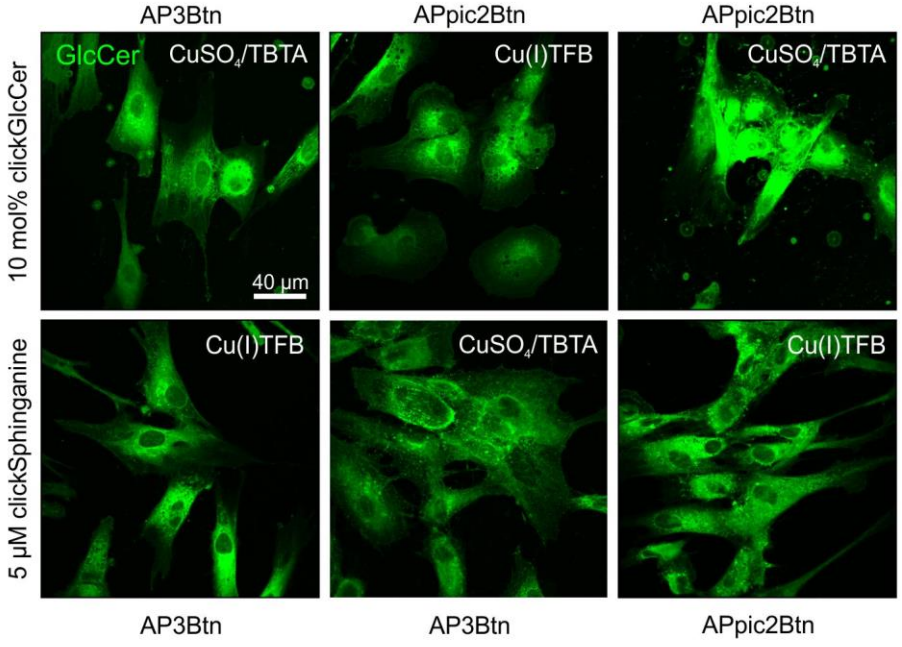
AP3Btn
APpic2Btn
APpic2Btn
GlcCer
CuSO4/TBTA
Cu(I)TFB
CuSO4/TBTA
10 mol% clickGlcCer
40 µm
Cu(I)TFB
CuSO4/TBTA
Cu(I)TFB
5 µM clickSphinganine
AP3Btn
AP3Btn
APpic2Btn

Figure 72: Analysis of different Cu-based click catalysts and azido-biotin derivatives. Control fibroblasts were pulsed with 18 µM hGLTP and DOPC liposomes, containing 10 mol% clickGlcCer (green) or 5 µM clickSphinganine (green), for 15 minutes and chased for 1 h. ClickSphinganine was pulsed for 1 h without further chase. The lipids were clicked in the presence of either Cu(I)TFB or $CuSO_4$/TBTA to AP3Btn or APpic2Btn. ClickGlcCer was detected via a streptavidin coupled to Alexa488. **(a)** Structures of AP3Btn, APpic2Btn, and ApicSBDP. Published in (Gaebler et al., 2016). **(b)** Detection with APpic2Btn was more sensitive than AP3Btn and Cu(I)TFB showed less dirt than $CuSO_4$/TBTA. Scale bar is indicated. A: Azido, PX: Polyethylenglycol spacer with length of x ethylene glycol units, pic: linker contains picolyl moiety, Btn: Biotin, BDP: BODIPY/ boron-dipyrromethene, CuSO4: Copper (II) sulfate, TBTA: Tris(benzyltriazolylmethyl)amine, GlcCer: Glucosylceramide, DOPC: 1,2-Dioleoyl-sn-glycero-3-phosphocholine, GLTP: Glycolipid transfer protein. Scale bar is indicated.

Besides testing different azido-biotins and click catalysts, I also tested a protocol to deliver clickGlcCer to the plasma membrane of cells in a complex with bovine serum albumin (BSA). Albumin is the most abundant protein found in blood plasma where it e.g. binds hydrophobic molecules to carry them through the body (He&Carter, 1992). Since lipids are mainly hydrophobic and, thus, cannot simply be fed to cells in aqueous solutions, they have been complexed to BSA for this purpose since many years (Lambeth et al., 1988). I prepared clickGlcCer/BSA complexes by lyophilisation (personal communication with Dr. Ü. Coskun, DZD-Paul Langerhans Institute, Technische Universität Dresden, Dresden) and pulsed control dermal fibroblasts with or without 2, 20, or 200 µM of the complex re-suspended in sterile PBS for 15 minutes and chased the lipids for 1 h (Figure 73). As a control, I also prepared DOPC liposomes containing no or 10 mol% clickGlcCer and followed the same feeding protocol using GLTP-mediated transfer as previously described (Figure 70). As previously shown (Figure 72b), cells pulsed with 10 mol% clickGlcCer diluted 1:2.5 in PBS in presence of 18 µM GLTP and clicked to streptavidin-Alexa488 catalysed by Cu(I)TFB displayed a strong signal compared to cells pulsed without clickGlcCer (lower panel, Figure 73). In comparison, there was barely any fluorescence detectable in cells pulsed with different amounts of clickGlcCer complexed to BSA (upper panel, Figure 73). Thus, I continued with the protocol using GLTP-mediated transfer of clickGlcCer for further experiments.

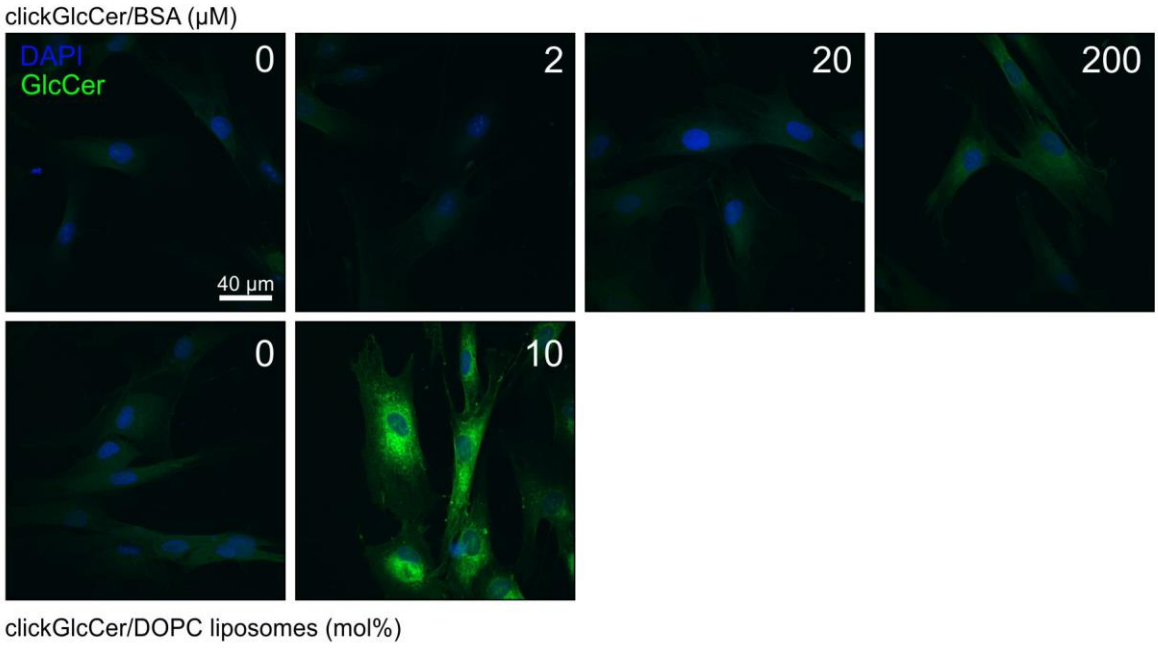

Figure 73: Transfer of clickGlcCer to cells in complex with BSA. ClickGlcCer/BSA complexes were prepared via lyophilisation and control fibroblasts were incubated with 0, 2, 20, or 200 µM clickGlcCer for 15 minutes. Lipids were chased for 1 h and clicked to APpic2Btn in the presence of Cu(I)TFB. APpic2Btn was visualised using streptavidin-Alexa488 (upper panel). As controls, cells were incubated with DOPC liposomes containing no or 10 mol% clickGlcCer (lower panel). There was almost no fluorescence detectable in cells pulsed with different amounts of clickGlcCer/BSA (upper panel). GLTP-mediated transfer of clickGlcCer worked nicely with liposomes containing 10 mol% clickGlcCer compared to the controls (lower panel). Blue channel: DAPI. GlcCer: Glucosylceramide, BSA: Bovine serum albumin, GLTP: Glycolipid transfer protein, DOPC: 1,2-Dioleoyl-sn-glycero-3-phosphocholine. Scale bar is indicated.

To increase the subcellular resolution of clickGlcCer, I switched from biotin-conjugated azides to ApicSBDP (azido-picolyl-sulfo-tetramethyl-BODIPY), an azide that carries a BODIPY moiety (Figure 72a and Figure 74) (Gaebler et al., 2016). BODIPY (boron-dipyrromethene) is a fluorescent dye that has been extensively used to study the structure of membranes (Kaiser&London, 1998). BODIPY possesses sharp excitation and emission peaks in the visible light range and is highly soluble in organic solvents (Karolin et al., 1994). Most importantly, directly using a dye-conjugated azide to detect clickGlcCer simplifies the staining protocol and should also provide a better resolution since the dye is much closer to the lipid.

As previously described, fibroblasts from control and type I *Gaucher* patients were pulsed with either 0 or 10 mol% clickGlcCer/DOPC liposomes for 1 h or 24 h (Figure 74 - Figure 76). Cells pulsed for 1 h were subsequently chased for 23 h (Figure 74 and

Figure 75). Afterwards, lipids were extracted, clicked to 3-azido-7-hydroxycoumarin, and either analysed by TLC (Figure 74) or fixed using 4% PFA in PBS and blocked using a buffer containing cold-water fish gelatine, saponine, and PBS (Figure 75 and Figure 76). To reveal the subcellular localisation of clickGlcCer at certain organelles, cells were immunocytochemically labelled using antibodies against the lysosomal marker protein LAMP1 (Lysosomal-associated membrane protein 1) (Chen et al., 1985) or the Golgi marker giantin (Linstedt&Hauri, 1993). Primary antibodies were detected using Cy3- and Alexa647-conjugated secondary antibodies before the cells were clicked to ApicSBDP in presence of Cu(I)TFB and imaged using a fluorescence microscope (Figure 75 and Figure 76).

TLC analysis showed that both, control and *Gaucher* fibroblasts, took up clickGlcCer equally well (Figure 74). Here, pulsing for 24 h resulted in a much stronger clickGlcCer signal than pulsing for only 1 h (Figure 74). On the other hand, since additional bands appeared in the samples pulsed for 24 h, clickGlcCer was partially metabolised to sphingomyelin and phosphatidylcholine (Figure 74). These bands were not visible in cells pulsed for only 1 h (Figure 74).

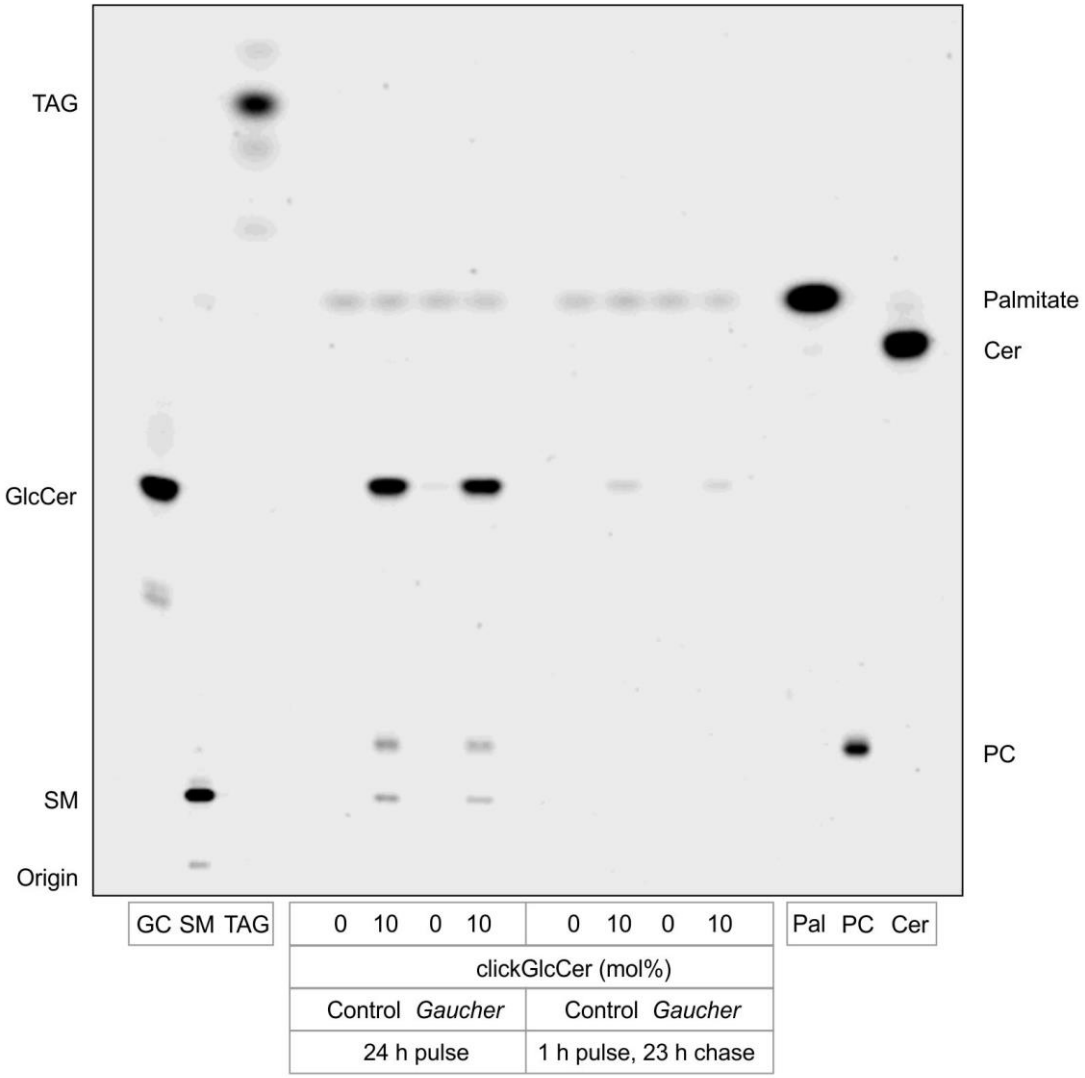

Figure 74: Analysis of clickGlcCer in control and *Gaucher* fibroblasts by TLC. Fibroblasts from control and *Gaucher* patients were incubated with 18 µM hGLTP and DOPC liposomes containing no or 10 mol% clickGlcCer to facilitate GLTP-mediated transfer of click-GlcCer to the plasma membrane. Cells were pulsed with clickGlcCer for 1 h and chased for 23 h or only pulsed for 24 h. Lipids extracted from the cells were clicked to 3-azido-7-hydroxycoumarin and analysed by TLC at 404 nm. Pulsing for 24 h resulted in a stronger signal than the shorter pulsing time. ClickGlcCer was partially metabolised to sphingomyelin and phosphatidylcholine during longer pulsing times. TAG: triacylglyerol, GlcCer/GC: Glucosylceramide, SM: sphingomyelin, Cer: Ceramide, Pal: Palmitic acid, PC: phosphatidylcholine, GLTP: Glycolipid transfer protein, DOPC: 1,2-Dioleoyl-sn-glycero-3-phosphocholine.

The ratio of clickGlcCer uptake between pulsing times of 1 h *versus* 24 h was also reflected in the fluorescence intensity of immunocytochemically stained samples: There was barely any difference visible between cells incubated with no or 10 mol% clickGlcCer (Figure 75). As also displayed on the TLC, there were no obvious differences between control and *Gaucher* fibroblasts (Figure 74).

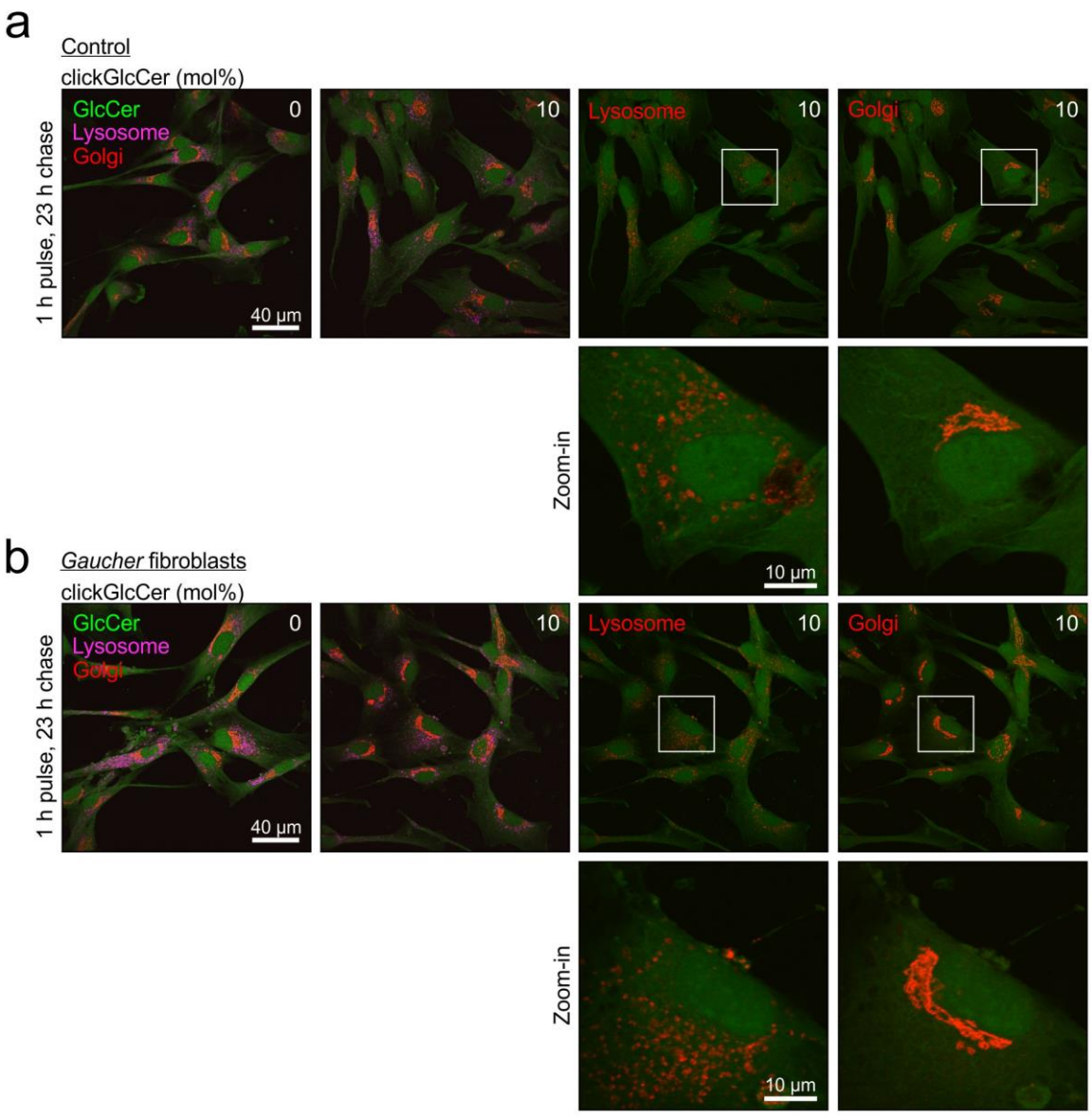

Figure 75: Microscopic analysis of control and *Gaucher* fibroblasts pulsed with clickGlcCer. Fibroblasts from control and *Gaucher* patients were incubated with 18 µM hGLTP and DOPC liposomes containing 0 or 10 mol% clickGlcCer (green) to facilitate GLTP-mediated transfer of clickGlcCer to the plasma membrane. Cells were pulsed with clickGlcCer for 1 h and chased for 23 h. Cells were fixed with 4% PFA in PBS and immunostained using the lysosomal marker protein LAMP1 (magenta, red) and the Golgi marker protein giantin (red). ClickGlcCer was clicked to ApicSBDP and visualised at 488 nm. The signal intensity of clickGlcCer was very weak in **(a)** control and **(b)** *Gaucher* fibroblasts. The antibody staining clearly showed lysosomal and Golgi structures. Lower pictures were zoomed-in. GlcCer: Glucosylceramide, GLTP: Glycolipid transfer protein, DOPC: 1,2-Dioleoyl-sn-glycero-3-phosphocholine. Scale bars are indicated.

In comparison, signal intensity was much stronger in cells incubated with 10 mol% clickGlcCer for 24 h (Figure 76). Here, a clear difference between cells incubated with

0 or 10 mol% clickGlcCer was visible (Figure 76). BODIPY-labelled clickGlcCer staining was detected throughout the whole cell with a prominent staining that co-localised with the Golgi marker, resulting in a yellow signal in both, control and *Gaucher* fibroblasts (Figure 76). ClickGlcCer also seemed to localise to lysosomal structures, but did not co-localise with LAMP1 (Figure 76).

In summary, clickGlcCer was found to localise predominantly to the Golgi in both, control and *Gaucher* fibroblasts, when pulsed for 24 h (Figure 76). Even though a minor portion of clickGlcCer was metabolised during this time, the majority of the signals still originated from clickGlcCer (Figure 74). Thus, there were no obvious difference between the localisation of clickGlcCer in fibroblasts from control and *Gaucher* patients. Due to time limitations, the experiment was not further optimised.

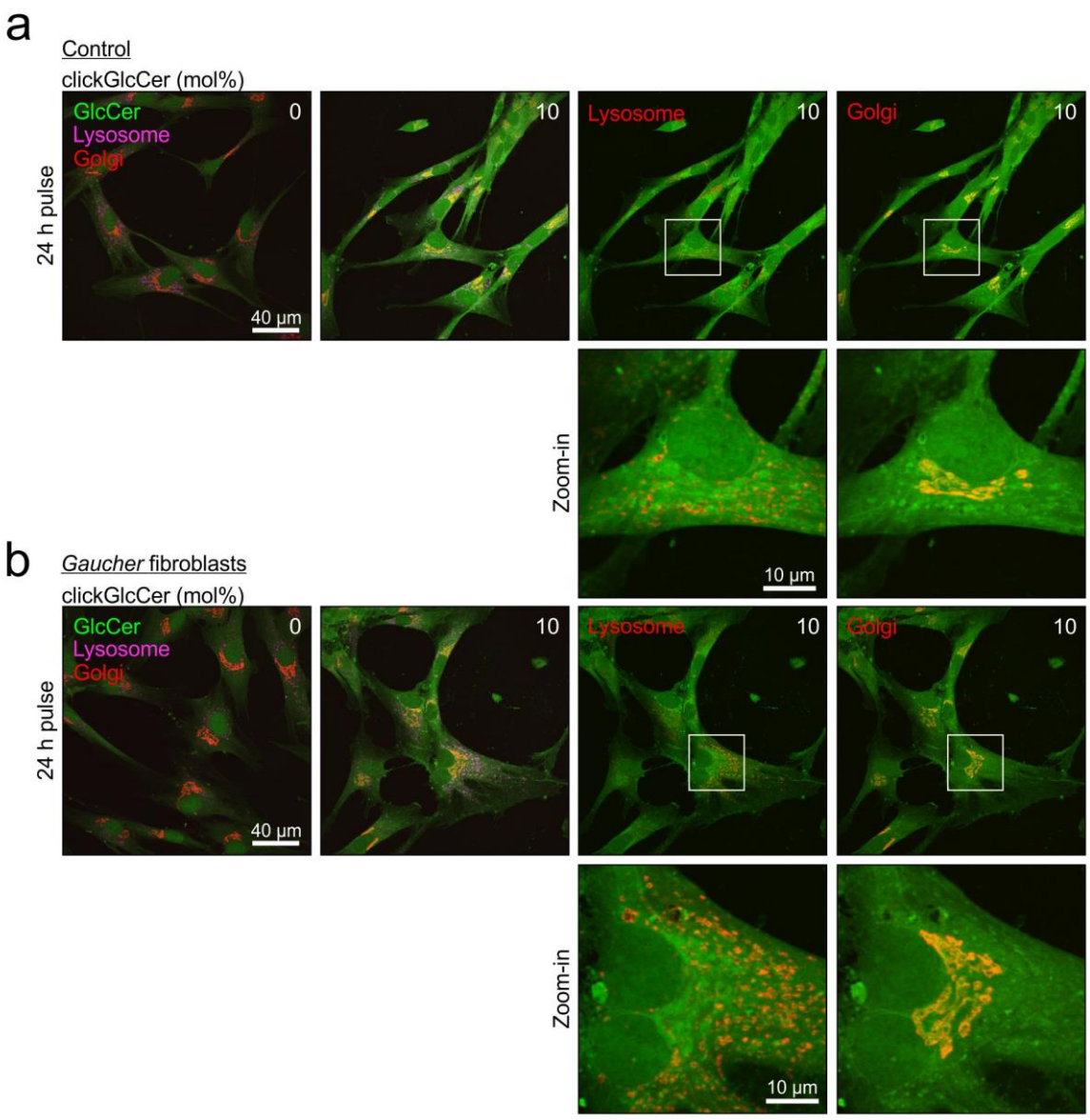

Figure 76: Microscopic analysis of control and *Gaucher* fibroblasts pulsed with clickGlcCer. Fibroblasts from control and *Gaucher* patients were incubated with 18 µM hGLTP and DOPC liposomes containing 0 or 10 mol% clickGlcCer (green) to facilitate GLTP-mediated transfer of clickGlcCer to the plasma membrane. Cells were pulsed with clickGlcCer for 24 h. Cells were fixed with 4% PFA in PBS and immunostained using the lysosomal marker protein LAMP1 (magenta, red) and the Golgi marker protein giantin (red). ClickGlcCer was clicked to ApicSBDP and visualised with light at 488 nm. There was a clear difference in signal intensity visible between cells pulsed with or without clickGlcCer. **(a)** Control and **(b)** *Gaucher* fibroblasts took up clickGlcCer equally well. The antibody staining clearly showed lysosomal and Golgi structures. ClickGlcCer localised predominantly to the Golgi in both, control and *Gaucher* fibroblasts. Lower pictures were zoomed-in. GlcCer: Glucosylceramide, GLTP: Glycolipid transfer protein, DOPC: 1,2-Dioleoyl-sn-glycero-3-phosphocholine. Scale bars are indicated.

3.15.2 Studying the interaction of sphingosine and GBA2

3.15.2.1 Photoactivatable and clickable sphingosine (pacSph)

To further investigate the binding of sphingosine to GBA2, I designed an assay using a bifunctional sphingosine derivative. Photoactivatable and clickable sphingosine (pacSph) features a photoactivatable diazarine ring that covalently binds to proteins in close proximity upon activation with UV-light (Haberkant et al., 2016). Furthermore, pacSph is equipped with a terminal alkyne group that can be subsequently labelled by click chemistry to visualise protein-lipid complexes (Haberkant et al., 2016).

3.15.2.2 Assay to pull-down sphingosine-binding proteins

By using pacSph, Dr. P. Haberkant could already show that pacSph directly binds to GBA1 (non-published data). This finding is supported by my results showing that GBA1 activity is sensitive to sphingosine (see Figure 61a). Thus, I aimed to study the interaction between both, GBA1 and GBA2, using pacSph, while GBA1 served as a positive control. During the respective assay, either intact cells or protein lysates were incubated with pacSph and, subsequently, with azido-biotin. The protocol contains several protein precipitation steps to separate pacSph that was neither cross-linked nor clicked. Thus, I first tested two different protein precipitation protocols to verify that GBA1 and GBA2 are not lost during precipitation. First, I prepared hypotonic protein lysates from CHO cells stably over-expressing mGBA1-HA and mGBA2-HA and precipitated the proteins three times using chloroform/methanol (Figure 77a). Unfortunately, a lot of both, GBA1 and GBA2, was already lost after the first precipitation step and there was barely any protein visible after the third precipitation (Figure 77a). Thus, I switched to a different precipitation protocol using ethanol. Here, almost all protein from the input was successfully recovered after the third precipitation (Figure 77b). Therefore, I chose the latter protocol for the assay.

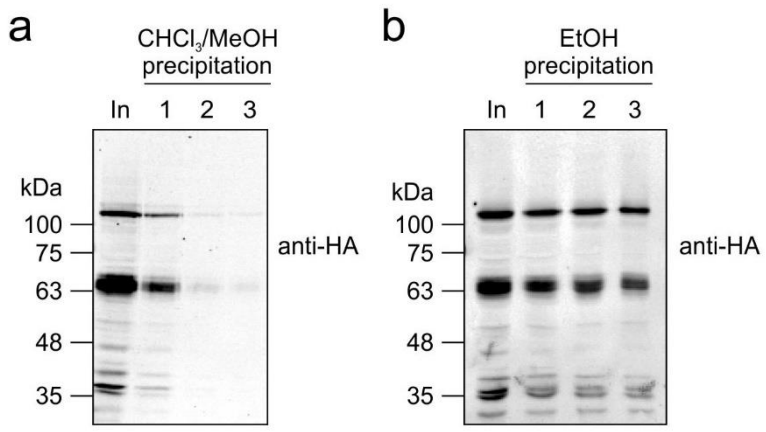

Figure 77: Comparison of protein precipitation using $CHCl_3$/MeOH or EtOH. Analysis of presence GBA1 and GBA2 in hypotonic lysates of CHO cells stably over-expressing mGBA1 and mGBA2 after three rounds of protein precipitation by Western blot using a specific anti-HA antibody (Kremmer). **(a)** GBA1 and GBA2 were already almost completely lost during the first precipitation when precipitated with $CHCl_3$/MeOH. **(b)** EtOH precipitation of GBA1 and GBA2 almost full recovered both proteins after three precipitations. kDa: Kilo Dalton.

In a first attempt, CHO cells stably over-expressing mGBA1-HA and mGBA2-HA were incubated with 6 µM pacSph for 4 h. Then, cells were washed and incubated in PBS for UV-radiation using a LED lamp (1.25 mA) for 5 min (UV+). In parallel, a control plate was incubated without UV-radiation (UV-, Figure 78b). The cells were harvested and lysed using hypotonic buffer (L, Figure 78b, c) and proteins were precipitated using ethanol to separate the remaining, non-cross-linked pacSph from the protein-lipid complexes (Precipitation 1, Figure 78b, c). The protein pellets were re-suspended in HEPES buffer and the suspension was clicked to azido-biotin (AP3Btn, see Figure 72a) at 37 °C for 3 h. Afterwards, proteins were precipitated again to remove residual, non-clicked azido-biotin from the sample (Precipitation 2, Figure 78b, c). The protein pellets were re-suspended in PBS and loaded to a neutravidin column. Neutravidin is a derivative of streptavidin, a protein purified from *Streptomyces avidinii*, which has a very high affinity for biotin (Gyorgy et al., 1940). The neutravidin beads in the column bind biotinylated proteins and, thus, every protein that has bound to pacSph. In a final step, proteins were eluted (E, Figure 78b, c) and the samples, including the beads, were analysed by Western blot using an anti-HA antibody (Figure 78b, c). Although protein precipitation using ethanol was successfully tested before (compare Figure 77b), the majority of GBA2 was lost during the precipitation and only a small amount of GBA2 was loaded to the neutravidin column (Figure 78c). Some GBA2 protein was

detected in the flow-through fraction (FT, Figure 78c), but there was also GBA2 present in the elution and the bead fraction after elution in the UV+ samples (Figure 78c), indicating that GBA2 had directly bound to sphingosine. Similar results were obtained for GBA1, which was generally more expressed than GBA2 and showed a clear band in the input and elution fraction of the UV+ sample, supporting the results from Dr. P. Haberkant (Figure 78c). The samples without UV irradiation (UV-, Figure 78b) served as a negative control because without cross-linking, no proteins should have covalently bound to pacSph and, thus, have bound to the column material. However, there were faint GBA1 bands visible in the elution fraction of the UV- samples, suggesting that the binding of GBA1 and pacSph was either extremely strong or that there was some non-specific binding of GBA1 to the column material (Figure 78b).

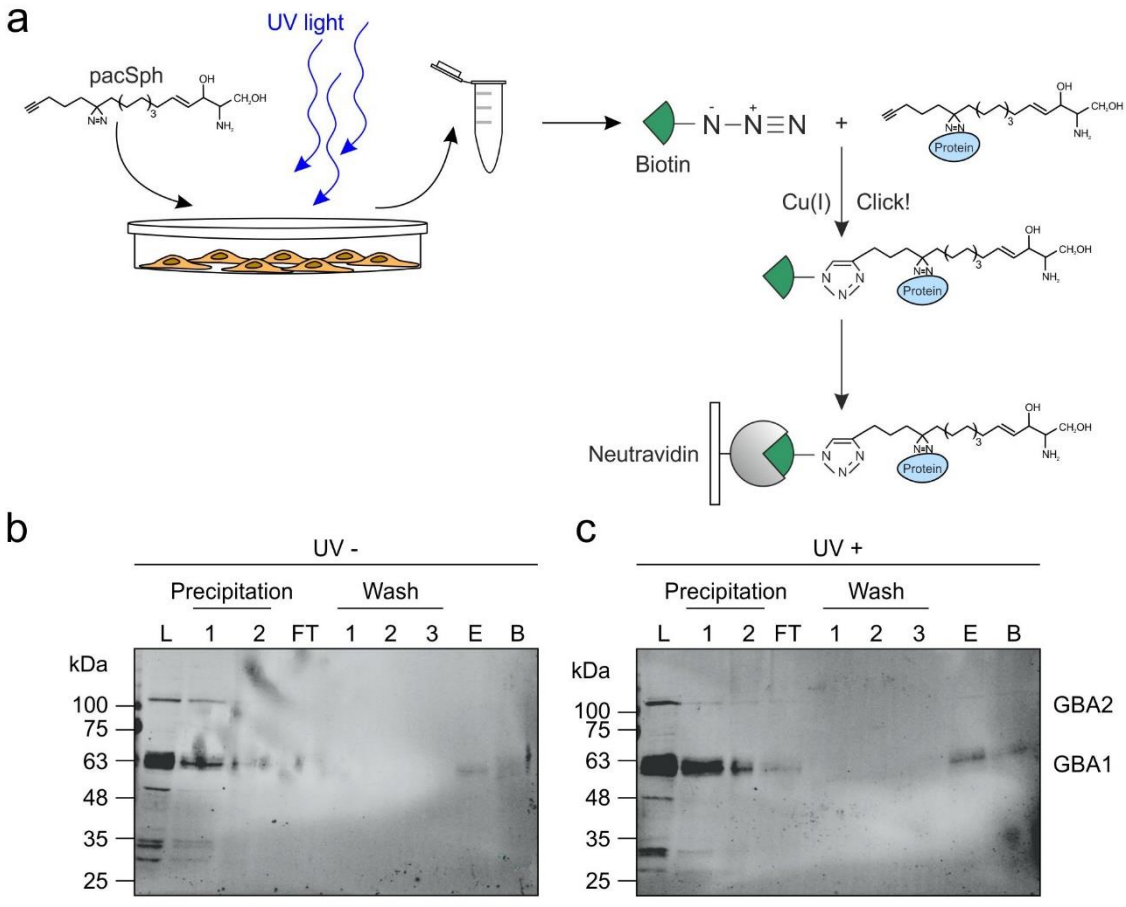

Figure 78: Photo-crosslinking and clicking of pacSph in CHO cells stably over-expressing mGBA1 and mGBA2. CHO cells stably over-expressing mGBA1 and mGBA2 were fed with 6 µM pacSph before irradiation with UV light to photo-crosslink binding proteins. Western blot analysis and immunostaining of GBA1 and GBA2 by a specific anti-HA antibody (Kremmer) after clicking pacSph to biotin-azide and precipitating biotinylated proteins via neutravidin beads. **(a)** Flow-chart of the experiment. The protocol is described in the text. **(b)** There were faint GBA1 bands visible in the elution

fraction of samples without UV irradiation. **(c)** Faint bands of both, GBA1 and GBA2, were visible in the elution fraction when samples were UV irradiated. L: Lysate, FT: Flow-through, E: Elution, B: Beads boiled in SDS sample buffer, kDa: Kilo Dalton.

As previously mentioned, sphingosine is not only a precursor for higher-order GSLs, but also for glycerolipids (Figure 1, Figure 79). Sphingosine is released from GSLs in the lysosome and then transported back to the ER, where it can be re-used to produce ceramide via the salvage pathway (Schwarzmann&Sandhoff, 1990). Here, sphingosine can be phosphorylated by S1P kinases to produce S1P (Spiegel&Milstien, 2003), which can be irreversibly cleaved by S1P lyase (SGPL1) to produce hexadecenal and phosphoethanolamine (Serra&Saba, 2010), which enters the biosynthesis pathway for glycerolipids (Nakahara et al., 2012).

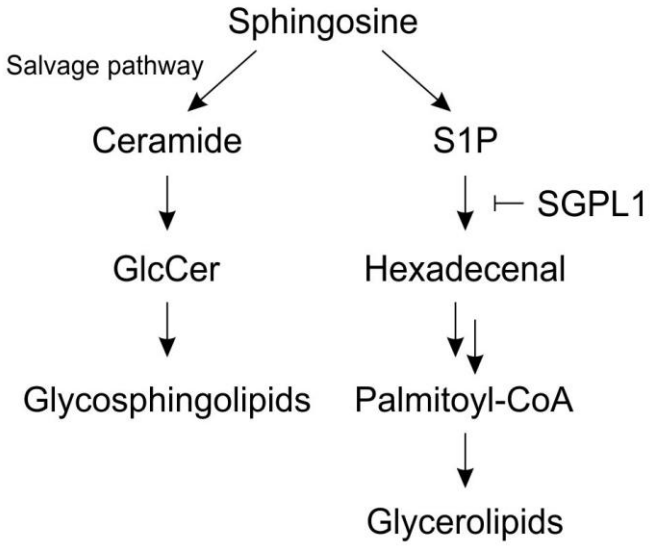

Figure 79: Sphingosine is a precursor for both, glycosphingolipids and glycerolipids. The different synthesis pathways are described in the text. S1P: Sphingosine-1-phosphate, SGPL1: Sphingosine-1-phosphate lyase, GlcCer: Glucosylceramide.

During the aforementioned assay, pacSph is incubated with cells for 4 h. Here, Haberkant et al. showed that pacSph was already metabolised and incorporated into the glycerolipid phosphatidylcholine after incubation for only 1 h (Haberkant et al., 2016). This effect had also been recognised by others, where radioactive or fluorescently labelled sphingosine was found to be rapidly degraded and subjected to the glycerolipid pathway when incubated with cells (Kim et al., 2013; Riboni et al., 1999). In this case, binding of glycerolipids such as phosphatidylcholine and GBA1 or GBA2, but not the interaction between pacSph and the beta-glucosidases would be

observed. To prevent that, I switched to delta SGPL1 HeLa cells that were generated using the CRISPR/Cas9 system (Figure 80) (Gerl et al., 2016; Haberkant et al., 2016). First, I tested the heterologous expression of mGBA1 and mGBA2 in this cell type. Delta SGPL1 HeLa cells were transfected using PEI and harvested 24 h later to perform hypotonic cell lysis. The ectopic expression of both proteins was analysed by Western blot using an anti-HA antibody (Figure 80). As shown in Figure 80, both, GBA1 and GBA2, are expressed in delta SGPL1 HeLa cells.

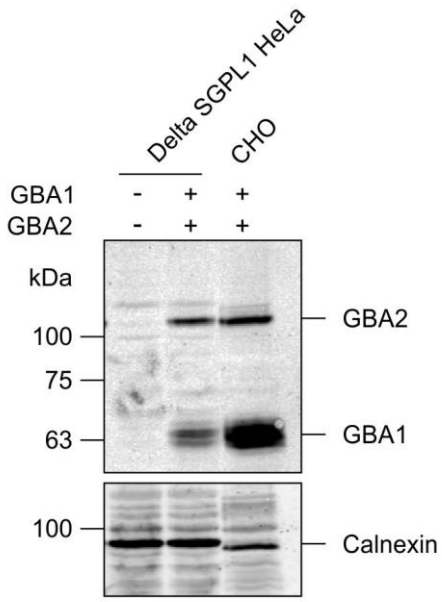

Figure 80: Expression of mGBA1 and mGBA2 in delta SGPL1 HeLa cells. Delta SGPL1 HeLa cells were transfected with mGBA1 and mGBA2 using polyethylenimine (PEI) and expression was compared to non-transfected controls by Western blot using a specific anti-HA antibody (Kremmer). Calnexin was used as a loading control. HeLa cells showed detectable levels of ectopically expressed GBA1 and GBA2 after transfection. SGPL1: Sphingosine-1-phosphate lyase, KO: knock-out, kDa: Kilo Dalton.

As a negative control for the assay, I co-expressed GFP - a protein that would most likely not bind to pacSph and could, therefore, serve as a quality control for the assay itself. I first tested whether the ethanol precipitation protocol also works for GFP (Figure 81). GFP was successfully recovered in the protein pellet even after three precipitation steps, albeit not as efficiently as GBA1 and GBA2 (Figure 81, compare Figure 77b).

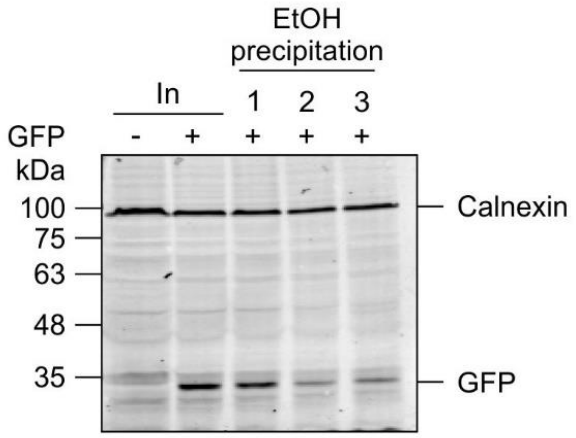

Figure 81: Precipitation of GFP from hypotonic cell lysates using EtOH. GFP was co-expressed with mGBA1 and mGBA2 in delta SGPL1 HeLa cells and the recovery of GFP after EtOH precipitation was analysed by Western blot using a specific anti-GFP antibody (Abcam). Calnexin was used as a control. GFP was recovered in the protein pellet even after three precipitation steps, albeit some protein was lost. In: Input, kDa: Kilo Dalton.

The pacSph assay was performed with delta SGPL1 HeLa cells heterologously expressing GFP, mGBA1, and mGBA2 (Figure 82). Here, both, GBA1 and GBA2, could be recovered in the elution fraction of the UV+ sample (Figure 82b). GFP, which served as a putative negative control, showed a faint band in the elution fraction, representing the background of non-specific protein binding to the column material (Figure 82b). I quantified the amount of GBA1 and GBA2 present in the elution fraction relative to the input. GBA1 was 2-fold and GBA2 was 1.6-fold more abundant in the elution fraction than GFP (background) (Figure 82b). Thus, pacSph directly binds to both, GBA1 and GBA2. A fact that was quite puzzling was that the results for the UV- samples looked very similar (Figure 82a). Even if GBA1 and GBA2 had a very high affinity for pacSph, I would expect that, without a covalent linkage, most of the proteins bound to pacSph would be washed off during the experiment, resulting in much fewer signal and an overall different result compared to the UV+ sample. To verify my results, I tackled the question with a different approach.

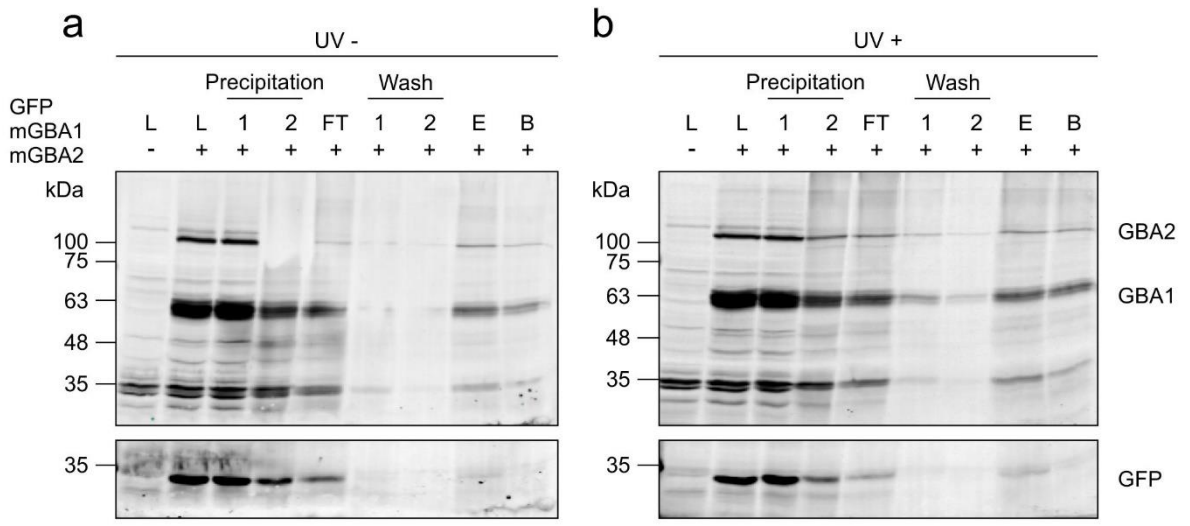

Figure 82: Purification of GBA1 and GBA2 via pacSph. Delta SGPL1 HeLa cells transiently expressing mGBA1, mGBA2, and GFP were fed with 6 µM pacSph for 4 h before irradiation with UV light to photo-crosslink pacSph-binding proteins. After clicking pacSph to biotin-azide and purifying bound proteins via neutravidin beads, protein lysates were subjected to Western blot analysis using an anti-HA specific antibody to detect GBA1 and GBA2 (Kremmer). **(a)** GBA1 and GBA2 were partially recovered in the elution fraction in samples without UV irradiation. **(b)** GBA1, GBA2, and GFP were recovered in the elution fraction in samples photo-crosslinked by UV light. GBA1 was 2-fold more abundant and GBA2 was 1.6-fold more abundant than GFP. L: Lysate, FT: Flow-through, E: Elution, B: Beads boiled in SDS sample buffer, kDa: Kilo Dalton.

I repeated the experiment by incubating lysates from delta SGPL1 HeLa cells heterologously expressing GFP, mGBA1, or mGBA2 with 6 µM pacSph *in vitro* using protein lysates rather than intact cells (Haberkant et al., 2016). Furthermore, I introduced another negative control, AR451 (Dr. A. Rennhack, caesar, non-published, see Table 31). AR451 is a marker and potent modulator for gamma-secretase. It was synthesised to label gamma-secretase via UV-crosslinking of its diazarine group and can subsequently be detected by clicking a marker carrying an azido moiety to its terminal alkyne group (Dr. A. Rennhack, non-published). Lastly, pacSph was also incubated with lysates from delta SGPL1 cells heterologously expressing JAM3, a protein that has been shown to specifically bind to pacSph (Haberkant et al., 2016) (Figure 83). Protein lysates were UV-irradiated before clicking to azido-DY-654 (Dyomics) and separation by size via SDS-PAGE (Figure 83). According to Dr. P. Haberkant, pacSph-protein complexes should turn up as strong DY-654-positive bands already visible in in-gel fluorescence in the UV+ sample compared to the UV- lane when excited with light of 680 nm wavelength (Figure 83). JAM3 is supposed to run at a height of 35-55 kDa (personal communication with Dr. P. Haberkant). However,

Figure 83 only shows a distinct change in fluorescence intensity between the UV- and UV+ sample at around 65 kDa. Thus, I could not reproduce the results obtained by Dr. P. Haberkant. As there were also no clear differences visible between non-transfected and transfected GFP/mGBA1/mGBA2 samples and the UV+ sample and UV- controls, I decided to transfer the proteins to a nitrocellulose membrane by Western blotting and specifically detect the proteins using an anti-HA antibody.

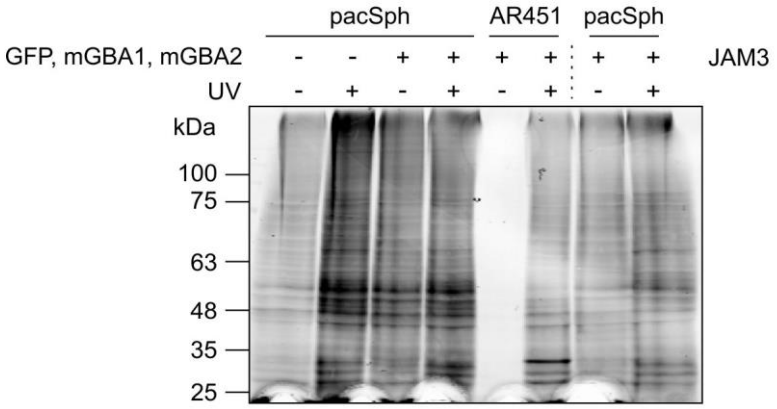

Figure 83: In-gel fluorescence of pacSph and AR451 clicked to azido-DY-654. Lysates from delta SGPL1 cells transiently expressing mGBA1, mGBA2, and GFP, or JAM3 were incubated with 6 µM pacSph before irradiation with UV light to photo-crosslink binding proteins. In-gel fluorescence of pacSph- or AR451-binding proteins after labelling with azido-DY-654 (Dyomics). No distinct bands at the height of GBA1 (55-69 kDa) or GBA2 (~120 kDa) were visible in samples incubated with pacSph or AR451. There was also no band visible in JAM3-expressing samples at around 35-55 kDa. AR451: marker and potent modulator for gamma-secretase, kDa: Kilo Dalton. Representative blot for n = 3 experiments.

After transfer, pacSph-DY-654-labelled proteins were still fluorescent when excited at 680 nm (Figure 84, displayed in red channel). According to the signal pattern, many different proteins of different sizes were bound to pacSph, whereas there were fewer signals visible in the UV+ lane of the sample incubated with AR451 (Figure 84). Here, only one protein band was highlighted at around 30 kDa (Figure 84). In cell lysates expressing mGBA1 and mGBA2, two thin but distinct bands appeared at around 120 kDa, the height of mGBA2 (Figure 84, left). GBA1 and GBA2 were detected using an anti-HA antibody and a fluorescently labelled secondary anti-rat antibody. GBA1 bands were visible at around 60 kDa and GBA2 bands were present at around 120 kDa (Figure 84, displayed in green channel). When both channels were merged, the bands arising from the pacSph-labelled protein co-localised with the GBA2 band resulting in a yellow signal (Figure 84, merged channels), demonstrating that pacSph binds to

GBA2. The pacSph-DY-654 band was also visible in the non-transfected control, most likely due to binding to endogenous GBA2 (Figure 84). In contrast, pacSph did not bind to GBA1, indicating that I could not reproduce the findings from Dr. P. Haberkant (personal communication with Dr. P. Haberkant) (Figure 84). The negative control AR451 neither bound to GBA1 nor to GBA2 (Figure 84). The anti-HA antibody displayed a lot of background labelling with proteins of low molecular weight, making it difficult to clearly see GFP with an anti-GFP staining (Figure 84). However, there are distinct bands visible in the transfected samples that do not co-localise with pacSph or AR451 (Figure 84). Thus, GBA2 but not GBA1 or GFP specifically bound to pacSph.

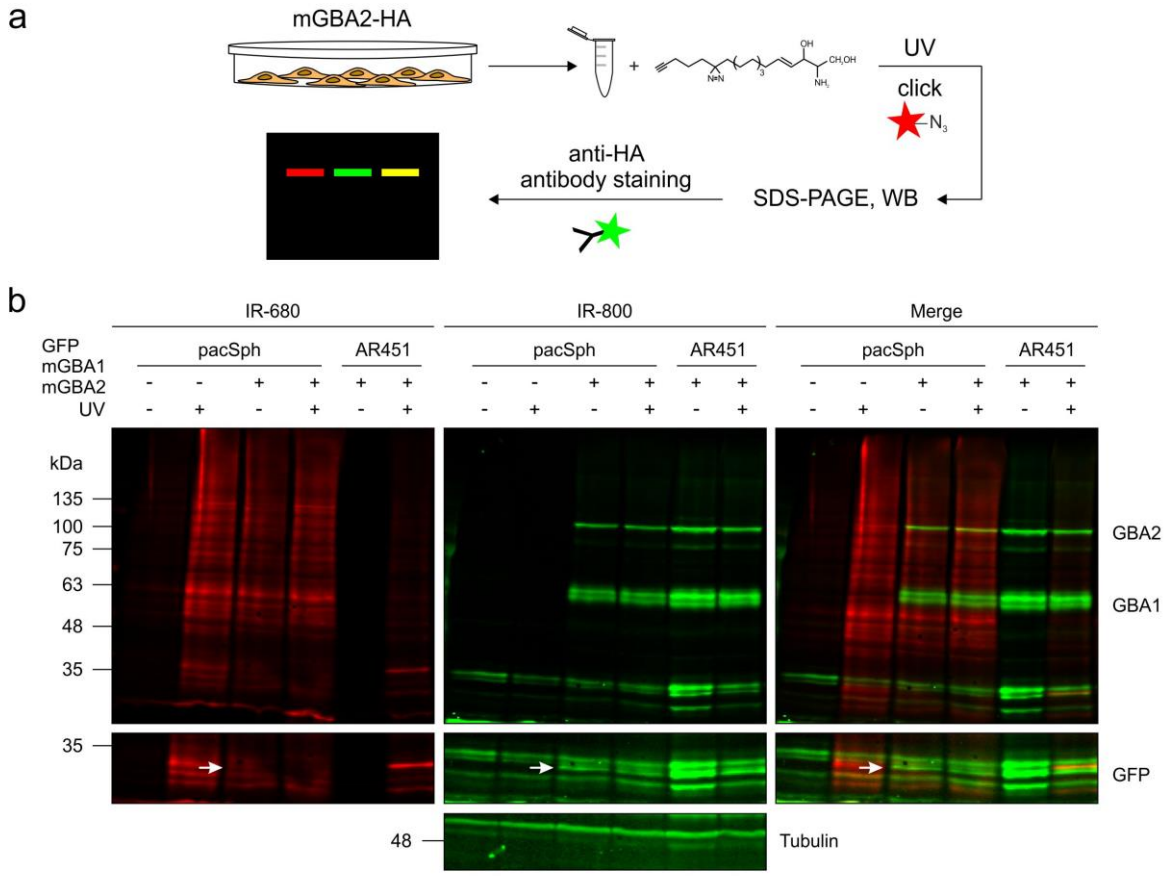

Figure 84: Labelling of GBA2 with pacSph *in vitro*. Lysates from delta SGPL1 cells transiently expressing mGBA1, mGBA2, and GFP also displayed in Figure 83 were analysed by Western blot using a specific anti-HA (Kremmer) and anti-GFP (Abcam) antibody and a fluorescently labelled secondary antibody (IR 800). **(a)** Flow-chart of the experiment. The protocol is described in the text. **(b)** A thin but distinct band was visible at the height of GBA2 (~120 kDa) in samples endogenously and heterologously expressing GBA1 and GBA2 incubated with pacSph and visualised by clicking to azido-DY-654 (Dyomics, red channel). Bands at 120 kDa co-localised with GBA2 (green channel), resulting in a yellow signal (merge channel). Neither GBA1 nor GFP co-localised with pacSph. SDS-PAGE: sodium dodecyl

sulfate polyacrylamide gel electrophoresis, WB: Western blot, IR-680: Infrared wavelength 680 nm, IR-800: Infrared wavelength 800 nm, AR451: marker and potent modulator for gamma-secretase, kDa: Kilo Dalton. Representative blots for n = 3 experiments.

In a final experiment, I wanted to test whether the experimental set up described above would also work when incubating intact delta SGPL1 HeLa cells expressing mGBA1 and mGBA2 with 6 µM pacSph for 4 h before cell lysis (Figure 85). Thus, I repeated the experiment *in vivo*, harvested the cells, and induced the UV-mediated cross linking of pacSph *in vitro* (Figure 85a). Again, the samples were clicked to azido-DY-654 before separating the proteins by SDS-PAGE (Figure 85). In Western blot analysis, GBA1 and GBA2 were detected by an anti-HA antibody and an IRDye800-labelled secondary antibody (IR-800, Figure 85b). As seen in the previous experiment, many different proteins had bound to pacSph, which resulted in several prominent bands at different heights (IR-680, Figure 85b). Nevertheless, the red channel again displayed a band at 120 kDa that co-localised with mGBA2 in the green channel (Figure 85b). GBA1, however, did not bind to pacSph. In summary, these data show that GBA2 specifically binds to pacSph when incubated in a cell lysate or in intact cells.

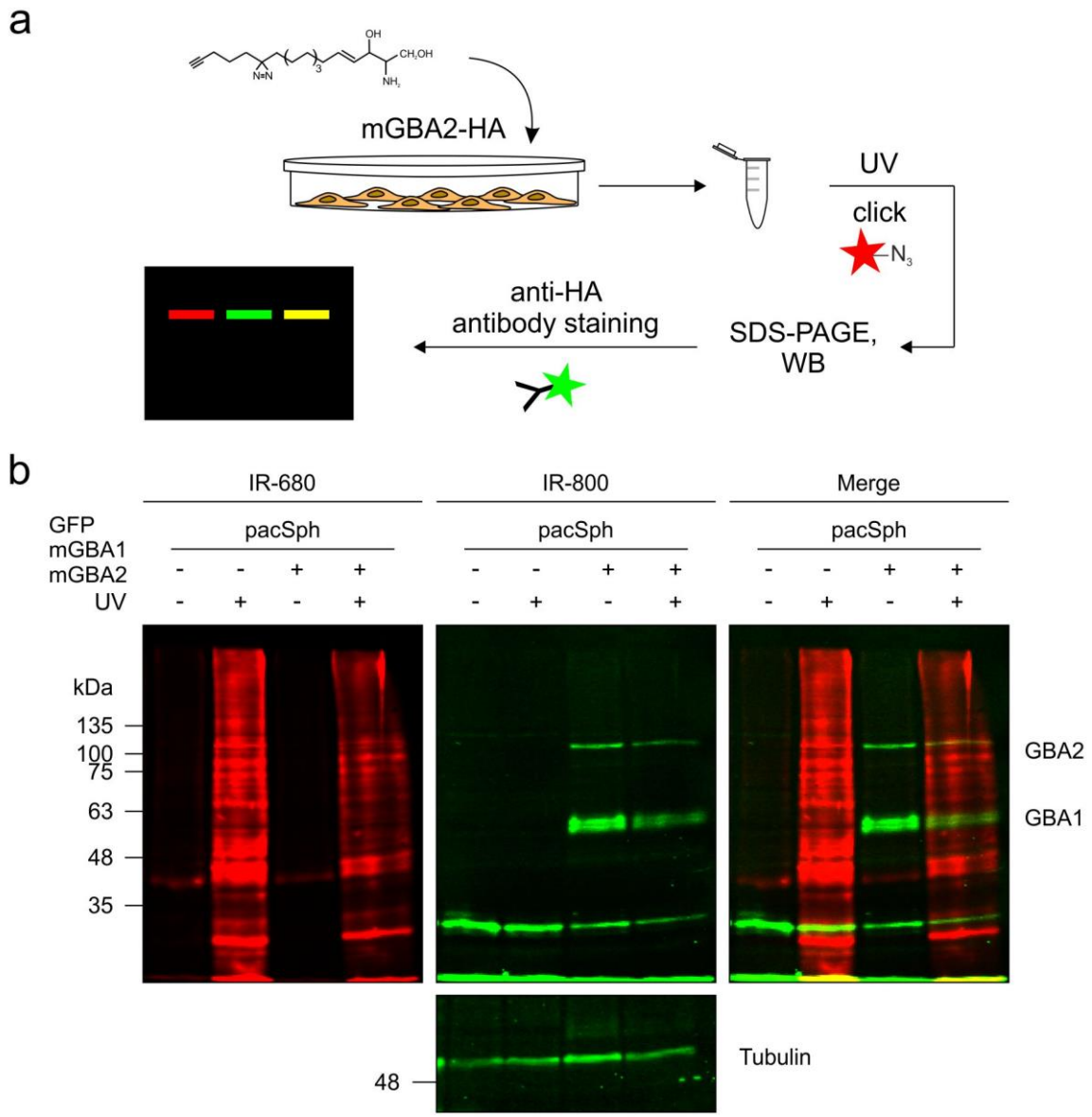

Figure 85: Labelling of GBA2 with pacSph *in vivo.* Delta SGPL1 cells transiently expressing mGBA1, mGBA2, and GFP were fed with 6 µM pacSph before harvesting and irradiation with UV light to photo-crosslink binding proteins. PacSph-bound proteins were visualised by clicking pacSph to azido-DY-654 (Dyomics); GBA1 and GBA2 were detected with an anti-HA specific antibody and a fluorescently labelled secondary antibody (IR-800). **(a)** Flow-chart of the experiment. The protocol is described in the text. **(b)** A thin but distinct band was visible at the height of GBA2 in samples endogenously and heterologously expressing GBA1 and GBA2 incubated with pacSph and visualised by clicking to azido-DY-654 (red channel). Bands at 120 kDa co-localised with GBA2 (green channel), resulting in a yellow signal (merge channel). SDS-PAGE: sodium dodecyl sulfate polyacrylamide gel electrophoresis, WB: Western blot, IR-680: Infrared wavelength 680 nm, IR-800: Infrared wavelength 800 nm, kDa: Kilo Dalton. Representative blots for n = 1 experiment.

To validate that pacSph is not metabolised when incubated with protein lysates from delta SGPL1 HeLa cells transiently expressing mGBA1-HA and mGBA2-HA, the *in vitro* protocol was repeated and lipids were extracted using methanol/chloroform after incubating the samples with 6 µM pacSph for 1 h. The lipids were clicked to 3-azido-7-hydroxycoumarin and analysed by TLC (Figure 86b). Quantification of the bands revealed that pacSph is partially, albeit not predominantly, metabolised to pacCer (14% of the total signal intensity *versus* 1.5% without incubation (Figure 86c). Thus, the amount of pacSph in the samples was decreased to 85% of the total signal intensity (Figure 86c). A minor part of pacSph was also metabolised to pacPC (increase in signal intensity from 0.02% to 1.6%) (Figure 86c). Thus, the bands visible in Figure 84 and Figure 85 arouse from pacSph.

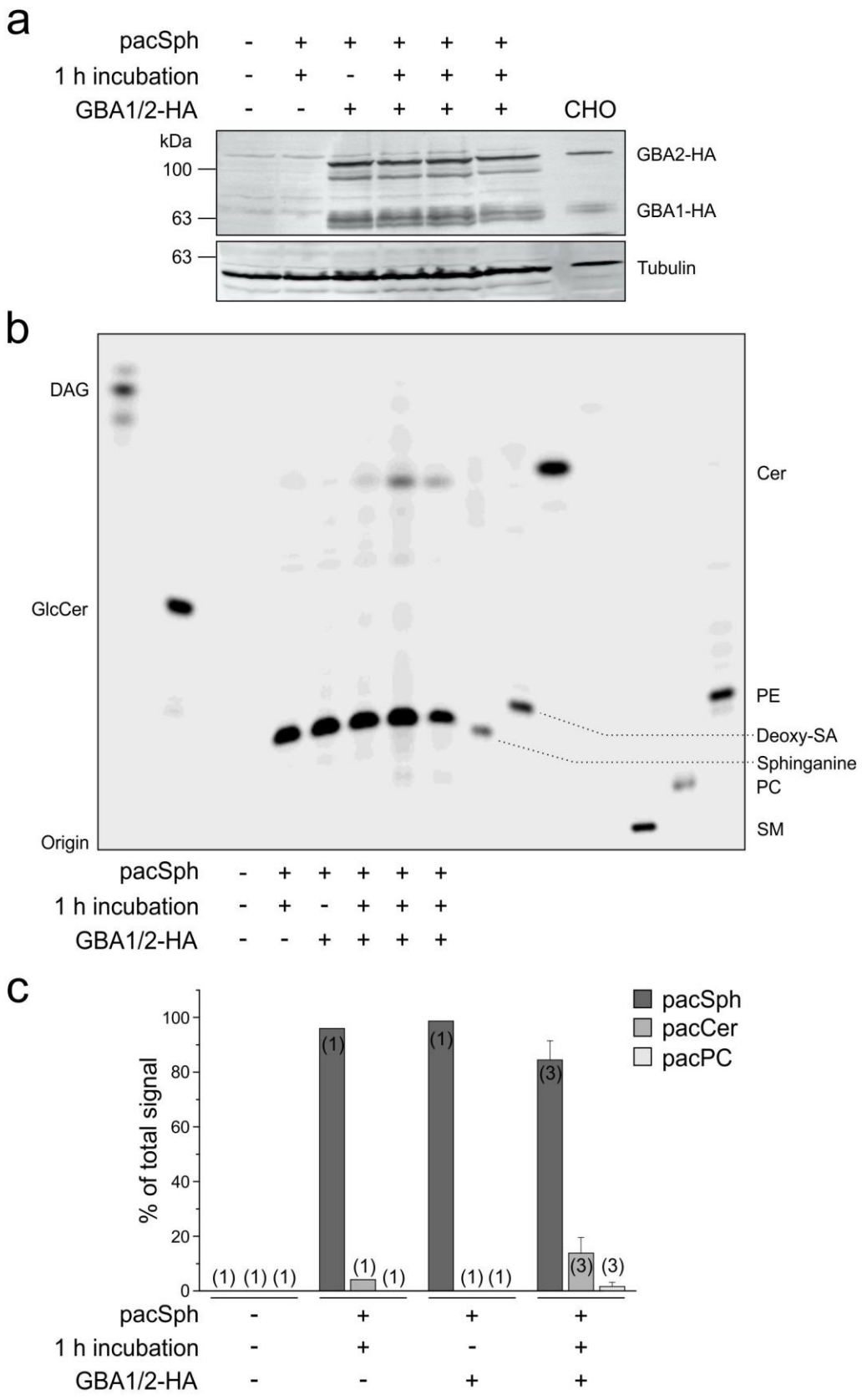

Figure 86: Analysis of pacSph in protein lysates from delta SGPL1 HeLa cells transiently expressing mGBA1-HA and mGBA2-HA. Delta SGPL1 HeLa cells transiently expressing mGBA1-HA and mGBA2-HA were lysed and incubated with 6 µM pacSph for 1 h. **(a)** Western blot analysis using an

anti-HA specific antibody to detect GBA1 and GBA2 (Kremmer). Beta-tubulin was used as a loading control. **(b)** Lipids extracted from the cells were clicked to 3-azido-7-hydroxycoumarin and analysed by TLC at 404 nm. PacSph was partially metabolised to pacCer and pacPC. **(c)** Quantification of **(b)** expressed as % of total signal intensity. DAG: Diacylglycerol, GlcCer: Glucosylceramide, Cer: Ceramide, PE: Phosphatidylethanolamine, Deox-SA: Deoxysphinganine, PC: Phosphatidylcholine, SM: Sphingomyelin, pacSph: photoactivatable and clickable sphingosine. Data are presented as mean + SD. N numbers are indicated in brackets.

3.16 Sphingosine – a “bioactive lipid”

My results demonstrate that sphingosine binds to GBA2. However, sphingosine is also a “bioactive lipid” (Contreras et al., 2012). It either exerts its effect by directly binding to a protein and/or it indirectly changes the properties of cell membranes and, thereby, protein function. Sphingosine is a surface active agent (surfactant), which attains its function due to its amphipathic structure: The head group carries an amide and two hydroxyl groups, which represent the hydrophilic part, while the carbon tail is highly hydrophobic. Thus, sphingosine forms micelles above a critical micelle concentration (cmc) of 18 µM (Slavik, 1982). GBA2 activity is diminished in presence of detergents like Triton X-100 or sodium taurocholate (Körschen et al., 2013). Detergents solubilise membrane proteins by mimicking the lipid bilayer environment, but also severely change the properties of membranes themselves (le Maire et al., 2000). Their amphipathic nature enables them to incorporate into the lipid bilayer and, at concentrations around or greater than the cmc, to produce protein-detergent complexes as well as mixed micelles, consisting of detergent molecules and membrane lipids (le Maire et al., 2000). Why GBA2 activity is lost in presence of detergents is not known. Three scenarios could be envisioned: i) detergents solubilise a GBA2-binding protein that is necessary for the activity of the enzyme, just as GBA1 needs saposin C to lift GlcCer from the luminal membrane of the lysosome to exert its activity (Alattia et al., 2006), or ii) detergents alter the membrane properties, e.g. the membrane curvature or integrity of distinct lipid platforms, preventing GBA2 from binding and sensing its substrate, or, finally, iii) detergents detach GBA2 from membranes.

3.16.1 Establishing an immunoprecipitation protocol for GBA2

Proteins interacting with GBA2 are not know. Thus, I set-out to first search for GBA2-binding proteins. The method-of-choice to study protein-protein interaction is co-immunoprecipitation, short co-IP (summarised in the Protein Interactions Handbook by

Thermo Fischer Scientific, 2010). Here, the protein of interest is isolated from a protein solution using a specific antibody that can be coupled to a matrix to “pull” the protein of interest out of the solution. Proteins strongly interacting with the protein of interest are isolated in a protein complex and can be identified by mass spectrometry.

The basis for the co-IP is a GBA2-specific antibody. In the past, we have generated nine different monoclonal rat antibodies against four different mGBA2 peptides (Figure 87 and Table 64) (Körschen et al., 2013). To immunoprecipitate GBA2 out of a protein solution, the anti-GBA2 antibody is coupled to a sepharose matrix. Sepharose (Separation-Pharmacia-Agarose) is the trade name for a cross-linked, beaded-form of agarose, a polysaccharide material extracted from seaweed (GE Healthcare). The link between the sepharose beads and the antibody is either protein A or G, two proteins that bind antibodies with high affinity (Bjorck&Kronvall, 1984). Both proteins bind to the IgG class of antibodies, but their binding properties differ among species and subclasses of IgG. Protein A prefers rabbit, pig, dog, and cat IgG, and protein G rather binds to human, mouse, and rat IgG. Thus, sepharose beads coupled to protein G were used (GE Healthcare).

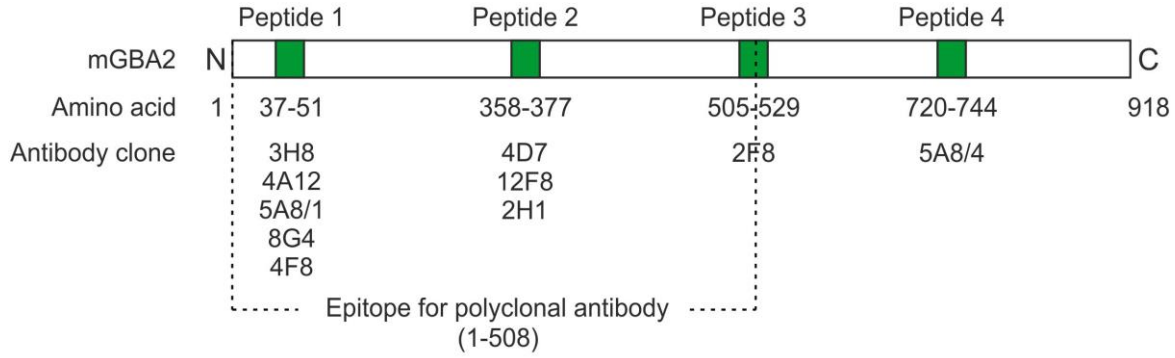

Figure 87: Topology of mouse GBA2. Monoclonal rat antibodies were generated against four different epitopes of mGBA2 (gray boxes, 1-4). Data published in Körschen et al. (Körschen et al., 2013). A polyclonal antibody against mGBA2 was produced in rabbit (Yildiz et al., 2006).

Table 64: Monoclonal rat antibodies generated against four different peptides of mGBA2. Data published in Körschen et al. (Körschen et al., 2013).

Name	Epitope/peptide	Clone	Species	Isotype
GBA2-1	1	3H8	Rat	IgG_{2b}
GBA2-1	1	4A12	Rat	IgG_{1}
GBA2-1	1	5A8/1	Rat	IgG_{2b}
GBA2-1	1	8G4	Rat	IgG_{2b}
GBA2-1	1	4F8	Rat	IgG_{2c}
GBA2-2	2	4D7	Rat	IgG_{2c}
GBA2-2	2	12F8	Rat	IgG_{2c}
GBA2-2	2	2H1	Rat	IgG_{2a}
GBA2-3	3	2F8	Rat	IgG_{2b}
GBA2-4	4	5A8/4	Rat	IgG_{2b}

In a first step, I tested, which of the aforementioned antibodies is the most specific one and shows the least cross reactivity to other proteins (Figure 88). Our monoclonal anti-GBA2 antibodies are produced from hybridoma cells that are cell fusions of myeloma cells and B cells from rat spleen (Kohler&Milstein, 1975). There are five different antibody isotypes known, of which IgG is the most common one released by B cells. IgG can be further divided into four subclasses named IgG_1, IgG_2, IgG_3, and IgG_4, named in order of abundance in human serum with IgG_1 being most abundant (Schur, 1988). The four different subclasses differ in molecular mass, the amino acids present in the hinge region, and their antibody response to e.g. proteins or polysaccharides (Vidarsson et al., 2014).

I tested all monoclonal rat antibodies besides 4A12, which had already been tested in a co-IP protocol, but failed in the quality control (Dr. D. N. Raju, unpublished data) and 4F8, which does not detect GBA2 (unpublished data). Clones 8G4, 2H1, 2F8, and

5A8/4 were tested in a Western blot using hypotonic brain and testis lysates from control and GBA2-deficient mice (upper panel, Figure 88). As shown in Figure 88, all tested antibodies displayed a band slightly above the predicted molecular weight of 103 kDa (NP_766280.2) in control samples, but not in samples from GBA2-deficient mice. Clone 8G4 showed additional, non–specific bands in control and GBA2-deficient samples at around 65 kDa and overall gave the highest background (upper panel, Figure 88). GBA2 detection by antibody clone 2H1 was very weak in both tested organs and there were non-specific bands in both, control and GBA2-deficient brains at around 180 kDa. Clones 2F8 and 5A8/4 both showed some background in either brain or testis samples but overall, 2F8 gave very little background, but strong GBA2 band signals. Clones 3H8, 5A8/1, 4D7, and 12F8 were tested in a Western blot using hypotonic brain lysates from control and GBA2-deficient mice (lower panel, Figure 88). Clone 3H8 showed nice bands in the control sample without any signal in the GBA2-deficient sample, but unfortunately predominant bands at around 50 kDa in lysates from both genotypes were observed (lower panel, Figure 88). This result was quite similar to clone 5A8/1, but the non-specific signal at 50 kDa was less pronounced (lower panel, Figure 88). Clones 4D7 and 12F8, however, did not label any protein (lower panel, Figure 88). Unfortunately, those antibodies with IgG subclasses that strongly bind to protein G ($IgG2_a$: clone 2H1, $IgG2_c$: clones 4F8, 4D7 and 12F8) did not or only poorly detect GBA2 in control brain lysates (Figure 88). Thus, I chose clone 2F8 for the experiment, even though protein G binding to IgG_{2b} rat antibodies is supposed to be rather weak (Table 64 and Figure 88).

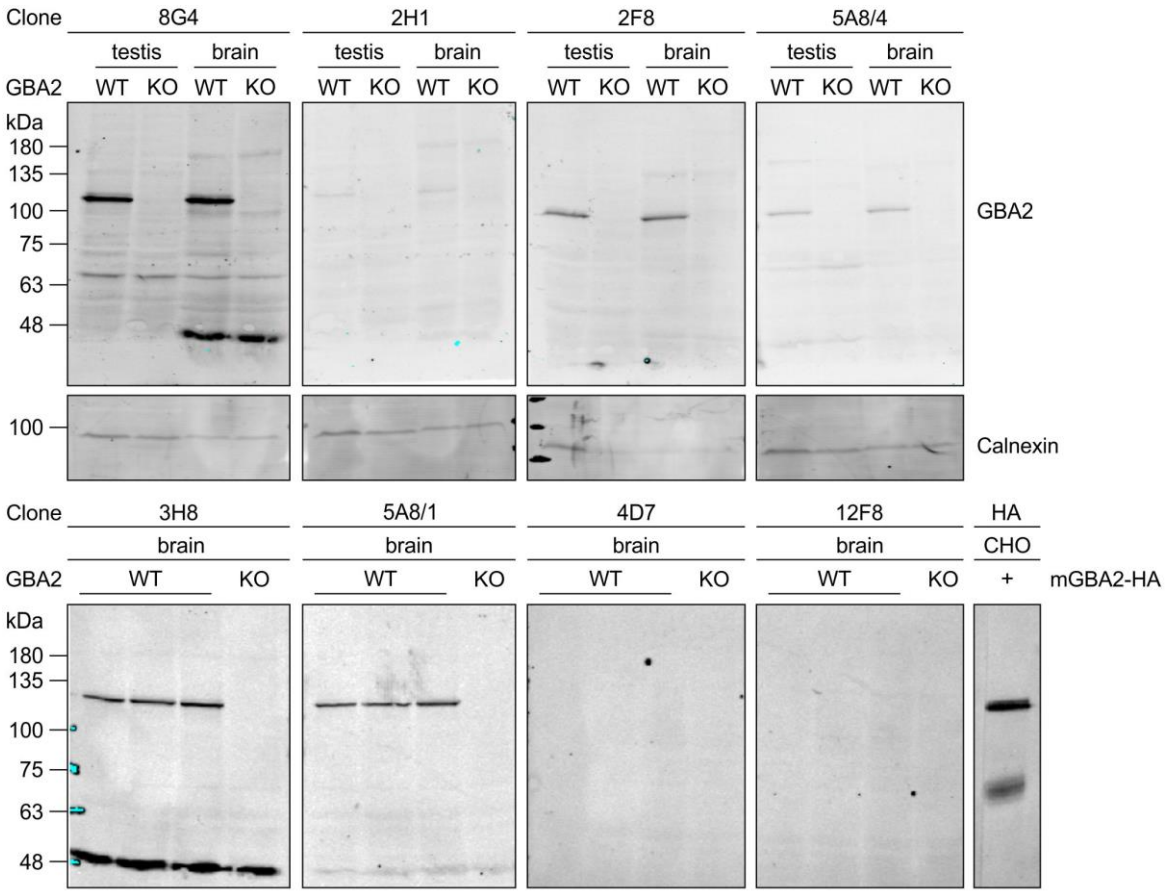

Figure 88: Test of monoclonal rat antibodies against mGBA2. Monoclonal antibodies summarised in Table 1 were tested for their specificity against mGBA2 in hypotonic brain and testis lysates from control and GBA2-deficient mice. A CHO cell lysate expressing mGBA1 and mGBA2 was used as positive control. WT: wild-type, KO: knockout.

Next, anti-GBA2 antibody clone 2F8 was coupled to protein G sepharose and the efficiency of coupling was validated by Western blot analysis using a fluorescently-labelled secondary anti-rat antibody (Figure 89). Figure 89 shows that less antibody was present in the supernatant after binding, demonstrating that some antibody had bound to the protein G coupled beads (2F8 antibody before and after, Figure 89). However, some antibody was lost during the following washing steps (W, Figure 89) and buffer exchange (ExB, exchange to boric acid, Figure 89), but after cross-linking the antibody to protein G via dimethylpimelimidate, there were no antibody signals detectable anymore on the Western blot, showing that the remaining antibody on the column was cross-linked (X, Figure 89). In a final step after exchanging the buffer to ethanolamine (ExE, Figure 89) and then to PBS (ExP, Figure 89), the column material was boiled to detect the antibody that is bound to the column. Indeed, antibody was

present, demonstrating that the 2F8 antibody was successfully cross-linked to the column (B, Figure 89, “2F8 column”).

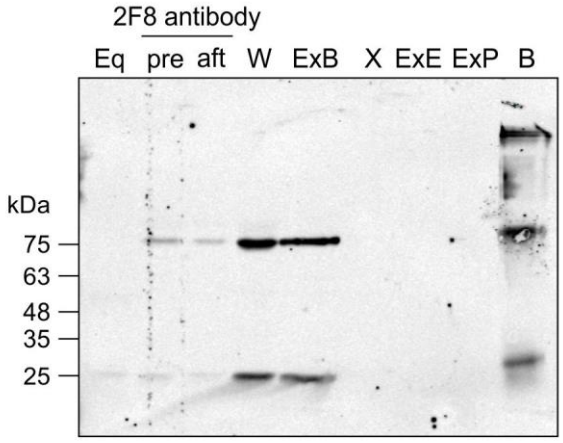

Figure 89: Coupling of monoclonal antibody clone 2F8 to protein G sepharose. Antibody clone 2F8 was coupled to protein G sepharose by covalently cross-linking the antibody with the column material via demithylpimelimidate. After the cross-linking step, no antibody was washed off from the column; only when beads were boiled, the antibody was eluted. Eq: Equilibration step, pre: Previous, aft: After, W: Wash, ExB: Buffer exchange to boric acid, X: Cross-linking, ExE: Buffer exchange to ethanolamine, ExP: Buffer exchange to PBS, B: Beads, kDa: Kilo Dalton.

The antibody to detect GBA2 after immunoprecipitation on the Western blot (“detection antibody”) needs to be preferably produced in a different animal species to avoid labelling of the heavy and light antibody chains of the 2F8 antibody used for immunoprecipitation. First, an anti-HA antibody produced in mouse (Sigma) was tested for detection on Western blot using lysates from control and mGBA2-HA over-expressing CHO cells (#G4A11) (Dilution: Left: 1:5,000, right: 1:10,000, Figure 90). Unfortunately, the signals obtained from this antibody were very weak and also showed some non-specific background in the control cells (Figure 90).

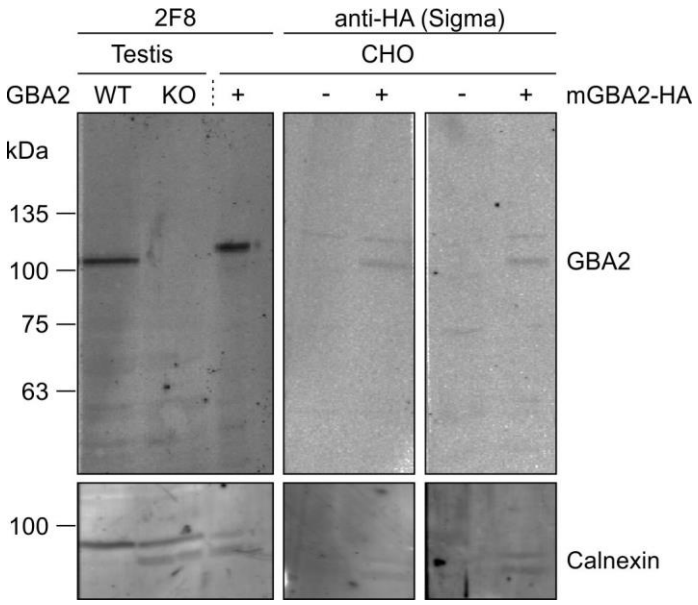

Figure 90: Detection of GBA2 via an anti-HA antibody from mouse. Lysates from CHO control cells and cell stably over-expressing mGBA2 (15 µg/sample) and testis lysates from control and GBA2-deficient mice (50 µg/sample) analysed by Western blot and the monoclonal rat antibody clone 2F8 (left) or an anti-HA antibody produced in mouse (Sigma, dilution on the left: 1:5,000, dilution on the right: 1:10,000). Calnexin was used as loading control. Only very faint signals were detected using the anti-HA antibody. WT: wild-type, KO: knockout, kDa: Kilo Dalton.

I then tested a polyclonal anti-GBA2 antibody that was produced in rabbit (Yildiz et al., 2006) on lysates from CHO control cells and different protein amounts of cells over-expressing mGBA2-HA as well as on testis lysates from control and GBA2-deficient mice (Figure 91). The polyclonal anti-GBA2 antibody gave very nice signals in both, CHO cells and testis lysates without showing any signal in the GBA2-deficient sample (Figure 91).

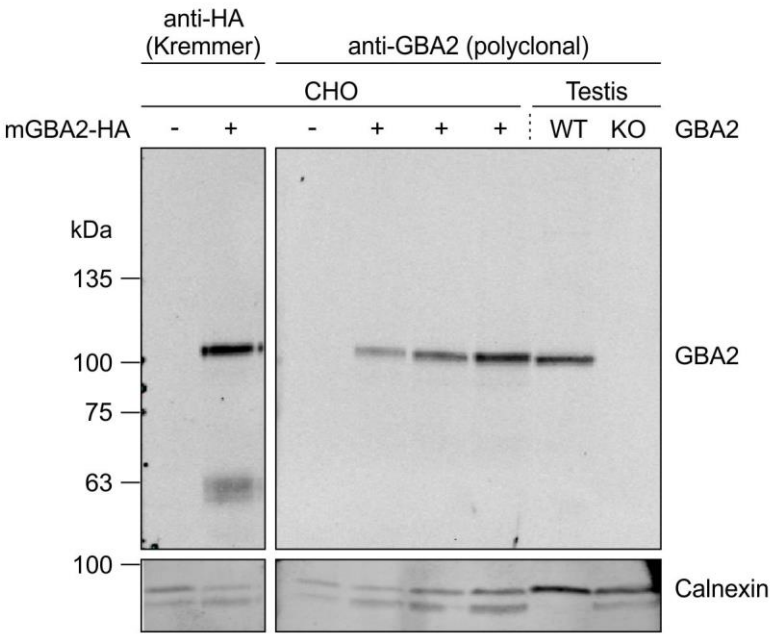

Figure 91: Detection of GBA2 via a polyclonal anti-GBA2 antibody from rabbit. Lysates from CHO control cells and cell stably over-expressing mGBA2 (15 – 50 µg/sample) and testis lysates from control and GBA2-deficient mice (50 µg/sample) analysed by Western blot using and the anti-HA antibody from rat (left, Kremmer) or a polyclonal antibody produced in rabbit (Yildiz et al., 2006). Calnexin was used as loading control. The polyclonal anti-GBA2 antibody showed a clear staining in both, CHO cells and testis lysates, while not showing any signal in the GBA2-deficient sample. WT: wild-type, KO: knockout, kDa: Kilo Dalton.

I started to establish the co-IP protocol using hypotonic lysates of CHO cells stably over-expressing mGBA2-HA (#G4A11) (Figure 92a). First, the protein lysate was incubated with protein G sepharose beads without the 2F8 antibody to remove proteins that non-specifically bind to the column material (Pre clearing step, Figure 92b). The pre-cleared protein lysate was then incubated with the 2F8 column material to allow antibody-GBA2 binding. On the next day, the non-bound proteins were collected (Flow-through, Figure 92b) and the column was washed five times (Washes, Figure 92b) before proteins were eluted by adding SDS (E, Figure 92b). Likewise, proteins that had non-specifically bound to the empty column material (Pre-clearing step) were also eluted by SDS. The samples were analysed by Western blot using the polyclonal anti-GBA2 antibody (Yildiz et al., 2006) (Figure 92b), which nicely labelled a band in protein lysates from CHO cells over-expressing mGBA2-HA (Figure 92b). There was no non-specific binding to the protein G sepharose (Pre-clearing fraction, Figure 92b) but, unfortunately, GBA2 also did not bind to the 2F8 column (E, Figure 92b). Thus, almost all proteins from the input were recovered in the flow-through fraction (FT, Figure 92b).

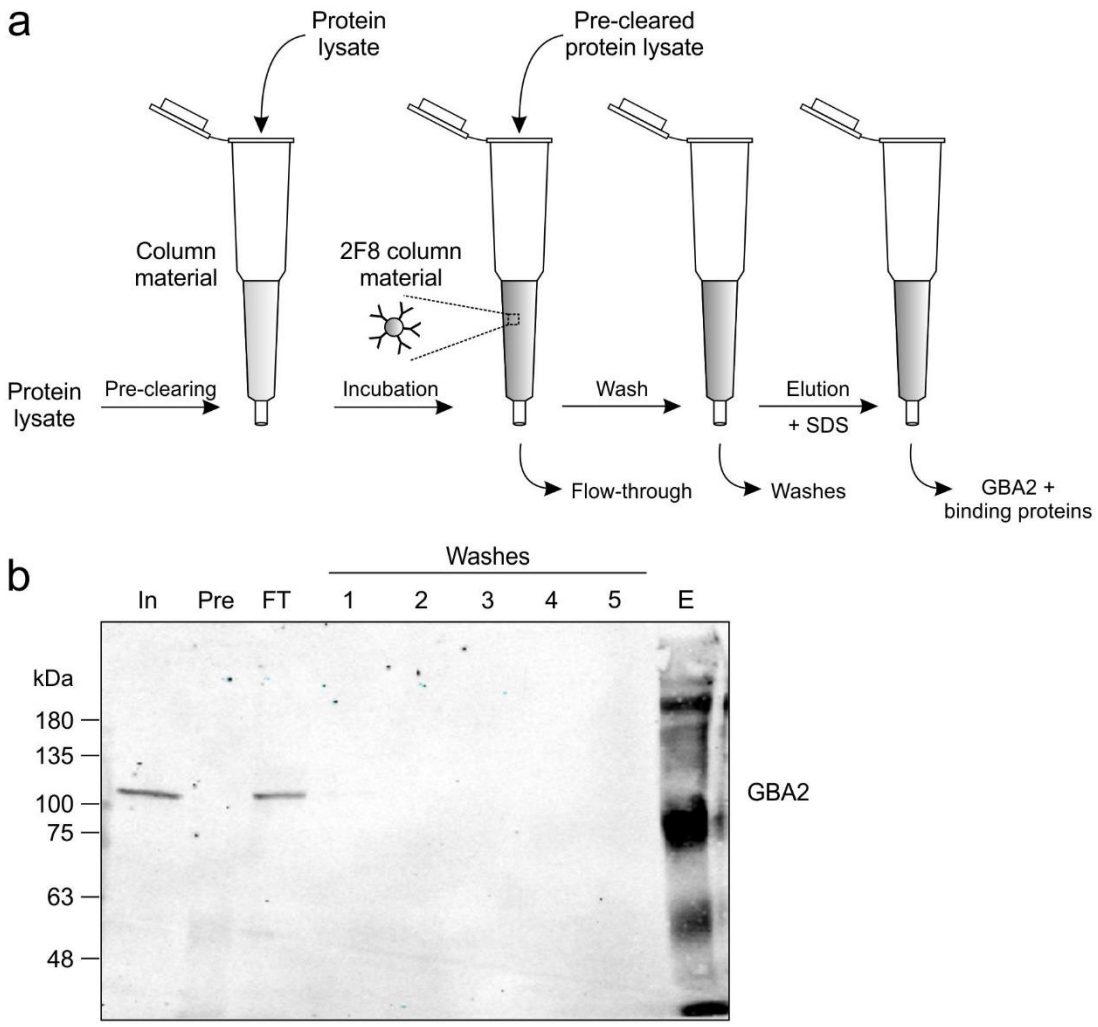

Figure 92: Immunoprecipitation of GBA2 in lysates from CHO cells stably over-expressing mGBA2 via anti-GBA2 antibody clone 2F8. Protein G sepharose beads covalently linked to monoclonal antibody clone 2F8 were incubated with hypotonic lysates of CHO cells stably over-expressing mGBA2. Protein samples were subjected to Western blot analysis using a polyclonal antibody from rabbit against GBA2 (Yildiz et al., 2006). **(a)** Flow-chart of the experiment. **(b)** The anti-GBA2 antibody showed that GBA2 did not bind to the column and was fully recovered in the flow-through. There was no GBA2 band visible in the elution fraction. In: Input, Pre: Pre-incubation, FT: Flow-through, E: Elution.

To test whether presence of a detergent would favour specific binding of mGBA2-HA to 2F8, the same approach was repeated with total cell lysates (containing 1% Triton X-100) from CHO cells over-expressing mGBA2-HA (#G4A11) (Figure 93). Again, mGBA2-HA was still present in the column flow-through (FT, Figure 93), but the signal was weaker compared to the input (In, Figure 93), indicating that some GBA2 protein had bound to the column.

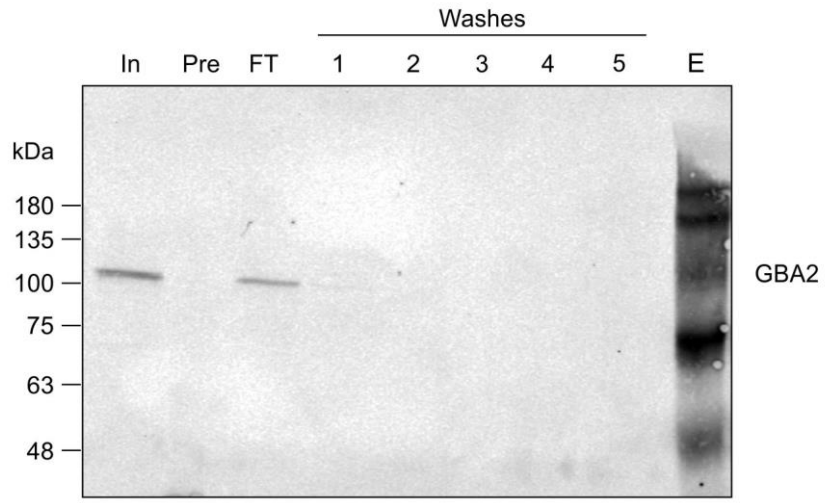

Figure 93: Immunoprecipitation of GBA2 from total protein lysates of CHO cells stably over-expressing mGBA2 via anti-GBA2 antibody clone 2F8. Protein G sepharose beads covalently linked to monoclonal antibody clone 2F8 were incubated with total lysates from CHO cells stably over-expressing mGBA2 containing Triton X-100 according to the text. Protein samples were subjected to Western blot analysis using a polyclonal antibody from rabbit against GBA2 (Yildiz et al., 2006). The anti-GBA2 antibody showed that GBA2 did not bind to the column even in presence of a detergent and was fully recovered in the flow-through. There was no GBA2 band visible in the elution fraction. In: Input, Pre: Pre-incubation, FT: Flow-through, E: Elution.

Unfortunately, the elution fraction in both trials (Figure 92b and Figure 93) showed a high background staining that is probably due to cross-reactivity of the anti-rabbit secondary antibody with the 2F8 rat antibody being eluted from the column. To experimentally verify the cross-reactivity of the antibody, I ran pure 2F8 anti-GBA2 rat antibody on a SDS-PAGE, performed a Western blot, and incubated the blots with anti-rabbit or anti-rat secondary antibodies, respectively (Figure 94). While the anti-rat antibody labelled the 2F8 antibody in a dose-dependent manner, the anti-rabbit antibody did not show any staining, meaning that the background on the previous Western blots was not due to cross-reactivity of the secondary antibody (Figure 94).

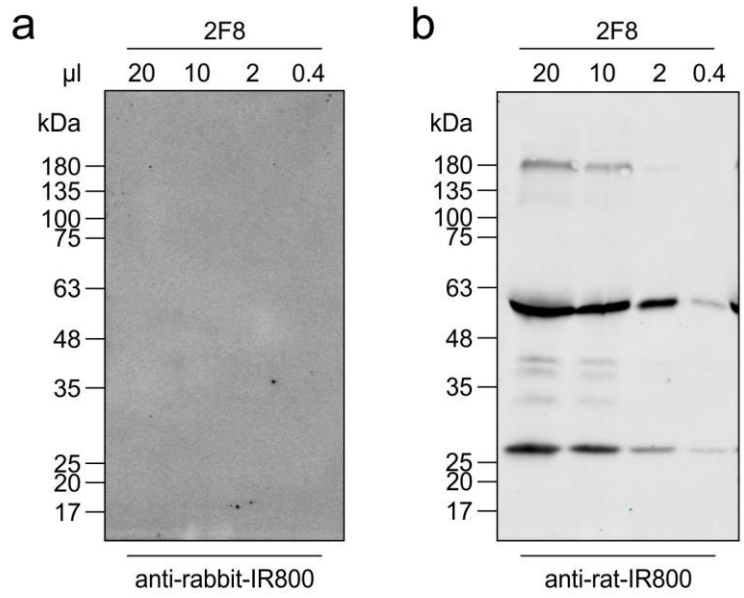

Figure 94: Analysis of the cross-reactivity of the anti-rabbit-IR800 secondary antibody. Western blot analysis of 0.4 – 20 µl pure clone 2F8 anti-GBA2 rat antibody and immunostaining with an anti-rabbit or anti-rat secondary antibody. **(a)** The anti-rabbit secondary antibody did not recognise the 2F8 antibody from rat, whereas **(b)** the anti-rat antibody labelled the 2F8 antibody in a dose-dependent manner. kDa: Kilo Dalton.

To further test, where the strong background came from, I boiled and loaded pure protein G sepharose, the 2F8 column material, and an old elution fraction for comparison on a SDS gel, performed a Western blot, and incubated the blot with the polyclonal anti-GBA2 rabbit antibody (Figure 95). Here, the antibody did not show any non-specific binding to the pure column material, whereas the background bands appeared in the 2F8 column material, showing that the primary, polyclonal anti-GBA2 antibody itself was responsible for the background signal (Figure 95). Thus, the combination of antibodies used so far did not allow to establish a GBA2 co-IP protocol.

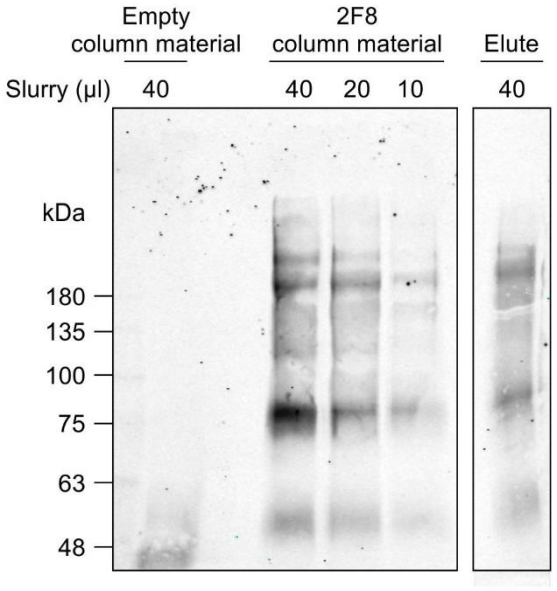

Figure 95: Analysis of the cross-reactivity of the polyclonal anti-GBA2 rabbit antibody. Western blot analysis of pure 40 µl pure column material, 10 – 40 µl 2F8 column material, and an old elution fraction from 2F8 column material after boiling and immunostaining with the polyclonal anti-GBA2 antibody from rabbit. The antibody did not bind non-specifically to the pure column material, whereas the background bands appeared in the 2F8 column material, showing that the primary, polyclonal anti-GBA2 antibody itself was responsible for the background signal. kDa: Kilo Dalton.

In a final approach, the co-IP strategy was changed as follows: protein G has high affinity for all mouse-derived antibodies; thus, the bead matrix was first coupled to an anti-rat-IgG_{2b} antibody produced in mouse (green antibody in schematic, Figure 96a). Next, the monoclonal anti-GBA2 2F8 antibody from rat was bound to the column material via its interaction with the anti-rat-IgG_{2b} antibody (black antibody in schematic, Figure 96a). The column was then incubated with a total brain lysate (NP-40/Igepal) from a control mouse overnight at 4 °C following the normal protocol (Figure 96). After performing an SDS-PAGE and Western blot, GBA2 was detected with the 2F8 antibody, but three different HRP-coupled anti-rat secondary antibodies (Green: mouse-anti-rt-IgG2b, blue: goat-anti-rat-IgG, orange: mouse-anti-rat-kappa) to test, which secondary antibody shows the least background (Figure 96b-d). All three secondary anti-rat antibodies detected the heavy chains from the 2F8 column antibody in the elution fraction, with the anti-rt-IgG2b antibody showing the least background, but also no strong GBA2 band in the input lane (Figure 96b). The anti-rat-IgG_{2b} antibody showed a very faint signal in the elution fractions, which could be at the same height as the input band. The anti-rat-IgG antibody clearly showed a GBA2 band in the input lane, but no signal at the same height in the elution fraction (Figure 96c). Lastly,

the anti-rat-kappa antibody gave the best result, while also detecting the heavy and light chain complexes of the column antibody (clone 2F8). However, there were bands visible in the elution fractions at the height of the mGBA2, indicating that this approach is suitable to immunoprecipitate GBA2 (Figure 96d).

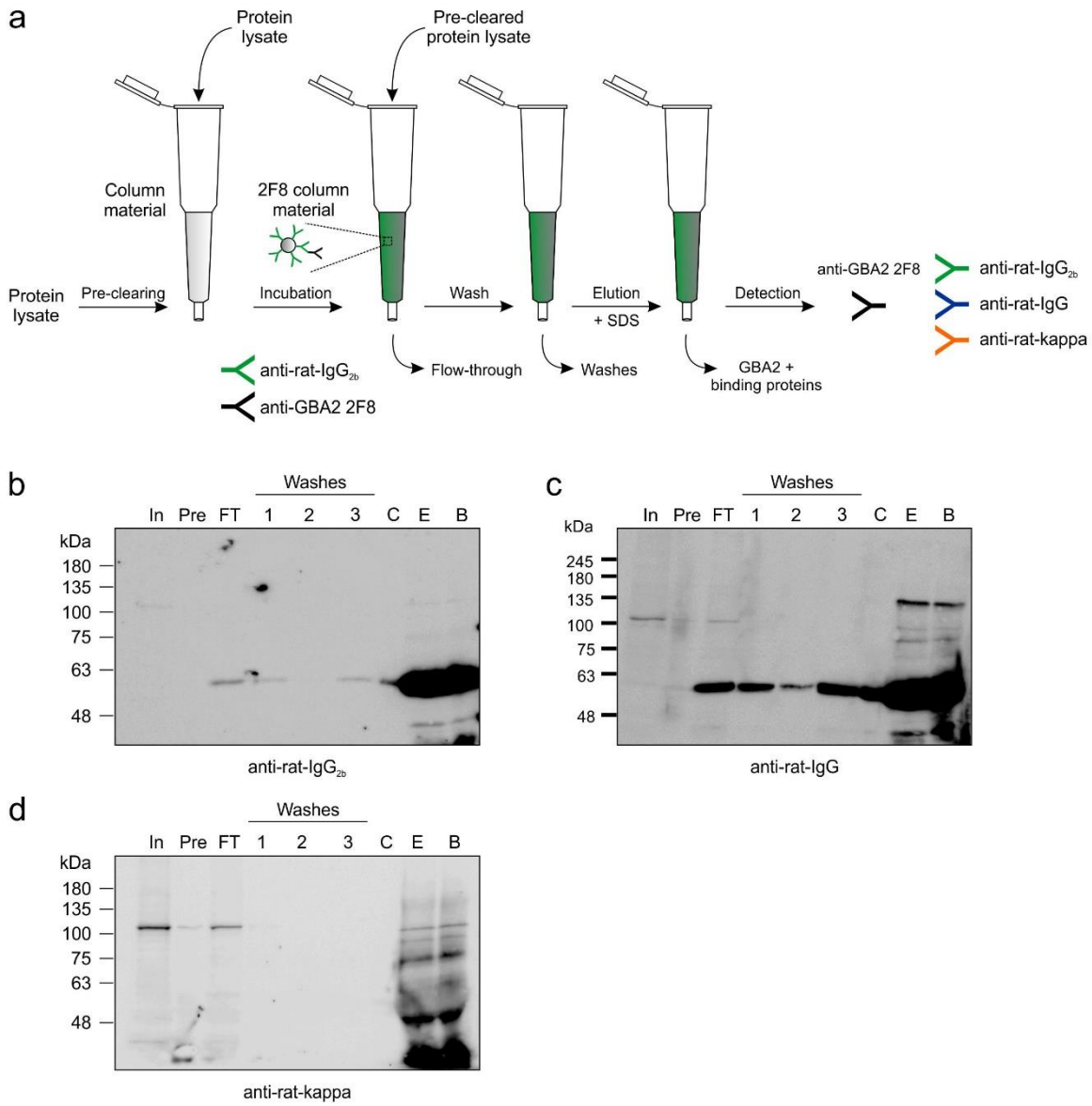

Figure 96: Immunoprecipitation of GBA2 using the same "column" and "detection" antibody. Incubation of a total brain lysate with protein G sepharose coupled to an anti-rat antibody produced in mouse and bound to the anti-GBA2 antibody clone 2F8 from rat. All fractions were analysed by Western blot using the GBA2-specific antibody clone 2F8. **(a)** Flow-chart of the experiment. **(b)** Decoration of antibody clone 2F8 with an HRP-coupled anti-rat-IgG2b secondary antibody. There were faint bands at around 120 kDa visible in the elution fraction. **(c)** Same as **(b)** using an anti-rat-IgG HRP-coupled secondary antibody. There was no GBA2 band visible in the elution. **(d)** As for **(b)** using an anti-rat-kappa HRP-coupled secondary antibody. This antibody gave the clearest result with bands in the elution

fractions at around 120 kDa. In: Input, Pre: Pre-incubation, FT: Flow-through, C: Boiled column without protein lysate, E: Elution, B: Boiled beads, kDa: Kilo Dalton.

To test whether these bands were indeed GBA2, the same approach was repeated using total brain lysates (NP-40/Igepal) from wild-type and GBA2-deficient mice (Figure 97). Although the detection of GBA2 worked in the input of the control, the results of the previous experiment could not be reproduced (Figure 97). Furthermore, there was a very faint band visible in the input and flow-through fraction of the GBA2-deficient sample, suggesting that the animal was rather a heterozygous or wild-type animal or that there was non-specific binding of the antibody to a protein of a similar size, which would be due to a general detection problem using these antibodies (arrows, Figure 97b). Due to time limitations, the experiment was not further optimised. Thus, it is not clear yet whether a GBA2-binding protein is solubilised in presence of sphingosine, which would explain the reduction of GBA2 activity in presence of sphingoid bases.

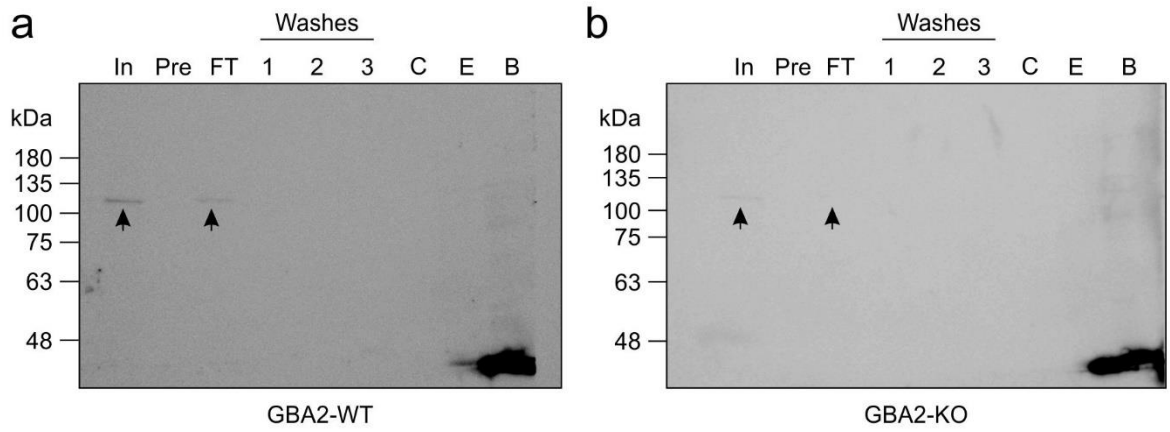

Figure 97: Immunoprecipitation of GBA2 from total brain lysates from control and GBA2-deficient mice via anti-GBA2 antibody clone 2F8. Total brain lysates containing NP-40 were incubated with the 2F8 column material and processed as previously mentioned. Western blot analysis and immunostaining using the anti-GBA2 antibody clone 2F8 and the HRP-coupled secondary anti-rat-kappa antibody to test the presence of GBA2 in **(a)** control and **(b)** GBA2-deficient brain lysates. **(a)** There were signals of different intensities visible in the input and flow-through fraction of the control sample, suggesting that some GBA2 had bound to the column. **(b)** There was also a very faint band visible in the input and flow-through fraction of the GBA2-deficient sample, suggesting that this animal was rather heterozygous. In both samples, no GBA2 bands was detectable in the elution fraction. In: Input, Pre: Pre-incubation, FT: Flow-through, C: Boiled column without protein lysate, E: Elution, B: Boiled beads, kDa: Kilo Dalton.

3.16.2 Recovery of GBA2 activity is similar at membranes derived from control and GBA1-deficient cells

As previously stated, surfactants like sphingosine alter the membrane properties, e.g. by changing the membrane curvature or by modifying the composition of distinct lipid platforms, preventing GBA2 from binding and sensing its substrate (Contreras et al., 2006). We have shown that the membrane surrounding is crucial for the activity of GBA2 (Körschen et al., 2013). When separating a protein lysate into a membrane and soluble fraction, GBA2 was partially recovered in the supernatant. However, GBA2 activity was barely detectable in the supernatant. In Körschen et al., we demonstrated that addition of membranes from GBA2-deficient brain “rescued” the GBA2 activity in the soluble fraction, underlining the importance of membranes for the activity of GBA2 (Körschen et al., 2013). Thus, I wondered whether a local increase of sphingosine in GBA1-deficient cells could alter the membrane properties and in turn, diminish GBA2 activity at the membrane.

To test this hypothesis, the recovery of GBA2 activity in supernatants from HEK293 cells stably over-expressing mGBA2 was analysed by adding membranes from control, GBA1-deficient, or GBA2-deficient HAP1 cells (Figure 98). HEK293 cells stably over-expressing mGBA2 were lysed and proteins were separated into a soluble and membrane fraction by ultracentrifugation. I followed the distribution of mGBA2 after ultracentrifugation by Western blot analysis: GBA2 was detected in both, the membrane and the soluble fraction (Figure 98a). The GBA2 activity measured in both fractions did not sum up to the total input activity, underlining that GBA2 activity is lost in absence of membranes (Figure 98b). Next, membranes from either control, GBA1-deficient, or GBA2-deficient HAP1 cells were added in equal amounts to the supernatant of HEK293 cells stably over-expressing mGBA2 (Figure 98c). Of note, the endogenous GBA2 activity in HAP1 cells was negligible compared to over-expressed mGBA2 in the HEK293 cell supernatants. Addition of membranes slightly boosted the GBA2 activity from 19% (HEK293 supernatant only) to 29-30% (Figure 98c). There was no difference in activity between membranes from control, GBA1-deficient, or GBA2-deficient HAP1 cells, showing that GBA2 seems to exhibit equal activity at both, control and GBA1-deficient membranes (Figure 98c).

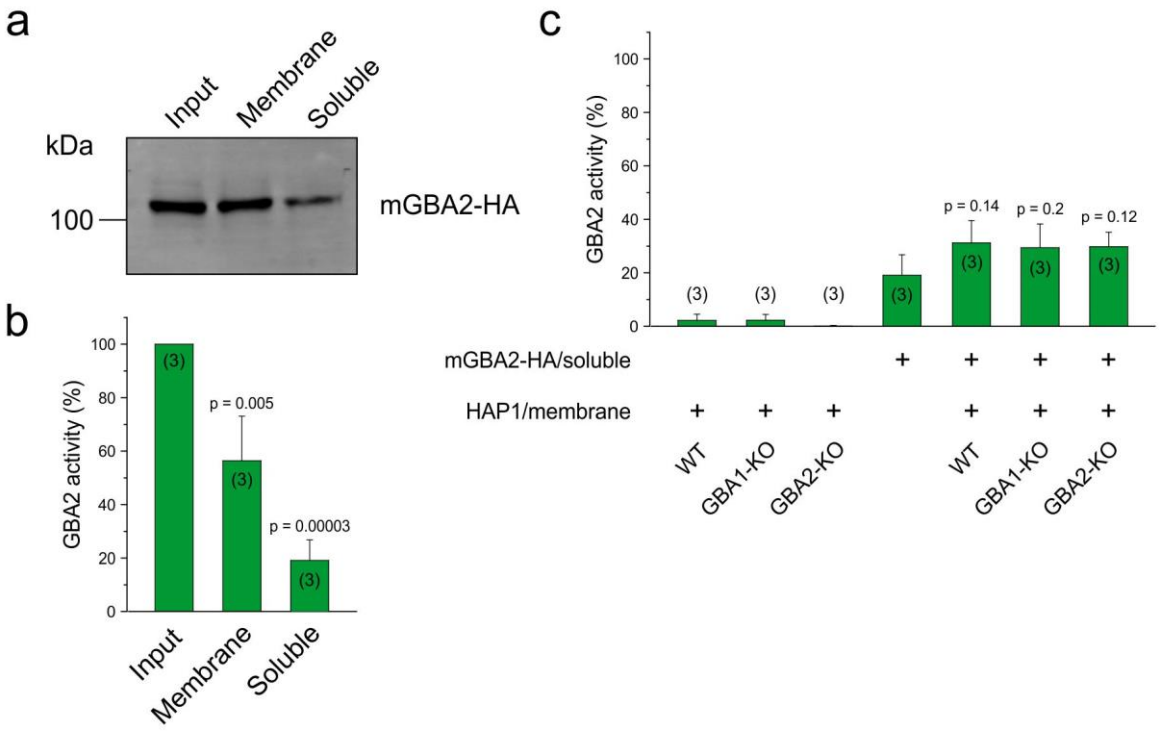

Figure 98: GBA2 activity in the absence or presence of membranes. HEK293 cell lysates stably over-expressing mGBA2 were subjected to ultracentrifugation to separate soluble GBA2 from membrane-associated GBA2. The distribution of GBA2 was analysed by Western blot using an anti-HA antibody (Kremmer). GBA2 activity was assayed in hypotonic lysates in presence of 1.67 mM 4-MUG. **(a)** GBA2 was found in both, the membrane fraction and the soluble fraction after ultracentrifugation. **(b)** GBA2 is less active in the absence of membranes. **(c)** To recover GBA2 activity, membrane fractions from HAP1 control cells and cells deficient for either GBA1 or GBA2 were added. All three HAP1 cell lines possessed very low endogenous GBA2 activity. Addition of membrane fractions resulted in an equal increase in GBA2 activity from 19% to 29-30%. 4-MUG: 4-Methylumbelliferyl beta-D-glucopyranoside. Data are presented as mean + SD. N numbers are indicated in brackets. P values were determined using Student's t-test **(b)** and One-way ANOVA **(c)**.

3.16.3 GBA2 is sensitive to lipids with detergent-like properties

Besides being a membrane lipid, sphingosine also possesses sufficient aqueous solubility to move between membranes (Hannun&Obeid, 2008). Thus, Khan et al. have estimated that around 70% of intracellular sphingosine resides in membranes at physiological pH, whereas the remaining 30% are soluble (Khan et al., 1991). Higher cytoplasmic levels of sphingosine might not only incorporate into adjacent membranes and change its local properties, but could also be present in solution. As previously mentioned, Slavik and co-workers showed that sphingosine forms micelles above a cmc of 18 µM (Slavik, 1982). This concentration is very similar to the IC_{50} of 25.04 ±

0.2 µM of sphingosine inhibition of GBA2 in GBA2-expressing bacteria lysates (see Figure 52). As the effect that I saw was reversible (Figure 58) and non-competitive (see Figure 59 and Figure 60), I wondered whether the inhibition of GBA2 activity upon addition of sphingosine might be due to a detergent-like effect of sphingosine. Thus, sphingosine could also exert its surfactant activity by forming detergent-protein complexes with soluble GBA2 itself and, thereby, preventing it from being active at a membrane.

To test this hypothesis, I searched for an amphipathic lipid that exerts similar surfactant properties as sphingosine, but is not involved in glycosphingolipid metabolism. C16 carnitine (palmitoylcarnitine, 3-(palmitoyloxy)-4-(trimethylammonio) butanoate) is present in all animal species, many microorganisms, and also in some plants, and is required during fatty acid oxidation in mitochondria (Bremer, 1983; Fritz, 1955). To test whether the activity of GBA2 is also sensitive to a sphingosine-like molecule with a similar cmc, I analysed the effect of C16 carnitine on GBA2 activity in bacterial lysates (Figure 99). C16 carnitine is a long-chain fatty acyl ester with a cmc of 10 µM (Goni et al., 1996). Adams and co-workers have shown that this structural sphingosine analogue initiates changes in the structure and function of the cardiac sarcoplasmic reticulum and the sarcolemmal Na^+-K^+-ATPase, while functioning as a “natural occurring detergent” (Adams et al., 1979). Echabe et al. showed that C16 carnitine induced alterations in membrane fluidity of erythrocytes (Echabe et al., 1995). Requero and co-workers showed that C16 carnitine that is added to a liposome suspension becomes almost completely membrane-bound, while the concentration of free C16 carnitine approaches the cmc (Requero et al., 1995). When analysing the GBA2 activity in the presence of C16 carnitine, a dose-dependent inhibition of GBA2 activity with an IC_{50} of 31.31 ± 2.68 µM was determined (Figure 99). Thus, C16 carnitine as a surfactant might form protein-detergent complexes with GBA2 and, thereby, hinders it from being active at the membrane. Of note, as previously seen for sphingosine/sphinganine and GBA1 (compare Figure 52, Figure 53, and Figure 61), C16 carnitine did not evoke a full block of GBA2 activity even at high concentrations (Figure 99). Because of its lipid properties, C16 carnitine (and sphingosine, sphinganine) might cluster at higher concentrations and, therefore, loses its effect on GBA2.

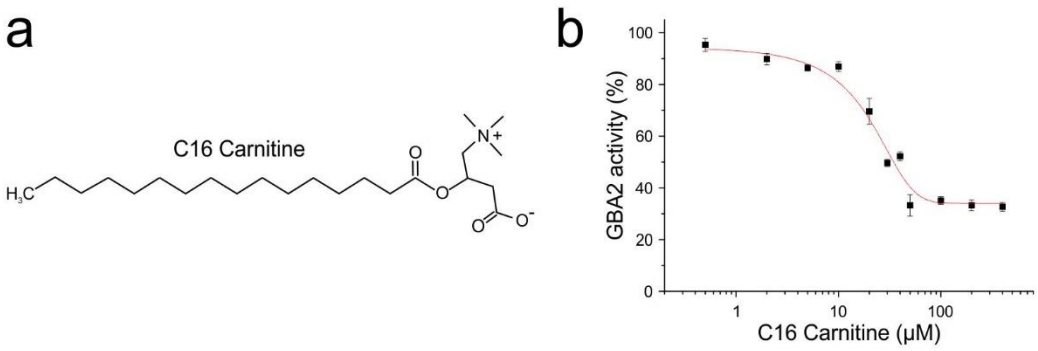

Figure 99: Dose-response relationship of GBA2 to C16 carnitine. Analysis of the GBA2 activity in bacterial lysates over-expressing mGBA2 in presence of a serial dilution of C16 carnitine and 1.67 mM 4-MUG at pH 6. Data were normalised to a non-treated control. **(a)** Structure of C16 carnitine. **(b)** The IC_{50} for C16 carnitine in bacterial lysates over-expressing mGBA2 was 31.31 ± 2.68 µM. Representative plot for n = 3 experiments, data are presented as mean of quadruples ± SD.

3.16.4 Detergent-like properties of lipids detach GBA2 from membranes

Previous experiments have shown that soluble GBA2 is equally active at membranes obtained from HAP1 control and GBA1-deficient cells, suggesting that there is no change in intra-membranous sphingosine levels or, if so, that this does not affect the activity of GBA2 (compare 3.16.2). As mentioned above, around 30% of sphingosine in the cell are soluble (Khan et al., 1991). Results from the dose-response analysis of GBA2 and C16 carnitine showed that lipids with similar chemical properties like sphingosine might form protein-lipid/detergent complexes, which could interfere with GBA2 finding/binding to its substrate at the membrane (compare 3.16.3). Thus, increased amounts of soluble sphingosine might detach GBA2 from the membrane in GBA1-deficient cells.

To test this hypothesis, wild-type and GBA1-deficient HAP1 cells transiently expressing mGBA2 were lysed and proteins were separated into a soluble and membrane fraction by ultracentrifugation (3.16.2). mGBA2 was detected in both, the membrane and the soluble fraction, whereas the mGBA2 signal was a bit stronger in the soluble fraction of the GBA1-deficient samples compared to the wild-type control (Figure 100a). I quantified the band signals, normalised the signals from the soluble fraction to the input fraction, and compared the ratios between samples with a wild-type and a GBA1-deficient background. Interestingly, there was significantly more mGBA2 present in the soluble fractions from GBA1-deficient cells compared to wild-type cells compared to the respective input. This means that less GBA2 is bound to

the membrane, resulting in less active GBA2 present in GBA1-deficient cells (Figure 100b). Of note, the input was similar in wild-type and GBA1-deficient samples (Figure 100c). These results suggest that increased amounts of (soluble) sphingosine in GBA1-deficient cells form reversible lipid-protein complexes with GBA2, which disables the binding of GBA2 to the membrane and, thereby, reduces its enzymatic activity.

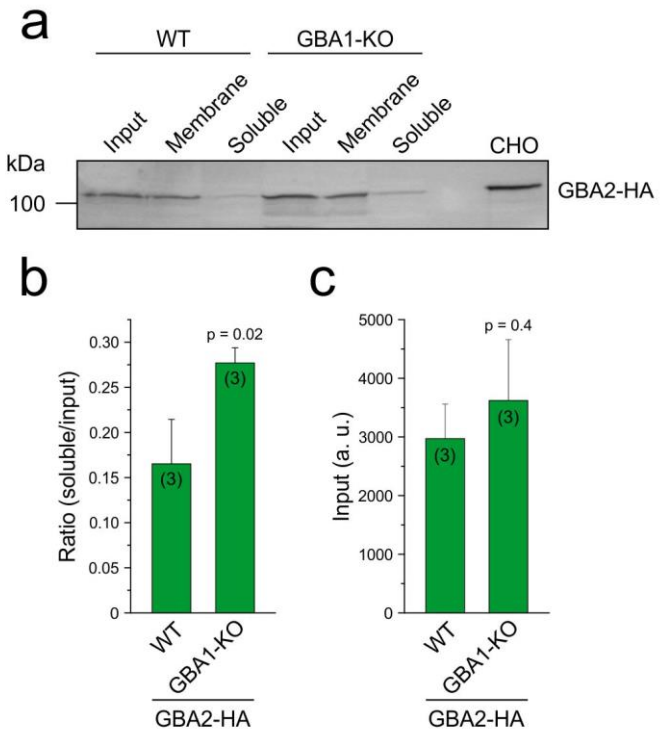

Figure 100: GBA2 membrane-association in HAP1 control and GBA1-deficient cells. HAP1 cell lysates transiently expressing mGBA2 were subjected to ultracentrifugation to separate soluble GBA2 from membrane-associated GBA2. The distribution of GBA2 was analysed by Western blot using an anti-HA antibody (Kremmer). CHO cells stably expressing mGBA2-HA were used as a positive control. **(a)** The GBA2 signal in the soluble fraction of the GBA1-deficient sample was slightly stronger than in the control sample. **(b)** Ratio of mGBA2 signals in the soluble compared to the input fraction in wild-type and GBA1-deficient samples. The amount of mGBA2 in the soluble fraction of GBA1-deficient HAP1 cell lysates was significantly increased compared to control cells. **(c)** The input signal intensity is similar in wild-type and GBA1-deficient samples. WT. Wild-type, KO. Knockout, kDa: Kilo Dalton, CHO: Chinese hamster ovary cells. Data are presented as mean + SD. N numbers are indicated in brackets. Representative Western blot for n = 3 experiments. P values were determined One-way ANOVA.

4 Discussion

4.1 The effect of GBA1 on GBA2 activity

In my PhD thesis, I have demonstrated that the GBA2 activity is reduced in genetic and pharmacologic models that lack active GBA1 *in vitro* and *in vivo*. Mistry et al. proposed that accumulating GlcCer and GlcSph spill over into the cytoplasm in GBA1-deficient cells, which leads to a breakdown of these metabolites by GBA2 and an increase in cytotoxic sphingosine (Mistry et al., 2014). I could show that sphingosine directly binds to GBA2 and inhibits its activity.

Based on the findings presented in this study, I developed the following model underlying the GBA1-dependent regulation of GBA2 activity in *Gaucher* cells (Figure 101): In wild-type cells, GBA1 breaks GlcCer down to glucose and ceramide in the lysosome, whereas an acid ceramidase cleaves GlcCer to GlcSph and a fatty acid. GBA2 cleaves GlcCer to glucose and ceramide at the *cis* Golgi and the ER. In *Gaucher* cells, GBA1 is almost inactive, resulting in the accumulation of GlcCer and GlcSph in the lysosome. Both metabolites spill over into the cytoplasm, where they become a substrate for GBA2. Here, GBA2 breaks GlcCer and GlcSph down to release ceramide and sphingosine, whereas ceramide is further broken down to sphingosine and a fatty acid by a neutral ceramidase, resulting in the cytoplasmic accumulation of cytotoxic sphingosine. Application of NB-DNJ/Zavesca in *Gaucher* disease inhibits both, GlcCerS and GBA2, resulting in fewer production of GlcCer and reduction in cytoplasmic sphingosine levels.

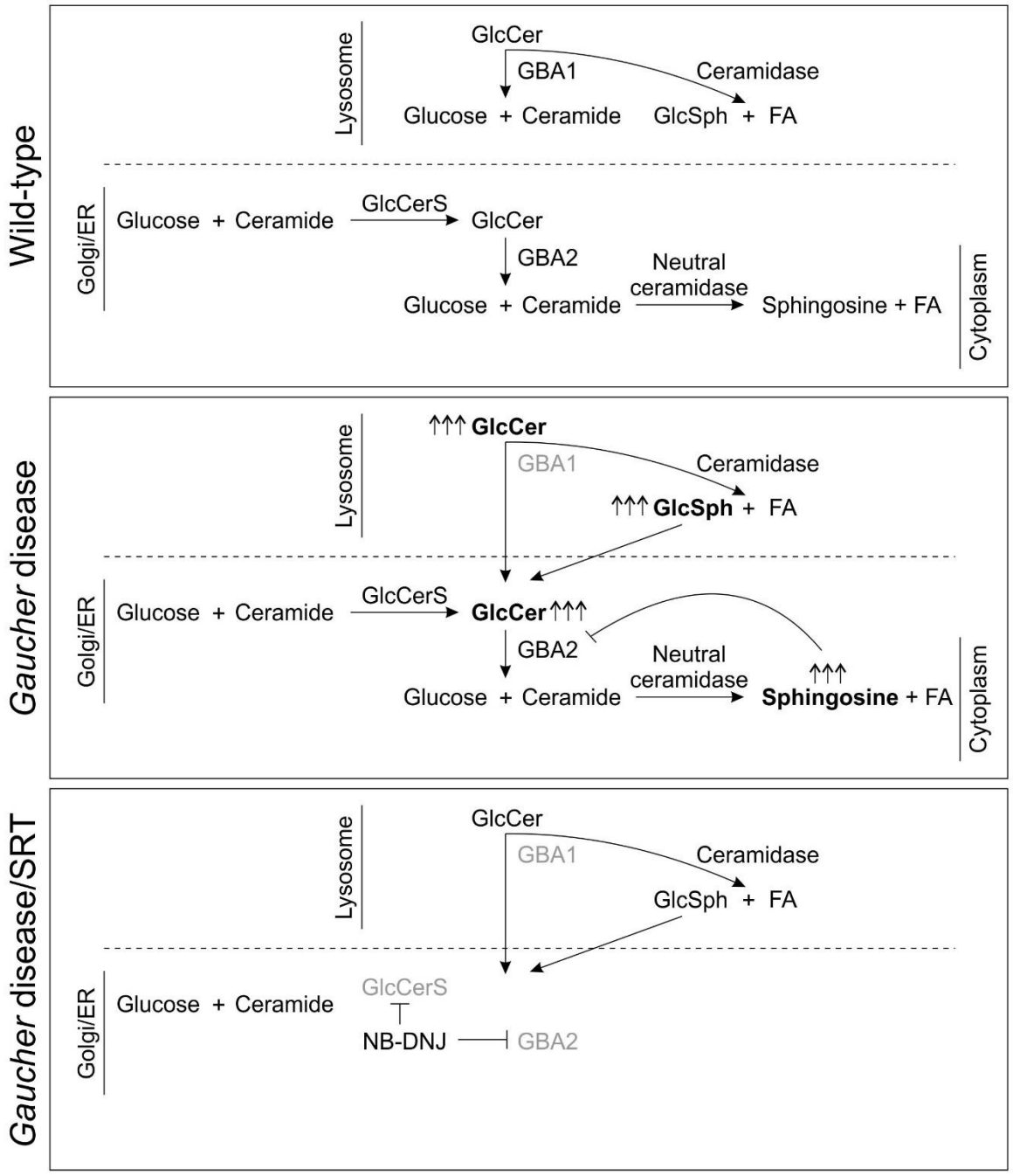

Figure 101: The GBA1-dependent regulation of GBA2 activity in *Gaucher* disease. The model is decribed in the text. ER: Endoplasmic reticulum, GlcCer: Glucosylceramide, GBA1: acid beta-glucosidase, GBA2: non-lysosomal beta-glucosidase, GlcSph: Glucosylsphingosine, FA: Fatty acid, GlcCerS: Glucosylceramide synthase, NB-DNJ: N-butyl-deoxynojirimycin.

4.2 The GBA1-dependent control of GBA2 activity – a closer look

4.2.1 Mimicking the effect of sphingosine on GBA2 activity

To demonstrate that sphingosine is indeed the metabolite that regulates GBA2 activity, cytoplasmic sphingosine levels can be increased by either feeding cells with

sphingosine or over-expressing an enzyme that is involved in sphingosine metabolism. The former has already been tried in this study, where incubation of GBA1-deficient cells with 20 µM sphingosine resulted in a decrease in GBA2 activity (see Figure 41). The latter could be done by over-expression of neutral ceramidase (EC 3.5.1.23), which cleaves ceramide to release fatty acids and sphingosine (El Bawab et al., 2000).

Besides the recent finding that sphingosine serum levels are elevated in GBA1-deficient mice (Mistry et al., 2014), both, sphingosine and sphinganine, have previously been reported to be accumulating in different lysosomal storage disorders. However, the underlying molecular mechanisms are ill-defined. Sphinganine levels are increased in liver from CerS2-deficient mice (Pewzner-Jung et al., 2010). In CerS2-deficient liver, GBA2 was slightly less active compared to control livers, but the change was not significant (Figure 37). Thus, sphinganine levels were most likely not high enough to evoke an effect on GBA1 and/or GBA2 activity, e.g. because the total amount of sphinganine was diluted during sample preparation and performance of the activity assay. Sphingosine accumulates in the lysosomes of macrophages treated with U18666A, a drug that is used to pharmacologically induce a *Niemann-Pick* type C (NP-C) phenotype in cells (Lloyd-Evans et al., 2008), but is also known to accumulate in brain, liver, and spleen from NP-C-deficient mice (te Vruchte et al., 2004). My data show that both, GBA1 and GBA2 activity, are significantly reduced in dermal fibroblasts from NP-C patients (Figure 36). Thus, it is difficult to distinguish between a GBA1-dependent and -independent effect on GBA2 activity because GBA1 activity was also reduced. However, under acidic conditions, sphingosine is protonated (pK_a of 8.9) (Kagedal et al., 2001) and cannot leave the lysosome unless actively shuttled by e.g. a transporter (Lloyd-Evans et al., 2008). Thus, it is unlikely that the GBA2 activity is reduced due to increased levels of sphingosine in NP-C cells. However, my data also show that GBA1 is sensitive to sphingosine (compare Figure 40 and Figure 61) (Erickson et al., 1985; Grabowski et al., 1985). Thus, the accumulation of sphingosine in lysosomes of NP-C cells could block GBA1, leading to accumulation of GlcCer and, thereby, to a reduction of GBA2 activity in a GBA1-dependent manner. Of note, during my binding studies with pacSph, GBA1 did not directly bind to sphingosine, in contrast to what Dr. P. Haberkant observed (personal communication, non-published data). This result is puzzling because sphingosine and sphinganine blocked GBA1 in a dose-dependent manner (Figure 61).

4.3 Reversing the GBA1-dependent effect on GBA2 activity

To restore GBA2 activity in a GBA1-dependent manner, I over-expressed mGBA1 in GBA1-deficient cells. However, GBA1 activity could not be fully restored. Accordingly, the GBA2 activity remained unchanged. Two main factors are known, which are crucial for the activity of GBA1: Its glycosylation pattern and the presence of saposin C, which catalyses the binding of GBA1 and GlcCer at the membrane (Alattia et al., 2006; Bergmann&Grabowski, 1989). Thus, heterologously expressed GBA1 might not be fully glycosylated, resulting in protein expression but very little activity.

Another approach would be to feed recombinant GBA1 (imiglucerase or Cerezyme, Genzyme Corporation, Cambridge, MA, USA) to cells. Imiglucerase carries mannose-type oligosaccharide side chains, which bind to mannose receptors present on the cell surface of e.g. macrophages and fibroblasts (Bergmann&Grabowski, 1989; Sheikh et al., 2000). Once internalised, imiglucerase reaches the lysosome via the endocytic pathway. Because of its high water solubility, I tested the activity of imiglucerase under our assay conditions. Imiglucerase (Cerezyme Finished Product, Part No 4285, obtained from E. Monlleó Mas, Institute of Advanced Chemistry of Catalonia, Spain) was dissolved to a concentration of 0.2 mg/ml in hypotonic buffer and analysed at pH 4, 5, 6, and 7 to find its optimal pH value (Figure 102). The enzyme was only active at pH 5 and the activity was partially blocked by 25 µM CBE, but insensitive to 8.3 µM NB-DNJ (Figure 102). To study the GBA1-dependent effect on GBA2 activity in more detail, GBA1-deficient cells could be fed with imiglucerase to increase the amount of active GBA1 and, thereby, restore GlcCer and GlcSph levels to control levels.

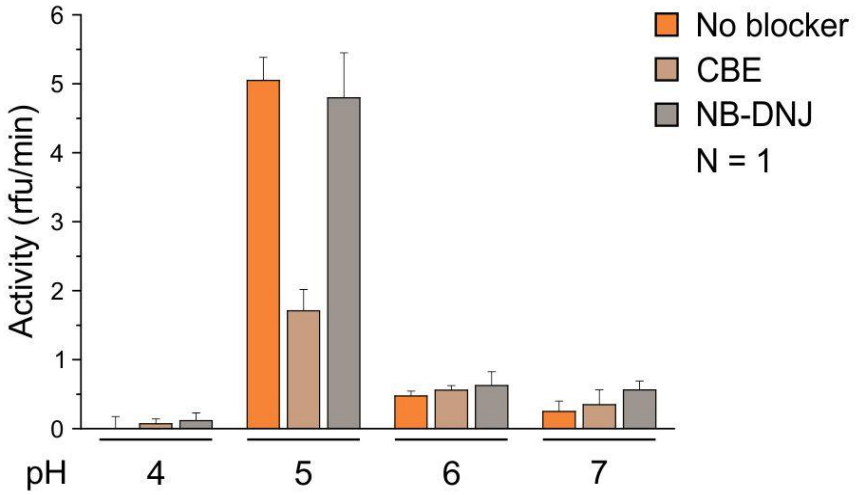

Figure 102: Imiglucerase activity at different pH values. Imiglucerase was dissolved to 0.2 mg/ml in hypotonic buffer and analysed at pH 4, 5, 6, and 7 in presence of 1.67 mM 4-MUG. There was no CBE-blockable activity detectable at pH 4, 6, and 7 but robust activity at pH 5, which was partially blockable by CBE. 4-MUG: 4-Methylumbelliferyl beta-D-glucopyranoside, CBE: Conduritol B epoxide. Data are presented as mean + SD of quadruples. The N number is indicated.

4.4 Regulation of GBA2

Results presented in this study show that sphingosine reversibly binds to an allosteric site of GBA2, which results in mixed-type enzyme inhibition (see 3.14.4). Even though GBA2 was first purified from human liver in 1997 and cloned in 2001, little is known about its functional domains and no crystal structure has been published so far (Matern et al., 2001; Matern et al., 1997). Thus, it is difficult to predict an allosteric site controlling lipid-dependent regulation of GBA2 activity. Data presented by others but also in this study (Figure 40 and Figure 61) show that GBA1 is also sensitive to sphingosine (Erickson&Radin, 1973; Grabowski et al., 1985). As previously mentioned, three domains are crucial for GBA1 activity, of which one interacts with sphingosine derivatives (Grabowski et al., 1986). This third domain was found to reversibly bind to sphingosine with an IC_{50} value of 40 µM (Grabowski et al., 1985). Interestingly, mutated GBA1 obtained from different *Gaucher* patients either showed similar behaviour towards sphingosine, or, in some cases, the sphingosine concentration had to be fivefold greater to achieve a half-maximal enzyme inhibition (Grabowski et al., 1985). Thus, point mutations, which result in an amino acid exchange in close proximity to the third domain of GBA1, seemed to reduce sphingosine binding (Grabowski et al., 1985). Likewise, point mutations could be introduced into the *GBA2* gene to identify residues that are crucial for aglycon binding. Unfortunately, truncated or mutated forms of GBA2

are inactive and single point mutations already result in a complete loss of GBA2 activity (Sultana et al., 2015) (personal observation in our lab). Recently, the crystal structure of a glycoside hydrolase family GH116 enzyme from the bacterium *Thermoanaerobacterium xylanolyticum* has been solved. The protein shares 40% sequence identity with the predicted catalytic domain of human GBA2, but does not cleave GlcCer (Charoenwattanasatien et al., 2016). Instead, the enzyme hydrolyses alkyl glycosides, including n-heptyl glucoside and n-octyl glucoside. Its structure supports the peripheral membrane localisation of GBA2 that we have also described previously (Körschen et al., 2013). Interestingly, loss-of-function mutations similar to those found in GBA2 also showed loss of activity, most likely due to reduced substrate binding and reduced enzyme stability (Charoenwattanasatien et al., 2016). Thus, a crystal structure of GBA2 is needed to study its regulatory domains in more detail.

4.5 The function of GBA2 in the cell

Since degradation of most GSLs occurs through GBA1 in the lysosomes, the cellular function of GBA2 is a matter of ongoing debate. GBA2 is associated with membranes at the cytosolic side of the *cis* Golgi and the ER, where it cleaves GlcCer to glucose and ceramide (Körschen et al., 2013). Thus, GBA2 is localised in close proximity to GlcCerS and the synthesis pathway of its substrate, GlcCer (Schweizer et al., 1994), suggesting that GBA2 could be a “fine-tuner” for intracellular GlcCer levels. However, the fact that the GBA2 activity remains unchanged in complete absence of GlcCer argues against GBA2 being a sensor for GlcCer levels at the Golgi and ER membrane (see Figure 39).

To date, the function of GBA2 can only be described by the effect of its loss and the subsequent accumulation of GlcCer. Loss of GBA2 activity in pharmacologic and genetic models results in impaired male fertility caused by accumulation of GlcCer, which alters cytoskeletal dynamics during sperm development (Raju et al., 2015; van der Spoel et al., 2002; Yildiz et al., 2006). Thus, GBA2 might indeed primarily function as a regulator of GlcCer levels in membranes at the Golgi and the ER, which, in turn, could affect downstream signalling pathways. It is well known that membrane lipid composition determines its characteristics and directly controls protein function (van Meer et al., 2003). Depletion of cholesterol enhances auto-phosphorylation of the EGF receptor (epidermal growth factor receptor), leading to an increase in tyrosine kinase activity (Pike&Casey, 2002). Furthermore, it has been shown that GM3 can regulate

the transition from an inactive to an active EGF receptor independent from ligand binding (Coskun et al., 2011).

In a previous study, we have shown that the accumulation of GlcCer in membranes derived from GBA2-deficient cells leads to more ordered lipid packaging, which seemed to affect the activity of proteins in or at the membrane (Raju et al., 2015). Since GBA2 is associated with the Golgi membrane, I wondered whether accumulation of its substrate, GlcCer, would also occur in Golgi membranes. Thus, I tried to establish an immunogold labelling protocol using an anti-GlcCer antibody that has previously been used to study the subcellular localisation of GlcCer (Brade et al., 2000; Vielhaber et al., 2001). Unfortunately, my experiments revealed that the anti-GlcCer antibody neither recognised GlcCer in control cells nor in DOPC liposomes containing GlcCer (see 3.15.1). Thus, I could not reveal, where GlcCer accumulates in GBA2-deficient cells.

Sorli et al. have demonstrated that GBA2 is down-regulated in melanoma cells (Sorli et al., 2013). In turn, heterologous expression of GBA2 in melanoma cells led to degradation of GlcCer, accompanied by UPR-dependent apoptosis and reduced tumour growth (Sorli et al., 2013). In a different study, it was recognised that GlcCerS-deficient cells (also used in Figure 39) were incapable of forming melanin, the pigment found in skin cells, even though all enzymes associated with pigmentation were present in these cells (Sprong et al., 2001). Interestingly, lack of GlcCer (and more complex GSLs) resulted in a mis-localisation of tyrosinase, an enzyme that is required in melanosomes, but was retained in the Golgi in GlcCerS-deficient cells. Heterologous expression of GlcCerS in GlcCerS-deficient cells restored pigmentation, whereas exogenous addition of GlcCer did not (Sprong et al., 2001). In total, these and other reports demonstrate that homeostasis of GSLs, and GlcCer in particular, is needed to maintain even basic cellular functions. Here, GBA2 as a non-lysosomal beta-glucosidase has become a key enzyme in the field of GSL research (Aureli et al., 2016).

4.6 GBA2 in *Gaucher* disease

Besides the present study, other reports have also analysed GBA2 activity in the context of *Gaucher* disease, showing an increase in GBA2 activity in brain from GBA1-deficient mice and in fibroblasts from *Gaucher* disease patients (Aureli et al., 2012; Burke et al., 2013). These results are in contrast to my findings and the reason for this

discrepancy is not known. One explanation could be a difference in the experimental set-up and how GBA2 activity was measured. However, in none of the *in vitro* or *in vivo* models that I tested, GBA2 expression or activity was higher in the absence of GBA1, arguing against earlier findings described above.

Analysis of the GBA2 activity in dermal fibroblasts from *Gaucher* type I, II, and III patients revealed that the GBA2 activity is similarly reduced in patients with a different genotypic and phenotypic background of the disease (Figure 14). From this I concluded that GBA2 does not play a role in genotype-phenotype correlation of *Gaucher* disease. However, even though the residual GBA2 activity might be equal in all tested patient cell lines, the effect of its partial loss might vary in the different phenotypes. As previously mentioned, type I *Gaucher* patients obtain a daily infusion of NB-DNJ/Zavesca (Actelion Pharmaceuticals, Basel, Switzerland) during substrate reduction therapy (SRT, also see 1.1.4.1.4) to block GlcCerS and subsequently reduce accumulation of GlcCer. According to dose-response analyses performed in our lab and also by others, treatment with NB-DNJ in the aforementioned concentration should completely inhibit GBA2 in *Gaucher* patients. According to my model presented above, the beneficial effect of NB-DNJ treatment might not only be due to a reduction in GlcCer, but also due to a reduction in GBA2 activity and, hence, the reduction of cytotoxic sphingosine levels (Figure 101). This hypothesis also matches the data generated by Mistry et al., who could reverse some of the symptoms previously seen in their type I *Gaucher* mouse by either applying NB-DNJ or genetically knocking out GBA2 (Mistry et al., 2014).

On the other hand, SRT does not exert a beneficial effect in the treatment of type II *Gaucher* patients suffering from severe neurologic conditions. Of note, NB-DNJ/Zavesca does not cross the blood-brain barrier (Coutinho et al., 2016). Still, the endogenous GBA2 activity is reduced in cells from type II *Gaucher* patients via the mechanism presented in this study. It has been shown that the GBA2 activity increases during neuronal differentiation, suggesting an important role for GBA2 during neuron development (Aureli et al., 2012). Furthermore, knock-down of GBA2 in zebrafish larvae resulted in abnormalities in motor behaviour and axonal outgrowth of motor neurons (Martin et al., 2013). GBA2 loss-of-function mutations have recently been connected to neuronal disorders such as hereditary spastic paraplegia and autosomal-recessive cerebellar ataxia with spasticity, underlining the importance of GBA2 in neuron function (Citterio et al., 2014; Hammer et al., 2013; Martin et al., 2013; Sultana

et al., 2015; Votsi et al., 2014). Thus, the probably beneficial effect of reduced GBA2 activity in type I *Gaucher* patients might be the opposite in type II and III patients suffering from neurologic symptoms. Here, a PDMP (1-phenyl-2-decanoylamino-3-morpholino-1-propanol)-based compound capable of crossing the blood-brain barrier might be of great advantage to reduce accumulation of GlcCer without further reducing the activity of GBA2, since PDMP inhibits GlcCerS, but not GBA2 (Shayman&Larsen, 2014).

In conclusion, the present study reveals the regulation of GBA2 activity by sphingosine in *Gaucher* disease. Thus, my results add a new chapter to the understaning of the molecular mechanisms underlying *Gaucher* disease pathology, presenting new ideas for the therapy of this severe lysosomal storage disorder.

5 References

Adams, R. J., Pitts, B. J., Woods, J. M., Gende, O. A., Wallick, E. T. & Schwartz, A. (1979) "Effect of palmitylcarnitine on ouabain binding to Na, K-ATPase" *Journal of molecular and cellular cardiology* 11, 941-959

Aerts, J. M., Hollak, C. E., Boot, R. G., Groener, J. E. & Maas, M. (2006) "Substrate reduction therapy of glycosphingolipid storage disorders" *Journal of inherited metabolic disease* 29, 449-456

Alattia, J. R., Shaw, J. E., Yip, C. M. & Prive, G. G. (2006) "Direct visualization of saposin remodelling of lipid bilayers" *Journal of molecular biology* 362, 943-953

Amory, J. K., Muller, C. H., Page, S. T., Leifke, E., Pagel, E. R., Bhandari, A., Subramanyam, B., Bone, W., Radlmaier, A. & Bremner, W. J. (2007) "Miglustat has no apparent effect on spermatogenesis in normal men" *Human reproduction* 22, 702-707

Aureli, M., Gritti, A., Bassi, R., Loberto, N., Ricca, A., Chigorno, V., Prinetti, A. & Sonnino, S. (2012) "Plasma membrane-associated glycohydrolases along differentiation of murine neural stem cells" *Neurochemical research* 37, 1344-1354

Aureli, M., Masilamani, A. P., Illuzzi, G., Loberto, N., Scandroglio, F., Prinetti, A., Chigorno, V. & Sonnino, S. (2009) "Activity of plasma membrane beta-galactosidase and beta-glucosidase" *FEBS letters* 583, 2469-2473

Aureli, M., Samarani, M., Loberto, N., Mancini, G., Murdica, V., Chiricozzi, E., Prinetti, A., Bassi, R. & Sonnino, S. (2016) "Current and Novel Aspects on the Non-lysosomal beta-Glucosylceramidase GBA2" *Neurochemical research* 41, 210-220

Basu, S., Kaufman, B. & Roseman, S. (1968) "Enzymatic synthesis of ceramide-glucose and ceramide-lactose by glycosyltransferases from embryonic chicken brain" *The Journal of biological chemistry* 243, 5802-5804

Bentz, J. & Duzgunes, N. (1985) "Fusogenic capacities of divalent cations and effect of liposome size" *Biochemistry* 24, 5436-5443

Berg-Fussman, A., Grace, M. E., Ioannou, Y. & Grabowski, G. A. (1993) "Human acid beta-glucosidase. N-glycosylation site occupancy and the effect of glycosylation on enzymatic activity" *The Journal of biological chemistry* 268, 14861-14866

Bergmann, J. E. & Grabowski, G. A. (1989) "Posttranslational processing of human lysosomal acid beta-glucosidase: a continuum of defects in Gaucher disease type 1 and type 2 fibroblasts" *American journal of human genetics* 44, 741-750

Bertolotti, A., Zhang, Y., Hendershot, L. M., Harding, H. P. & Ron, D. (2000) "Dynamic interaction of BiP and ER stress transducers in the unfolded-protein response" *Nature cell biology* 2, 326-332

Bjorck, L. & Kronvall, G. (1984) "Purification and some properties of streptococcal protein G, a novel IgG-binding reagent" *Journal of immunology* 133, 969-974

Bodennec, J., Pelled, D., Riebeling, C., Trajkovic, S. & Futerman, A. H. (2002) "Phosphatidylcholine synthesis is elevated in neuronal models of Gaucher disease due to direct activation of CTP:phosphocholine cytidylyltransferase by glucosylceramide" *FASEB journal : official publication of the Federation of American Societies for Experimental Biology* 16, 1814-1816

Boot, R. G., Verhoek, M., Donker-Koopman, W., Strijland, A., van Marle, J., Overkleeft, H. S., Wennekes, T. & Aerts, J. M. (2007) "Identification of the non-lysosomal glucosylceramidase as beta-glucosidase 2" *The Journal of biological chemistry* 282, 1305-1312

Brade, L., Vielhaber, G., Heinz, E. & Brade, H. (2000) "In vitro characterization of anti-glucosylceramide rabbit antisera" *Glycobiology* 10, 629-636

Brady, R. O., Barton, N. W. & Grabowski, G. A. (1993) "The role of neurogenetics in Gaucher disease" *Archives of neurology* 50, 1212-1224

Brady, R. O., Kanfer, J. N. & Shapiro, D. (1965) "Metabolism of Glucocerebrosides. Ii. Evidence of an Enzymatic Deficiency in Gaucher's Disease" *Biochemical and biophysical research communications* 18, 221-225

Brady, R. O., Pentchev, P. G., Gal, A. E., Hibbert, S. R. & Dekaban, A. S. (1974) "Replacement therapy for inherited enzyme deficiency. Use of purified glucocerebrosidase in Gaucher's disease" *The New England journal of medicine* 291, 989-993

Braun, P. E. & Snell, E. E. (1968) "Biosynthesis of sphingolipid bases. II. Keto intermediates in synthesis of sphingosine and dihydrosphingosine by cell-free extracts of Hansenula ciferri" *The Journal of biological chemistry* 243, 3775-3783

Bremer, J. (1983) "Carnitine--metabolism and functions" *Physiological reviews* 63, 1420-1480

Brinkmann, V., Davis, M. D., Heise, C. E., Albert, R., Cottens, S., Hof, R., Bruns, C., Prieschl, E., Baumruker, T., Hiestand, P., Foster, C. A., Zollinger, M. & Lynch, K. R. (2002) "The immune modulator FTY720 targets sphingosine 1-phosphate receptors" *The Journal of biological chemistry* 277, 21453-21457

Brown, R. E. & Mattjus, P. (2007) "Glycolipid transfer proteins" *Biochimica et biophysica acta* 1771, 746-760

Burke, D. G., Rahim, A. A., Waddington, S. N., Karlsson, S., Enquist, I., Bhatia, K., Mehta, A., Vellodi, A. & Heales, S. (2013) "Increased glucocerebrosidase (GBA) 2 activity in GBA1 deficient mice brains and in Gaucher leucocytes" *Journal of inherited metabolic disease* 36, 869-872

Buton, X., Herve, P., Kubelt, J., Tannert, A., Burger, K. N., Fellmann, P., Muller, P., Herrmann, A., Seigneuret, M. & Devaux, P. F. (2002) "Transbilayer movement of monohexosylsphingolipids in endoplasmic reticulum and Golgi membranes" *Biochemistry* 41, 13106-13115

Cao, S. S. & Kaufman, R. J. (2012) "Unfolded protein response" *Current biology : CB* 22, R622-626

Carter, H. E., Glick, F. J., Norris, W. P. & Phillips, G. E. (1947) "Biochemistry of the Sphingolipides .3. Structure of Sphingosine" *Journal of Biological Chemistry* 170, 285-294

Chalat, M., Menon, I., Turan, Z. & Menon, A. K. (2012) "Reconstitution of glucosylceramide flip-flop across endoplasmic reticulum: implications for mechanism of glycosphingolipid biosynthesis" *The Journal of biological chemistry* 287, 15523-15532

Charoenwattanasatien, R., Pengthaisong, S., Breen, I., Mutoh, R., Sansenya, S., Hua, Y., Tankrathok, A., Wu, L., Songsiriritthigul, C., Tanaka, H., Williams, S. J., Davies, G. J., Kurisu, G. & Cairns, J. R. (2016) "Bacterial beta-Glucosidase Reveals the Structural and Functional Basis of Genetic Defects in Human Glucocerebrosidase 2 (GBA2)" *ACS chemical biology* 11, 1891-1900

Chen, J. W., Pan, W., D'Souza, M. P. & August, J. T. (1985) "Lysosome-associated membrane proteins: characterization of LAMP-1 of macrophage P388 and mouse embryo 3T3 cultured cells" *Archives of biochemistry and biophysics* 239, 574-586

Chun, J. & Hartung, H. P. (2010) "Mechanism of action of oral fingolimod (FTY720) in multiple sclerosis" *Clinical neuropharmacology* 33, 91-101

Citterio, A., Arnoldi, A., Panzeri, E., D'Angelo, M. G., Filosto, M., Dilena, R., Arrigoni, F., Castelli, M., Maghini, C., Germiniasi, C., Menni, F., Martinuzzi, A., Bresolin, N. & Bassi, M. T. (2014) "Mutations in CYP2U1, DDHD2 and GBA2 genes are rare causes of complicated forms of hereditary spastic paraparesis" *Journal of neurology* 261, 373-381

Claude, A. (1946) "Fractionation of mammalian liver cells by differential centrifugation; problems, methods, and preparation of extract" *The Journal of experimental medicine* 84, 51-59

Clermont, Y. (1972) "Kinetics of spermatogenesis in mammals: seminiferous epithelium cycle and spermatogonial renewal" *Physiological reviews* 52, 198-236

Contreras, F. X., Ernst, A. M., Haberkant, P., Bjorkholm, P., Lindahl, E., Gonen, B., Tischer, C., Elofsson, A., von Heijne, G., Thiele, C., Pepperkok, R., Wieland, F. & Brugger, B. (2012) "Molecular recognition of a single sphingolipid species by a protein's transmembrane domain" *Nature* 481, 525-529

Contreras, F. X., Sot, J., Alonso, A. & Goni, F. M. (2006) "Sphingosine increases the permeability of model and cell membranes" *Biophysical journal* 90, 4085-4092

Coskun, U., Grzybek, M., Drechsel, D. & Simons, K. (2011) "Regulation of human EGF receptor by lipids" *Proceedings of the National Academy of Sciences of the United States of America* 108, 9044-9048

Coutinho, M. F., Prata, M. J. & Alves, S. (2012) "Mannose-6-phosphate pathway: a review on its role in lysosomal function and dysfunction" *Molecular genetics and metabolism* 105, 542-550

Coutinho, M. F., Santos, J. I. & Alves, S. (2016) "Less Is More: Substrate Reduction Therapy for Lysosomal Storage Disorders" *International journal of molecular sciences* 17

Cox, T. M. (2001) "Gaucher disease: understanding the molecular pathogenesis of sphingolipidoses" *Journal of inherited metabolic disease* 24 Suppl 2, 106-121; discussion 187-108

Crocker, A. C. (1961) "The cerebral defect in Tay-Sachs disease and Niemann-Pick disease" *Journal of neurochemistry* 7, 69-80

D'Angelo, G., Polishchuk, E., Di Tullio, G., Santoro, M., Di Campli, A., Godi, A., West, G., Bielawski, J., Chuang, C. C., van der Spoel, A. C., Platt, F. M., Hannun, Y. A., Polishchuk, R., Mattjus, P. & De Matteis, M. A. (2007) "Glycosphingolipid synthesis requires FAPP2 transfer of glucosylceramide" *Nature* 449, 62-67

De Duve, C., Pressman, B. C., Gianetto, R., Wattiaux, R. & Appelmans, F. (1955) "Tissue fractionation studies. 6. Intracellular distribution patterns of enzymes in rat-liver tissue" *The Biochemical journal* 60, 604-617

Deduve, C. (1964) "From Cytases to Lysosomes" *Federation proceedings* 23, 1045-1049

Dwek, R. A., Butters, T. D., Platt, F. M. & Zitzmann, N. (2002) "Targeting glycosylation as a therapeutic approach" *Nature reviews. Drug discovery* 1, 65-75

Echabe, I., Requero, M. A., Goni, F. M., Arrondo, J. L. & Alonso, A. (1995) "An infrared investigation of palmitoyl-coenzyme A and palmitoylcarnitine interaction with perdeuterated-chain phospholipid bilayers" *European journal of biochemistry / FEBS* 231, 199-203

El Bawab, S., Roddy, P., Qian, T., Bielawska, A., Lemasters, J. J. & Hannun, Y. A. (2000) "Molecular cloning and characterization of a human mitochondrial ceramidase" *The Journal of biological chemistry* 275, 21508-21513

Enquist, I. B., Nilsson, E., Ooka, A., Mansson, J. E., Olsson, K., Ehinger, M., Brady, R. O., Richter, J. & Karlsson, S. (2006) "Effective cell and gene therapy in a murine model of Gaucher disease" *Proceedings of the National Academy of Sciences of the United States of America* 103, 13819-13824

Erickson, A. H., Ginns, E. I. & Barranger, J. A. (1985) "Biosynthesis of the lysosomal enzyme glucocerebrosidase" *The Journal of biological chemistry* 260, 14319-14324

Erickson, J. S. & Radin, N. S. (1973) "N-hexyl-O-glucosyl sphingosine, an inhibitor of glucosyl ceramide -glucosidase" *Journal of lipid research* 14, 133-137

Erikson, A., Bembi, B. & Schiffmann, R. (1997) "Neuronopathic forms of Gaucher's disease" *Bailliere Clin Haem* 10, 711-723

Farfel-Becker, T., Vitner, E., Dekel, H., Leshem, N., Enquist, I. B., Karlsson, S. & Futerman, A. H. (2009) "No evidence for activation of the unfolded protein response in neuronopathic models of Gaucher disease" *Human molecular genetics* 18, 1482-1488

Farfel-Becker, T., Vitner, E. B. & Futerman, A. H. (2011) "Animal models for Gaucher disease research" *Disease models & mechanisms* 4, 746-752

Ferraz, M. J., Marques, A. R., Appelman, M. D., Verhoek, M., Strijland, A., Mirzaian, M., Scheij, S., Ouairy, C. M., Lahav, D., Wisse, P., Overkleeft, H. S., Boot, R. G. &

Aerts, J. M. (2016) "Lysosomal glycosphingolipid catabolism by acid ceramidase: formation of glycosphingoid bases during deficiency of glycosidases" *FEBS letters* 590, 716-725

Filocamo, M., Mazzotti, R., Corsolini, F., Stroppiano, M., Stroppiana, G., Grossi, S., Lualdi, S., Tappino, B., Lanza, F., Galotto, S. & Biancheri, R. (2014) "Cell Line and DNA Biobank From Patients Affected by Genetic Diseases" *Open Journal of Bioresources* 1, e2

Fritz, I. (1955) "The effect of muscle extracts on the oxidation of palmitic acid by liver slices and homogenates" *Acta physiologica Scandinavica* 34, 367-385

Fuller, M., Rozaklis, T., Lovejoy, M., Zarrinkalam, K., Hopwood, J. J. & Meikle, P. J. (2008) "Glucosylceramide accumulation is not confined to the lysosome in fibroblasts from patients with Gaucher disease" *Molecular genetics and metabolism* 93, 437-443

Furst, W. & Sandhoff, K. (1992) "Activator proteins and topology of lysosomal sphingolipid catabolism" *Biochimica et biophysica acta* 1126, 1-16

Futerman, A. H., Stieger, B., Hubbard, A. L. & Pagano, R. E. (1990) "Sphingomyelin synthesis in rat liver occurs predominantly at the cis and medial cisternae of the Golgi apparatus" *The Journal of biological chemistry* 265, 8650-8657

Gaebler, A., Penno, A., Kuerschner, L. & Thiele, C. (2016) "A highly sensitive protocol for microscopy of alkyne lipids and fluorescently tagged or immunostained proteins" *Journal of lipid research* 57, 1934-1947

Gallo, J. M. (2001) "Pharmacokinetics: Model structure and transport systems (Reprinted from Transport Processes in Pharmaceutical Systems, pg 55-86, 2000)" *Clin Res Regul Aff* 18, 235-266

Gatt, S. (1963) "Enzymic Hydrolysis and Synthesis of Ceramides" *The Journal of biological chemistry* 238, 3131-3133

Geeraert, L., Mannaerts, G. P. & van Veldhoven, P. P. (1997) "Conversion of dihydroceramide into ceramide: involvement of a desaturase" *The Biochemical journal* 327 (Pt 1), 125-132

Gerl, M. J., Bittl, V., Kirchner, S., Sachsenheimer, T., Brunner, H. L., Luchtenborg, C., Ozbalci, C., Wiedemann, H., Wegehingel, S., Nickel, W., Haberkant, P., Schultz, C., Kruger, M. & Brugger, B. (2016) "Sphingosine-1-Phosphate Lyase Deficient Cells as a Tool to Study Protein Lipid Interactions" *PloS one* 11, e0153009

Ginkel, C., Hartmann, D., vom Dorp, K., Zlomuzica, A., Farwanah, H., Eckhardt, M., Sandhoff, R., Degen, J., Rabionet, M., Dere, E., Dormann, P., Sandhoff, K. & Willecke, K. (2012) "Ablation of neuronal ceramide synthase 1 in mice decreases ganglioside levels and expression of myelin-associated glycoprotein in oligodendrocytes" *The Journal of biological chemistry* 287, 41888-41902

Godi, A., Di Campli, A., Konstantakopoulos, A., Di Tullio, G., Alessi, D. R., Kular, G. S., Daniele, T., Marra, P., Lucocq, J. M. & De Matteis, M. A. (2004) "FAPPs control Golgi-to-cell-surface membrane traffic by binding to ARF and PtdIns(4)P" *Nature cell biology* 6, 393-404

Goldstone, A. & Koenig, H. (1973) "Physicochemical modifications of lysosomal hydrolases during intracellular transport" *The Biochemical journal* 132, 267-282

Goni, F. M., Requero, M. A. & Alonso, A. (1996) "Palmitoylcarnitine, a surface-active metabolite" *FEBS letters* 390, 1-5

Gonzalez-Carmona, M. A., Sandhoff, R., Tacke, F., Vogt, A., Weber, S., Canbay, A. E., Rogler, G., Sauerbruch, T., Lammert, F. & Yildiz, Y. (2012) "Beta-glucosidase 2 knockout mice with increased glucosylceramide show impaired liver regeneration" *Liver international : official journal of the International Association for the Study of the Liver* 32, 1354-1362

Grabowski, G. A. (2001) "Gaucher's disease. Enzyme therapy is not enough" *Lancet* 358 Suppl, S29

Grabowski, G. A., Dinur, T., Osiecki, K. M., Kruse, J. R., Legler, G. & Gatt, S. (1985) "Gaucher disease types 1, 2, and 3: differential mutations of the acid beta-glucosidase active site identified with conduritol B epoxide derivatives and sphingosine" *American journal of human genetics* 37, 499-510

Grabowski, G. A., Gatt, S., Kruse, J. & Desnick, R. J. (1984) "Human lysosomal beta-glucosidase: kinetic characterization of the catalytic, aglycon, and hydrophobic binding sites" *Archives of biochemistry and biophysics* 231, 144-157

Grabowski, G. A. & Hopkin, R. J. (2003) "Enzyme therapy for lysosomal storage disease: principles, practice, and prospects" *Annual review of genomics and human genetics* 4, 403-436

Grabowski, G. A., Osiecki-Newman, K., Dinur, T., Fabbro, D., Legler, G., Gatt, S. & Desnick, R. J. (1986) "Human acid beta-glucosidase. Use of conduritol B epoxide derivatives to investigate the catalytically active normal and Gaucher disease enzymes" *The Journal of biological chemistry* 261, 8263-8269

Grace, M. E., Newman, K. M., Scheinker, V., Berg-Fussman, A. & Grabowski, G. A. (1994) "Analysis of human acid beta-glucosidase by site-directed mutagenesis and heterologous expression" *The Journal of biological chemistry* 269, 2283-2291

Graham, F. L., Smiley, J., Russell, W. C. & Nairn, R. (1977) "Characteristics of a human cell line transformed by DNA from human adenovirus type 5" *The Journal of general virology* 36, 59-74

Grant, B. D. & Donaldson, J. G. (2009) "Pathways and mechanisms of endocytic recycling" *Nature reviews. Molecular cell biology* 10, 597-608

Gyorgy, P., Melville, D. B., Burk, D. & V, D. U. V. (1940) "The Possible Identity of Vitamin H with Biotin and Coenzyme R" *Science* 91, 243-245

Haberkant, P., Stein, F., Hoglinger, D., Gerl, M. J., Brugger, B., Van Veldhoven, P. P., Krijgsveld, J., Gavin, A. C. & Schultz, C. (2016) "Bifunctional Sphingosine for Cell-Based Analysis of Protein-Sphingolipid Interactions" *ACS chemical biology* 11, 222-230

Hakomori, S. (1981) "Glycosphingolipids in cellular interaction, differentiation, and oncogenesis" *Annual review of biochemistry* 50, 733-764

Hakomori Si, S. I. (2002) "The glycosynapse" *Proceedings of the National Academy of Sciences of the United States of America* 99, 225-232

Halter, D., Neumann, S., van Dijk, S. M., Wolthoorn, J., de Maziere, A. M., Vieira, O. V., Mattjus, P., Klumperman, J., van Meer, G. & Sprong, H. (2007) "Pre- and post-Golgi translocation of glucosylceramide in glycosphingolipid synthesis" *The Journal of cell biology* 179, 101-115

Hammer, M. B., Eleuch-Fayache, G., Schottlaender, L. V., Nehdi, H., Gibbs, J. R., Arepalli, S. K., Chong, S. B., Hernandez, D. G., Sailer, A., Liu, G., Mistry, P. K., Cai, H., Shrader, G., Sassi, C., Bouhlal, Y., Houlden, H., Hentati, F., Amouri, R. & Singleton, A. B. (2013) "Mutations in GBA2 cause autosomal-recessive cerebellar ataxia with spasticity" *American journal of human genetics* 92, 245-251

Hanada, K., Kumagai, K., Yasuda, S., Miura, Y., Kawano, M., Fukasawa, M. & Nishijima, M. (2003) "Molecular machinery for non-vesicular trafficking of ceramide" *Nature* 426, 803-809

Hannun, Y. A. & Obeid, L. M. (2008) "Principles of bioactive lipid signalling: lessons from sphingolipids" *Nature reviews. Molecular cell biology* 9, 139-150

He, X. M. & Carter, D. C. (1992) "Atomic structure and chemistry of human serum albumin" *Nature* 358, 209-215

Hoekstra, D. & Kok, J. W. (1992) "Trafficking of glycosphingolipids in eukaryotic cells; sorting and recycling of lipids" *Biochimica et biophysica acta* 1113, 277-294

Hruska, K. S., LaMarca, M. E., Scott, C. R. & Sidransky, E. (2008) "Gaucher disease: mutation and polymorphism spectrum in the glucocerebrosidase gene (GBA)" *Human mutation* 29, 567-583

Ichikawa, S., Nakajo, N., Sakiyama, H. & Hirabayashi, Y. (1994) "A mouse B16 melanoma mutant deficient in glycolipids" *Proceedings of the National Academy of Sciences of the United States of America* 91, 2703-2707

Imgrund, S., Hartmann, D., Farwanah, H., Eckhardt, M., Sandhoff, R., Degen, J., Gieselmann, V., Sandhoff, K. & Willecke, K. (2009) "Adult ceramide synthase 2 (CERS2)-deficient mice exhibit myelin sheath defects, cerebellar degeneration, and hepatocarcinomas" *The Journal of biological chemistry* 284, 33549-33560

Iwabuchi, K., Handa, K. & Hakomori, S. (1998) "Separation of "glycosphingolipid signaling domain" from caveolin-containing membrane fraction in mouse melanoma B16 cells and its role in cell adhesion coupled with signaling" *The Journal of biological chemistry* 273, 33766-33773

Jacewicz, M., Clausen, H., Nudelman, E., Donohue-Rolfe, A. & Keusch, G. T. (1986) "Pathogenesis of shigella diarrhea. XI. Isolation of a shigella toxin-binding glycolipid from rabbit jejunum and HeLa cells and its identification as globotriaosylceramide" *The Journal of experimental medicine* 163, 1391-1404

Kagedal, K., Zhao, M., Svensson, I. & Brunk, U. T. (2001) "Sphingosine-induced apoptosis is dependent on lysosomal proteases" *The Biochemical journal* 359, 335-343

Kaiser, R. D. & London, E. (1998) "Determination of the depth of BODIPY probes in model membranes by parallax analysis of fluorescence quenching" *Biochimica et biophysica acta* 1375, 13-22

Kanfer, J. N., Legler, G., Sullivan, J., Raghavan, S. S. & Mumford, R. A. (1975) "The Gaucher mouse" *Biochemical and biophysical research communications* 67, 85-90

Kappos, L., Radue, E. W., O'Connor, P., Polman, C., Hohlfeld, R., Calabresi, P., Selmaj, K., Agoropoulou, C., Leyk, M., Zhang-Auberson, L., Burtin, P. & Group, F. S. (2010) "A placebo-controlled trial of oral fingolimod in relapsing multiple sclerosis" *The New England journal of medicine* 362, 387-401

Karlsson, K. A. (1989) "Animal glycosphingolipids as membrane attachment sites for bacteria" *Annual review of biochemistry* 58, 309-350

Karolin, J., Johansson, L. B. A., Strandberg, L. & Ny, T. (1994) "Fluorescence and Absorption Spectroscopic Properties of Dipyrrometheneboron Difluoride (Bodipy) Derivatives in Liquids, Lipid-Membranes, and Proteins" *J Am Chem Soc* 116, 7801-7806

Kaufman, R. J. (2002) "Orchestrating the unfolded protein response in health and disease" *Journal of Clinical Investigation* 110, 1389-1398

Khan, W. A., Mascarella, S. W., Lewin, A. H., Wyrick, C. D., Carroll, F. I. & Hannun, Y. A. (1991) "Use of D-erythro-sphingosine as a pharmacological inhibitor of protein kinase C in human platelets" *The Biochemical journal* 278 (Pt 2), 387-392

Kim, R., Lou, K. & Kraft, M. L. (2013) "A new, long-wavelength borondipyrromethene sphingosine for studying sphingolipid dynamics in live cells" *Journal of lipid research* 54, 265-275

Klein, A. D., Ferreira, N. S., Ben-Dor, S., Duan, J., Hardy, J., Cox, T. M., Merrill, A. H., Jr. & Futerman, A. H. (2016) "Identification of Modifier Genes in a Mouse Model of Gaucher Disease" *Cell reports* 16, 2546-2553

Klenk, E. (1951) "[Contribution to the concept of gangliosides]" *Hoppe-Seyler's Zeitschrift fur physiologische Chemie* 288, 216-220

Klenk, E. & Lauenstein, K. (1952) "[The carbohydrate groups of the submaxillar mucin and uromucoproteids. Isolation of neuramic acid as metabolite]" *Hoppe-Seyler's Zeitschrift fur physiologische Chemie* 291, 147-152

Kohler, G. & Milstein, C. (1975) "Continuous cultures of fused cells secreting antibody of predefined specificity" *Nature* 256, 495-497

Korkotian, E., Schwarz, A., Pelled, D., Schwarzmann, G., Segal, M. & Futerman, A. H. (1999) "Elevation of intracellular glucosylceramide levels results in an increase in endoplasmic reticulum density and in functional calcium stores in cultured neurons" *The Journal of biological chemistry* 274, 21673-21678

Körschen, H. G., Yildiz, Y., Raju, D. N., Schonauer, S., Bonigk, W., Jansen, V., Kremmer, E., Kaupp, U. B. & Wachten, D. (2013) "The non-lysosomal beta-glucosidase GBA2 is a non-integral membrane-associated protein at the endoplasmic reticulum (ER) and Golgi" *The Journal of biological chemistry* 288, 3381-3393

Kuziemko, G. M., Stroh, M. & Stevens, R. C. (1996) "Cholera toxin binding affinity and specificity for gangliosides determined by surface plasmon resonance" *Biochemistry* 35, 6375-6384

Laemmli, U. K. (1970) "Cleavage of structural proteins during the assembly of the head of bacteriophage T4" *Nature* 227, 680-685

Lambeth, J. D., Burnham, D. N. & Tyagi, S. R. (1988) "Sphinganine effects on chemoattractant-induced diacylglycerol generation, calcium fluxes, superoxide production, and on cell viability in the human neutrophil. Delivery of sphinganine with bovine serum albumin minimizes cytotoxicity without affecting inhibition of the respiratory burst" *The Journal of biological chemistry* 263, 3818-3822

Lannert, H., Bunning, C., Jeckel, D. & Wieland, F. T. (1994) "Lactosylceramide is synthesized in the lumen of the Golgi apparatus" *FEBS letters* 342, 91-96

Lauria, I., van Uum, J., Mjumjunov-Crncevic, E., Walrafen, D., Spitta, L., Thiele, C. & Lang, T. (2013) "GLTP mediated non-vesicular GM1 transport between native membranes" *PloS one* 8, e59871

le Maire, M., Champeil, P. & Moller, J. V. (2000) "Interaction of membrane proteins and lipids with solubilizing detergents" *Biochimica et biophysica acta* 1508, 86-111

Lee, A. S. (2005) "The ER chaperone and signaling regulator GRP78/BiP as a monitor of endoplasmic reticulum stress" *Methods* 35, 373-381

Levy, M. & Futerman, A. H. (2010) "Mammalian ceramide synthases" *IUBMB life* 62, 347-356

Lin, X., Mattjus, P., Pike, H. M., Windebank, A. J. & Brown, R. E. (2000) "Cloning and expression of glycolipid transfer protein from bovine and porcine brain" *The Journal of biological chemistry* 275, 5104-5110

Lingwood, C. A. (2011) "Glycosphingolipid functions" *Cold Spring Harbor perspectives in biology* 3

Linstedt, A. D. & Hauri, H. P. (1993) "Giantin, a novel conserved Golgi membrane protein containing a cytoplasmic domain of at least 350 kDa" *Molecular biology of the cell* 4, 679-693

Lloyd-Evans, E., Morgan, A. J., He, X., Smith, D. A., Elliot-Smith, E., Sillence, D. J., Churchill, G. C., Schuchman, E. H., Galione, A. & Platt, F. M. (2008) "Niemann-Pick

disease type C1 is a sphingosine storage disease that causes deregulation of lysosomal calcium" *Nature medicine* 14, 1247-1255

Lofgren, H. & Pascher, I. (1977) "Molecular arrangements of sphingolipids. The monolayer behaviour of ceramides" *Chemistry and physics of lipids* 20, 273-284

Mandel, M. & Higa, A. (1970) "Calcium-dependent bacteriophage DNA infection" *Journal of molecular biology* 53, 159-162

Mandon, E. C., Ehses, I., Rother, J., van Echten, G. & Sandhoff, K. (1992) "Subcellular localization and membrane topology of serine palmitoyltransferase, 3-dehydrosphinganine reductase, and sphinganine N-acyltransferase in mouse liver" *The Journal of biological chemistry* 267, 11144-11148

Maor, G., Rencus-Lazar, S., Filocamo, M., Steller, H., Segal, D. & Horowitz, M. (2013) "Unfolded protein response in Gaucher disease: from human to Drosophila" *Orphanet journal of rare diseases* 8, 140

Marasas, W. F. (2001) "Discovery and occurrence of the fumonisins: a historical perspective" *Environmental health perspectives* 109 Suppl 2, 239-243

Marks, D. L., Wu, K., Paul, P., Kamisaka, Y., Watanabe, R. & Pagano, R. E. (1999) "Oligomerization and topology of the Golgi membrane protein glucosylceramide synthase" *The Journal of biological chemistry* 274, 451-456

Marques, A. R., Aten, J., Ottenhoff, R., van Roomen, C. P., Herrera Moro, D., Claessen, N., Vinueza Veloz, M. F., Zhou, K., Lin, Z., Mirzaian, M., Boot, R. G., De Zeeuw, C. I., Overkleeft, H. S., Yildiz, Y. & Aerts, J. M. (2015) "Reducing GBA2 Activity Ameliorates Neuropathology in Niemann-Pick Type C Mice" *PloS one* 10, e0135889

Martin, E., Schule, R., Smets, K., Rastetter, A., Boukhris, A., Loureiro, J. L., Gonzalez, M. A., Mundwiller, E., Deconinck, T., Wessner, M., Jornea, L., Oteyza, A. C., Durr, A., Martin, J. J., Schols, L., Mhiri, C., Lamari, F., Zuchner, S., De Jonghe, P., Kabashi, E., Brice, A. & Stevanin, G. (2013) "Loss of function of glucocerebrosidase GBA2 is responsible for motor neuron defects in hereditary spastic paraplegia" *American journal of human genetics* 92, 238-244

Matern, H., Boermans, H., Lottspeich, F. & Matern, S. (2001) "Molecular cloning and expression of human bile acid beta-glucosidase" *The Journal of biological chemistry* 276, 37929-37933

Matern, H., Gartzen, R. & Matern, S. (1992) "Beta-glucosidase activity towards a bile acid glucoside in human liver" *FEBS letters* 314, 183-186

Matern, H., Heinemann, H., Legler, G. & Matern, S. (1997) "Purification and characterization of a microsomal bile acid beta-glucosidase from human liver" *The Journal of biological chemistry* 272, 11261-11267

Maxfield, F. R. & Yamashiro, D. J. (1987) "Endosome acidification and the pathways of receptor-mediated endocytosis" *Advances in experimental medicine and biology* 225, 189-198

Mayor, S. & Pagano, R. E. (2007) "Pathways of clathrin-independent endocytosis" *Nature reviews. Molecular cell biology* 8, 603-612

Meivar-Levy, I., Horowitz, M. & Futerman, A. H. (1994) "Analysis of glucocerebrosidase activity using N-(1-[14C]hexanoyl)-D-erythroglucosylsphingosine demonstrates a correlation between levels of residual enzyme activity and the type of Gaucher disease" *The Biochemical journal* 303 (Pt 2), 377-382

Merrill, A. H., Jr. (2002) "De novo sphingolipid biosynthesis: a necessary, but dangerous, pathway" *The Journal of biological chemistry* 277, 25843-25846

Merrill, A. H., Jr., Hannun, Y. A. & Bell, R. M. (1993a) "Introduction: sphingolipids and their metabolites in cell regulation" *Advances in lipid research* 25, 1-24

Merrill, A. H., Jr., van Echten, G., Wang, E. & Sandhoff, K. (1993b) "Fumonisin B1 inhibits sphingosine (sphinganine) N-acyltransferase and de novo sphingolipid biosynthesis in cultured neurons in situ" *The Journal of biological chemistry* 268, 27299-27306

Merrill, A. H., Jr. & Wang, E. (1992) "Enzymes of ceramide biosynthesis" *Methods in enzymology* 209, 427-437

Metz, R. J. & Radin, N. S. (1980) "Glucosylceramide uptake protein from spleen cytosol" *The Journal of biological chemistry* 255, 4463-4467

Miller-Prodraza, H. & Fishman, P. H. (1984) "Effect of drugs and temperature on biosynthesis and transport of glycosphingolipids in cultured neurotumor cells" *Biochimica et biophysica acta* 804, 44-51

Mistry, P. K., Liu, J., Sun, L., Chuang, W. L., Yuen, T., Yang, R., Lu, P., Zhang, K., Li, J., Keutzer, J., Stachnik, A., Mennone, A., Boyer, J. L., Jain, D., Brady, R. O., New, M. I. & Zaidi, M. (2014) "Glucocerebrosidase 2 gene deletion rescues type 1 Gaucher disease" *Proceedings of the National Academy of Sciences of the United States of America* 111, 4934-4939

Nakahara, K., Ohkuni, A., Kitamura, T., Abe, K., Naganuma, T., Ohno, Y., Zoeller, R. A. & Kihara, A. (2012) "The Sjogren-Larsson syndrome gene encodes a hexadecenal dehydrogenase of the sphingosine 1-phosphate degradation pathway" *Molecular cell* 46, 461-471

Nozue, M., Sakiyama, H., Tsuchiya, K., Hirabayashi, Y. & Taniguchi, M. (1988) "Melanoma antigen expression and metastatic ability of mutant B16 melanoma clones" *International journal of cancer* 42, 734-738

Overkleeft, H. S., Renkema, G. H., Neele, J., Vianello, P., Hung, I. O., Strijland, A., van der Burg, A. M., Koomen, G. J., Pandit, U. K. & Aerts, J. M. (1998) "Generation of specific deoxynojirimycin-type inhibitors of the non-lysosomal glucosylceramidase" *The Journal of biological chemistry* 273, 26522-26527

Oyadomari, S. & Mori, M. (2004) "Roles of CHOP/GADD153 in endoplasmic reticulum stress" *Cell death and differentiation* 11, 381-389

Pelled, D., Trajkovic-Bodennec, S., Lloyd-Evans, E., Sidransky, E., Schiffmann, R. & Futerman, A. H. (2005) "Enhanced calcium release in the acute neuronopathic form of Gaucher disease" *Neurobiology of disease* 18, 83-88

Pennelli, N., Scaravilli, F. & Zacchello, F. (1969) "The morphogenesis of Gaucher cells investigated by electron microscopy" *Blood* 34, 331-347

Pentchev, P. G., Blanchette-Mackie, E. J. & Dawidowicz, E. A. (1994) "The NP-C gene: a key to pathways of intracellular cholesterol transport" *Trends in cell biology* 4, 365-369

Pentchev, P. G., Brady, R. O., Hibbert, S. R., Gal, A. E. & Shapiro, D. (1973) "Isolation and characterization of glucocerebrosidase from human placental tissue" *The Journal of biological chemistry* 248, 5256-5261

Peters, C. & von Figura, K. (1994) "Biogenesis of lysosomal membranes" *FEBS letters* 346, 108-114

Pewzner-Jung, Y., Ben-Dor, S. & Futerman, A. H. (2006) "When do Lasses (longevity assurance genes) become CerS (ceramide synthases)?: Insights into the regulation of ceramide synthesis" *The Journal of biological chemistry* 281, 25001-25005

Pewzner-Jung, Y., Park, H., Laviad, E. L., Silva, L. C., Lahiri, S., Stiban, J., Erez-Roman, R., Brugger, B., Sachsenheimer, T., Wieland, F., Prieto, M., Merrill, A. H., Jr. & Futerman, A. H. (2010) "A critical role for ceramide synthase 2 in liver homeostasis:

I. alterations in lipid metabolic pathways" *The Journal of biological chemistry* 285, 10902-10910

Pike, L. J. & Casey, L. (2002) "Cholesterol levels modulate EGF receptor-mediated signaling by altering receptor function and trafficking" *Biochemistry* 41, 10315-10322

Platt, F. M., Neises, G. R., Dwek, R. A. & Butters, T. D. (1994) "N-butyldeoxynojirimycin is a novel inhibitor of glycolipid biosynthesis" *The Journal of biological chemistry* 269, 8362-8365

Platt, F. M., Reinkensmeier, G., Dwek, R. A. & Butters, T. D. (1997) "Extensive glycosphingolipid depletion in the liver and lymphoid organs of mice treated with N-butyldeoxynojirimycin" *The Journal of biological chemistry* 272, 19365-19372

Premkumar, L., Sawkar, A. R., Boldin-Adamsky, S., Toker, L., Silman, I., Kelly, J. W., Futerman, A. H. & Sussman, J. L. (2005) "X-ray structure of human acid-beta-glucosidase covalently bound to conduritol-B-epoxide. Implications for Gaucher disease" *The Journal of biological chemistry* 280, 23815-23819

Radin, N. S. (1996) "Treatment of Gaucher disease with an enzyme inhibitor" *Glycoconjugate journal* 13, 153-157

Raju, D., Schonauer, S., Hamzeh, H., Flynn, K. C., Bradke, F., Vom Dorp, K., Dormann, P., Yildiz, Y., Trotschel, C., Poetsch, A., Breiden, B., Sandhoff, K., Korschen, H. G. & Wachten, D. (2015) "Accumulation of glucosylceramide in the absence of the beta-glucosidase GBA2 alters cytoskeletal dynamics" *PLoS genetics* 11, e1005063

Ramstedt, B. & Slotte, J. P. (2002) "Membrane properties of sphingomyelins" *FEBS letters* 531, 33-37

Reczek, D., Schwake, M., Schroder, J., Hughes, H., Blanz, J., Jin, X., Brondyk, W., Van Patten, S., Edmunds, T. & Saftig, P. (2007) "LIMP-2 is a receptor for lysosomal mannose-6-phosphate-independent targeting of beta-glucocerebrosidase" *Cell* 131, 770-783

Requero, M. A., Goni, F. M. & Alonso, A. (1995) "The membrane-perturbing properties of palmitoyl-coenzyme A and palmitoylcarnitine. A comparative study" *Biochemistry* 34, 10400-10405

Riboni, L., Bassi, R., Prinetti, A., Viani, P. & Tettamanti, G. (1999) "Predominance of the acylation route in the metabolic processing of exogenous sphingosine in neural and extraneural cells in culture" *The Biochemical journal* 338 (Pt 1), 147-151

Ridley, C. M., Thur, K. E., Shanahan, J., Thillaiappan, N. B., Shen, A., Uhl, K., Walden, C. M., Rahim, A. A., Waddington, S. N., Platt, F. M. & van der Spoel, A. C. (2013) "beta-Glucosidase 2 (GBA2) activity and imino sugar pharmacology" *The Journal of biological chemistry* 288, 26052-26066

Rink, T. J., Tsien, R. Y. & Pozzan, T. (1982) "Cytoplasmic pH and free Mg2+ in lymphocytes" *The Journal of cell biology* 95, 189-196

Ron, D. & Habener, J. F. (1992) "CHOP, a novel developmentally regulated nuclear protein that dimerizes with transcription factors C/EBP and LAP and functions as a dominant-negative inhibitor of gene transcription" *Genes & development* 6, 439-453

Rosenberg, A. & Chargaff, E. (1958) "A reinvestigation of the cerebroside deposited in Gaucher's disease" *The Journal of biological chemistry* 233, 1323-1326

Rosenthal, M. D. (1987) "Fatty acid metabolism of isolated mammalian cells" *Progress in lipid research* 26, 87-124

Rother, J., van Echten, G., Schwarzmann, G. & Sandhoff, K. (1992) "Biosynthesis of sphingolipids: dihydroceramide and not sphinganine is desaturated by cultured cells" *Biochemical and biophysical research communications* 189, 14-20

Rutkowski, D. T. & Kaufman, R. J. (2004) "A trip to the ER: coping with stress" *Trends in Cell Biology* 14, 20-28

Sako, F., Gasa, S. & Makita, A. (1987) "Characterization of neutral glycosphingolipids from porcine erythrocyte membranes" *The International journal of biochemistry* 19, 923-929

Sasaki, T. (1990) "Glycolipid transfer protein and intracellular traffic of glucosylceramide" *Experientia* 46, 611-616

Schiffmann, R., Fitzgibbon, E. J., Harris, C., DeVile, C., Davies, E. H., Abel, L., van Schaik, I. N., Benko, W., Timmons, M., Ries, M. & Vellodi, A. (2008) "Randomized, controlled trial of miglustat in Gaucher's disease type 3" *Annals of neurology* 64, 514-522

Schuchman, E. H. (2010) "Acid sphingomyelinase, cell membranes and human disease: lessons from Niemann-Pick disease" *FEBS letters* 584, 1895-1900

Schulze, H., Kolter, T. & Sandhoff, K. (2009) "Principles of lysosomal membrane degradation: Cellular topology and biochemistry of lysosomal lipid degradation" *Biochimica et biophysica acta* 1793, 674-683

Schur, P. H. (1988) "IgG subclasses. A historical perspective" *Monographs in allergy* 23, 1-11

Schwarzmann, G. & Sandhoff, K. (1990) "Metabolism and intracellular transport of glycosphingolipids" *Biochemistry* 29, 10865-10871

Schweizer, A., Clausen, H., van Meer, G. & Hauri, H. P. (1994) "Localization of O-glycan initiation, sphingomyelin synthesis, and glucosylceramide synthesis in Vero cells with respect to the endoplasmic reticulum-Golgi intermediate compartment" *The Journal of biological chemistry* 269, 4035-4041

Scriver, C. R. (1995) "The metabolic and molecular bases of inherited disease".

Serra, M. & Saba, J. D. (2010) "Sphingosine 1-phosphate lyase, a key regulator of sphingosine 1-phosphate signaling and function" *Advances in enzyme regulation* 50, 349-362

Shayman, J. A. & Larsen, S. D. (2014) "The development and use of small molecule inhibitors of glycosphingolipid metabolism for lysosomal storage diseases" *Journal of lipid research* 55, 1215-1225

Sheikh, H., Yarwood, H., Ashworth, A. & Isacke, C. M. (2000) "Endo180, an endocytic recycling glycoprotein related to the macrophage mannose receptor is expressed on fibroblasts, endothelial cells and macrophages and functions as a lectin receptor" *Journal of cell science* 113 (Pt 6), 1021-1032

Sidransky, E., Sherer, D. M. & Ginns, E. I. (1992) "Gaucher disease in the neonate: a distinct Gaucher phenotype is analogous to a mouse model created by targeted disruption of the glucocerebrosidase gene" *Pediatric research* 32, 494-498

Simons, K. & van Meer, G. (1988) "Lipid sorting in epithelial cells" *Biochemistry* 27, 6197-6202

Sivakumar, K., Xie, F., Cash, B. M., Long, S., Barnhill, H. N. & Wang, Q. (2004) "A fluorogenic 1,3-dipolar cycloaddition reaction of 3-azidocoumarins and acetylenes" *Organic letters* 6, 4603-4606

Slavik, J. (1982) "Anilinonaphthalene sulfonate as a probe of membrane composition and function" *Biochimica et biophysica acta* 694, 1-25

Sleat, D. E., Wiseman, J. A., El-Banna, M., Price, S. M., Verot, L., Shen, M. M., Tint, G. S., Vanier, M. T., Walkley, S. U. & Lobel, P. (2004) "Genetic evidence for

nonredundant functional cooperativity between NPC1 and NPC2 in lipid transport" *Proceedings of the National Academy of Sciences of the United States of America* 101, 5886-5891

Sorice, M., Garofalo, T., Misasi, R., Longo, A., Mattei, V., Sale, P., Dolo, V., Gradini, R. & Pavan, A. (2001) "Evidence for cell surface association between CXCR4 and ganglioside GM3 after gp120 binding in SupT1 lymphoblastoid cells" *FEBS letters* 506, 55-60

Sorli, S. C., Colie, S., Albinet, V., Dubrac, A., Touriol, C., Guilbaud, N., Bedia, C., Fabrias, G., Casas, J., Segui, B., Levade, T. & Andrieu-Abadie, N. (2013) "The nonlysosomal beta-glucosidase GBA2 promotes endoplasmic reticulum stress and impairs tumorigenicity of human melanoma cells" *FASEB journal : official publication of the Federation of American Societies for Experimental Biology* 27, 489-498

Spiegel, S. & Milstien, S. (2003) "Sphingosine-1-phosphate: an enigmatic signalling lipid" *Nature reviews. Molecular cell biology* 4, 397-407

Sprong, H., Degroote, S., Claessens, T., van Drunen, J., Oorschot, V., Westerink, B. H., Hirabayashi, Y., Klumperman, J., van der Sluijs, P. & van Meer, G. (2001) "Glycosphingolipids are required for sorting melanosomal proteins in the Golgi complex" *The Journal of cell biology* 155, 369-380

Stahl, P. D., Rodman, J. S., Miller, M. J. & Schlesinger, P. H. (1978) "Evidence for receptor-mediated binding of glycoproteins, glycoconjugates, and lysosomal glycosidases by alveolar macrophages" *Proceedings of the National Academy of Sciences of the United States of America* 75, 1399-1403

Starzyk, K., Richards, S., Yee, J., Smith, S. E. & Kingma, W. (2007) "The long-term international safety experience of imiglucerase therapy for Gaucher disease" *Molecular genetics and metabolism* 90, 157-163

Steinman, R. M., Mellman, I. S., Muller, W. A. & Cohn, Z. A. (1983) "Endocytosis and the recycling of plasma membrane" *The Journal of cell biology* 96, 1-27

Stephens, M. C., Bernatsky, A., Burachinsky, V., Legler, G. & Kanfer, J. N. (1978) "The Gaucher mouse: differential action of conduritol B epoxide and reversibility of its effects" *Journal of neurochemistry* 30, 1023-1027

Stoffel, W., LeKim, D. & Sticht, G. (1968) "Metabolism of sphingosine bases. 8. Distribution, isolation and properties of D-3-oxosphinganine reductase. Stereospecificity of the NADPH-dependent reaction of 3-oxodihydrospingosine (2-amino-1-hydroxyoctadecane-3-one)" *Hoppe-Seyler's Zeitschrift fur physiologische Chemie* 349, 1637-1644

Sultana, S., Reichbauer, J., Schule, R., Mochel, F., Synofzik, M. & van der Spoel, A. C. (2015) "Lack of enzyme activity in GBA2 mutants associated with hereditary spastic paraplegia/cerebellar ataxia (SPG46)" *Biochemical and biophysical research communications* 465, 35-40

Takizawa, M., Nomura, T., Wakisaka, E., Yoshizuka, N., Aoki, J., Arai, H., Inoue, K., Hattori, M. & Matsuo, N. (1999) "cDNA cloning and expression of human lactosylceramide synthase" *Biochimica et biophysica acta* 1438, 301-304

te Vruchte, D., Lloyd-Evans, E., Veldman, R. J., Neville, D. C., Dwek, R. A., Platt, F. M., van Blitterswijk, W. J. & Sillence, D. J. (2004) "Accumulation of glycosphingolipids in Niemann-Pick C disease disrupts endosomal transport" *The Journal of biological chemistry* 279, 26167-26175

Tettamanti, G. & Riboni, L. (1994) "Gangliosides turnover and neural cells function: a new perspective" *Progress in brain research* 101, 77-100

Thiele, C., Papan, C., Hoelper, D., Kusserow, K., Gaebler, A., Schoene, M., Piotrowitz, K., Lohmann, D., Spandl, J., Stevanovic, A., Shevchenko, A. & Kuerschner, L. (2012) "Tracing fatty acid metabolism by click chemistry" *ACS chemical biology* 7, 2004-2011

Thudichum, J. L. W. (1901) "Die chemische Konstitution des Gehirns des Menschen und der Tiere", xii, 339 p.

Trajkovic-Bodennec, S., Bodennec, J. & Futerman, A. H. (2004) "Phosphatidylcholine metabolism is altered in a monocyte-derived macrophage model of Gaucher disease but not in lymphocytes" *Blood cells, molecules & diseases* 33, 77-82

Tybulewicz, V. L., Tremblay, M. L., LaMarca, M. E., Willemsen, R., Stubblefield, B. K., Winfield, S., Zablocka, B., Sidransky, E., Martin, B. M., Huang, S. P. & et al. (1992) "Animal model of Gaucher's disease from targeted disruption of the mouse glucocerebrosidase gene" *Nature* 357, 407-410

van der Spoel, A. C., Jeyakumar, M., Butters, T. D., Charlton, H. M., Moore, H. D., Dwek, R. A. & Platt, F. M. (2002) "Reversible infertility in male mice after oral administration of alkylated imino sugars: a nonhormonal approach to male contraception" *Proceedings of the National Academy of Sciences of the United States of America* 99, 17173-17178

van Echten, G. & Sandhoff, K. (1993) "Ganglioside metabolism. Enzymology, Topology, and regulation" *The Journal of biological chemistry* 268, 5341-5344

van Meer, G., Wolthoorn, J. & Degroote, S. (2003) "The fate and function of glycosphingolipid glucosylceramide" *Philosophical transactions of the Royal Society of London. Series B, Biological sciences* 358, 869-873

Van Weely, S., Aerts, J. M., Van Leeuwen, M. B., Heikoop, J. C., Donker-Koopman, W. E., Barranger, J. A., Tager, J. M. & Schram, A. W. (1990) "Function of oligosaccharide modification in glucocerebrosidase, a membrane-associated lysosomal hydrolase" *European journal of biochemistry / FEBS* 191, 669-677

van Weely, S., Brandsma, M., Strijland, A., Tager, J. M. & Aerts, J. M. (1993) "Demonstration of the existence of a second, non-lysosomal glucocerebrosidase that is not deficient in Gaucher disease" *Biochimica et biophysica acta* 1181, 55-62

Vanier, M. T. (1983) "Biochemical studies in Niemann-Pick disease. I. Major sphingolipids of liver and spleen" *Biochimica et biophysica acta* 750, 178-184

Vanier, M. T. (2010) "Niemann-Pick disease type C" *Orphanet journal of rare diseases* 5, 16

Vanier, M. T. & Millat, G. (2003) "Niemann-Pick disease type C" *Clinical genetics* 64, 269-281

Vardi, A., Zigdon, H., Meshcheriakova, A., Klein, A. D., Yaacobi, C., Eilam, R., Kenwood, B. M., Rahim, A. A., Massaro, G., Merrill, A. H., Jr., Vitner, E. B. & Futerman, A. H. (2016) "Delineating pathological pathways in a chemically induced mouse model of Gaucher disease" *The Journal of pathology* 239, 496-509

Varki, A. (1993) "Biological roles of oligosaccharides: all of the theories are correct" *Glycobiology* 3, 97-130

Varki, A. (1994) "Selectin ligands" *Proceedings of the National Academy of Sciences of the United States of America* 91, 7390-7397

Vidarsson, G., Dekkers, G. & Rispens, T. (2014) "IgG subclasses and allotypes: from structure to effector functions" *Frontiers in immunology* 5, 520

Vielhaber, G., Pfeiffer, S., Brade, L., Lindner, B., Goldmann, T., Vollmer, E., Hintze, U., Wittern, K. P. & Wepf, R. (2001) "Localization of ceramide and glucosylceramide in human epidermis by immunogold electron microscopy" *The Journal of investigative dermatology* 117, 1126-1136

Votsi, C., Zamba-Papanicolaou, E., Middleton, L. T., Pantzaris, M. & Christodoulou, K. (2014) "A novel GBA2 gene missense mutation in spastic ataxia" *Annals of human genetics* 78, 13-22

Wacker, M., Linton, D., Hitchen, P. G., Nita-Lazar, M., Haslam, S. M., North, S. J., Panico, M., Morris, H. R., Dell, A., Wren, B. W. & Aebi, M. (2002) "N-linked glycosylation in Campylobacter jejuni and its functional transfer into E. coli" *Science* 298, 1790-1793

Walter, P. & Ron, D. (2011) "The unfolded protein response: from stress pathway to homeostatic regulation" *Science* 334, 1081-1086

Wang, X. Q., Sun, P., O'Gorman, M., Tai, T. & Paller, A. S. (2001) "Epidermal growth factor receptor glycosylation is required for ganglioside GM3 binding and GM3-mediated suppression [correction of suppresion] of activation" *Glycobiology* 11, 515-522

Warnock, D. E., Lutz, M. S., Blackburn, W. A., Young, W. W., Jr. & Baenziger, J. U. (1994) "Transport of newly synthesized glucosylceramide to the plasma membrane by a non-Golgi pathway" *Proceedings of the National Academy of Sciences of the United States of America* 91, 2708-2712

Wei, H., Kim, S. J., Zhang, Z., Tsai, P. C., Wisniewski, K. E. & Mukherjee, A. B. (2008) "ER and oxidative stresses are common mediators of apoptosis in both neurodegenerative and non-neurodegenerative lysosomal storage disorders and are alleviated by chemical chaperones" *Human molecular genetics* 17, 469-477

Weinreb, N. J., Charrow, J., Andersson, H. C., Kaplan, P., Kolodny, E. H., Mistry, P., Pastores, G., Rosenbloom, B. E., Scott, C. R., Wappner, R. S. & Zimran, A. (2002) "Effectiveness of enzyme replacement therapy in 1028 patients with type 1 Gaucher disease after 2 to 5 years of treatment: a report from the Gaucher Registry" *The American journal of medicine* 113, 112-119

Wennekes, T., Meijer, A. J., Groen, A. K., Boot, R. G., Groener, J. E., van Eijk, M., Ottenhoff, R., Bijl, N., Ghauharali, K., Song, H., O'Shea, T. J., Liu, H., Yew, N., Copeland, D., van den Berg, R. J., van der Marel, G. A., Overkleeft, H. S. & Aerts, J. M. (2010) "Dual-action lipophilic iminosugar improves glycemic control in obese rodents by reduction of visceral glycosphingolipids and buffering of carbohydrate assimilation" *Journal of medicinal chemistry* 53, 689-698

Xu, Y. H., Reboulet, R., Quinn, B., Huelsken, J., Witte, D. & Grabowski, G. A. (2008) "Dependence of reversibility and progression of mouse neuronopathic Gaucher disease on acid beta-glucosidase residual activity levels" *Molecular genetics and metabolism* 94, 190-203

Yamanaka, S., Johnson, M. D., Grinberg, A., Westphal, H., Crawley, J. N., Taniike, M., Suzuki, K. & Proia, R. L. (1994) "Targeted disruption of the Hexa gene results in mice with biochemical and pathologic features of Tay-Sachs disease" *Proceedings of the National Academy of Sciences of the United States of America* 91, 9975-9979

Ye, J., Rawson, R. B., Komuro, R., Chen, X., Dave, U. P., Prywes, R., Brown, M. S. & Goldstein, J. L. (2000) "ER stress induces cleavage of membrane-bound ATF6 by the same proteases that process SREBPs" *Molecular cell* 6, 1355-1364

Yildiz, Y., Hoffmann, P., Vom Dahl, S., Breiden, B., Sandhoff, R., Niederau, C., Horwitz, M., Karlsson, S., Filocamo, M., Elstein, D., Beck, M., Sandhoff, K., Mengel, E., Gonzalez, M. C., Nothen, M. M., Sidransky, E., Zimran, A. & Mattheisen, M. (2013) "Functional and genetic characterization of the non-lysosomal glucosylceramidase 2 as a modifier for Gaucher disease" *Orphanet journal of rare diseases* 8, 151

Yildiz, Y., Matern, H., Thompson, B., Allegood, J. C., Warren, R. L., Ramirez, D. M., Hammer, R. E., Hamra, F. K., Matern, S. & Russell, D. W. (2006) "Mutation of beta-glucosidase 2 causes glycolipid storage disease and impaired male fertility" *The Journal of clinical investigation* 116, 2985-2994

Zimran, A., Gelbart, T., Westwood, B., Grabowski, G. A. & Beutler, E. (1991) "High frequency of the Gaucher disease mutation at nucleotide 1226 among Ashkenazi Jews" *American journal of human genetics* 49, 855-859

Danksagung

Diese Arbeit wurde in der Max-Planck-Forschungsgruppe Molekulare Physiologie am Forschungszentrum Caesar in Bonn angefertigt. Ich danke allen Mitarbeitern und Mitarbeiterinnen für die Unterstützung und gute Zusammenarbeit.

Insbesondere gilt mein Dank:

- PD Dr. Dagmar Wachten, für das Anvertrauen eines spannenden Projekts, das mir über die Jahre sehr ans Herz gewachsen ist und mir große Freude bereitet hat. Danke für Deine Unterstützung in jeglicher Lebenslage!
- Prof. Dr. Christoph Thiele, für seine Diskussionsbereitschaft und die erfolgreiche Zusammenarbeit, die maßgeblich am Erfolg dieses Projekts beteiligt war.
- Prof. Dr. Günther Mayer und Prof. Dr. Anton Bovier, für ihre Beteiligung an der Prüfungskommission.
- Dr. Heinze Körschen, für seine unermüdliche Unterstützung seit Beginn meiner Arbeit. Danke, dass Du immer ein offenes Ohr für meine Fragen hattest und ich von Deinem riesigen Wissensschatz profitieren durfte!
- Prof. Dr. Tony Futerman, for all the lively (and hilarious!) discussions and the help with my project during the past years.
- Dr. Wolfgang Bönigk, für seine Hilfe bei molekularbiologischen Arbeiten. Die Plasmide waren ein Traum!
- Dr. Jan Jikeli, für seine Hilfe bei der Analyse von Daten und die hierfür aufgebrachte Geduld.
- Dr. Bernadette Breiden, für ihre Hilfe auf Lipid-Territorium und für ihre herzliche Art.
- Dr. Diana N. Raju, for sharing her (scientific) thoughts, laughter, and cookies with me. You are a wonderful colleague and I am lucky to call you my friend!
- Jens-Henning Krause, für seine Hilfe und eine außergewöhnlich schöne Zeit, sowohl im Büro als auch im Labor! Danke, dass Du mich aufgebaut und mit mir gelacht hast (was auch immer gerade nötiger war).
- Dr. Anke Penno, für ihre Freundschaft und Unterstützung sowohl im als auch außerhalb des Labors. Danke, Anke (haha!), dass Du immer für mich da warst!

- Allen Mitgliedern der AG Wachten. Danke an Melanie und Marina für eine tolle Zeit!
- Meinen Mitdoktoranden, für die wissenschaftliche Unterstützung und ein gutes Miteinander.
- Jessica Hierer und Stefanie Sonnenburg für ihre helfenden Hände in der Zellkultur.

Mein persönlicher Dank gilt meinen Freunden, die mir sowohl in guten als auch in schlechten Zeiten nicht von der Seite gewichen sind. Helen, mit dir zusammen ist das Leben gleich viel lebenswerter und ich bin froh, in Dir so eine wundervolle Freundin gefunden zu haben! Carina, Du hast mich immer aufgefangen und gibst so viel, ohne selbst etwas zu erwarten. Danke, für all die gemeinsamen Erlebnisse! Christian, es ist immer wieder eine Freude mit Dir über jegliches Thema zu sinnieren! Und natürlich: Dominik, denn Du bist ein Meister darin, den Grumpy-Cat-Modus in den Fluffy-Unicorn-Modus umzuwandeln! :-)

Ich bin stolz darauf, so tolle Eltern zu haben, die mich nicht nur im Studium und bei der Promotion unterstützt, sondern auch alle Hebel in Bewegung gesetzt haben, um mir parallel den Reitsport zu ermöglichen. Das eine wäre ohne das andere nicht möglich gewesen und ich bin sehr dankbar, dass ihr mir immer den Rücken freigehalten habt. Danke, Mama, dass Du Dich um alles gekümmert und mich bedingungslos unterstützt hast.